JOURNAL OF ENGINEERING RESEARCH & SCIENCES

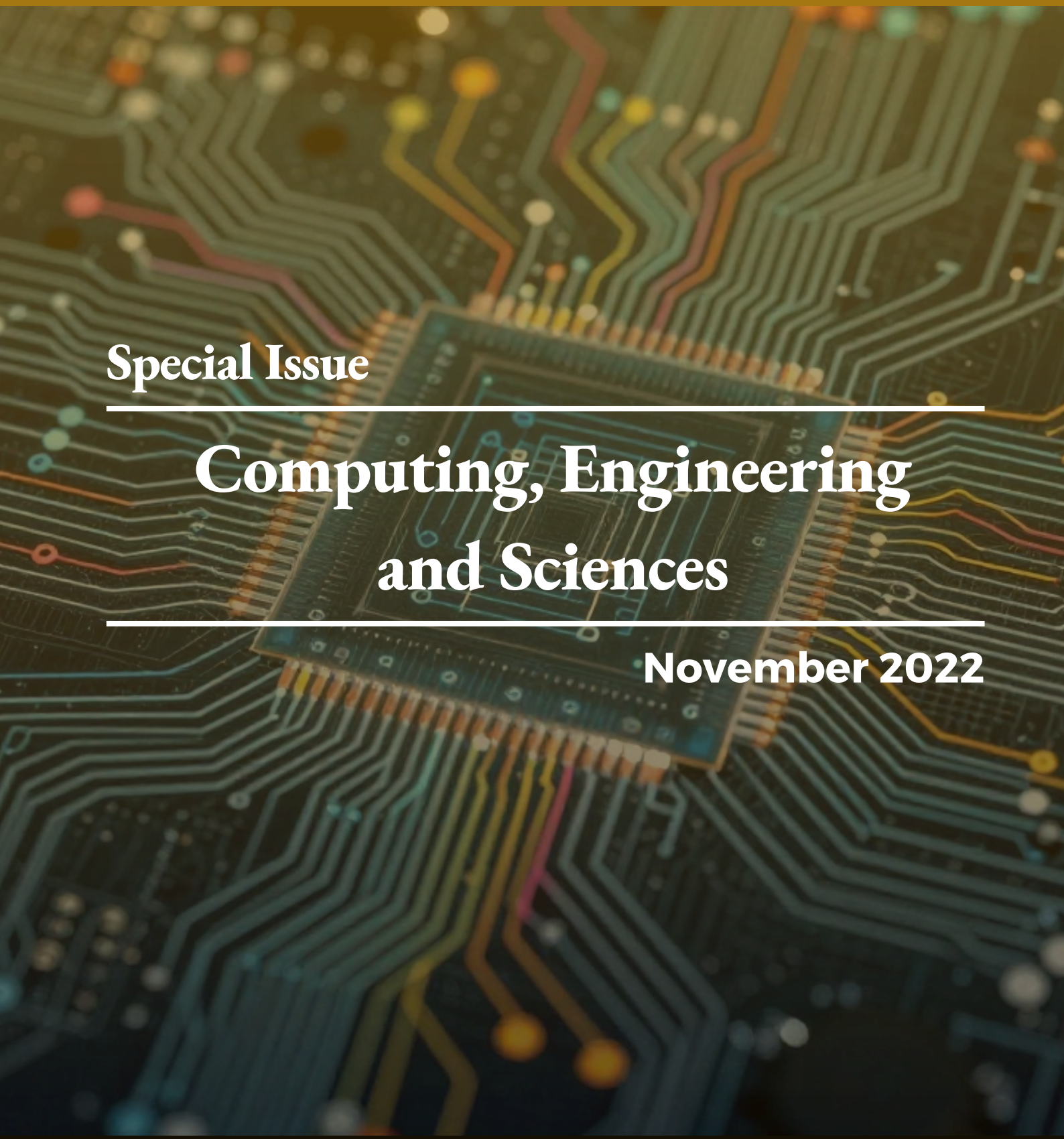

Special Issue

# Computing, Engineering and Sciences

November 2022

www.jenrs.com
ISSN: 2831-4085

JENRS

# EDITORIAL BOARD
# (Special Issue)

## Guest Editor

**Prof. Paul Andrew**
Department of Electrical Engineering, Universidade De São Paulo, Brazil

# Editorial

The convergence of computing, engineering, and scientific inquiry has become a defining characteristic of modern research and innovation. It is with great pleasure that we present this special issue of the *Journal of Engineering Research and Sciences*, devoted to the theme of *Computing, Engineering and Sciences*. This issue brings together a diverse collection of scholarly works that illustrate how computational advancements are reshaping engineering practices and scientific exploration, ultimately enabling more efficient, intelligent, and impactful solutions to contemporary challenges.

In recent years, the integration of computing technologies into engineering and scientific domains has accelerated at an unprecedented pace. High-performance computing, artificial intelligence, data analytics, and simulation techniques have become indispensable tools across a wide range of disciplines. The contributions featured in this issue highlight how these technologies are not only enhancing traditional methodologies but also redefining the boundaries of what is possible. From predictive modeling in engineering systems to data-driven discoveries in scientific research, the role of computing as a transformative force is clearly evident.

A central theme of this special issue is the seamless interaction between theoretical foundations and practical applications. Authors have explored innovative approaches that bridge computational theory with engineering design and scientific experimentation. This integration enables the development of optimized systems, improved decision-making processes, and scalable solutions that can adapt to evolving requirements. The interdisciplinary nature of the research presented here underscores the importance of collaboration among experts from computing, engineering, and scientific backgrounds.

Furthermore, the issue emphasizes the growing importance of intelligent systems and automation. Advances in machine learning, deep learning, and embedded systems are enabling the creation of smart technologies that can analyze complex datasets, learn from patterns, and make autonomous decisions. These capabilities are being applied in areas such as smart manufacturing, healthcare technologies, environmental monitoring, and infrastructure management. The research contributions in this issue demonstrate how intelligent systems are contributing to increased efficiency, accuracy, and reliability in both engineering and scientific applications.

Another significant aspect highlighted in this issue is the role of simulation and modeling in advancing knowledge and innovation. Computational simulations allow researchers to explore scenarios that may be difficult, costly, or time-consuming to replicate in real-world environments. By leveraging these tools, researchers can test hypotheses, optimize designs, and gain deeper insights into complex systems. The studies presented here showcase the power of simulation in addressing challenges across various domains, including materials science, fluid dynamics, and energy systems.

The editorial team would like to extend its sincere gratitude to all authors for their valuable contributions and to the reviewers for their diligent efforts in maintaining the high standards of the journal. Their expertise and commitment have ensured the quality, rigor, and relevance of the research presented in this special issue.

As we present this collection of articles, we hope it will inspire continued exploration and collaboration at the intersection of computing, engineering, and sciences. The challenges faced by society today require integrated approaches that leverage the strengths of multiple disciplines. By fostering such collaboration, the research community can continue to develop innovative solutions that address global needs and contribute to sustainable progress.

We invite readers to engage with the insights and advancements presented in this issue and to contribute to the ongoing dialogue in this dynamic and evolving field. The future of computing, engineering, and sciences lies in the continued integration of knowledge, the advancement of technology, and the pursuit of excellence in research and innovation.

**Guest Editor**

**Prof. Paul Andrew**

**JOURNAL OF ENGINEERING RESEARCH AND SCIENCES**

**Special Issue** **November 2022**

# CONTENTS

Received: 08 September 2022, Revised: 11 November 2022, Accepted: 12 November 2022, Online: 27 November 2022

DOI: https://dx.doi.org/10.55708/js0111001

# Using Interaction Geography to Explore Building Occupant Behaviors in Virtual Reality: A Pilot Study

**Hoa Vo*, Peter Huesemann-Odom**

Welch School of Art and Design, College of the Arts, Georgia State University, Atlanta, 30303, USA
*Corresponding author: Hoa Vo, AH 362,10 Peachtree Center Ave. SE, Atlanta, GA 30303, USA, (+1)404-413-5143, kvo@gsu.edu

**ABSTRACT:** The sole focus of current occupant behavior research on environmental and contextual factors (i.e., physical attributes) in buildings is a missed opportunity. Psychological, physiological, social, time, and random factors also influence building occupants. In this pilot study ($n = 10$), the authors used Interaction Geography to capture human movements across space and time in a Virtual Reality (VR) museum to dissect building occupant behavior. Results indicated that study majors (i.e., psychological) and personal connections (i.e., social) with the space affected how participants explored and spent time in the VR museum.

**KEYWORDS:** Interaction Geography, Building Occupant Behavior, Virtual Reality

## 1. Introduction

Building occupant behaviors are the direct indicators of how well the built environment (e.g., interior spaces) promotes human physical and psychological well-being. The current approach to comprehending said behaviors focuses on occupant assessments of the physical design or subjective ratings of indoor environmental quality (IEQ) factors such as acoustics, cleanliness, and furnishings [1]. Occupancy evaluations exemplify this approach by asking occupants to rate their satisfaction with IEQ factors on survey-based Likert-scale items (e.g., 1 = dissatisfied; 7 = satisfied) [2]. This approach may seem like an objective way to measure IEQ; however, the following problems cloud the resulting data. First, retrospective data collection relies on occupants' memories of a space. Subjects might mis-remember or fail to recall their experience with the building [3]. Therefore, their ratings of IEQ factors are inadequate and incomplete reflections of their real-time experiences which dictate their behaviors in the building. Second, the tendency to reduce cognitive load means that occupants frequently select the middle choice of complex multiple-choice questions [4].

These biases challenge researchers who study the built environment to develop more comprehensive methods for assessing occupants' behaviors. One exemplary method is implementing agent-based simulation (ABS), autonomous computational agents interacting with one another and their surroundings [5], to predict occupant behaviors in buildings. ABS is most effective in modeling behavioral patterns in hypothesized scenarios to schedule working shifts, regulate energy usage, evacuate for emergencies, and so on [6–8]. One caveat of using ABS in the built environment is that the computational system disregards the complexities underlying occupant behaviors (e.g., age, gender, and psychological state) [6]. This argument also applies to sensor-based and GPS-enabled data collection, with a heavy emphasis on the physical characteristics of the building, not the psychological aspects of occupants [9], [10].

Interaction geography, a novel approach to describing, representing, and interpreting human interactions with their environments across space and time [11], offers one solution to these challenges. Current implementations of interaction geography in the built environment include assessing occupant travel patterns in a museum [12] and in teacher-student-interactions in the classroom [13], [14]. Such implementations are limited, yet growing interest in interaction geography is evident through multiple studies focusing on the movements of building occupants [15–17]. However, tracking movements is an intensive and time-consuming data collection process that uses wearable sensors or camera recordings [12], [17].

This paper presents a time-and-cost efficient approach to exploring building occupant behavior via movements using Virtual Reality (VR) technology. In a pilot study, the authors analyzed the movements of 10 participants in a

virtual museum to examine the extent to which interaction geography further the current understandings of building occupant behavior with the research question:

"What insights can Interaction Geography offer to the understanding of participant behavior in a VR museum?"

The authors, thus, explored movement patterns (obtained via Interaction Geography) to identify how participants interacted with a building setting via real-time data.

## 2. Literature Review

### *2.1. Building Occupant Behavior Research*

Building occupant behavior is under the influences of environmental, contextual, psychological, physiological, social, time, and random factors (Figure 1) [18]. Lighting, temperature, and indoor air are environmental factors. Building features such as orientation and construction are contextual; gender, age, and occupation are psychological; individual perceptions of temperature are physiological, cultural groups and organizational regulations are social factors [19]. Time-related events (e.g., working shifts) and random movements are influential as well [20]. Studies on building occupant behavior focus on environmental and contextual factors due to their quantifiable nature. For instance, researchers operationalize environmental factors as Indoor Environmental Quality (IEQ) variables that are measurable using satisfaction surveys (e.g., pre-and post-occupancy evaluations) and real-time devices (e.g., light meters, sensors) [21].

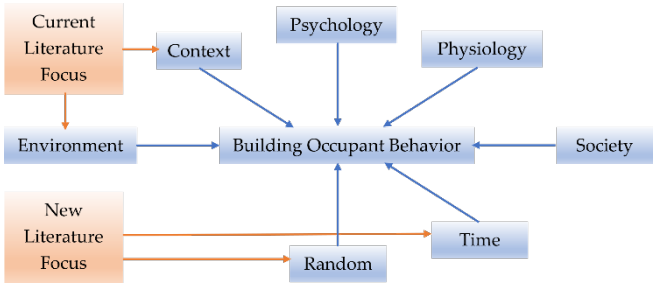


Figure 1: Factors that Influence Building Occupant Behavior

In the typical approach of post-occupancy evaluation (POE), occupants will complete a survey nine to twelve months after moving into a building. The two components that make up POE include (i) subjective perceptions (i.e., comfort and satisfaction) and (ii) physical measurements (i.e., building features) [9]. Both components contain IEQ variables such as temperature, light, noise, privacy, view, decoration, cleanliness, and so on. Occupants use Likert ratings to indicate their subjective perceptions of IEQ variables and their impacts. For example, the Building Use Studies (BUS) survey includes 7-point rating scales (e.g., uncomfortable to comfortable) for 11 IEQ variables (e.g., thermal, acoustic, appearance) [22]. Among IEQ variables, noise, air quality, light, and thermal are most influential to building occupants [1], [23].

Regarding physical measurements, devices like meters and sensors help researchers estimate how IEQ variables might influence building occupants over time. Energy and water consumption plus IEQ variables such as thermal, lighting, air quality, and acoustics make up most of this component [10]. Electricity usage (e.g., applicant loads), window, fan, and air conditioning operation are occupant behaviors of interest within residential and commercial buildings; these studies dominate the corresponding literature [19]. In [18], the authors discussed the current state of building occupant behavior through the following environmental and contextual factors (i.e., IEQ variables): window, lighting, shading, and air conditioning (AC). The focus on this subset of factors/variables is reasonable as professionals (e.g., engineers, architects, designers) and stakeholders (e.g., managers, owners) are concerned with the social and financial costs of energy consumption and life cycle of buildings. The authors in [24] also projected a decline in energy purchasing power of $11,258,2019 by 2099, implying that low-income populations would suffer from the inability to consume energy in response to climate change (i.e., global warming). According to the authors in [25], residential buildings that withstand a wide temperature fluctuation (e.g., from – 20°C to + 30°C) are costly, especially with a deficit in Gross Domestic Product (e.g., – 2% in 2017) due to global warming. Said costs explain why environmental and contextual factors (i.e., IEQ variables) predominate the current state of building occupant behavior research (Figure 1).

Viewing building occupant behavior as stochastic (i.e., random) with the variants between occupants that evolve over time represents a research paradigm shift [15]. Recent additions to POE include visual records, data of building structure/service/system, window sensors, GPS-tracked mobility, and so on [10]. In [6] the authors utilized an agent-based simulation (ABS) model and sensor-based data to predict probabilities of window operation in commercial buildings. This model reduces stochastic uncertainties by cross-referencing multiple IEQ variables like temperature, air, and humidity, in a single behavior: opening a window. However, the ABS model did not take into account the complex occupant interactions in real-world settings and the underlying psychological factors.

### *2.2. Interaction Geography*

Interaction Geography is the comprehensive analysis of audiovisual data of interactions via sociocultural and social lenses [11]. Originating from interaction analysis in Computer Supported Collaborative Learning (CSCL), this approach converts and presents selective subsets of verbal and physical behaviors into transcripts so researchers can comprehend social events from insider perspectives [26]. The transcript is not merely a record of audiovisual data but a portrait that captures the emotions, behaviors, and potential intentions of people who engage in a social event

[27]. Transcripts are vital to interaction analysis, but their production techniques have evolved little over the years. Language-processing software such as Microsoft Word is typically used to produce transcripts that include conversations and gestures or multimodal transcription [28]. Through the "presentation of text," researchers preserve data integrity by not correcting "particulars" or "tiny things" that might reveal the sociocultural backgrounds or underlying thoughts of the event in participants [27], [29].

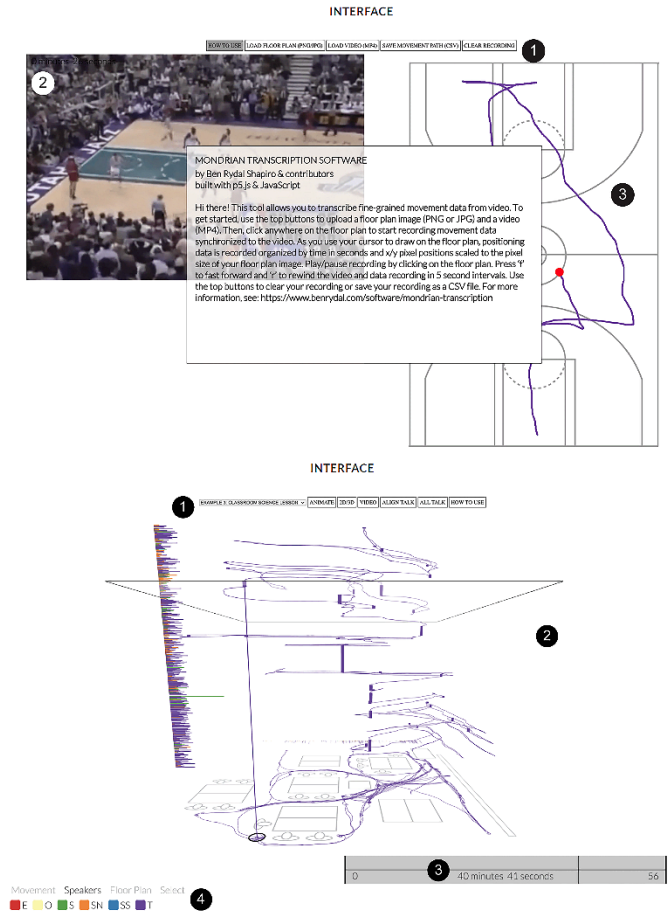


Figure 2: Mondrian Transcription and IGS Interfaces [12]

However, language-based transcription is inadequate to represent the intrinsic complexity of social behaviors. Interaction Geography combines qualitative analysis with time geography (i.e., time-space coordination of human behaviors in social events) to analyze audiovisual data [30], [31]. In [11], the author offered a cutting-edge method for Interaction Geography with two key components (Figure 2). First, via Mondrian Transcription web-based software, the author extracted and encoded participant movements and conversations over space and time from audiovisual data. This process resulted in a spreadsheet containing the pixel positions and movement transcripts of participants. Mondrian Transcription is among the earliest tools that transcribe movements and conversations (i.e., pixel positions and timed verbal exchanges). Second is Interaction Geography Slicer (IGS), a tool that syncs transcripts of movements and conversations with specific time frames in audiovisual data. IGS, therefore, enables exploratory analyses and dynamic visualizations of Mondrian transcription [26].

One application of Interaction Geography in buildings was to study museum visitor traveling patterns [12] and classroom interactions of teachers and students [13]. In [12], the authors analyzed 22 case studies with 72 hours of audio and video recordings of museum visitors to determine their movements, interactions, and technology use. The data illustrated how "visitors' personal and social history, prior knowledge, and relationship to one another" influenced their choice of navigation and experience in a museum setting. In [13], the authors analyzed audiovisual excerpts of teacher-student interactions in two classrooms. Results indicated that the teachers developed repetitive circulation patterns around projector and tables. Their travel patterns also fluctuated during classroom hours, depending on the changes in instructional content. The findings raised concerns regarding how teachers should monitor their classroom movements and interactions to ensure effective teaching. Interaction Geography, thus, is helpful for the stochastic paradigm in building occupant behavior research as it reveals the randomness underlies occupants' behavior across space and time.

## 3. Methodology

In this paper, the authors proposed a novel application of Interaction Geography in building occupant behavior research using Virtual Reality (VR). Like the authors in [12], we also chose a museum setting to explore occupant behaviors across time and space. VR technology enabled a time- and cost-efficient simulation of a museum and therefore was fundamental for piloting occupant behavior study in the chosen setting.

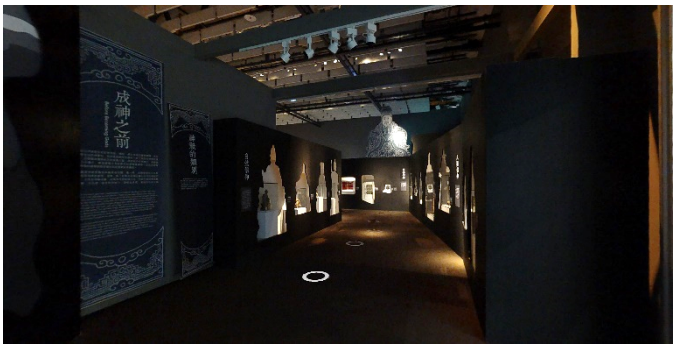

Figure 3: The VR Museum [32] as Seen in a Meta Quest 2 Headset

### *3.1. VR Museum Session*

This pilot study utilized a public VR museum (Figure 3) from the Matterport website (https://matterport.com/) [32]. Participants ($n = 10$) each attended a VR session, which included 10 minutes of training and 20 minutes (or more) of exploring the VR museum. Using Meta Quest 2 headsets, the authors recorded VR sessions (in video and audio) as participants explored the virtual building space.

Using the hand controllers, participants moved through the space by pointing at the white circles on the floor. The participants, however, could not interact with the artifacts (e.g., statues) and spatial elements (e.g., door) in the virtual museum as they are only 360-degree photographs.

### *3.2. Interaction Geography Transcription*

Mondrian Transcription (https://www.benrydal.com/software/mondrian-transcription) [12] helped transcribe recorded movements and interactions into pixel positions on a scale diagram that illustrates space arrangements in a building (i.e., a floor plan). The museum floor plan and the audiovisual recordings of the VR sessions were uploaded to Mondrian Transcription's web-based interface (Figure 4) for manual tracing. Both files were then visible next to each other on a computer screen. By hovering the mouse cursor over the floor plan, the authors displayed a path that followed the participants' movements as shown in the recording. The authors accurately traced the time-specific movements using the keyboard to play, rewind, and pause the recording. Analysis results included a traced floorplan demonstrating a two-dimensional (2-D) movement path and a spreadsheet logging every step of the participant in the space with x- and y-coordinates. The authors repeated this process with all recordings.


Figure 4: Mondrian Transcription's Web-based Interface with Manual Tracing of Participant's Movements

IGS (https://www.benrydal.com/software/igs) [12] was another process the authors used to visualize the traced movement paths of participants over time. We uploaded Mondrian Transcription transcripts (i.e., the spreadsheets with x- and y-coordinates) and the corresponding VR recordings to this web-based interface. IGS synchronized all movements and conversations of each participant following a timeline that equaled the length of each recording. This process resulted in an animated floor plan illustrating the 2-D movement path over a corresponding three-dimensional (3-D) conversation timeline. Hovering the cursor on top of the animated floor plan allowed the authors to rewind and analyze participant movements and conversations at a specific point in time.

## 4. Results

Participants ($n = 10$) in this pilot study were all college students in the 18 – 34 age group, with 67 % female and 33 % male. This was a convenient sample of volunteers who dedicated their time to participate in this study without compensation. Table 1 summarizes the demographics and logistics of all participants.

Table 1: Demographics and Logistics of Participants

| ID No. | Time in VR | Use VR | Major |
|---|---|---|---|
| P_1 | 12 minutes | Monthly | Design |
| P_2 | 15 minutes | Yearly | Design |
| P_3 | 20 minutes | Never | Design |
| P_4 | 28 minutes | Never | Non-design |
| P_5 | 17 minutes | Never | Non-design |
| P_6 | 14 minutes | Never | Non-design |
| P_7 | 14 minutes | Never | Non-design |
| P_8 | 12 minutes | Never | Non-design |
| P_9 | 30 minutes | Never | Design |
| P_10 | 12 minutes | Monthly | Design |

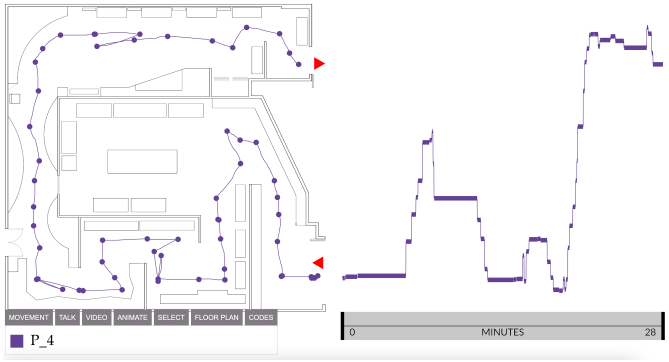


Figure 5: Floor plan of the VR museum with the Traced Movements Across Time and Space of a Participant

### *4.1. Participant Behavior in a Virtual Space*

Most participants (70%) had minimal prior exposure to VR technology, and the average time they spent exploring the virtual museum was around 17 minutes. Participants all completed the VR session from start to finish. The floor plan (Figure 5) indicates the entrance (i.e., the upper red arrow) and the exit (i.e., the lower red arrow), with representations of objects (i.e., artifacts), display cases, and furniture in the VR museum. Although the white circles predetermined the VR museum navigation, participants were free to skip circles, come back, and stay for a certain amount of time at specific points. Such behaviors reflected how participants behaved in the VR museum regarding the space arrangement (e.g., whether display cases with the artifacts captured participant attention as planned by the interior designer). Figure 5 below illustrates the fourth participant's (P_4) movements across space and time. P_4's travel path is depicted on the museum floor plan, and the adjacent timeline displays the periods they spent in each area of the space throughout their recording. For 28 minutes, P_4 (a non-design major) traveled across the VR museum yet entirely skipped the central exhibition with multiple display cases and artifacts. This observation

is one of the behavior discrepancies among participants. The section below summarizes notable findings from the movements across space and time of all participants in this pilot study. Instead of discussing the movements across space and time of each participant, the authors stacked the travel paths of those with the same background (i.e., design vs. non-design) together for a better comparison.

### *4.2. Movement Density and Personal Background*

The authors analyzed all the transcripts and organized them into two categories based on movement density: design and non-design major participants. To give a comprehensive view of the results, the authors overlaid the traced paths of participants together on the floor plan for each category. Figure 6 depicts the paths of five participants who major in design (P_1, P_2, P_3, P_9, and P_10).

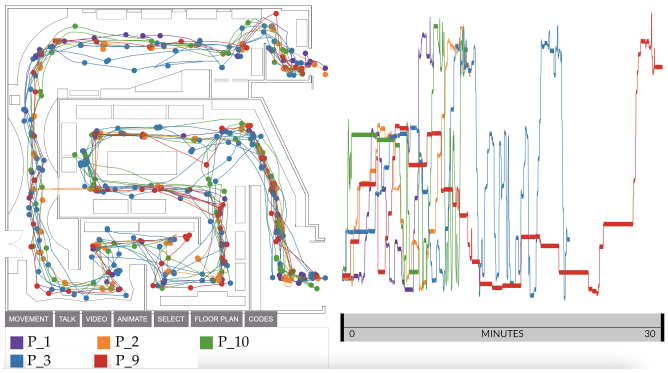


Figure 6: Overlays of Movements Across Time and Space of Design Participants

- Design-major participants had intense movement density; as shown in Figure 6, these participants spent more time at the entrance and exit (as shown in multiple traced points). They also returned to specific spots (as their paths overlapped several times). None of them skipped the central exhibition, and all followed the intended design of the floor plan.
- P_2 discovered the door that led directly to the central exhibition while exploring the lower part of the central exhibition. P_2 then crossed the door to a hallway previously visited and went back to the central exhibition to complete the upper part (the orange path in Figure 6). Notably, P_2 indicated only yearly use of VR, which is less prior experience than P_1 and P_10 indicated. The other participants all navigated from the entrance toward the long hallway leading to the central exhibition and ended at the exit.
- The synchronized timeline on the right of Figure 6 also reveals time durations spent throughout the VR museum. P_1 and P_3, for example, spent more time exploring at the beginning (about one-fourth and one-half of their time, respectively) but later skimmed through the space. Meanwhile, P_2, P_9, and P_10 divided their time more evenly across the VR museum.

Figure 7 illustrates the paths of five participants who were in non-design majors (P_4., P_5, P_6, P_7, and P_8). Their behavior showed some differences compared to their design counterparts.

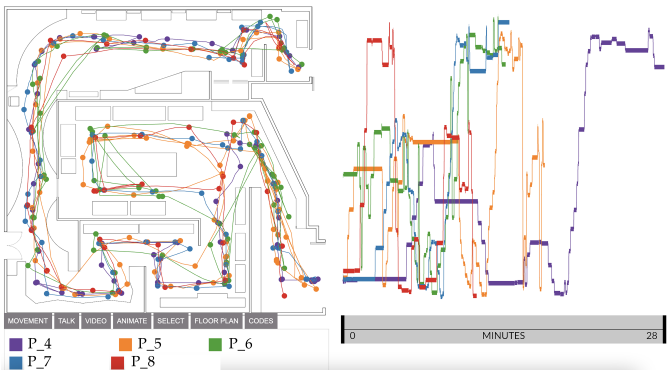


Figure 7: Overlays of Movements Across Time and Space of Non-design Participants

- The movement density was less condensed for non-design participants. Figure 7 shows that non-design participants spent equal time throughout the VR museum (i.e., as shown in the straightforward and less-overlapped paths). P_4, as a notable case, even skipped the central exhibition altogether (Figure 5). Especially, no participant ever noticed the door connecting the hallway and the central exhibition.
- The traced paths also differed from one participant to another. For instance, P_4 had the most straightforward path that started at the entrance and flowed through the hallway to the exit. P_5, on the contrary, explored the VR museum twice using the same path. P_6 repeatedly visited the upper left curved display in the hallway, the left upper corner display cases in the central exhibition, and three display cases at the end of the museum (as shown in the overlaps in the green traced path). P_7 showed a similar travel path to those of the design participants (i.e., following the intended navigation of the floor plan) yet visited each spot only once. P_8 revisited the first half of the VR museum yet skimmed through the last half. This participant also explored the central exhibition counterclockwise, thus, differing from the rest. It's worth noting that all non-design participants had never used VR technology before.
- The synchronized timeline on the right of Figure 7 also reveals time durations spent in the VR museum. P_4 and P_5, for instance, spent more time exploring at the beginning (about one-half of their time) and moved faster at the end. P_6, P_7, and P_8 divided their time into small durations evenly spanned over the exploration.

## 5. Conclusion

Participants all finished the VR museum with an average time of 17 minutes from start to finish, except P_4,

who skipped the central exhibition. Prior experience in VR technology, therefore, was not an influential factor in participant behavior. Similar to the authors in [12], this pilot study also found that "personal history" and "prior knowledge" (i.e., design vs. non-design majors) affected how participants navigated and experienced the virtual museum.

First, design-major participants explored the space more thoroughly than their non-design counterparts. They also spent extended time at the entrance and exit, where there were artifacts, signs, and display cases; revisited specific spots; and examined the central exhibition equally as the hallway. P_2 even found the door leading directly to the central exhibition, possibly due to their design knowledge (i.e., the psychological factor of occupation) which helped them navigate and engage with the space more effectively. The non-design participants paid less attention to the space, as evidenced by their behavior: for example, they did not go back to check artifacts and display cases along the paths, and P_4 skipped the central exhibition altogether. Said behaviors raise concerns about whether all occupants perceived space design intentions equally.

Second, either design or non-design participants explored the VR museum at their own pace. Some spent more time in the beginning and rushed at the end; others spent equal time periods in the whole space. This observation shows an underlying social factor relating to personal interests and connection to certain artifacts or display cases. The degree of personal interest one has with the space might affect their behaviors [12].

One limitation of this pilot study is that each participant explored the VR museum independently, which does not account for social interactions between them. Moreover, the VR museum is a 360-degree-captured environment or a compilation of multiple 2-D images of a real space. Participants could not interact with artifacts, display cases, and furniture. Future research will use an interactive VR environment so that participants can interact with the objects in their surroundings. The authors hope to gain further insights into occupant behavior via Interaction Geography and more sophisticated VR technology.

## Conflict of Interest

The authors declare no conflict of interest.

## Acknowledgment

The authors thank James Amann and the student workers at the Creative Media Industries Institute, Georgia State University for their hospitality and support. This study is supported by the 2022 Summer Research Fund for faculty from Welch School of Art and Design, College of the Arts, Georgia State University.

## References

[1] L. T. Graham, T. Parkinson, S. Schiavon, "Lessons learned from 20 years of CBE's occupant surveys", *Buildings and Cities*, vol. 2, no. 1, pp. 166–184, 2021. http://doi.org/10.5334/bc.76

[2] C. D. Roa, S. Schiavon, T. Parkinson, "Targeted occupant surveys: A novel method to effectively relate occupant feedback with environmental conditions", *Building and Environment*, pp. 107129, 2020. https://doi.org/10.1016/j.buildenv.2020.107129

[3] K. A. Young, "Direct from the source: the value of'think-aloud'data in understanding learning", *Journal of Educational Enquiry*, 2005. http://hdl.handle.net/10453/6348

[4] C. D. Darker, D. P. French, "What sense do people make of a theory of planned behaviour questionnaire? A think-aloud study", *Journal of health psychology*, vol. 14, no. 7, pp. 861–871, 2009. https://doi.org/10.1177/1359105309340983

[5] C. Macal, M. North, "Introductory tutorial: Agent-based modeling and simulation", *Proceedings of the winter simulation conference 2014*, pp. 6–20, 2014. https://doi.org/10.1109/WSC.2014.7019874.

[6] M. Jia et al., "A systematic development and validation approach to a novel agent-based modeling of occupant behaviors in commercial buildings", *Energy and Buildings*, vol. 199, pp. 352–367, 2019. https://doi.org/10.1016/j.enbuild.2019.07.009

[7] S. Norouziasl, A. Jafari, C. Wang, "An agent-based simulation of occupancy schedule in office buildings", *Building and Environment*, vol. 186, pp. 107352, 2020. https://doi.org/10.1016/j.buildenv.2020.107352

[8] K. R. Rozo et al., "Modelling building emergency evacuation plans considering the dynamic behaviour of pedestrians using agent-based simulation", *Safety science*, vol. 113, pp. 276–284, 2019. https://doi.org/10.1016/j.ssci.2018.11.028

[9] P. Li, T. M. Froese, G. Brager, "Post-occupancy evaluation: State-of-the-art analysis and state-of-the-practice review", *Building and Environment*, vol. 133, pp. 187–202, 2018. https://doi.org/10.1016/j.buildenv.2018.02.024

[10] D. Sanchez Leitner, N. Christine Sotsek, A. de Paula Lacerda Santos, "Postoccupancy evaluation in buildings: Systematic literature review", *Journal of Performance of Constructed Facilities*, vol. 34, no. 1, pp. 03119002, 2020. . https://doi.org/10.1061/(asce)cf.1943-5509.0001389

[11] B. R. Shapiro, "What About Interaction Geography to Evaluate Physical Learning Spaces?", *Teacher Transition into Innovative Learning Environments*, pp. 167–179, 2021. https://doi.org/10.1007/978-981-15-7497-9_14

[12] B. R. Shapiro, R. P. Hall, D. A. Owens, "Developing & using interaction geography in a museum", *International Journal of Computer-Supported Collaborative Learning*, vol. 12, no. 4, pp. 377–399, 2017. https://doi.org/10.1007/s11412-017-9264-8

[13] B. R. Shapiro, B. Garner, "Classroom interaction geography: visualizing space & time in classroom interaction", *Journal of Research on Technology in Education*, pp. 1–15, 2021. https://doi.org/10.1080/15391523.2021.1927265

[14] G. Fernandez-Nieto et al., "Classroom Dandelions: Visualising Participant Position, Trajectory and Body Orientation Augments Teachers' Sensemaking", *CHI Conference on Human Factors in Computing Systems*, pp. 1–17, 2022. https://doi.org/10.1145/3491102.3517736

[15] S. Carlucci et al., "Modeling occupant behavior in buildings", *Building and Environment*, vol. 174, pp. 106768, 2020. https://doi.org/10.1016/j.buildenv.2020.106768

[16] M. Arslan, C. Cruz, D. Ginhac, "Understanding occupant behaviors in dynamic environments using OBiDE framework", *Building and environment*, vol. 166, pp. 106412, 2019. https://doi.org/10.1016/j.buildenv.2019.106412

[17] N. Haidar et al., "Towards a new graph-based occupant behavior modeling in smart building", *2019 15th International Wireless Communications & Mobile Computing Conference (IWCMC)*, pp. 1809–1814, 2019. https://doi.org/10.1109/IWCMC.2019.8766569

[18] F. Stazi, F. Naspi, M. D'Orazio, "A literature review on driving factors and contextual events influencing occupants' behaviours in buildings", *Building and Environment*, vol. 118, pp. 40–66, 2017. https://doi.org/10.1016/j.buildenv.2017.03.021

[19] E. Delzendeh et al., "The impact of occupants' behaviours on building energy analysis: A research review", *Renewable and sustainable energy reviews*, vol. 80, pp. 1061–1071, 2017. https://doi.org/10.1016/j.rser.2017.05.264

[20] S. Chen et al., "The impacts of occupant behavior on building energy consumption: A review", *Sustainable Energy Technologies and Assessments*, vol. 45, pp. 101212, 2021. https://doi.org/10.1016/j.seta.2021.101212

[21] C. Shen, K. Zhao, J. Ge, "An overview of the green building performance database", *Journal of Engineering*, vol. 2020, 2020. https://doi.org/10.1155/2020/3780595

[22] Arup, "BUS methodology." https://busmethodology.org.uk/ . (accessed: 05-Oct-2021).

[23] I. A. Sakellaris et al., "Perceived indoor environment and occupants' comfort in European "modern" office buildings: The OFFICAIR study", *International journal of environmental research and public health*, vol. 13, no. 5, pp. 444, 2016. https://doi.org/10.3390/ijerph13050444

[24] A. Rode et al., "Estimating a social cost of carbon for global energy consumption", *Nature*, vol. 598, no. 7880, pp. 308–314, 2021. https://doi.org/10.1038/s41586-021-03883-8

[25] N. Stern, J. E. Stiglitz, *The social cost of carbon, risk, distribution, market failures: An alternative approach*, vol. 15, , National Bureau of Economic Research Cambridge, MA, USA, 2021. https://files.static-nzz.ch/2021/4/26/7e32b21f-81b9-4033-907c-7aaeba85e7a5.pdf

[26] A. Mathur, B. R. Shapiro, "Interactive Transcription Techniques for Interaction Analysis", *16th International Conference of the Learning Sciences (ICLS)*, pg. 19-26, 2022. https://scholarworks.gsu.edu/ltd_facpub/46

[27] A. Hepburn, G. B. Bolden, *Transcribing for social research*, Sage, 2017.

[28] J. Bezemer, D. Mavers, "Multimodal transcription as academic practice: A social semiotic perspective", *International Journal of Social Research Methodology*, vol. 14, no. 3, pp. 191–206, 2011. https://doi.org/10.1080/13645579.2011.563616

[29] G. Jefferson, "Glossary of transcript symbols with an introduction", *Pragmatics and Beyond New Series*, vol. 125, pp. 13–34, 2004.

[30] T. Hägerstrand, "Reflections on "what about people in regional science?"", *Papers of the Regional Science Association*, vol. 66, no. 1, pp. 1–6, 1989. https://doi.org/10.1007/BF01954291

[31] B. Jordan, A. Henderson, "Interaction analysis: Foundations and practice", *The journal of the learning sciences*, vol. 4, no. 1, pp. 39–103, 1995. https://doi.org/10.1207/s15327809jls0401_2

[32] Matterport Inc., "Matterport." https://matterport.com/ . (accessed: 03-Sep-2022).



**Dr. Hoa Vo** is an Assistant professor in Interior Design at the Welch School of Art and Design, College of the Arts, Georgia State University. She earned her Ph.D. degree in Interior Design from the University of Minnesota in 2021.

Her research covers adaptive technologies (AR, VR, digital modeling and fabrication) in teaching, intersectional collaborations in design, creativity and feedback practices in design, and physical experiences in the built environment. She has published in Journal of Creativity (JOC), Sustainability of MDPI, International Journal of Designs for Learning (IJDL), Archnet-IJAR: International Journal of Architectural Research, Academic Exchange Quarterly (AEQ), and multiple peer-reviewed conference proceedings.

**Peter Huesemann-Odom** is a M.F.A. candidate in Interior Design (expecting 2024) at the Welch School of Art and Design, College of the Arts, Georgia State University. With over fifteen years working in creative departments and a Bachelor of Arts degree in business administration, he consults, supports, as well as inspires design aesthetics worldwide.

He lived in Brazil, Germany, Sweden, and now the States to research how much space we need to live a happy life, what we define as "home," and how consumers will shop in the future.

Received: 28 October, 2022, Revised: 11 December 2022, Accepted: 18 December, 2022, Online: 28 January, 2023

DOI: https://dx.doi.org/10.55708/js0201001

# Modelling, Simulation and Sensitivity Analysis of Generator Control Systems using Coexisting and Cooperative Tools

**Javier Urquizo[1,*], Diover Bonilla[1], Francisco Rivera[1], Rommel Chang[2]**

[1]Escuela Superior Politécnica del Litoral, ESPOL, FIEC, Campus Gustavo Galindo Km. 30.5 Via Perimetral, Guayaquil, Ecuador
[2]CELEC EP Unidad de Negocio Hidronación, Central Baba, Kilómetro 39 vía Quevedo -- Santo Domingo, Ecuador
*Corresponding author: Javier Urquizo, ESPOL/FIEC, Km. 30.5 Via Perimetral, +593982226142 jurquizo@espol.edu.ec

**ABSTRACT:** This research is about tuning the automatic generator control (AGC) unit within the National Transmission System (NTG) and is intended to provide a set of key insights into problems related to generator control systems oscillations and the possible available solutions. The case study is the Baba Hydroelectric Power Plant in Ecuador. The aim is to model, simulate and validate the controls of the Baba generating units for an optimal and stable response. Both controllers, the Automatic Voltage Regulator (AVR) and Power System Stabilizer (PSS) were tuned using both a component-based approach using an object-orientated tool where the model structure resembles the original system, and a coexisting power flow tool in a signal orientated environment. A key part of this tuning is the adaptation of the model to different operating conditions by testing scenarios where signals ought to be defined before the start of the simulation and others be chosen for visualisation without any limitation, therefore, this paper is about finding a multi-framework environment. Also, the model was disturbed so to observe the field Voltage and terminal voltage values using a simplified and reduced part of the NTG. Results show that a high gain AVR helps the steady state and transient stabilities but may reduce the oscillatory stability and the PSS can provide significant stabilization of such oscillations. The validation strategy uses the average quadratic mean square error statistical method.

**KEYWORDS:** Electric Power Systems, Automatic Voltage Regulator, Coexisting and Collaborative tools, Power System Stabilizer, Stability Assessment, Sensitivity Analysis

## 1. Introduction

Hydroelectric power plants are the foundation of Ecuador's power generation capacity. Hydropower plants account for 57.67% [1] of the country's installed capacity by 2017. Our case study is the Baba Multi-Purpose Project (BMP), consisting of four dikes and three channels in Los Ríos province, used for irrigation, flood control, water supply and hydroelectric power generation. The BMP includes water supply to the reservoir and the Daule-Peripa reservoir, construction of the hydroelectric power plant and associated transmission lines. Therefore, the main purpose of the BMPs is water storage and transmission, not hydropower. Upland rice is dominant in Los Rios and no-tillage is the dominant crop cultivation method. About 60 percent of the farmers farm less than five hectares per person and three percent are large farmers cultivating 100 hectares per person [2]. With 3,000 hectares of land at risk of flooding, protesters against the Baba dam had a major impact on the construction of the dam and saved the community from flooding [3]. Capable of generating 42 MW, covering 40-50% of the demand in Los Ríos. The Baba hydropower station has two of his Kaplan direct shaft turbines submerged by a spiral cover or scroll area.

This paper concerns the feasible enhancement controls which may allow the countrywide electricity grid to perform reliably over broader tiers of loading and system operational point. Hydro-turbines controllers are tuned for assumed situations withinside the relaxation of the electricity grid; however, as grid situations vary, the controllers eventually 'malfunction' in one-of-a-kind ways (ranging being too sluggish and/or of inadequate ability or loss of coordination) [4]; consequently, it is hard to ensure system-wide performance; therefore, the general tendency is not to rely on control outside normal regions and find

out where are the opportunities to operate efficiently. A method is wanted for dealing with the machine throughout a huge variety of running condition, for this is important to display electricity-flows and adjust those consistent with the higher described generator interconnection standards making sure viable electricity exchanges without compromising machine reliability; however, at the same time, the design has to be completed in order that every generator maintains its decentralized, self-sufficient operation, whilst coordinating with turbines of the nearby electricity grid.

Literature review shows different ways authors can implement controls. For example, Std 421.5™-2005 [5] describes a model structure intended to facilitate the use of field test data as a means of obtaining model parameters. In North America model validation is mandated according to the Reliability Council (NERC) Modelling, Data, and Analysis (MOD) series of standards. NERC MOD-033-1 [6] specifies consistent validation requirements to facilitate the collection of accurate data and the development of planning models for reliability analysis of interconnected transmission systems. In Europe, [7] designed a robust controller to address both local area and inter-area oscillations. The controller is a second-order state-space regulator. In Ecuador, [8] is developing tools for displaying oscillation modes and their damping, and for provisional localization of a PSS in the Ecuadorian NTG. An online model estimation scheme was also used to validate and/or tune a small-signal model of the power system using synchro phasor data [9] at the Paute-Molino power plant in Ecuador [10]. In Modelica [11] there was an effort on design principles and a prototype for modelling the pan-European electricity grid to be used by European transmission system operators.

The controls are an Automatic Voltage Regulator (AVR) and a Power System Stabilizer (PSS). The AVR regulates the terminal voltage of the generator. A fast-response high-gain AVR improves large-signal transient stability in the sense that it improves the network's ability to maintain synchronism when subjected to severe transient disturbances. There is a trade-off between synchronous torque provided by the AVR and the damping torque provided by the PSS [12,13]. PSS tuning is for a wide oscillation damping applications. PSS requires a reliable model of the system in a software package such as DigSILENT PowerFactory (PF). The early stages of this research involved extensive data management, cleansing, and restructuring to the NTG initial dataset in the PF package. The development of these controllers uses an object-oriented and non-causal modelling approach in which individual parts of the model are directly described as equations using a declarative approach [14] but also coexisting in good cooperation with signal-orientated tools.

## 2. Methodology

### *2.1. Generation unit modelling*

The Baba power generation unit will generate 161 GWh/year by pumping water to the Santa Elena Peninsula at up to 234 $m^3$/sec. During the rainy season (January to October), the reservoir only provides a downstream flow of 10 - 15 $m^3$/sec. The generating units are two horizontal axis Kaplan turbines, each of 21 MW, with a maximum operating flow of 86 $m^3$/ sec. The difference from the maximum flow rate, approximate 62 $m^3$/sec, is discharged via a by-pass installed next to the pressure line [15]. Clarke and Park transforms are commonly used in field-oriented control of three-phase AC machines. The Clarke transform converts the time domain components of a three-phase system (in abc frame) to two components in an orthogonal stationary frame (αβ). The Power System Analysis Toolbox (PSAT) hydroelectric salient pole machine is modelled as Order V Type 2 model [16], which more closely resembles the Baba generator characteristics. Both follows Van-Cutsem and Papangelis [17] proposed data (see Figure 1). Baba generator parameters and initial NTG values are shown in Table 1. The internal parameters of the generator are the same for Isolated and in NTG operation modes, but their initialization values differ depending on the controller's mode of operation. Table 1 also shows the initial values for the Isolated - NTG generator. To view the controller's response, a voltage disturbance in the form of a pulse generator was applied to the $V_{ref}$ input. The 'Pulse Generator' parameters are shown in Table 2.

The generation model corresponds to a three-phase synchronous generator and a classic electromechanical model with transfer functions to model the direct and quadrature inductances. Assuming an additional circuit for the direct axis, the state variables can be described as in the following equations [18]. A curious reader would have to read the GitHub repository for all the models and parameters used from the OpenIPSL library.

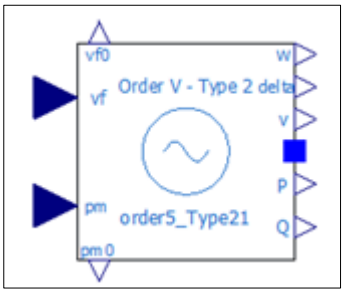


Figure 1: Machine - Generator Order V Type 2

The Model Parameters are Synchronous reactance - d axis (pu) Xd, Synchronous reactance - q axis (pu) $X_q$, Sub-transient reactance - d axis (pu) $X_{2d}$, Open circuit transient time constant - d axis (pu) $T_{1d0}$, Open circuit sub-transient time constant - d axis (pu) $T_{2d0}$, Open circuit sub-transient time constant - q axis (pu) $T_{2q0}$, Nominal Power (MVA) $S_n$,

Nominal Voltage (kV) $V_n$, Armature Resistance (pu) $R_a$, Transient Reactance - d axis (pu) $X_{1d}$, Mechanical inertia coefficient M and Damping D.

Table 1: Parameters of the Baba Generator

| Parameter | Value | Parameter | Value |
|---|---|---|---|
| $X_d$ | 0.97 | $e_{1q}$.start | 0.950539 \| 1.49748 |
| $X_q$ | 0.78 | $e_{2q}$.start | 1.00027 \| 1.47345 |
| $X_{2d}$ | 0.29 | $e_{2d}$.start | 0 \| 0.285123 |
| $X_{2q}$ | 0.38 | w.start | 0 \| 0 |
| $T_{1d0}$ | 3.56 | v.start | 1.00027 \| 0.945013 |
| T2d0 | 0.028 | P.start | 0 \| 1.88565 |
| T2q0 | 0.006 | Q.start | 0 \| 1.47173 |
| $T_{aa}$ | 0.177 | $V_f$. start | 1.00027 \| 3.125 |
| Sn MVA | 23.4 | $P_{m0}$.start | 0.900957 \| 0.900957 |
| $V_n$ kV | 13.8 | $p_m$.start | 0.900957 \| 0.900957 |
| $R_a$ | 0.0022 | $v_d$.start | 0 \| 0.551147 |
| $X_{1d}$ | 0.36 | $v_q$.start | 1.00027 \| 0.76767 |
| M | 10 | $i_d$ start | 0 \| 2.42869 |
| D | 0 | $i_q$.start | 0 \| 0.712775 |

Table 2: Parameters of the pulse generator

| Pulse | Value |
|---|---|
| Extent | -0.03 |
| Pulse width (%) | 50 |
| Period (s) | 1 |
| Initialization | 5.65 |

AVR modelling is in Section 2-2 and PSS is in Section 2-3. The closed-loop response has two outputs, **P** (power) and **w** (velocity), which are connected to the corresponding inputs of the PSS. A frequency **f** block was added that allows to change the speed to frequency and therefore being able to meet the number of equations and unknowns for the Generator validation. Enhancements have also been made to the PSS output to address what-if scenarios. The internal block diagram is shown in Figure 2 and the external block diagram is shown in Figure 3.

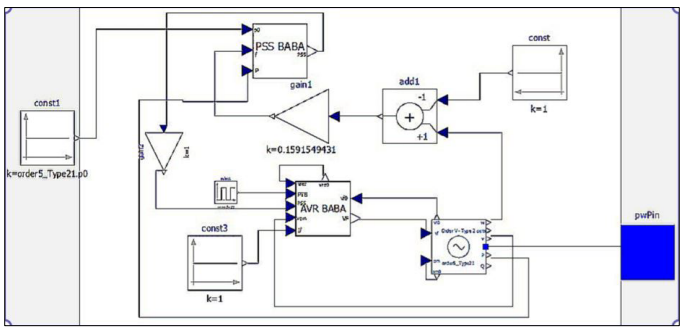


Figure 2: Baba generator internal block

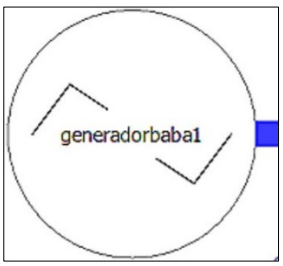


Figure 3: Baba generator external block

## 2.2. AVR Modelling

The IEEE 421.5 standard [5] is the IEEE recommended practice for excitation system models for power system stability studies. The models apply for frequency deviations of ±5\% from nominal frequency and oscillation frequencies up to 3 Hz. The Baba excitation system follows the IEEE 421.5 ST6B model. The AVR is shown in Figure 4 and consists of a field voltage regulator and a PI voltage regulator with a feedforward control in the inner loop. The field voltage controller implements proportional control.

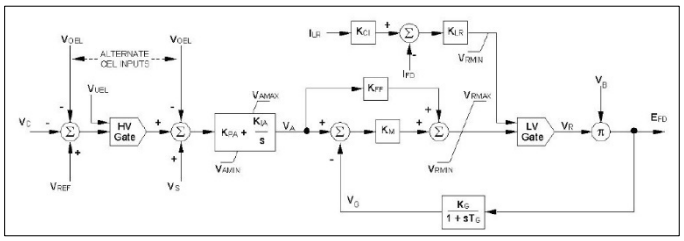


Figure 4: ST6B static potential - source excitation system with field current limiter [5]

The AVR appeared in Figure 4 comprises of a PI voltage regulator with an internal loop field voltage regulator and pre-control. The field voltage regulator executes a proportional control. The pre-control and the delay in the feedback circuit increase the dynamic response. VR represents the limits of the power rectifier. The ceiling current IFD limitation is included in this model. The power for the rectifier, VB, may be supplied from the generator terminals or from an independent source. Inputs are provided for external models of the over-excitation limiter (VOEL), under-excitation limiter (VUEL), and PSS (VS).

Baba has a static excitation system in which the generator stator voltage is rectified by a thyristor bridge. This DC excitation voltage is fed through the slip ring to the rotor windings to excite the rotor. As the energized rotor rotates within the stator, an AC voltage is generated at the stator terminals, i.e., stator voltage variations directly affect the excitation voltage. Figure 5 shows the main exciter structure underlying the exciter modelled in the simulation tool.

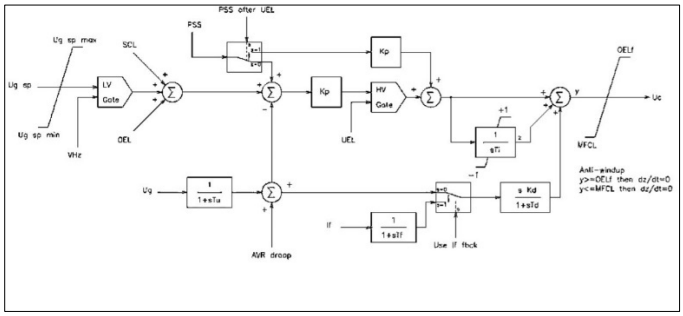


Figure 5: Excitation System, main structure [19]

The variables and parameters in Figure 5 are the maximum allowed AVR reference $U_{g\ sp\ max}$ (VHZ), the minimum allowed AVR reference $U_{g\ sp\ min}$, the transducer time constant $T_u$, field current time constant $T_f$, proportional gain $K_p$, integral time $T_i$, derivative gain $K_d$, derivative time constant $T_d$, Field current $I_f$, Use If the feedback in the loop control Use $I_{f\ fdbck}$, PSS after UEL, Field undercurrent limiter output MCLF, overdrive limiter output OEL, overdrive fast limiter output $OEL_f$, AVR compensation loop output AVR droop, Stator current limiter output SCL, Under-drive Limiter Output UEL, PSS output signal PSS, Volts hertz limiter output VHz. Typical parameter values are $U_{g\ sp\ max}$ 1.1, $U_{g\ sp\ min}$ 0.9, $T_u$ 20 ms, $T_f$ 20 ms, $K_p$ 10, $T_i$ 2 s, $K_d$ 0, $T_d$ 5 s, Use $I_{f\ fdbck}$ 0 (Only for brushless excitation systems), PSS after UEL 1.

Our research focuses on damping of small signal swings, so we have simplified Figure 5. It is important to model the limiter in conjunction with the voltage regulator. Under excitation limiting is especially used in turbo generators. This is because without a limiter the reactive power output from the generator could be too high, leading to erroneous simulation results. Small turbo generators connected to powerful networks are sensitive to this kind of phenomenon [20]. The purpose of the over-excited limit is to protect the generator from overheating due to prolonged field over-current.

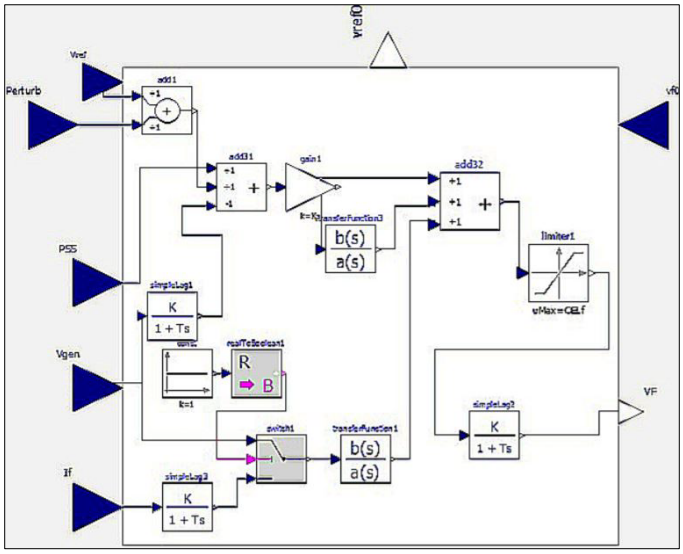


Figure 6: AVR implemented in a non-causal approach.

Figure 6 is a simplified non-causal AVR approach to modelling the Baba excitation system. Traditional approaches are based on block-oriented schemes in which causality plays a key role. However, new concepts based on object-oriented approaches, physics-oriented connections, and algebraic manipulation enable non-causal modelling, where blocks represent the interactions of equations.

Each of the transfer functions (TF) in Figure 6 has initialization parameter calibrated to stable values according to its response, either isolated or NTG modes. See Table 3.

Table 3: TF Initialization Isolated - NTG modes

| Transfer Functions | Initial Isolated | Initial NTG |
|---|---|---|
| Simple Lag1 | 1.00027 | 0.94503 |
| Simple Lag2 | 1 | 1 |
| Simple Lag3 | 1.00027 | 3.12500 |
| TransferFuntion1 | 0 | 0 |
| TransferFuntion3 | 0.160044 | 0.499815 |

The AVR's operating parameters are adjusted according to a manufacturer's specified ranges and are shown in Table 4.

Table 4: Isolated and NTG AVR Parameters

| Parameters | Isolated Values | NTG Values |
|---|---|---|
| $K_p$ | 10 | 10 |
| $T_i$ | 1 | 2 |
| $K_d$ | -10 | 0 |
| $T_d$ | 10 | 5 |
| $T_f$ | 0.02 | 0.02 |
| Tu | 0.02 | 0.02 |
| $K_{br}$ | 6.25 | 6.25 |
| $T_{br}$ | 0.0014 | 0.0014 |
| $OEL_f$ | 0.5 | 0.7 |
| MFCL | -0.5 | -0.5 |
| $V_0$ | 0.75 | 0.7384 |
| $V_{00}$ | FIXED=False | FIXED=False |

### *2.3. PSS Modelling*

The IEEE 2005 421.5 standard [5] introduced a PSS structure called IEEE PSS4B. The PSS4B model represents a structure based on multiple operating frequency bands, as shown in Figure 7. Three separate bands, each dedicated to the low-, medium- and high-frequency oscillations modes, are used in the delta-omega (velocity input). Baba uses the IEEE Std 421.5™-2016 Dual-Input Power System Stabilizer ($PSS_2C$) [21] to improve electrical

system stability, as shown in Figure 8. A key element is the Limiter. The Limiter is used to keep the PSS output voltage within a range of values and the PSS output protection should also match the output limiter. Additional damping can be achieved to improve transient stability by setting the PSS output limit. As a result, the PSS performance improves under larger system disturbances [22].

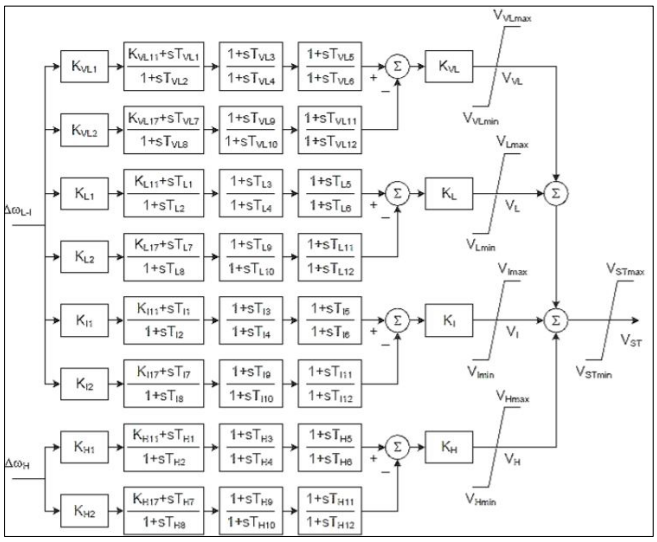

Figure 7: The multi-band stabilizer, IEEE PSS4B [5]

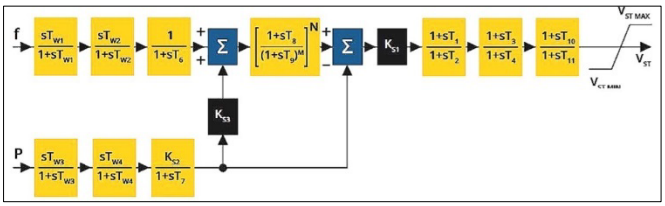

Figure 8: Power system stabilizer – PSS [21]

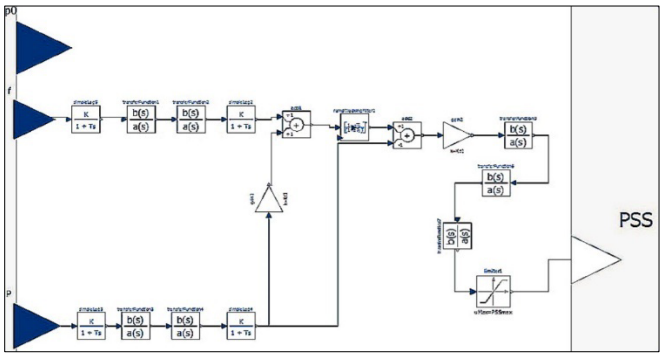


Figure 9: PSS implemented in non-causal approach.

The PSS controller has a large number of 'simple lag' and 'TransferFunction', constants, limiters, input and output signals. It also has a 'RampTrackingFilter' for attenuating the signal. Non-casual modelling is shown in Figure 9.

Each of the transfer functions (TF) of Figure 9 have initialization parameters calibrated to stable values according to their response either isolated or NTG modes. See Table 5.

Table 5: TF Initialization Isolated -- NTG modes

| TF | Isolated | NTG | TF | Isolated | NTG |
|---|---|---|---|---|---|
| Simple Lag 5 | 0 | 0 | Transfer Function3 | 0 | 0 |
| Simple Lag2 | 0 | 0 | Transfer Function4 | 0 | 0 |
| Simple Lag3 | 0 | 1.87338 | Transfer Function5 | 0 | 0 |
| Simple Lag 4 | 0 | 0 | Transfer Function6 | 0 | 0 |
| Transfer Function1 | 0.0430175 | -0,0476977 | Transfer Function7 | 0 | 0 |
| Transfer Function2 | 0 | 0 | | | |

The operating parameters of the PSS were adjusted according to the ranges specified by the manufacturer. Parameters are shown in Table 6. $PSS_{min}$ is equal to zero.

Table 6: Isolated and NTG PSS Parameters

| Parameter | Isolated | NTG | Parameter | Isolated | NTG |
|---|---|---|---|---|---|
| $T_f$ | 0.02 | 0.02 | $T_9$ | 0.01 | 0.1 |
| $T_p$ | 0.02 | 0.02 | M | 4 | 4 |
| $T_{w1}$ | 3 | 3 | N | 2 | 1 |
| $T_{w2}$ | 3 | 3 | $K_{s1}$ | 0.01 | 0.1 |
| $T_{w3}$ | 3 | 3 | $T_1$ | 0.12 | 0.12 |
| $T_{w4}$ | 3 | 3 | $T_2$ | 0.03 | 0.03 |
| $T_6$ | 4.6 | 0 | $T_3$ | 0.09 | 0.03 |
| $T_7$ | 3 | 3 | $T_4$ | 0.03 | 0.03 |
| $K_{s2}$ | 0.3 | 0.3 | $T_{10}$ | 4.7 | 2.06 |
| $K_{s3}$ | 1 | 1 | $T_{11}$ | 0.37 | 1.3 |
| $T_8$ | 0.2 | 0.4 | $PSS_{max}$ | 0.05 | 0.05 |

In addition, the PSS controller is not a separate controller that is used with the generator, but it is a controller that input signals to the AVR by entering a signal into the AVR to improve the response after a failure.

### *2.4 National Transmission Grid*

The early stages of this research involved extensive data management, cleansing, restructuring and additions to this initial dataset. In addition, real time test values of power flows were available via a robust PF power system tool. Figure 10 shows a reduced portion of the NTG with synchronous machines, transformers, transmission lines and system buses.

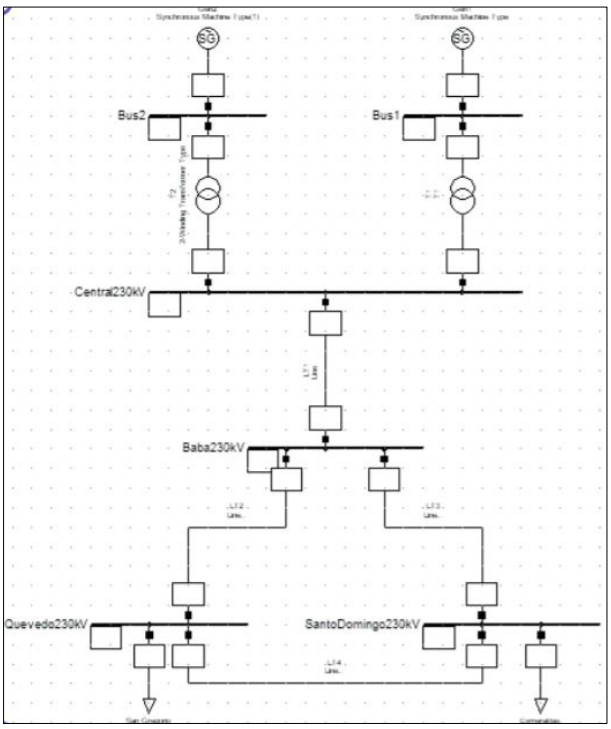


Figure 10: Reduced portion of the NTG for Baba stability studies

### 2.5 Transformers

Two elevating transformers (13.8:230 kV) were used for the implementation of the reduced grid. The transformer is connected to the synchronous generator. The primary winding of each transformer is connected to the generator's armature winding at 13.8 kV. A circuit breaker is installed close to transformer on the upper (230 kV) voltage side. In this arrangement any generator perturbations and grid disturbances have an effect on the transformers. Transformers implemented in our system does have serial reactance and do not have iron losses. The transformer connection is grounded wye - delta. The grounded connection will provide a path for a line-to-ground fault current (back feed current) for a fault upstream from the transformer. The parameters are shown in Table 7.

Table 7: Transformers parameters

| Parameters | Values (pu) |
|---|---|
| $K_T$ | 13.8/230 |
| x | 0.5036 |
| r | 0.5 |

Simulation tools like PF facilitates the user with varied types of power system studies. It also obtains more detailed and accurate power-flow simulation solutions. However, the libraries integrated in the tools are normally closed for modifications. The values of power-flow that are entered in the non-causal model of transformers, generator, transmission lines and buses are acquired from PF.

### 2.6 Transmission Lines

A NTG transmission line is modelled with an equivalent ∏ circuit in the non-casual tool. The resistance (R) data is entered, whereas reactance (X), conductance (G) and susceptance (B) are obtained from DIgSILENT's NTG block. All values are in p.u, but the units in PF are Ω/km and need to be converted using the Zbase into per unit. Zbase is calculated from Equation 1.

$$Zbase = \frac{V^2}{P} = \frac{13{,}800^2}{46{,}760{,}000} = 4.072712\ [\Omega] \quad (1)$$

Zbase allows to compute all the lines from a reduced Baba grid. The line parameters are shown in Figure 11.

| | Plant line to Baba Substation 230 Kv | Baba Substation Line to Quevedo 230 Kv | Baba Substation Line to S.Domingo 230 Kv | Line S. Domingo to Quevedo 230 Kv | Line S.Domingo to Esmeraldas 230 Kv | Line Quevedo to San Gregorio 230 Kv |
|---|---|---|---|---|---|---|
| R (Ω/Km) | 0.101485 | 0.059085 | 0.059085 | 0.059085 | 0.05192 | 0.059085 |
| X (Ω/Km) | 0.49082 | 0.472668 | 0.472668 | 0.472668 | 0.4866 | 0.472668 |
| Long (Km) | 1.4 | 45 | 62 | 104 | 155 | 110 |
| R (Ω) | 0.142079 | 2.658825 | 3.66327 | 6.14484 | 8.0476 | 6.49935 |
| X (Ω) | 0.687148 | 21.27006 | 29.305416 | 49.157472 | 75.423 | 51.99348 |
| Zbase (Ω) | 4.072712 | | | | | |
| R (pu) | 0.0348856 | 0.6528390 | 0.899467 | 1.508783 | 1.975981 | 1.595829 |
| X (pu) | 0.1687200 | 5.2225793 | 7.195554 | 12.186018 | 18.519111 | 12.766305 |
| G (pu) | 28.665122 | 1.5317712 | 1.111769 | 0.662786 | 0.506078 | 0.626633 |
| B (pu) | 5.9269796 | 0.1914763 | 0.138975 | 0.082061 | 0.053998 | 0.078331 |

Figure11: Transmission Line Parameters

### 2.7 Infinite Buses

An infinite bus is the main bus of a power system with constant frequency and voltage (both in magnitude and angle). This research analyses the problem of a machine connected to an infinite bus via a transmission line. In general, fast excitation systems are usually beneficial to transient stability following large impacts by driving the field to fast response without delay. However, these abrupt changes in excitation are not necessarily beneficial in damping the oscillations that follow the first swing, and they sometimes contribute growing oscillations several seconds after the occurrence of a large disturbance [23]. We properly design the exciter as a mean of enhancing stability in the dynamic range as well as in the first few cycles after a disturbance. We consider two infinite bus implementations: the Esmeraldas and San Gregorio 230 kV buses. Input power-flow data for the non-casual system in those buses were from PF and is shown in Figure 12 for Esmeraldas as an example.

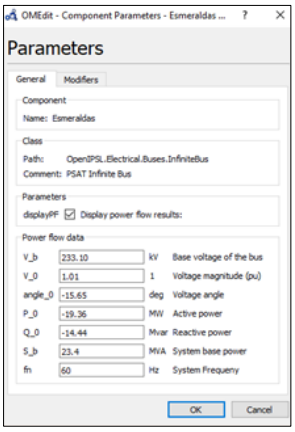


Figure 12: Esmeraldas's infinite bus parameters

*2.8 Equivalent system in OpenModelica*

To illustrate the effect of the excitation system on transient stability, we perform transient stability study on the equivalent system shown in Figure 13.

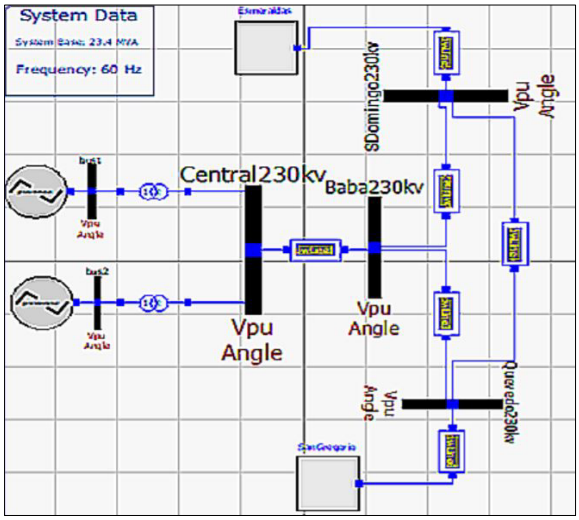


*Figure 13: NTG Equivalent System*

Figure 13 is the result after adding all the elements described in Sections 2.1 to 2.6. The generation parameters have been checked and AVR and PSS controller initialization values have also been adjusted as they are different from those in isolate mode.

Section 3-1 and Section 3-2 present the results and validation respectively of the system response. Validation tests are intended to later test the sensitivity estimates (see Section 3-4) derived from non-causal and causal approaches. This particular type of sensitivity analysis is being used in medicine [24]. Sensitivity helps identify potential risks in the power system.

## 3. Results

Related tests were performed on the Baba generation, including the AVR and PSS schemes shown in Figure 14. A gain follows the PSS output ('gain2' block in Figure 14) and also tracks frequency changes at the PSS input ('add1' block in Figure 14), both to understand the effect on the system response.

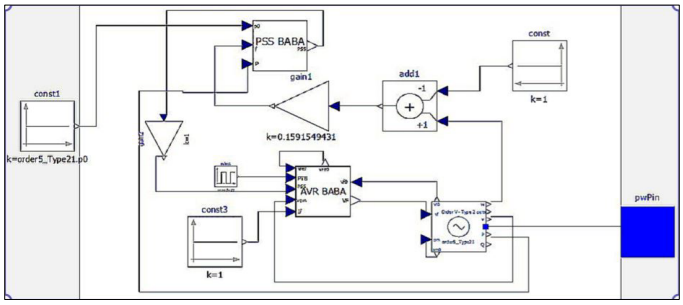


Figure 14: Baba Generator test schema

*3.1 Isolated test results*

An isolated test of the controller was performed using a 10 second pulse train with amplitude -0.03 starting at 5.65 seconds, so the system returns to normal in 15.65 seconds. The field voltage response under these conditions is shown in Figure 15. In this figure, 'gain2' is set to zero to show only-AVR isolated field and terminal voltages responses.

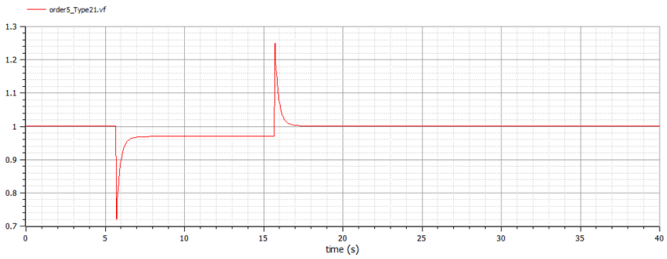


Figure 15: Baba isolated AVR field voltage response - non-causal mode

Figure 15 shows a stable response with a final value of 0.97 pu. Figure 16 shows the non-causal (red curve) and causal (blue curve) electric field voltage responses. Figure 16 shows that both curves are similar. A more detailed analysis of the differences using the mean squared error method follows in Section 3.4.

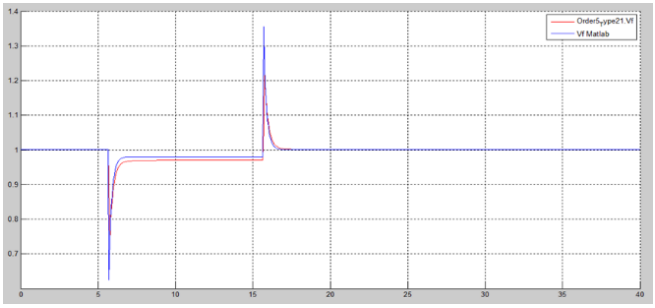


Figure 16: Isolated AVR field voltage response non-causal - causal comparative

Figure 17 shows the terminal voltage (non-causal mode) with the same disturbance as it has a stable response with the electric field voltage. Figure 18 shows a comparison of the terminal voltage responses in the non-causal mode (red curve) and the causal model (blue curve).

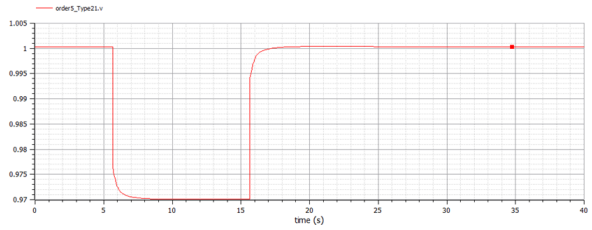


Figure 17: Isolated AVR terminal voltage response - non-causal mode

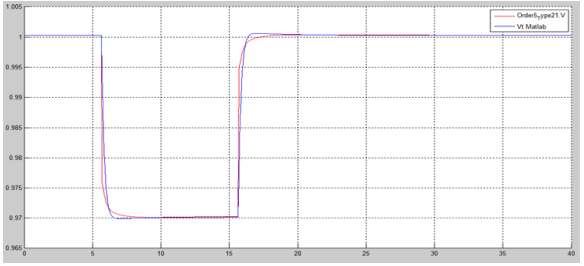


Figure 18: Isolated terminal voltage response non-causal - causal comparative

By changing 'gain2' from zero to one, Figure 19 shows the isolated AVR + PSS field voltage response. Figure 19 shows stable response. Figure 20 shows a comparison of the electric field voltage responses of the non-causal (red curve) and causal models (blue curve) of AVR + PSS. These differences are not relevant.

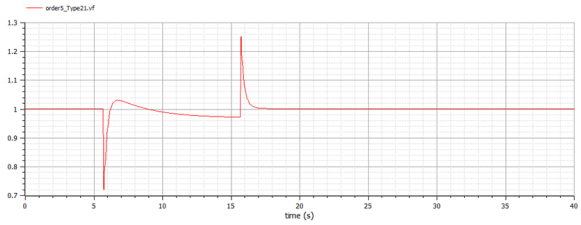

Figure 19: Isolated AVR + PSS field voltage response -- non-causal model

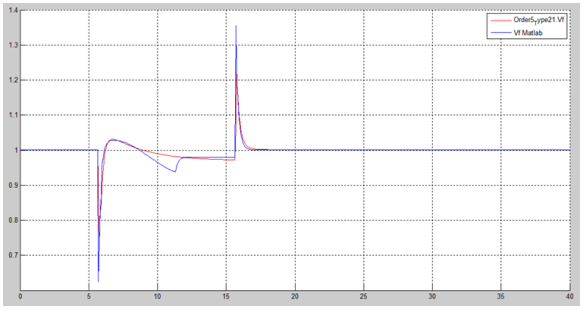

Figure 20: Isolated AVR + PSS field voltage response acasual - causal comparative

The AVR + PSS voltage response is shown in Figure 21 and the comparison is shown in Figure 22. Similar to the field voltage response, there is a stable response and small voltage difference between non-causal and causal modes.

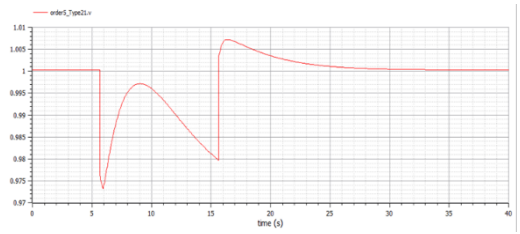

Figure 21: Isolated AVR + PSS terminal voltage response -- non-causal mode

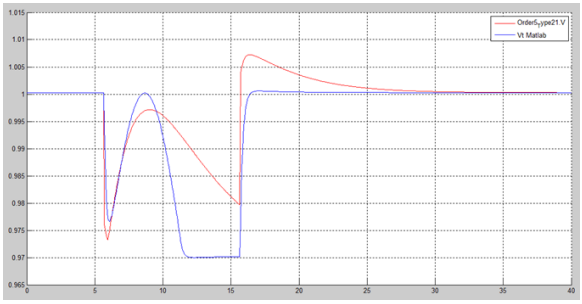

Figure 22: Isolated AVR + PSS terminal voltage response non-causal - causal comparative

In summary, this Section demonstrates the effectiveness of AVR-only and AVR + PSS controllers. This result demonstrates the effectiveness of a fast-response, high gain AVR controller in reducing the power system oscillation stability, thereby improving its transient stability. On the other hand, the AVR + PSS controller reduces transient stability by overriding the voltage signal to the exciter to improve oscillation stability. Basically, the AVR and PSS controller actions are dynamically linked as expected.

In conclusion, both non-causal and causal modes are equally suitable. This reflects the fact that either approach can be used to create schematics of large power grids, once the hard work of creating a model suitable for simulation is completed. Random changes in model parameters are straightforward in the physical (non-causal) declarative equation-based mode.

*3.2 NTG results*

This Section shows the NTG field voltages and terminal voltages using the infinitive bus described in Section 2.7. An equivalent schema is shown in Figure 13. The same disturbances are used as for the isolated test, i.e., start at 5.65 seconds with and amplitude equal to -0.03 using a pulse train of one period. Figure 23 shows the NTG field voltage in the non-causal model using the AVR controller and Figure 24 shows the AVR field voltage comparing the non-causal and causal responses. Figures 23 and 24 show a stable response.

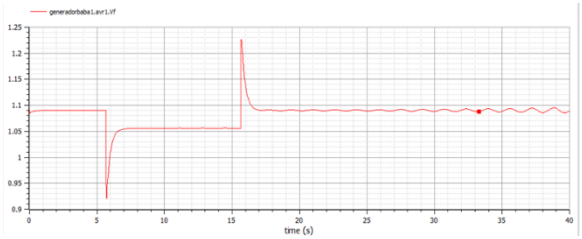

Figure 23: NTG AVR Field voltage response -- non-causal mode

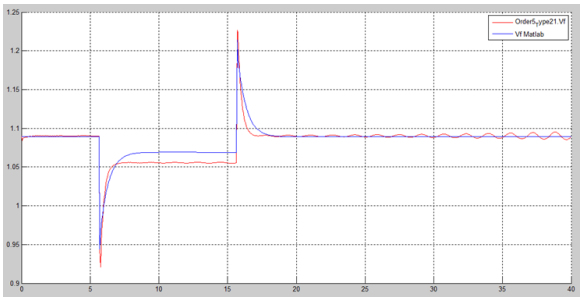

Figure 24: NTG AVR Field voltage comparative non-causal - causal responses

Figure 25 shows the terminal voltage response of the NTG AVR in non-causal mode and Figure 26 shows the NTG AVR response comparing non-causal and causal modes. Figures 25 and 26 show a stable response.

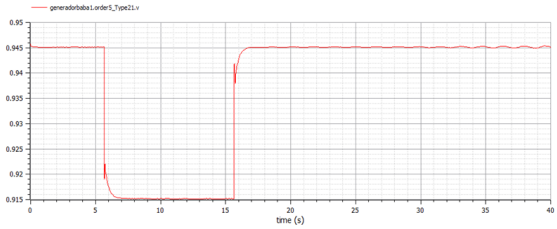

Figure 25: NTG AVR terminal voltage response - non-causal mode

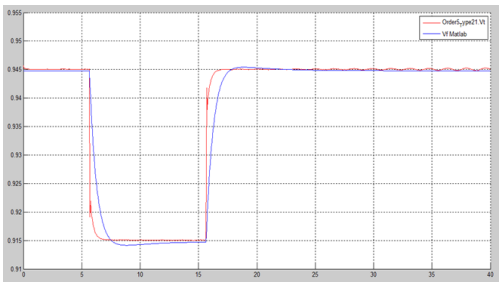

Figure 26: NTG AVR terminal voltage comparative non-causal - causal mode

Figure 27 shows the NTG AVR + PSS field voltage response. Figure 28 shows the comparative non-causal - causal of the NTG field voltage. Figures 27 and 28 show a stable response.

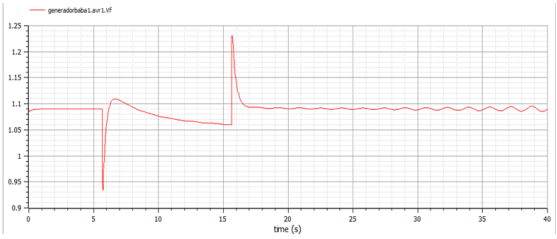

Figure 27: NTG AVR + PSS field voltage response - non-causal mode

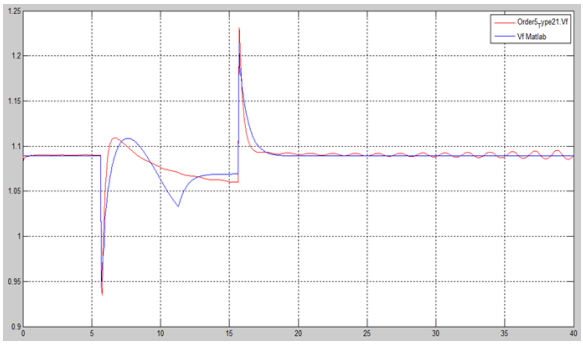

Figure 28: NTG AVR + PSS field voltage comparative non-causal - causal mode

Finally, Figure 29 shows the terminal voltages of NTG AVR + PSS in a non-causal mode, and Figure 30 shows a comparison of terminal voltages in non-causal and causal modes. From Figures 29 and Figure 30 show a stable response.

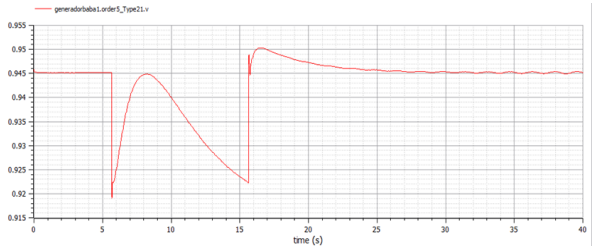

Figure 29: NTG AVR + PSS terminal voltage response -- non-causal mode

The execution time is proportional to its complexity i.e., NTS case study simulation time is longer as expected for the same computer power (see Table 8).

Table 8: Simulation time

| | |
|---|---|
| Isolated case study: 50.13 s | NTG case study: 1 min 12.63 s |

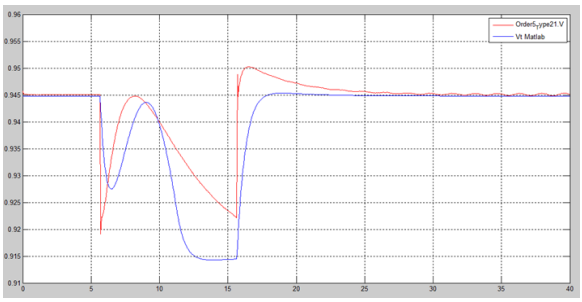

Figure 30: NTE AVR + PSS terminal voltage comparative non-causal and causal modes

In summary, in the Ecuadorian NTG has many disturbances that affect the power grid and can affect the generator reliability. Some disturbances are from large loads. When a large load is suddenly connected to the power grid, the power demand increases as shown in the diagrams of this Section. When a load is suddenly added, the Baba generator frequency begins to oscillate. In the case of small load, oscillation can be damped quickly. Figures of this Section also show that the PSS helps damp these oscillations by modulating the generator excitation.

For a full NTS grid, the grid becomes a complex non-linear system, and is often subject to low frequency oscillations, so these sections were tested with a reduced and simplified scheme [25]. A protective relay system disconnects the generator from the rest of the system and can cause an interruption in the power system.

*3.3 Reconciling Non-causal and causal mode*

Causal models are based on input-output relationships, while non-causal models describe the power system through implicit differential algebra equations (DAE). A fundamental limitation of the causal approach is the underlying explicit state-space formalism. Causal modelling tools reflects the computational process rather than the structure of the underlying model.

Non-causal model decide how computational causality is automatically assigned by equations rather than causation. While this approach is flexible for the model designer, it does not guarantee a smooth transition from design to simulation results. This is because when assembling multiple models in equations, there are multiple ways to decompose constraints into elementary equations. One of the most common decomposition methods is tearing which determines the computational time required to solve a given system of equations using sparsity patterns [26]. A typical implementation is triangular decomposition of the bottom block where only tearing is applied, which can lead to suboptimal results. A special case of the Dulmage-Mendelsohn decomposition [27] is the Block Lower Triangular (BLT) decomposition. In practice, a common approach to tearing is to perform a BLT decomposition first and then applies tearing to the diagonal irreducible blocks. There are also tearing

heuristics that require BLT decomposition, such as Cellier's tearing [28].

One way to reconcile both models is the root mean squared (RMS) error. The RMS (also known as the quadratic mean) is a special case of the generalized mean with exponent equal to two. RMS is defined as the integral of the squares of the instantaneous difference values during a simulation cycle of two continuously varying functions [29]. Table 9 shows the RMS error for the isolated (left) and NTG (right) case studies. Both cases, only-AVR and AVR + PSS controllers with field and terminal voltage output variables.

Table 9: RMS Isolated and NTG case studies

| | Only AVR | AVR + PSS | Only AVR | AVR + PSS |
|---|---|---|---|---|
| Vf | 4.97E-04 | 5.43E-04 | 2.09E-04 | 2.54E-04 |
| Vt | 6.19E-06 | 4.44E-05 | 1.24E-05 | 3.79E-05 |

Table 9 show that the RMS error of the values obtained using the non-causal mode as compared to causal mode over the entire simulation time is almost negligible, so it would be safe to conclude that the outputs are similar.

*3.4 Sensitivity Analysis*

Sensitivity Analysis (SA) technique consists of varying the input and examining the resulting variation across the output. Saltelli and Annoni [30] argue that local sensitivity analysis examines changes in a models' output variables based on small changes in the model's input parameters. The most common SA practice is One-Factor-at-a-Time (OAT). This consists of analysing the effect of varying one model input factor at a time while keeping everything else constant. In simple terms, sensitivity analysis considers the effect of independent varying parameters. SA is particularly important in this research because the accuracy of power system stability analysis depends on the regulation of the controllers used. Therefore, it is important to attempt to analyse the input controller factors; thus, allowing the planner to better understand of the stability margin of the system. Our sensitivity analysis finds the effect of $K_d$ and $T_d$ in the terminal and field voltages.

The sensitivity analysis case study is related to the NTG case study with an AVR controller with initial values of $T_d$=5, $K_d$ (derivative gain) = 0, but considering the limits allowed in [31], i.e., for the $K_d$ values between -40 and 0 (typical value of 0) and for $T_d$ (smoothed time constant) values between 0.1 s and 10 s (typical value of 5 s). Table 10 shows variations in percentage for field voltage and terminal voltage for $K_d$ values of -5, -15 and -30 and $T_d$ values of 1 and 10.

Table 10 shows that $K_d$ is a very sensitive parameter. When the ARV $K_d$ value is at the upper limit, the terminal voltage fluctuates by 6.693 percent. Therefore, a fast response AVR impacts both the oscillation stability as well as increasing transient stability of the power system.

Table 10. NTG AVR OAT Sensitivity Analysis

| | **Terminal Voltage (RMS percent variation)** | **Field Voltage (RMS percent variation)** |
|---|---|---|
| $K_d$ = -5 | 0.425 | 1.728 |
| $K_d$ = -15 | 1.491 | 5.512 |
| $K_d$ = -30 | 3.390 | 6.693 |
| $K_d$ = -1, $T_d$ = 10 s | 0.692 | 2.878 |
| $K_d$ = -1, $T_d$ = 1 s | 1.023 | 2.7020 |

## 4. Discussion

Section 2 shows how to estimate the Baba-generated field and terminal voltages in AVR and AVR + PSS controller modes using two case studies, i.e., isolated and NTG connected. Section 3 presents the application of this methodology to estimate the field voltage and terminal voltages in Baba generation. Case studies differ in system complexity. Section 3 is also an extension to the traditional sensitivity analysis, deconstructing the inputs to the path as the AVR derivative parameters flow through the Baba system and performing an innovative `what-if parameter sensitivity' scenario analysis. In this section, the methods, chart/table results, and sensitivities used to estimate the Baba generation are described in a broader context and discussed.

This paper began with a description of the power generation unit, AVR and PSS controller models, Transformers, Transmission lines and Infinite buses forming a simplified learning system (see Section 1). Two controller approaches: Only--AVR and AVR + PSS were developed in this research. In particular, the only-AVR controls the gate opening of the thyristor of the controlled rectifier. The entire system that controls and generates the excitation voltage is called the excitation system. For AVR + PSS controller, the main reason for implementing a PSS in the voltage regulator is to improve the small signal stability characteristics of the system. This study has shown that there is a trade-off between synchronous torque provided by the AVR and damping torque provided by the PSS.

This research has shown first and foremost that Generation data set components (see Section 2.1) are generally available in some form to many, if not all, Generation Business Units. Non-causal and causal models coexist as collaborative tools for simulating variables of interest in the simulation. The RMS error analysis using the non-causal mode is almost negligible compared to causal mode over the entire simulation time, so the outputs can be considered similar (see Section 3.3).

One of the issues highlighted is that in the initial phase of this research involved substantial data management,

cleansing, restructuring and additions to the NTG initial data set in PF package and the spatial extent complexity of the NTG case study surrounding Baba system. This study supports energy companies and stakeholders to model control systems in several ways: the first using either causal models based on input-output relations or non-causal models using implicit Differential Algebraic Equation (DAE). Second is the methodology for building the power generation control system. Third, to assess the impact of interventions, we explore the available tools that policy makers and city energy planners may need to identify reliability issues in the national power system.

In summary, this study has integrated a number of data sets in a way that it was able to integrate with well-respected standards such as the IEEE 421.5 standard, so every individual generation business unit can replicate this work. There are also issues with data collection methods and distribution restrictions.

This research proved that the strength is the framework approach not necessarily the model. The non-causal chosen is not necessarily suitable for large power systems. Therefore, an interesting application for future work is to take the framework developed in this study and adapt it to another hybrid model. This hybrid model can integrate power flow to control the physical properties of the system and multiple generators and their interrelations.

## 4. Conclusions

This study has shown that generation units' controller is affected by its parameters in all case studies. In some cases, these properties lead to output responses, suggesting that care should be taken when designing controller parameters from other studies instead of rigorous local analysis.

This paper proposes AVR and PSS with output limiters. This is because the key parameters that need to be controlled and kept within reasonable limits are the over-excitation and under-excitation indicators on the AVR output and saturation on the PSS output.

The stability analysis did not include models for low voltage load characteristics, tap changer behaviour under load, and relay protection, so the analysis includes manual manipulation. Further refinement of the stability analysis should include a physical understanding of these factors.

The work carried out within the framework of this research will make an important contribution to the research field of energy system modelling in several respects. First, the methodology used will greatly expand our theoretical understanding of existing complexities; second, to find new useful platforms to study power systems with their respective controls, with real conditions facilitating the study of different scenarios; and finally get the support of different tests and arrive at the same set of answers.

## References

[1]. International Renewable Energy Agency, "Sustainable development goal 7: Energy indicators". Technical Report. IRENA, 2017. URL: https://www.irena.org/IRENADocuments/Statistical_Profiles/SouthAmerica/Ecuador_SouthAmerica_RE_SP.pdf.

[2]. Food and Agriculture Organization of the United Nations, "Ecuador General Information". *Technical Report. FAO*, 2021. URL: http://www.fao.org/3/Y4347E/y4347e0n.htm.

[3]. J.P. Hidalgo-Bastidas, R. Boelens, "Hydraulic order and the politics of the governed: The Baba dam in coastal Ecuador". *Water* 11, 2019. URL: https://www.mdpi.com/2073-4441/11/3/409.

[4]. M. Ilic, J. Zaborszky, *Dynamics and Control of Large Electric Power Systems*. Wiley-IEEE Press, 2000.

[5]. IEEE Power Engineering Society, *IEEE Recommended Practice for Excitation System Models for Power System Stability Studies*. Technical Report, 2006.

[6]. NERC, *Steady-State and Dynamic System Model Validation*. Technical Report, 2017.

[7]. A. Elices, L. Rouco, H. Bourles, T. Margotin, "Design of robust controllers for damping interarea oscillations: application to the European power system". *IEEE Transactions on Power Systems* 19, 1058-1067, 2004. doi:10.1109/TPWRS.2003.821612.

[8]. P. Verdugo, J. Játiva, "Metodología de sintonización de parámetros del Estabilizador del Sistema de Potencia -PSS" [Power System Stabilizer parameter tuning methodology -PSS]. *Revista Técnica Energía* 10, 2014.

[9]. NASPI, *Model Validation Using Phasor Measurement Unit Data.* Technical Report, 2015.

[10]. W. Vargas, P. Verdugo, "Validación e identicación de modelos de centrales de generación empleando registros de perturbaciones de unidades de medición fasorial, aplicación práctica Central Paute – Molino" [validation and identication of generation plants models using disturbance records from phasor measurement units, practical application Paute - Molino Power Plant]. *Revista Técnica Energía* 16., 2020.

[11]. A. Bartolini, F. Casella, A. Guironnet, et al., "Towards pan-european power grid modelling in Modelica: Design principles and a prototype for a reference power system library", *13th International Modelica Conference*, pp. 627-636, 2019.

[12]. F. P. Demello, C. Concordia, "Concepts of synchronous machine stability as affected by excitation control". *IEEE Transactions on Power Apparatus and Systems PAS*-88, 316-329, 1969. doi:10.1109/TPAS.1969.292452.

[13]. P. Kundur, N.J. Balu, M.G. Lauby, *Power system stability and control*. New York: McGraw-Hill, 1994.

[14]. P. Fritzson, *Introduction to Modeling and Simulation of Technical and Physical Systems with Modelica*. Wiley-IEEE Press, 2011.

[15]. Consorcio Hidronergético del Litoral, *EIA definitivo Proyecto Hidroeléctrico Baba* [EAI final Baba Hydroelectric project]. Technical Report, 2006

[16]. L. Qi, "Modelica Driven Power System Modeling, Simulation and Validation". (Master's thesis, Royal Institute of Technology, 2014).

[17]. T. Van-Cutsem, L. Papangelis, *Description, Modeling and Simulation Results of a Test System for Voltage Stability Analysis*. Technical Report, 2013.

[18]. M. Baudette, M. Castro, T. Rabuzin, J. Lavenius, T. Bogodorova, L. Vanfretti, "Openipsl: Open-instance power system library | update 1.5 to itesla power systems library (ipsl): A modelica library

for phasor time-domain simulations". *SoftwareX* 7, 34-36, 2018. URL: https://www.sciencedirect.com/science/article/pii/S2352711018300050, doi :https://doi.org/10.1016/j.softx.2018. 01.002.

[19]. D. Mota, *Models for Power System Stability Studies, Thyricon(R) Excitation System*. Technical Report, 2010.

[20]. K. Walve, "Modelling of power system components at severe disturbances", *International conference on large high voltage electric systems*, 1986.URL: https://e-cigre.org/publication/38-18_1986-modelling-of-power-system-components-at-severe-disturbances.

[21]. IEEE Power and Energy Society, *IEEE Recommended Practice for Excitation System Models for Power System Stability Studies (Revision of IEEE Std 421.5-2005)*. Technical Report, 2016.

[22]. K.E. Bollinger, S.Z. Ao, "PSS performance as affected by its output limiter". *IEEE Transactions on Energy Conversion* 11, 118-124, 1996. doi:10.1109/60.486585.

[23]. P.M. Anderson, A.A. Fouad, *Power System Control and Stability*, Wiley-IEEE Press; 2nd edition, 2002.

[24]. V. Bari, E. Vaini, V. Pistuddi, A. Fantinato, B. Cairo, B. De-Maria, L.A. Dalla-Vecchia, M. Ranucci, A. Porta, "Comparison of causal and non-causal strategies for the assessment of baroreflex sensitivity in predicting acute kidney dysfunction after coronary artery bypass grafting". *Frontiers in Physiology* 10, 2019.

[25]. E.V. Larsen, D.A. Swann, "Applying Power System Stabilizers part iii: Practical Considerations". *IEEE Transactions on Power Apparatus and Systems PAS*100, 3034-3046, 1981. doi:10.1109/TPAS.1981.316411.

[26]. A. Baharev, A. Neumaier, H. Schichl, "Failure modes of tearing and a novel robust approach", *Proceedings of the 12th International Modelica Conference* pp 15-17, 2017.

[27]. A. Pothen, C.J. Fan, "Computing the block triangular form of a sparse matrix". *ACM Transactions on Mathematical Software*. 16, 303-324, 1990. URL: https://doi.org/10.1145/98267.98287, doi:10.1145/98267.98287.

[28]. P. Tauber, L. Ochel, W. Braun, B. Bachmann, "Practical realization and adaptation of Cellier's Tearing Method", *Proceedings of the 6th International Workshop on Equation-Based Object-Oriented Modeling Languages and Tools, Association for Computing Machinery*, New York, NY, USA. p. 11-19, 2014. URL: https://doi.org/10.1145/2666202.2666204,doi:10.1145/2666202.2666204.

[29]. M.J. Gibbard, P. Pourbeik, D.J. Bowles, "Small system stability, performance and control of power systems". *University of Adelaide Press*, 2015. Adelaide.

[30]. A. Saltelli, P. Annoni, "How to avoid a perfunctory sensitivity analysis". *Environmental Modelling and Software* 25, 1508-1517, 2010. URL: https://www.sciencedirect.com/science/article/pii/S1364815210001180, doi: https://doi.org/10.1016/j.envsoft.2010.04.012.

[31]. A. Hammer, "Analysis of IEEE Power System Stabilizer Models". (Master's Thesis. Norwegian University of Science and Technology, 2011). URL: https://ntnuopen.ntnu.no/ntnu-mlui/bitstream/handle/11250/257120/445805_FULLTEXT01.pdf?sequence=1.



**JAVIER URQUIZO,** after an undergraduate degree in Electric Power Systems in Ecuador, I did graduate master school in United States having a master's in electrical engineering from Stevens Institute of Technology, Hoboken New Jersey and a master's in civil and Environmental Engineering from University of New Orleans, Louisiana. I went to the United Kingdom in 2011 to pursue a doctoral degree in the Planning of Urban Energy Systems at Newcastle University. I did my VIVA in June 2015. The monograph I submitted informs domestic energy demand estimates to a number of EU, UK and Local Authority carbon and energy efficiency schemes. Currently I am doing research and teaching in an Ecuadorian University ESPOL, currently teaching Electric Power Distribution Systems, Renewable Processes and Sustainable Energy System Planning.

**DIOVER BONILLA,** after an undergraduate degree in Electric Power Systems at Escuela Superior Politécnica del Litoral ESPOL - Ecuador, I did graduate school in Renewable Energy I the European Centre of postgraduate studies, Madrid - Spain.

**FRANCISCO RIVERA,** I have an undergraduate degree in Electric Power Systems at Escuela Superior Politécnica del Litoral ESPOL – Ecuador

**ROMMEL CHANG** After an undergraduate degree in Electric Electronics and Industrial Automation at Escuela Superior Politécnica del Litoral (ESPOL), I did graduate school in Industrial Automation and Control at ESPOL. I work at Baba Generation Plant.

Received: 31 October 2022, Revised: 22 December 2022, Accepted: 29 December 2022, Online: 28 January 2023
DOI: https://dx.doi.org/10.55708/js0201002

# CAPEF: Context-Aware Policy Enforcement Framework for Android Applications

**Saad Inshi** [1], **Mahdi Elarbi** [1], **Rasel Chowdhury** [1,*], **Hakima Ould-Slimane** [2], **Chamseddine Talhi** [1]

[1] Department of Software Engineering and Information Technology, École de technologie supérieure, Montréal, Canada
[2] Département de Mathématiques et d'Informatique, Université du Québec à Trois-Rivières, Trois-Rivières, Canada
*Corresponding author: rasel.chowdhury.1@ens.etsmtl.ca

**ABSTRACT:** The notion of Context-Awareness of mobile applications is drawing more attention, where many applications need to adapt to physical environments of users and devices, such as location, time, connectivity, resources, etc. While these adaptive features can facilitate better communication and help users to access their information anywhere at any time, this however bring risks caused by the potential loss, misuse, or leak of users' confidential information. Therefore, a flexible policy-based access control system is needed to monitor critical functions executed by Android applications, especially, those requiring access to user's sensitive and crucial information. This paper introduces CAPEF, which is a policy specification framework that enforces context-aware inter-app security policies to mitigate privacy leakage across different Android applications. It also, provides an instrumentation framework to effectively enforce different behaviors based on automated context-aware policies to each Android application individually without modifying the underlying platform. Accordingly, the modified applications will be forced to communicate with our centralized policy engine to avoid any malware collusion that occur without the users' awareness. Experiments conducted on CAPEF shows an effective performance on the size of the enforced application after the instrumentation. The average size added was 705 bytes, which is about 0.063% of the size of the original applications, which is significantly small compared to other existing enforcement approaches. Also, we have denoted that the size and the execution time of the policy increases whenever the policies become more complex.

**KEYWORDS** Security, Android applications, Application instrumentation, Context-aware policies, Policy enforcement, Privacy

## 1. Introduction

Context awarenes service is a key driver for the modern mobile operating systems which are commonly prompting users by showing authorization dialog boxes asking for allowing or denying access to some functionalities. These services opened a big interest in defining, managing, and enforcing context-aware policies especially for those scenarios that put users under the risk of leaking or misusing their credential information. Yet, thousands of malicious applications are developed on the Android store and affecting millions of Android users worldwide. To safeguarded Android users, Google is frequently announcing the cracking down of such malicious applications. For instance, Google has removed over 700,000 malicious applications from the Play Store in 2017 only [1]. Based on Goggle statistics, this is 70% more than what Google removed in 2016. Very recently in 2022, Google has removed 16 bad apps that missuses mobile data and draining batteries. Surprisingly, these apps have been downloaded by more than 20 million users around the world [2].

Android system protects sensitive APIs by granting them permissions to amplify application privileges on the device, including access to stored data and services, such as network, memory, and so on. All permissions required to access the protected APIs in each application's manifest file (AndroidManifest.xml) [3] are necessarily set by the Android app developers. System permissions are divided into two categories, normal and dangerous. Normal permissions do not pose a direct threat to the privacy of the user, although dangerous permissions may allow the application to access the user's confidential data. Existing application authorization system in Android allows you to control only the permissions that are classified as dangerous, whereas our developed policy approach, offers the ability to control all monitored permissions as any application may cause a risk or conflict within a specific context without user awareness. Also, our model will mitigate malware collusion in which two or more malicious apps combine to accomplish their goals. For example, a user can choose to allow a camera app to access the camera, but not to the contact information without his consent or awareness. Another example, where normal applications can be granted permissions to collecting user's contacts, photos, videos,

locations, or banking information then sending it over the internet to a remote server and taking into consideration pre-defined context aware access control policies. Therefore, a flexible policy-based access control system is needed to monitor APIs functions in Android applications, especially those requiring access to the user's sensitive and crucial information. The current permission system of Android still has some limitations, where users must grant most permissions requested by an application to install it, without being able to automatically manage most of these permissions based on the user's context afterwards.

This drawback has motivated the researchers to propose context-aware policies and/or define policy languages to enforce the current Android permission system either by modifying the Android platform such as in [4]–[8] or by instrumenting the Android Applications [9]–[18] and more recently in [19]–[21] (more details and comparisons can be seen in the background and literature review section). While, existing works have demonstrated significant effectiveness in protecting users against threats, these approaches are still impeded by several drawbacks.

### *1.1. Challenges*

Defining and monitoring context-aware inter-app policies of sensitive APIs on Android applications presents several challenges. Especially, when we are trying to defend applications collaborating to create malicious contexts:

i Context-aware inter-app policies are difficult to predict as they frequently get changed and need to be updated accordingly for accuracy and correctness.

ii Beside the difficulty of representing the security policies in a logical language which can contain user contexts and semantics, a key challenge is how to design and develop effective and efficient algorithms to monitor private information leakage on semantics levels.

iii There is a need for a policy language that can provide certain agreements that empower users with the ability to prioritize specific mobile resource and specify the amount and kind of information that can be shared within particular contexts. For instance, a user should be able to share a personal data with a specific service provider based on his location or at a specific time of the day to ensure his privacy. In this case, the user must agree on a trade-off between data privacy and the needed service. As a result, a policy should be defined to ensure privacy, while certain context-based information can be shared.

iv Android Sandboxing is introduced in the recent Android version 13.0. Sandboxing protects apps data and permission from getting access from other apps. This new feature will have an impact on our inter-apps policy model, but our main goal still effective which is to allow the user to define his policies to work automatically depending on the context update, to the running apps etc. Therefore our, framework can fully protect the Android OS versions lower than 13.0 in which the installed apps can communicate between each others.

v Due to the resourced constrained mobile devices, we have to decide, in early stages the instrumentation and monitoring location, whether to be on device, external PC or App market.

### *1.2. Contributions*

This article is contributing solutions for the above-mentioned challenges and limitations by introducing:

i A formal context-aware policy specification framework for Android applications that effectively describe users defined consents.

ii A design and implementation of an instrumentation framework to mitigate privacy leakage across different Android applications.

iii Providing a centralized applications controller. This will allow users to manage all API calls performed by the applications installed on the device and to mitigate malware activities.

iv Effectively enforce different behaviors based on automated context-aware policies for each Android application individually without any modification to be entailed in the underlying platform.

v Experiments conducted on our CAPEF in terms of performance by analyzing the size of the enforced application after the instrumentation, also, the execution time of the policy decision, and the policy size which affects the complexity of the applied rules and conditions.

## 2. Background and Literature review

Android applications are distributed as APK files (Android Package). Each package consists of the application's manifest file, resources and application bytecode encoded for the Dalvik Virtual Machine (DVM) as a single classes.dex file. The APK file has to be signed for verifying its authenticity. Android signed package (Dex files) runs separately in its own DVM. Also, Android system is an open source platform where applications are published in different markets without being monitored or analyzed to guarantee their behavior. For that reason, Android platform protection mechanisms such as Application Sandboxing, Permission Model and Application Signing are developed for privacy and security purposes. Accordingly, at the time of installing Android applications, each application will get a unique user identifier (UID) [22]. Also, no application will be able to access other application's files. Besides, every application run into separate VMs. Accordingly, no vulnerable application will affect other applications.

For Android access control policies, context awareness have become an essential accessory in most mobile platforms and applications. This necessity has motivated many researchers to provide policy enforcement mechanisms to

define, manage and enforce different context aware policies. In this context, traditional access control models which generally refer to the process of determining what actions are allowed by a given subject upon objects and resources should be reinforced to fulfill the modern context-aware applications.

The most popular access control models are Discretionary Access Control (DAC), Mandatory Access Control (MAC), Role Based Access Control (RBAC) and Attribute Based Access Control (ABAC) [23] . For instance, RBAC is a model that uses "roles" to determine access control, also permissions are associated with these roles, and users are made members of appropriate roles. In ABAC, requests are granted or denied based on subject and resource attributes, environment conditions, and a set of policies specified in terms of those attributes and conditions. When it comes to using ABAC models, one of the well-known standard system implementations is XACML [24]. The XACML standard defines a declarative access control policy language implemented in XML and provides a processing model on how to evaluate access requests.

Thus, to adopt an effective context-aware access control model on Android platform and its application, there are series of work studying and proposing security mechanisms for privacy and security requirements. In this context, many reviewed efforts in [4]–[8] have been developed to extend the Android security framework in order to improve the standard permission control provided by the operating system. For example, SecureDroid [4] addressed the issue of controlling security policies while applications are executing in the Android environment. During the installation of an application, Android allows the user to grant permission for an application to use certain features of the system. Therefore, SecureDroid introduced an extension of Android's security framework in order to improve the standard permission control provided by the operating system. To achieve this goal, they introduced a new control mechanism adding granularity and flexibility. Moreover, their policy framework is based on customizing the XACML standard to work on the Android system. Also, they have provided the ability to add or edit a policy through a dedicated system service. This will allow users to specify which permissions to grant and which others to deny for each of the defined contexts.

However, modified Android platform has a number of major drawbacks such as the need of building different versions of firmware and platform codes, where applications will be limited by the security policies supported by the modified Android platform. Therefore, many researchers in [9]–[18] and more recently in [19]–[21] have provided solutions that are based on instrumenting Android Applications in ordered to enforce some security policies. These solutions require no modification to the Android platform and can be easily deployed. For instance, Aurasium [9] is a concurrent approach that rewrites Android application to sandbox important native API methods and monitors the behavior of the application to detect any security violations. Also, Capper [17] is a prototype for context-aware policy enforcement to mitigate privacy leakage in Android applications. This mechanism will enforce privacy policy based on user preferences. By using this system, when a user tries to install any Android application the bytecode rewriting engine called BRIFT will rewrite the program of this application by selectively inserts instrumentation code along taint propagation slices for monitoring and preventing any information leakage. Another interesting research called Weave Droid [18] has provided a framework for weaving AspectJ aspects into an Android application. The framework takes two inputs at the beginning: APK and a set of aspects that will be weaved into the APK. The weaving process will be performed on the Android device. Also, very recently in [21] They have developed a lightweight monitoring system to detect malware activities with the log file and they evaluated the proposed model according to Policy-based permissions.

Accordingly, some of the reviewed frameworks have provided enforcement mechanisms to mitigate Malware activities by enforcing context-related policies, however they didn't afford a policy specification language that runs on Android system as an application or a service without modifying the Android platform. Thus, this article is introducing a more featured policy specification language that allow regular users and any company to easily interpret and enforce their complex context-aware inter-apps policies on their Android mobile applications.

### *2.1. Summary of the literature reviews*

The table 1 shows the summary and differences between our research and the other works.

## 3. System Overview

This section gives an overview of our approach that automatically enforces user specific context-aware policies for android application and monitors all API calls that occur due to the interaction between enforced applications. Our developed system works in the application level of the Android framework, and its main components are illustrated in Fig. 1.

i From left, the first components represented the instrumentation of the targeted Android application (byte code or source code) by injecting monitoring code before each selected API method's call to intercept it at run time.

ii After the instrumentation, the applications will be forced to communicate with our controller that monitors the targeted context-aware inter-app calls.

iii Then, users will use CAPEF interface to create context-based rules and conditions in the form of security and privacy policies. More precisely, the policy represents a rule or set of rules based on a set of conditions and save it in the policies Database.

To motivate and illustrate our approach, we present the following scenario for vulnerability pattern that consider context-awareness policies. In this scenario, a user is using a public WiFi network in a coffee shop and he is trying to consult his credential banking information through his banking application. As the public network is not secure

Table 1: Comparison of related work

| Approach/ System | Methodology | Required modification | Policy Language | Context-aware inter-app Privacy Leakage Prevention |
|---|---|---|---|---|
| TaintDroid [25] | Dynamic Analysis | Android Platform | ✗ | ✗ |
| Appink [26] | Watermarking | Application | ✗ | ✗ |
| Apex [5] | Policy Enforcement | Application | ✗ | ✗ |
| TISSA [6] | Resources Access Control | Android Platform | ✗ | ✗ |
| AppFince [7] | Dynamic Analysis & Resources Access Control | Android Platform | ✗ | ✗ |
| Aurasium [9] | Rewriting Java Bytecode | Application | ✗ | ✗ |
| I-arm-droid [11] | Rewriting Dalvik bytecode | Application | ✗ | ✗ |
| AFrame [14] | Isolating Advertisements | Application | ✗ | ✗ |
| Capper [17] | Rewriting Java Bytecode | Application | ✗ | ✗ |
| SecureDroid [4] | Policy Enforcement | Android Platform | ✓ | ✗ |
| Weave Droid [18] | Isolating Advertisements | Application | ✗ | ✗ |
| [21] | Policy-based permissions | Application | ✗ | ✗ |
| CAPEF | Policy Language | Application | ✓ | ✓ |

and there are other people who use the same network, so there is a risk of sending requests to attackers and thefts of private data. Android system checks only if the user has been previously granted the permission of accessing WiFi network and doesn't provide any context-awareness policies to mitigate such dangers scenarios. CAPEF can provide more effective access control not only on the permissions declared in advance by the user but also at run time based on the context of the user, device, and resources. Thus, as a solution to the above-mentioned scenario, a user can use CAPEF to define a policy that prevent the use of banking applications while connecting to a public WiFi network. When an enforced bank application attempt to get public WiFi access, our application controller will first check if the permission is declared in the application manifest file. Then, will check if the user has defined any policies related to this permission in the policies database. Subsequently, the controller access decision will be based on the predefined policies for that specific API. As a result, the controller will notify the user for not being allowed to connect to public WiFi for banking activities.

## 4. CAPEF

Context-Aware policies are not static and might be changing over time to fulfill users' needs. Therefore, these policies could be used to control the behavior of the applications during run-time, which in our case, means monitoring and controlling all sensitive activities across different applications according to user's context. To achieve this goal, we provided a native Java-based CAPEF that allow regular users and enterprises to interpret and enforce their complex context-Aware policies. Contexts will represent various parameters including time, location, identity, activity, application, device status, resources etc. Moreover, these policies can be exported in multiple formats such as XML and JSON as they are widespread use today for data interchange and structured stores.

To develop the CAPEF language that allows the user to define contextual policies and transform them into security controls, we must rely on a flexible design that varies with the complexity of the policies, rational, able to execute all the conditions and easy to add new contexts.

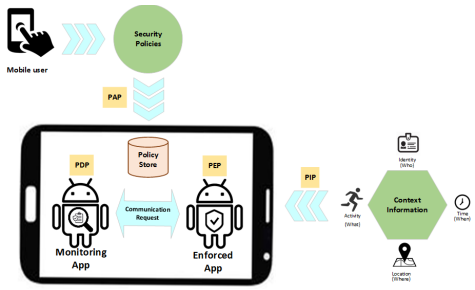


Figure 2: CAPEF Architecture

### 4.1. CAPEF Architecture

The main components of CAPEF are shown in Fig.2. which represents the following:

i **Security policies**: which is an interface for the user to define context aware policies and save them at the policy store. This component will act as a policy administration point (PAP) which is the source of the policies.

ii **Enforced Application**: Which plays the role of policy enforcement point (PEP) that receives the access request and move it to the Monitoring application for making access decision based on the predefined context aware policies.

iii **Context Information**: Provides context information in a form of attribute values about the targeted applications, resources, activates, actions and so on. This component will play the role of policy information point (PIP) in our system.

iv **Monitoring Application**: This component plays the role of policy decision point (PDP). It takes the access request from the PEP then interacts with PAP and PIP that capture the required context information to identify the appropriate policy. Then evaluates the

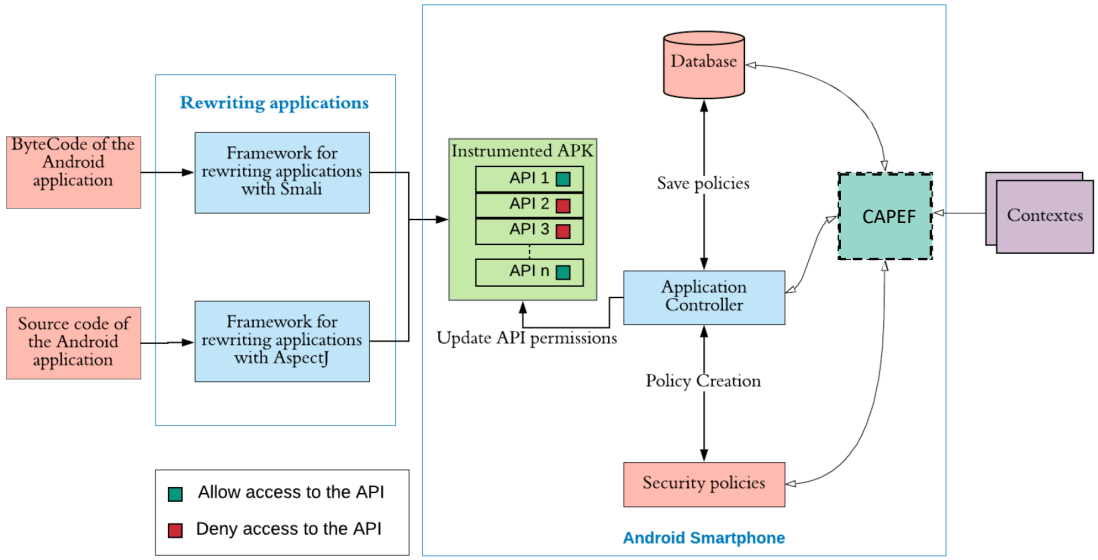


Figure 1: System Overview

request according to the applicable policy and returns the decision to the PEP.

### 4.2. Formal Definition

Hereafter, we formally define our ABAC policy model, which is composed of three main entities:

1. A, P, and C : sets of application, permissions (resources) and contexts, respectively;
2. AA , PA ,and CA are the pre-defined sets of attributes for applications, permissions, and contexts, respectively.

I An application *app* is a represented by a tuple as follows:

*app* <name, visibility, class, APIs>, where:

i visibility ∈ {background, foreground}

ii class ∈ { banking, communication, recording, games, media, location}

iii APIs: a set of APIs that can be invoked during execution

II A permissions *per* embeds the access to the resource, it is a represented by a tuple as follows:

*per* < name, resource, securityLevel >,

i resource ∈ { personal data, calendar, camera, wifi, account, calls, sms,Audio, GPS},

ii securityLevel ∈ { Normal, Dangerous },

III A context *c* is a represented by a tuple as follows:

*c* < time, location, fgApp, BgApps availableCPU, availableMEM, availableNRG >,

i fgApp indicates which application is running in foreground;

ii BgApps is the set of the applications running in background.

3 Attr(*app*),Attr(*per*), and Attr(*c*) are attribute assignment relations for application app, permission per and context c, we have respectively

I Attr(*app*) ⊆ name × visiblity × class × APIs;

II Attr(*per*) ⊆ name × resource × securityLevel;

III Attr(*c*) ⊆ time × location × fgApp × BGaps × availableCPU × availableMEM × availableNRG.

For the value assignment of each attribute, we use the following notation: **entity.attribute= value** ,

For example, for an application **app**, a permission **per** and a context **c**, we have the following assignments:

app.visiblity = 'background', per.securityLevel = 'Dangerous', c.location = 'Montreal'.

4 The ABAC policy rule that decides whether or not an application **app** is allowed is allowed to get the permission **per** under a particular context **c**, is denoted as a predicate **PR** over the attributes of **app**, **per** and **c** as follows:

**Rule** : Allow(app, per, c) ← PR(Attr(app), Attr(per), Attr(c))

Given all the attribute assignments of *app*, *per*, and *c*, if the predicate's evaluation is true, then the application **app** is allowed to get the permission **per** under the context **c**; otherwise, the permission is denied. Using the formal definition, we can have different types of policies for the *app*, for example:

1. A rule that dictates that " When a banking applications is being used, so the TakeScreenshot actions should be prevented from running" can be written as:

   $Allow_{screenShot}$(app, per, c) ← ( TakeScreenshot ∈ app.APIs) ∧ (per.resource==screen) ∧ (c.fgApp.class != banking)

2. A rule that dictates: "RecordVoice and RecordCall applications should be prevented from running when the user is dialing Skype from 9:00 to 10:00" can be written as:

   i $Allow_{recordVoice}$(app, per, c) ← ( RecordVoice ∈ app.APIs) ∧ (per.resource==voice) ∧ ((c.fgApp != 'skype') ∨ ( c.time <9:00 am ∨ c.time > 10:00am))

   ii $Allow_{recordCall}$(app, per, c) ←( RecordCall ∈ app.APIs) ∧ (per.resource==call) ∧ ((c.fgApp != 'skype') ∨ (c.time < 9:00am ∨ c.time > 10:00am))

   Or simply by combining the two rules as following:

   $Allow_{record}$(app, per, c) ←( RecordVoice , RecordCall ∩ app.APIs!= $\phi$) ∧ (per==voice ∨ per==call) ∧ ((c.fgApp != 'skype') ∨ ( c.time < 9:00am ∨ c.time > 10:00am))

### 4.3. CAPEF Policy Specification

CAPEF language is based on the definition of a policy that consists of a user ID, a policy name, a policy execution state, a control rule, and a list of applications to control. Each of these applications is characterized by a name, package name, execution status and a list of permissions. The permissions consist of a name and a execution state. The security rule consists of a list of objects that can be Parentheses, Conditions, Logical Operators, Conditional Operators, CPU, Time, Resource Used, Location and Battery.

As shown in Fig.3, user-defined security policies and its rules can contain multiple conditions, different contexts, multiple logical operators, and parentheses to specify priority between conditions. Also, these policies can be executed simultaneously in different inter-app activities across different applications. In this case, policy decision becomes more complex. Therefore, to facilitate and accelerate the execution of any compound policy, our algorithm will receive the current contexts and the control rule as parameters then returns the policy decision of the controller.

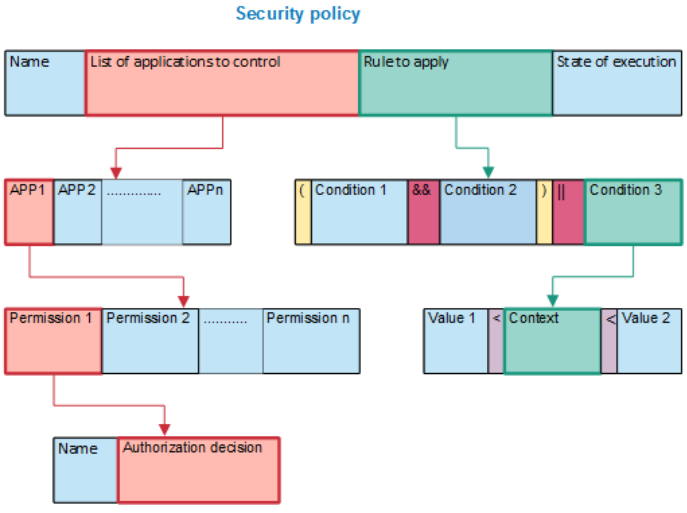


Figure 3: CAPEF Policy Execution Structure

In addition, the security rule might have sub-nodes of other rules, and themselves are sub-rules of the main rule. Therefore, we have adopted a recursive technique to reduce the complexity of the composed security rules. In this case, the algorithm will call itself, and recursion stops condition must be checked, otherwise the program will be stuck in an infinite loop.

To show the usefulness of our solution, we have chosen two examples of dangerous scenarios and we will translate them into security policies.

I Critical scenario 1: If the user uses his banking application to check his data and deposit a check in his account, while a TakeScreenshot application is installed on his smartphone.This application that takes screenshots automatic present a risk on banking data that is personal life data.

   i Solution: You must prevent the TakeScreenshot application and any screenshot function from running when the user is using their banking application.

   ii Security Policy: If [BankApp] is running, then stop the [TakeScreenShot] application.

II Critical Scenario 2: If the user is in a private work meeting every Monday from 9:00 am to 10:00 am by Skype while many other apps are able to record his speech and share it in public as RecordVoice and RecordCall applications.

   i Solution: RecordVoice and RecordCall applications should be prevented from running when the user is dialing Skype from 9:00 to 10:00.

   ii Security Policy: If ((CALL_PHONE in [Skype]) && (9: 00 <= Current_Time <= 10: 00)), then stop or prevent (if not yet executing) the application [RecordVoice && RecordCall].

To apply and evaluate the defined context aware policies, an application controller has been developed to allow users to define policies depending on different types of contexts and conditions.

## 5. Centralized Application Controller

The developed controller provides a user interface to translate the dangerous scenarios into security policies using the CAPEF. Based on the defined policies, the controller will make the adequate access control decision to allow or block applications from using certain permissions. Moreover, provide centralized control of installed applications which capture mandatory decisions that are automatically dependent on the current context.

Fig. 4, shows an example of how to define a security policy with our controller. The control scenario is to block the execution of the Camera resource in the Camera application if the user is in a meeting from 10:30 to 11:30 or from 13:30 to 15:30 otherwise it is in a meeting from 15:30 to 15:40 and that Bluetooth is enabled in the BluetoothShare Application.

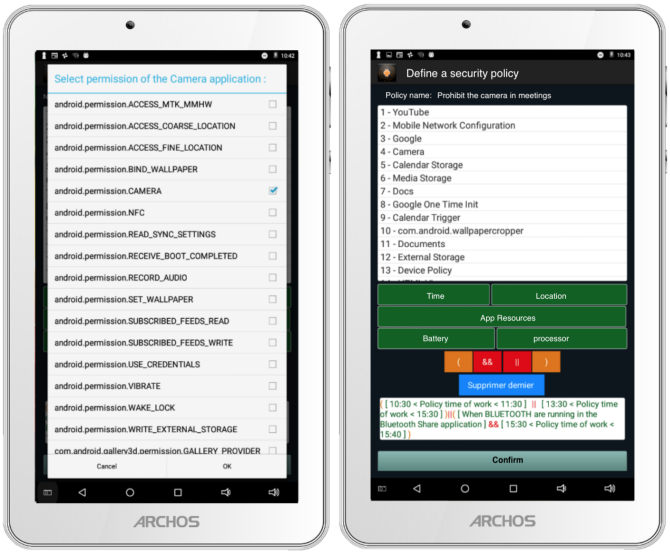


Figure 4: Screenshots of a policy definition within our controller

### 5.1. Managing Security Policies

The Application controller interface has been developed in a way that the user will be able to define any security policies in a few simple clicks. We chose our solution to be ergonomic, personalized, and user-centric design to have a convenient and easy-to-use service. It has also been taken into consideration that our user interface must reduce the search effort and limit data entry. In addition, all policies created by the user have been saved in a database. With the database, the user will be able to import, create, view, and modify security policies.

### 5.2. Export/Import Security Policies

Our developed solution allows the user to extract his defined policies and share them with other users of the controller or send them to nay server or cloud database. Therefore, our CAPEF flows same related policy language's architecture and structure. As discussed in the literature XACML is one of the good examples to extract our policies to its format. While Android system does not compile XACML language and all reviewed languages, our policies will be translated into java language to execute them, then will be extracted on different languages such as XML, JSON etc. Therefore, in order for our language to be compatible with other languages, we kept the same generic policy structure, objects and attributes applied by other languages as as shown in Table 2. Similar translation procedure will be applied when importing policies from other languages.

Among the values that can be assigned to attributes such as the names of applications, permissions, etc., we have defined symbols that allow us to simplify the rules, for example:

i ANY: it means no, for example a rental context, we do not need permission in this condition.

ii ALL: it means that we want to control all the permissions or all the applications it depends on the attributes used.

iii APPS: it means that we want to force the shutdown of an application.

iv API: that means we're going to apply the control on an API permission.

```
<?xml version="1.0" encoding="UTF-8"?>
<policy combine="deny-overrides" id="1" AUTHOR-KEY-CN="Mahdi" AUTHOR-KEY-FINGERPRINT="Mahdi">
   <target>
      <subject>
         <subject-match attr="id_ScreenShot" match="com.apps.TakeScreenShot" />
         <subject-match attr="id_BNC" match="com.apps.BNCbanque" />
      </subject>
   </target>
   <rule effect="deny">
      <condition>
         <ressources>
            <ressource>
               <ressource-match attr="APPS" subject-match="id_ScreenShot" match="ALL" />
            </ressource>
         </ressources>
         <contexts>
            <context>
               <context-match attr="UsedRessources" subject-match="id_BNC" match="android.permission.CAMERA" />
            </context>
         </contexts>
      </condition>
   </rule>
</policy>
```

Figure 5: An example of a security policy presented in the form of XML


```
{
    "@combine": "deny-overrides",
    "@id": "1",
    "@AUTHOR-KEY-CN": "Mahdi",
    "@AUTHOR-KEY-FINGERPRINT": "Mahdi",
    "target": {
        "subject": [
            {
                "@attr": "id_ScreenShot",
                "@match": "com.apps.TakeScreenShot"
            },
            {
                "@attr": "id_BNC",
                "@match": "com.apps.BNCbanque"
            }
        ]
    },
    "rule": {
        "@effect": "deny",
        "condition": {
            "ressources": {
                "ressource": {
                    "ressource-match": {
                        "@attr": "APPS",
                        "@subject-match": "id_ScreenShot",
                        "@match": "ALL"
                    }
                }
            },
            "contexts": {
                "context": {
                    "context-match": {
                        "@attr": "UsedRessources",
                        "@subject-match": "id_BNC",
                        "@match": "android.permission.CAMERA"
                    }
                }
            }
        }
    }
}
```


Figure 6: An example of a security policy presented in the form of JSON

The following scenario is established to extract CAPEF policies to communicate with other policy languages such as XML and JSON:

i Scenario: Prohibit launching the TakeScreenShot application that allows you to take automatic screenshots when the user opens the camera in his BankApp application to send a check.

Table 2: Generic policy description

| Element | Description |
|---|---|
| Policy-set | Presents a table that groups the list of policies. |
| Policy | Presents the policy object that contains the" Target and" Rule Sub-objects, as well as the attributes:" Combine "which presents the role of the policy, the" AUTHOR-KEY-CN attribute the author identifier of the policy and the attribute AUTHOR-KEY-FINGERPRINT" presents the fingerprint key of the author of the policy. |
| Target | This is the object that contains the definition of the target applications to control. |
| Rule | It is the object that defines the security rule, the attribute" effect "presents the decision of the control to give or withdraw the authorization. |
| Condition | Contains the permissions to remove and the contexts. |
| Resource-match | Contains different attributes:" attr "which can be an application to block or an API permission," subject-match "contains the application to control and" match "contains the permission to remove. |

ii Policy: if (CAMERA in [BNCApp]), then stop the application [TakeScreenShot].

Fig.5. shows the extraction of the above security policy scenario to XML and Fig.6. shows the extraction of the same scenario to JSON security policy.

## 6. Experimental results

This section presented the evaluation of our CAPEF and the application controller in terms of performance by analyzing: (1) the size of the enforced application after the instrumentation, 2) the execution time of the policy decision (3) The policy size due to the complexity of the applied rules and conditions.

### *6.1. Enforced Application Size*

To measure the effect of the instrumentation method on the original size of the applications, we have instrumented a set of 109 applications using our rewriting framework. Table 3 shows a sample of eighteen applications, the original size and the new size after the instrumented. Indeed, this percentage represents the size of the code added during the control of APIs calls for each application individually

For all instrumented 109 applications, the average size added was 705 bytes, which is about 0.063% of the size of the original applications. Also, as shown in Fig.7, it is very clear that the size added is very small and will have a very small impact on the size of the original applications.

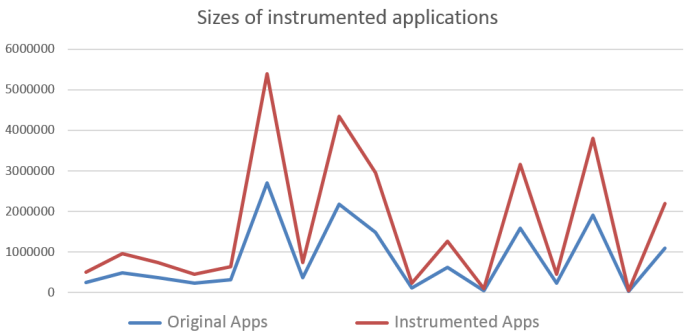


Figure 7: Average added size for 109 instrumented applications

### *6.2. Execution time of the policy decision*

To calculate and evaluate the execution time of our defined policies, we have calculated the decision execution time for several context aware policies with different rules and conditions based on some selected scenarios. The following is a set of scenarios that has been chosen among many others used during our tests. These scenarios will be ranked in ascending order according to their level of complexity.

1. **Scenario 1**: Prohibit launching the TakeScreenShot application that allows you to take automatic screenshots when the user opens the camera in his BankApp application to send a Check.

   **Policy**: $\text{Deny}_{TakeScreenShot}$(app, per, c) ← ( TakeScreenshot ∈ app.APIs) ∧ (per.resource==screen) ∧ (c.fgApp.class = banking)

2. **Scenario 2**: Prohibits the RecordAudioMedia application from recording when the user is making a phone call through the PhoneCall application.

   **Policy**: $\text{Deny}_{RecordAudioMedia}$ (app, per, c) ← (RecordAudioMedia ∈ app.APIs) ∧ (per.resource == microphone) ∧ (c.fgApp.class = (callPhone ∨ receivePhoneCall))

3. **Scenario 3**: Prohibit the FakeGPS application from changing the user's location when using one or more of these BankApp, Uber, and Google-Map applications.

   **Policy**: $\text{Deny}_{FakeGPS}$ (app, per, c) ← (FakeGPS ∈ apps.APIs) ∧ (per.resouce == (accessCoarseLocation ∧ accessFineLocation) ∧ (c.fgApp.Class = (BankApp ∧ UBER ∧ GoogleMap))

4. **Scenario 4**: Prohibition of the BankApp application to access the Internet or use the camera when the user is at TimHortons knowing that its longitude = 45.491318 and its latitude = -73.727987.

   **Policy**: $\text{Deny}_{internet \wedge camera}$ (app, per, c) ← ((internet ∧ camera) ∈ apps.APIs) ∧ (per.resource == (GPS = [45.491318, -73.727987]) ∧ (c.fgApp.Class = BankApp)

5. **Scenario 5**: When the user is at the meeting at ETS from 8am to 9am. Prohibit Facebook, Instagram and Gmail applications from accessing the Internet, the

Table 3: The size of applications before and after instrumentation

| Application | Original (Bytes) | Instrumented (Bytes) | Size added (Bytes) | Percentage |
|---|---|---|---|---|
| Contact Identicons | 246904 | 247965 | 603 | 0.24% |
| GPS tracker | 22420823 | 22421668 | 845 | 0.0037% |
| Show web view | 483839 | 484460 | 621 | 0.12% |
| Contact Search | 368610 | 369278 | 668 | 0.18% |
| Contacts Widget | 227386 | 228034 | 648 | 0.28% |
| Beta Updater for WhatsApp | 321673 | 322448 | 775 | 0.24% |
| Contact loader | 2701541 | 2702019 | 478 | 0.01% |
| Photo Manager | 366100 | 366668 | 568 | 0.15% |
| Wi-Fi setup | 2177239 | 2177747 | 508 | 0.02% |
| Time tracker | 1477841 | 1478711 | 870 | 0.06% |
| Calender Trigger | 119863 | 120732 | 869 | 0.72% |
| Calender Color | 629361 | 630232 | 871 | 0.13% |
| Calender Import Export | 45823 | 46772 | 949 | 2.07% |
| CamTimer | 1580753 | 1581393 | 640 | 0.04% |
| OpenCamera | 226585 | 227420 | 835 | 0.36% |
| Microphone | 1905254 | 1905910 | 656 | 0.03% |
| SMS backup | 26071 | 26984 | 913 | 3.50% |

camera and the location. Prohibit Message application from receiving SMS and MMS. Also, Prohibit the recording feature of RecordAudio application.

**Policy**: $\text{Deny}_{all}$ (app, per, c) ← ((Facebook ∧ Instagram ∧ Gmail∧ RecordAudioMedia ∧ SMS ∧ MMS) ∈ apps.APIs) ∧ (per.resouce ==(GPS = [45.491318, -73.727987] ∧ internet ∧ microphone ∧ phoneCall ∧ receiveCall )) ∧ (c.fgApp.Class = meeting ) ∧ (c.time >= 8am ∧ c.time <=9am )

The decision execution time has been calculated for each policy individually as following:

i For the Policy 1 and Policy 2, the test results were fixed because the context does not vary when entering random test values. The execution time for the first policy is 116 ms and for the second policy is 234 ms.

ii For the policy 3, the context is related to three different running applications, but it remains fixed. The execution time for the whole policy is 307 ms.

iii For the policy 4, our context is the location, so the results were more or less close, but they vary according to the change in GPS values. In this case the execution time of the whole policy is 314 ms.

iv For the policy 5, two different contexts were used time and location. The average execution time for notifying each application also was calculated. For the Skype application the execution time is 549 ms, for the Messages application is 592 ms, for the Instagram application is 634 ms, for the Gmail application is 758 ms and for Facebook is 814. Also, the average execution time for the whole policy is 818 ms.

Fig.8, shows the different policies execution times according to the complexity for each policy. All calculations and testes where repeated several times to ensure accuracy. As a result, we have noticed that as more the policy becomes complex the execution time becomes bigger.

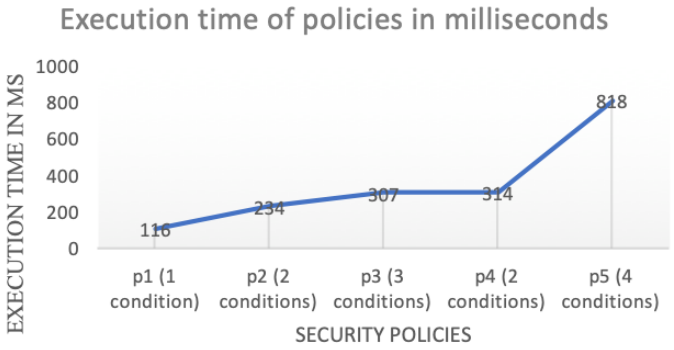


Figure 8: Policies execution times

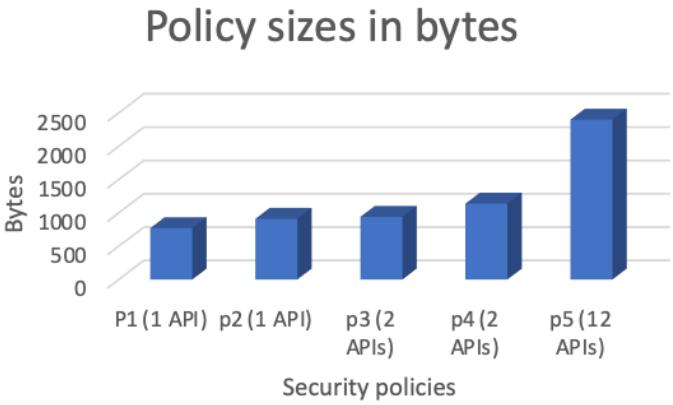


Figure 9: Policies sizes according to their complexities

### 6.3. Policy Size

The policy size is also changing due to the complexity of the applied rules and conditions. We have calculated the policy

sizes on the list of 109 enforced applications. Also, we took the same fife scenarios and their security policies mentioned above in the previous section to make our simulation. Fig. 9 shoes the progression of policy sizes according to their complexities.

## 7. Conclusion and Future Work

This work addressed problems related to context aware policies for Android applications as its one of the main targets of attackers. We, therefore developed CAPEF, which is a policy specification framework that enforces context-aware inter-app security policies to effectively describe users defined consents. Thorough experiments we have performed a study on the efficiency of CAPEF with respect to the size and execution time of the enforced applications. The evaluation results demonstrated the feasibility of our framework and the effectiveness of our policy specification language in enforcing complex context-aware policies on different Android applications.

In the future, we are planning to improve our model using different ML techniques for varying IoT smart environments. Furthermore, we will implement a security framework that is capable of data security and access control by encrypting all sensitive data and making it available only for the authorized service providers according to the pre-defined context-aware policies.

## References

[1] J. Maring, "Android central", Online[Access 12/07/2022] urlhttps://www.androidcentral.com/google-removed-over-700000-malicious-apps-play-store-2017, 2018.

[2] I. Rathore, "Google gets rid of these 16 apps having millions of downloads", Online[Access 15/09/2022] https://dazeinfo.com/2022/10/25/ google-removes-apps-that-have-affected-20-million-android-users-worldwide/, 2022.

[3] "Android developers", Online[Access 02/01/2022]urlhttps://developer.android.com /guide/topics/manifest/ manifest-intro.

[4] V. Arena, V. Catania, G. La Torre, S. Monteleone, F. Ricciato, "Securedroid: An android security framework extension for context-aware policy enforcement", "Privacy and Security in Mobile Systems (PRISMS), 2013 International Conference on", pp. 1–8, IEEE, 2013, doi:10.1109/PRISMS.2013.6927185.

[5] M. Nauman, S. Khan, X. Zhang, "Apex: extending android permission model and enforcement with user-defined runtime constraints", "Proceedings of the 5th ACM symposium on information, computer and communications security", pp. 328–332, 2010, doi:10.1145/1755688.1755732.

[6] Y. Zhou, X. Zhang, X. Jiang, V. W. Freeh, "Taming information-stealing smartphone applications (on android)", "International conference on Trust and trustworthy computing", pp. 93–107, Springer, 2011, doi:10.1007/978-3-642-21599-5_7.

[7] P. Hornyack, S. Han, J. Jung, S. Schechter, D. Wetherall, "These aren't the droids you're looking for: Retrofitting android to protect data from imperious applications", "Proceedings of the 18th ACM Conference on Computer and Communications Security", CCS '11, p. 639–652, Association for Computing Machinery, New York, NY, USA, 2011, doi:10.1145/2046707.2046780.

[8] D. Feth, A. Pretschner, "Flexible data-driven security for android", "Software Security and Reliability (SERE), 2012 IEEE Sixth International Conference on", pp. 41–50, IEEE, 2012, doi:10.1109/SERE.2012.14.

[9] R. Xu, H. Saidi, R. Anderson, "Aurasium: Practical policy enforcement for android applications", "21st USENIX Security Symposium (USENIX Security 12)", pp. 539–552, USENIX Association, 2012, 21st USENIX Security Symposium ; Conference date: 08-08-2012 Through 10-08-2012.

[10] J. Jeon, K. K. Micinski, J. A. Vaughan, A. Fogel, N. Reddy, J. S. Foster, T. Millstein, "Dr. android and mr. hide: Fine-grained permissions in android applications", "Proceedings of the Second ACM Workshop on Security and Privacy in Smartphones and Mobile Devices", SPSM '12, p. 3–14, Association for Computing Machinery, New York, NY, USA, 2012, doi:10.1145/2381934.2381938.

[11] B. Davis, B. Sanders, A. Khodaverdian, H. Chen, "I-arm-droid: A rewriting framework for in-app reference monitors for android applications", *Mobile Security Technologies*, vol. 2012, no. 2, p. 17, 2012.

[12] B. Davis, H. Chen, "Retroskeleton: Retrofitting android apps", "Proceeding of the 11th Annual International Conference on Mobile Systems, Applications, and Services", MobiSys '13, p. 181–192, Association for Computing Machinery, New York, NY, USA, 2013, doi:10.1145/2462456.2464462.

[13] P. von Styp-Rekowsky, S. Gerling, M. Backes, C. Hammer, "Idea: Callee-site rewriting of sealed system libraries", J. Jürjens, B. Livshits, R. Scandariato, eds., "Engineering Secure Software and Systems", pp. 33–41, Springer Berlin Heidelberg, Berlin, Heidelberg, 2013.

[14] X. Zhang, A. Ahlawat, W. Du, "Aframe: Isolating advertisements from mobile applications in android", "Proceedings of the 29th Annual Computer Security Applications Conference", ACSAC '13, p. 9–18, Association for Computing Machinery, New York, NY, USA, 2013, doi:10.1145/2523649.2523652.

[15] P. Pearce, A. P. Felt, G. Nunez, D. Wagner, "Addroid: Privilege separation for applications and advertisers in android", "Proceedings of the 7th ACM Symposium on Information, Computer and Communications Security", ASIACCS '12, p. 71–72, Association for Computing Machinery, New York, NY, USA, 2012, doi:10.1145/2414456.2414498.

[16] S. Shekhar, M. Dietz, D. S. Wallach, "Adsplit: Separating smartphone advertising from applications", "Presented as part of the 21st USENIX Security Symposium (USENIX Security 12)", pp. 553–567, 2012, doi:10.48550/arXiv.1202.4030.

[17] M. Zhang, H. Yin, "Efficient, context-aware privacy leakage confinement for android applications without firmware modding", "Proceedings of the 9th ACM Symposium on Information, Computer and Communications Security", ASIA CCS '14, p. 259–270, Association for Computing Machinery, New York, NY, USA, 2014, doi:10.1145/2590296.2590312.

[18] Y. Falcone, S. Currea, "Weave droid: aspect-oriented programming on android devices: fully embedded or in the cloud", "Proceedings of the 27th IEEE/ACM International Conference on Automated Software Engineering", pp. 350–353, 2012, doi:10.1145/2351676.2351744.

[19] O. Riganelli, D. Micucci, L. Mariani, "Controlling interactions with libraries in android apps through runtime enforcement", *ACM Trans. Auton. Adapt. Syst.*, vol. 14, no. 2, 2019, doi:10.1145/3368087.

[20] M. Alhanahnah, Q. Yan, H. Bagheri, H. Zhou, Y. Tsutano, W. Srisa-An, X. Luo, "Dina: Detecting hidden android inter-app communication in dynamic loaded code", *IEEE Transactions on Information Forensics and Security*, vol. 15, pp. 2782–2797, 2020, doi:10.1109/TIFS.2020.2976556.

[21] M. Grace, M. Sughasiny, "Behaviour analysis of inter-app communication using a lightweight monitoring app for malware detection", *Expert Systems with Applications*, vol. 210, p. 118404, 2022, doi:https://doi.org/10.1016/j.eswa.2022.118404.

[22] A. Developers, "Preparing for the android privacy sandbox beta", Online[Access 15/12/2022]urlhttps://android-developers.googleblog.com/2022/11/preparing-for-android-privacy-sandbox-beta.html , 2022.

[23] R. S. Sandhu, E. J. Coyne, H. L. Feinstein, C. E. Youman, "Role-based access control models", *Computer*, vol. 29, no. 2, pp. 38–47, 1996, doi:10.1109/2.485845.

[24] OASIS, "Oasis extensible access control markup language (xacml)", Online[Access 02/05/2017]urlhttp://www.oasis-open.org/committees/xacml, 2011.

[25] W. Enck, P. Gilbert, S. Han, V. Tendulkar, B.-G. Chun, L. P. Cox, J. Jung, P. McDaniel, A. N. Sheth, "Taintdroid: An information-flow tracking system for realtime privacy monitoring on smartphones", *ACM Trans. Comput. Syst.*, vol. 32, no. 2, 2014, doi:10.1145/2619091.

[26] W. Zhou, X. Zhang, X. Jiang, "Appink: Watermarking android apps for repackaging deterrence", ASIA CCS '13, p. 1–12, Association for Computing Machinery, New York, NY, USA, 2013, doi: 10.1145/2484313.2484315.



**SAAD INSHI** is currently pursuing his PhD in software engineering from École de technologie supérieure, University of Quebec, Montreal, Canada and completed his MASc degree in Information Systems Security from Concordia University, Montreal.

His research interests includes Android and IoT Privacy and security. He is also interested in Context aware privacy and security of devices.

**MAHDI ELARBI** has completed Masters from École de technologie supérieure, University of Quebec, Montreal, Canada. He is currently working as a senior Software Developer in Montreal.

His research interests includes Android and IoT security.

**RASEL CHOWDHURY** is pursuing his PhD in software engineering and completed his MSc degree in Information Technology Engineering from École de technologie supérieure, University of Quebec, Montreal, Canada.

His research interests includes Cloud Computing, Cloud Native orchestration, security and privacy of IoT, IoE and IoV.

**HAKIMA OULD-SLIMANE** is currently a professor at the Département de Mathématiques et d'Informatique, Université du Québec à Trois-Rivières, Trois-Rivières, Canada. She obtained her Ph.D. degree in Computer Science from Laval University, Québec, Canada.

Her research interests include mainly: information security, cryptography, preserving data privacy in smart environments, reliability of collaborative computing and formal methods.

**CHAMSEDDINE TALHI** is currently a Full Professor with the Department of Software Engineering and IT, École de Technologie Supérieure, University of Quebec, Montreal, Quebec, Canada.

He is leading a research group that investigates efficient security mechanisms for smartphone, IoT, edge and cloud infrastructures. His current research interests include cloud native telco services management and security, DevOps security, and federated learning for mobile cloud and IoT.

Received: 10 November, 2022, Revised: 03 January 2023, Accepted: 04 January 2023, Online: 28 January, 2023

DOI: https://doi.org/10.55708/js0201003

# A Tunable Dual-mode SIW Cavity Based Bandpass Filter with Wide Upper Stopband Characteristics

**Md. Atiqur Rahman*, Pankaj Sarkar**

Department of Electronics & Communication Engineering, School of Technology, North-Eastern Hill University, Shillong, 793022, India
*Corresponding author: Md. Atiqur Rahman, +91-7005468917 & atiqurece@gmail.com

**ABSTRACT:** A new approach to design a bandpass filter using substrate integrated waveguide (SIW) topology is presented here for 5G applications. The aim of the design is to produce a dual mode passband characteristic with wide upper stopband behaviour, centred at 4.7 GHz. Four identical Stepped Impedance Resonator (SIR) slots are etched into the top surface of the SIW cavity for the proposed filter structure. The SIR slots aid in reducing the cavity's resonant frequency and to generate the dual mode passband characteristics. The SIR slots also mitigate the higher modes in the SIW cavity which helps to accomplish a wide upper stopband response. In order to improve selectivity, the structure is further modified by introducing two E shaped resonator slots on the ground plane to produce two transmission zeros at 3.9 GHz and 6.2 GHz. Tunable characteristic is achieved by loading two surface mount varactor diodes diagonally on the top of the proposed structure. By suitably applying the bias voltage, the center frequency of the passband is tuned over a range of 600 MHz. The developed filter is fabricated in order to verify the simulated and measured results.

**KEYWORDS:** Substrate Integrated Waveguide Cavity, Bandpass Filter, Stepped Impedance Resonator slot, E-Shaped Resonator, Wide upper stopband, 5G Application.

## 1. Introduction

Substrate Integrated Waveguide (SIW) technology has attracted a great deal of attention in the research community due to its advantages such as low cost, light weight, ease of fabrication, minimal radiation loss, and good power handling. As a result, SIWs have demonstrated their viability as an innovation and continue to have significant potential as a crucial component of planer microwave circuits, such as highly selective filters, Voltage-Controlled Oscillators (VCOs) and antennas [1-3]. In [4], a compact SIW filter is reported with an E-shape slot etched on the topmost surface to reduce the filter's resonant frequency. In [5], a SIW bandpass filter is made using double-sided loading approach defective ground structure (DGS) bandpass filter (BPF). SIW based bandpass filter based on upper stopband performance are reported in [6-7].

One of our very recent developments shows the utilization of SIR slots on the SIW cavity to develop the dual-mode BPF [8]. A HMSIW doublet was created by employing the rectangular cavity's $TE_{102}$ and $TE_{301}$ modes as resonant, and $TE_{101}$ as a non-resonant mode reported in [9]. Several SIW-based tunable filter has been investigated by various researchers [10-12]. A tunable SIW dual mode dual-band filter using perturbing metalized via hole at the middle of the cavity is reported in [10]. In [11] a constant bandwidth highly selective tunable dual-mode BPF is investigated. A stub-loaded capacitor tunable dual-band HMSIW has been reported in [12].

In this manuscript, analytical and synthesis procedure is presented to implement the dual mode BPF for n79 band (4.4-5.0 GHz) of 5G New Radio (NR) application [13]. A rectangular cavity is designed in conjunction with four SIR slots to lower the resonating frequency. Additionally, two shaped-shaped resonators are introduced in the ground plane in order to improve the selectivity, and the upper stopband characteristic of the proposed filter. Finally, the proposed structure is tuned by loading two surface-mounted varactor diodes with two capacitors diagonally. For the design purpose, 1.00 mm thick FR4 substrate is employed. EM simulation is performed using CST Microwave Studio.

## 2. Filter Design

Top and the bottom views of the proposed tunable dual-mode SIW-based BPF are displayed in Figure 1(a) and Figure 1(b).

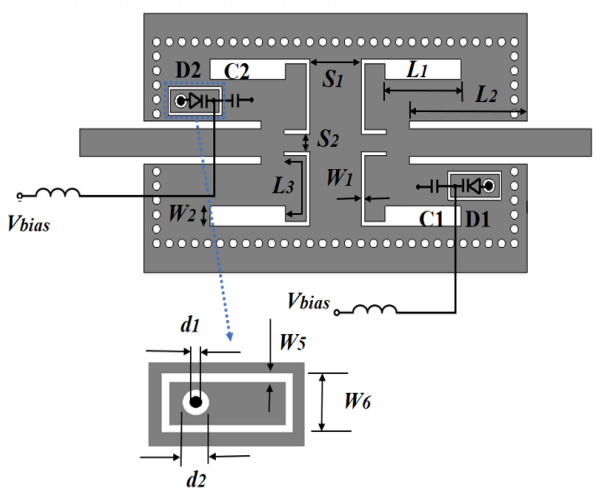


(a)

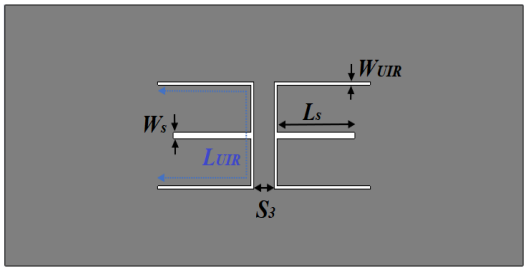


(b)

Figure 1: Proposed tunable bandpass filter layout and necessary tuning arrangements (a)Top view with $L_1$=7, $L_2$ =9.2 , $L_3$ =9.3 ,$W_1$=0.3 ,$W_2$=1.4 ,$S_1$=5.6 , $S_2$=1.2, $L_4$= 4.2, $W_5$= 0.2, $W_6$= 2, $d_1$= 0.6, $d_2$= 1.0 (*all dimensions in mm*). (b) Bottom view with $L_S$=6.1, $L_{UIR}$=21.6, $W_S$=0.3, $W_{UIR}$=1.4, $S_3$=5.6 (*all dimensions in mm*).

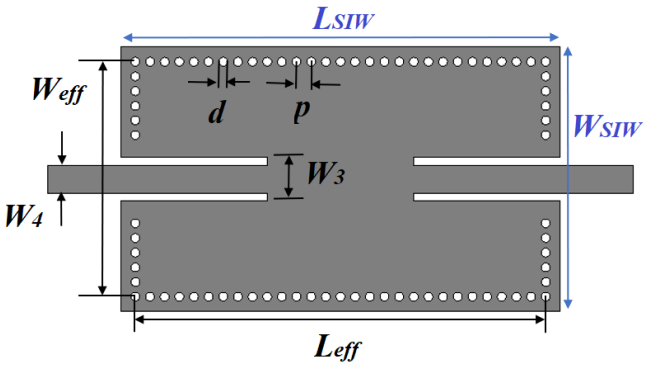


(a)

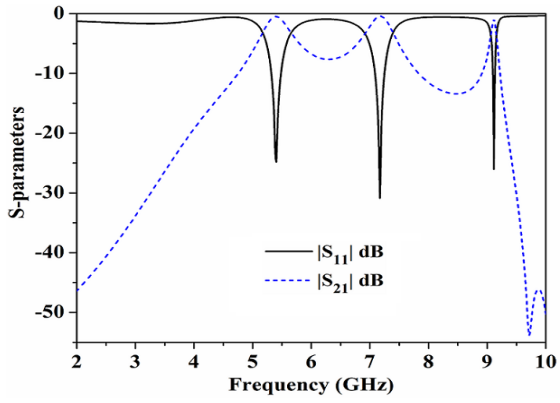


(b)

Figure 2: (a) SIW cavity layout with $L_{eff}$= 28, $L_{SIW}$= 30, $W_3$=3, $W_4$=1.9, $W_{eff}$ = 14, $W_{SIW}$ =16, $p$=1, $d$ = 0.6 (*all the dimensions in mm*). (b) SIW cavity's simulated S-parameters.

As shown in Figure 2(a), a SIW cavity is initially designed. The fundamental frequency of resonance of the proposed cavity is designed at 5.3 GHz [1]. The cavity resonance is kept a little high to minimize the area requirement. In Figure 2(b) the S-parameters of the simulated SIW cavity are illustrated. It can observe that the fundamental frequency of the resonator is 5.3 GHz. Up to 10 GHz, there are two spurious frequencies centered at 7.1 GHz and 9.1 GHz.

On top of the SIW cavity, stepped impedance resonators (SIRs) are placed to achieve dual-mode features and mitigate spurious frequency ranges. Inset in Figure 3 highlights the open-ended SIR's configuration. The SIR is made up of electrical sections $Z_1$ and $Z_2$ with corresponding electrical lengths of $\theta_1$ and $\theta_2$, and high and low impedance portions $Z_1$ and $Z_2$, respectively. An essential factor in modifying the SIR features is $R_Z$ = ($Z_2/Z_1$). The SIR input admittance is derived as:

$$Y_{in} = jY_2 \frac{Z_2 + Z_1 \cot\theta_1 \tan\theta_2}{Z_1 \cot\theta_1 - Z_2 \tan\theta_2} \quad (1)$$

The resonance condition is determined considering $Y_{in}$=0. Figure 3 plots the ratio of normalized first spurious frequency ($f_1$) and fundamental frequency ($f_0$) for various impedance ratios ($R_Z$), to easily extract the design parameters. To achieve the dual mode characteristics, fundamental resonant frequency is maintained at 4.5 GHz. The first spurious of SIR is predicted to be at 10.8 GHz, for a spurious free response up to 10 GHz. For fundamental frequency and the first spurious , the SIR has an impedance ratio of 0.57. $Z_2$ has a 60 Ω impedance, and its corresponding electrical length, $\theta_2$ is 68$^0$. The high impedance section's computed impedance $Z_1$ is 113Ω with an electrical length of 88$^0$. The dimensions of low impedance part has 7 mm in length, 1.4 mm in width, and for high impedance part are 9.3 mm and 0.3 mm, respectively.

Finally, the topmost surface of the cavity is etched with the SIR structure. For symmetry reasons, four SIRs are etched into the SIW cavity as, displayed in the inset of Figure 4(a). The classical filter design methods are adopted [14] to meet the design specification for n79 band (4.4-5.0 GHz), of 5G New Radio (NR). The circuit's coupling coefficient ($k$) and external quality factor ($Q_e$) components of a prototype lowpass filter is determined in order to develop the proposed filter. The $Q_e$ and $k$ for any designed filter can be calculated as provided in [13]. Figure 4(a) shows the $Q_e$ and $k$ for different separations $S_1$. It can be observed that the higher value of $Q_e$ can be obtained by increasing the $S_1$. The value of $k$ can also be significantly controlled by $S_1$. It can be inferred that the higher value of $k$ can be achieved by reducing $S_1$. To facilitate the design procedure, the value of $Q_e$ and $k$ is required to find for the

proposed filter. For the required passband from 4.4 GHz to 5.0 GHz the value of $Q_e$ is 10.2 whereas the calculated value of $k$ is 0.075. To accomplish the required $Q_e$ and $k$ the $S_1$ is determined to be 4.2 mm. The value of $S_1$ is revised further and selected to be 4.0 mm.

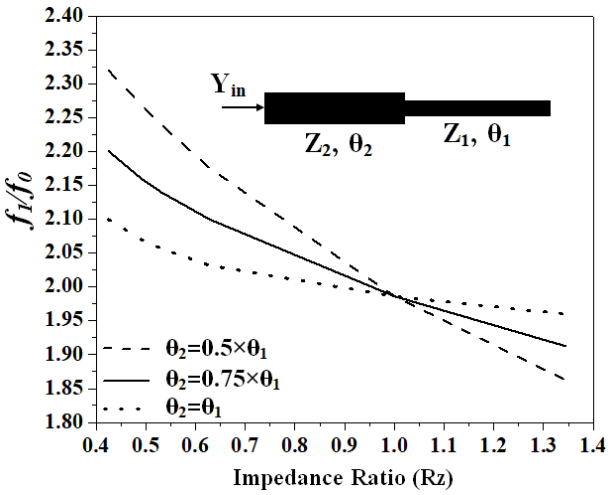


Figure 3: Ratio of first spurious to fundamental frequency vs impedance ratio plot of SIR.

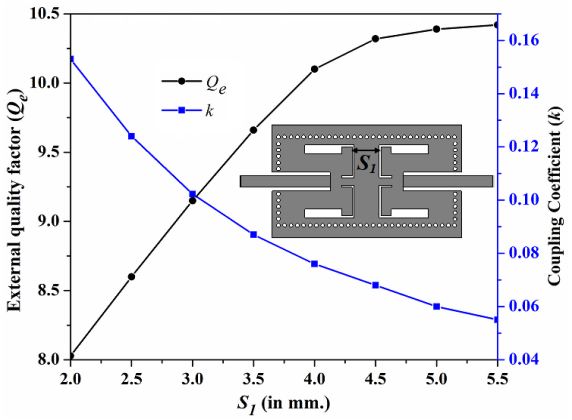


(a)

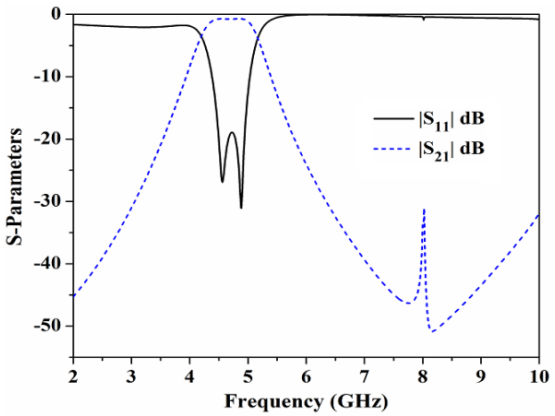


(b)

Figure 4: (a) For various values of $S_1$, the coupling coefficient ($k$) and the external quality factor ($Q_e$). (b) The dual mode filter's frequency response employing SIR slots.

Figure 4 (b) depicts the simulated filter S-parameters. It is clear that the suggested filter results in a dual-mode characteristic with a passband ranging from 4.4 GHz upto 5 GHz. Through the passband, the $S_{21}$ is better than -0.3 dB and the $S_{11}$ value is less than -19.0 dB. Additionally, it can be seen that the SIR's presence suppresses the spurious bands. The upper stopband response is satisfactory with attenuation levels greater than 30 dB are achieved up to 10 GHz.

Figure 4(b) inferred that the selectivity of the filter is poor. Therefore, to increase the selectivity, two E-shaped resonators are introduced in the ground plane. The basic -shaped stub structure is displayed in inset of Figure 5. A uniform impedance resonator (UIR) with electrical length $\theta_{UIR}$ and admittance $Y_1$ is used to realize the resonator. A stub of electrical length $\theta_S$ and admittance $Y_S$ is loaded into the center of the resonator. The input admittance is derived as follows for even and odd modes.

$$Y_{in,\,odd} = -jY_1\cot(\theta_{UIR}/2) \tag{2}$$

$$Y_{\text{in, even}} = jY_1\frac{Y_S\tan(\theta_S)+2Y_1\tan(\theta_{UIR}/2)}{2Y_1-Y_S\tan(\theta_S)\tan(\theta_{UIR}/2)} \tag{3}$$

The resonance condition can be determined by setting $Y_{in,odd}$=0, and $Y_{in,even}$=0. Resonating modes $f_o$ and $f_e$ are extracted by assuming $Y_1$=Ys/2. Figure 5 shows the normalized odd and even modes of resonant frequency for different values of $L_R$ and $L_S$. The E-shaped resonator is designed to form two modes at 4.0 GHz and 6.0 GHz. From the plot, it can be observed that the $f_o$ is fully depends on $L_R$ whereas the $f_e$ can be controlled by $L_R$ and $L_S$. The calculated value of $L_R$ and $L_S$ is tuned further to improve the performance. The resonating frequencies are chosen to improve the selectivity. For $L_R$ and $L_S$, optimal values are 10.5 mm and 6.0 mm, respectively. In order to generate a considerable degree of attenuation at the appropriate frequency, the inter-resonator spacing ($S_3$) is adjusted.

### *2.1. Reconfigurable Bandpass Filter Design*

In order to achieve the tunable characteristics, the proposed dual-mode BPF is loaded with two surface-mounted varactor diodes diagonally. Figure 1 depicted the proposed tunable bandpass filter where two SMV (1232-079LF and two DC blockers (C0603C330K5RACTU) are used. The anode terminal of the varactor diode is connected to the ground using a metallic post. The cathode terminal is landed on a rectangular island where bias voltage is applied. The diodes D1 and D2 are connected to the cavity through the two DC blockers C1 and C2 respectively. Through a 27 nH inductor, the bias voltage is applied to the varactor diode.

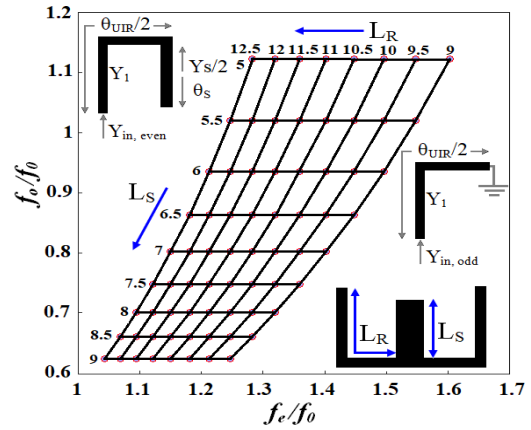


Figure 5: Normalized even and odd mode resonating frequencies for different values of $L_R$ and $L_S$.

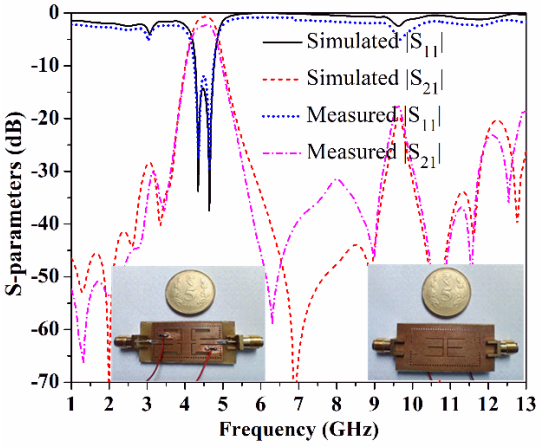


(a)

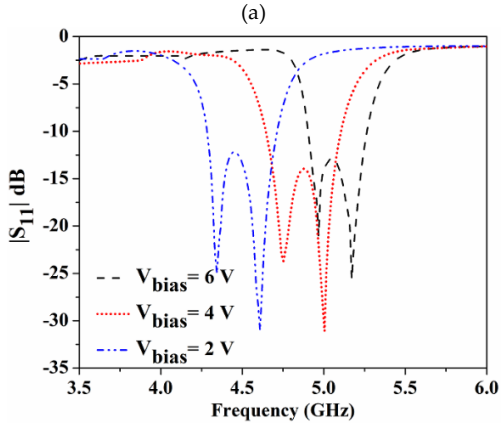


(b)

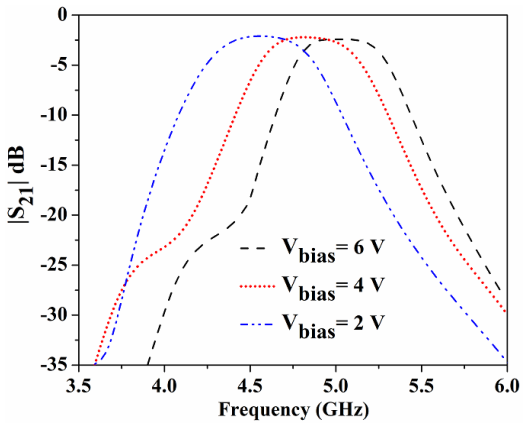


(c)

Figure 6: (a) Comparison of the proposed filter's S-parameters as simulated and measured. S-parameters simulations at various bias voltages (b) $|S_{11}|$ dB (c) $|S_{21}|$ dB.

## 3. Measured Results and Discussion

The fabricated prototype is displayed in Figure 6(a) as inset. The EM-simulated and measured S-parameters are compared in Figure 6(a). It can be seen that with the bias voltage $V_{bias}$=3V, the proposed filter gives a measured passband from 4.42 to 5.03 GHz. The measured $S_{11}$ is less than -12.0 dB throughout the passband, while the measured $S_{21}$ is better than -2.1 dB. Further observations include the suppression of spurious bands and the presence of two transmission zeros at frequencies of 3.85 GHz and 6.35 GHz. This improves the selectivity of the proposed filter. Three more number of transmission zeroes can be observed at 10.8 GHz, 11.7 GHz, and 12.6 GHz which increases the stopband range. More than 17 dB attenuation level is witnessed up to 13 GHz. Figure6(b) and 6(c) shows the $|S_{11}|$ and $|S_{21}|$ simulated results of the proposed tunable bandpass filter. By varying, the bias voltage of the varactor diode, which ranges from 2 to 6 V, the filter's center frequency can be tuned. Where can be observed, the passband center frequency can be moved from 4.5 GHz to 5.1 GHz as the reverse bias voltage rises. Over a bandwidth of 600 MHz structure is tuned. Throughout the tuning range, $S_{11}$ is below -12 dB, and the $S_{21}$ is better than -2.1 dB with excellent selectivity. Overall size of the filter is 30×18 mm². A comparative analysis is presented in Table 1 with previously published works. It can be observed that the proposed filter has better insertion loss compared to the work reported in [9] and [12]. The proposed filter has accomplished better stopband range and better fractional bandwidth compared to the filters presented in [7], [9], [10] and [12]. The filter structure exhibits a compact size compared to the filter reported in [7], [9] and [10]. The skirt factor, which is defined as the ratio of the passband's 3 dB bandwidth to its 20 dB bandwidth, is presented in order to explain selectivity. The skirt factor is 0.44 for the proposed filter which better compared to the filters presented in [7], [9], [10] and [12].

## 4. Conclusion

This manuscript presents a novel tunable dual-mode bandpass filter using SIW cavity. Etching SIRs into the top surface of the SIW cavity results in the dual-mode passband and a wide upper stopband performance. E-shaped resonators in the ground plane improve the selectivity. The resonating structures are properly analyzed and the resonating frequencies are determined. The tunable characteristic is achieved by employing two varactor diodes with good return loss and wide tuning range. The filter has compact size, low insertion loss, excellent selectivity, and wide upper stopband characteristics which are useful for modern communication systems.

Table 1: Performance comparison with some SIW based bandpass filter

| Ref. | Response | Tunable | Center Frequency ($f_0$ GHz) | FBW (%) Fractional Bandwidth | RL(dB) Return Loss | IL(dB) Insertion Loss | Skirt Factor | Stopband frequency (a× $f_0$) | Stopband attenuation (dB) | Size ($\lambda_g \times \lambda_g$) ($\lambda_g^2$) |
|---|---|---|---|---|---|---|---|---|---|---|
| [7] | SIW BPF | No | 13/13.2 | 4.6/4.5 | 15/10 | 1.7/1.5 | 0.4/0.35 | ($2f_0$) /($2.2 f_0$) | 20/20 | 0.9316 |
| [9] | Dual-Mode BPF | No | 10 | 5.3 | 18 | 2.4 | 0.34 | 1.05 $f_0$ | 30 | 1.75 |
| [10] | Dual-mode Dual-Band BPF | Yes | 17/19.36 | 2.01/4.1 | 17 | 2.1/1 | 0.38/0.18 | ($1.05f_0$) /($1.13 f_0$) | 20/20 | 2.62 |
| [12] | Dual-Band BPF | Yes | 2.25/4.5 | 13.33/8.8 | 15/17 | 2.33/3.38 | 0.25/0.25 | ($1.42f_0$) /($1.33 f_0$ | 20/20 | 0.04 |
| This work | Dual-Mode BPF with wide upper stopband characteristics | Yes | 4.7 | 14.89 | 12 | 2.1 | 0.43 | (2.85 $f_0$) | 17 | 0.44 |

$\lambda_g$ is the guided wavelength derived at the passband's center frequency passband, RL stands for Return Loss, IL for Insertion Loss, and FBW for Fractional Bandwidth.

## References

[1] D. Deslandes and K. Wu, "Single-substrate integration technique of planar circuits and waveguide filters," *IEEE Transactions on Microwave Theory and Techniques*, vol. 51, no. 2, pp. 593-596, 2003, doi: 10.1109/TMTT.2002.807820.

[2] A. Parameswaran and S. Raghavan, "Novel siw dual mode band pass filter with high skirt selectivity," *2nd International Conference for Convergence in Technology (I2CT)*, 2017, pp. 189-191, doi: 10.1109/I2CT.2017.8226118.

[3] M. Almalkawi, M. Westrick, V. Devabhaktuni, M. Alam, L. Zhu and J. Deng, "Design of a dual-band dual-mode substrate integrated waveguide filter with symmetric transmission zeros," *IEEE Applied Electromagnetics Conference (AEMC)*, 2011, pp. 1-3, doi: 10.1109/AEMC.2011.6256872.

[4] H. Zhang, W. Kang and W. Wu, "Miniaturized Dual-Band SIW Filters Using E-Shaped Slotlines With Controllable Center Frequencies," *IEEE Microwave and Wireless Components Letters*, vol. 28, no. 4, pp. 311-313, 2018, doi: 10.1109/LMWC.2018.2811251.

[5] S. Xu, K. Ma, F. Meng and K. S. Yeo, "Novel Defected Ground Structure and Two-Side Loading Scheme for Miniaturized Dual-Band SIW Bandpass Filter Designs," *IEEE Microwave and Wireless Components Letters*, vol. 25, no. 4, pp. 217-219, 2015, doi: 10.1109/LMWC.2015.2400916.

[6] S. Wang, D. Zhang, Y. Zhang, L. Qing and D. Zhou, "Novel Dual-Mode Bandpass Filters Based on SIW Resonators under Different Boundaries," *IEEE Microwave and Wireless Components Letters*, vol. 27, no. 1, pp. 28-30, 2017, doi: 10.1109/LMWC.2016.2629963.

[7] D. Jia, Q. Feng, Q. Xiang and K. Wu, "Multilayer Substrate Integrated Waveguide (SIW) Filters With Higher-Order Mode Suppression," *IEEE Microwave and Wireless Components Letters*, vol. 26, no. 9, pp. 678-680, 2016, doi: 10.1109/LMWC.2016.2597222.

[8] M. A. Rahman and P. Sarkar, "A Novel Compact Dual-Mode Substrate Integrated Waveguide Cavity based Bandpass Filter for WLAN Applications," *International Conference on Computational Performance Evaluation (ComPE)*, 2020, pp. 059-061, doi: 10.1109/ComPE49325.2020.9200038.

[9] F. Zhu, G. Q. Luo, Z. Liao, X. W. Dai and K. Wu, "Compact Dual-Mode Bandpass Filters Based on Half-Mode Substrate-Integrated Waveguide Cavities," *IEEE Microwave and Wireless Components Letters*, vol. 31, no. 5, pp. 441-444, 2021, doi: 10.1109/LMWC.2021.3066569.

[10] M. F. Abbas, and A. J. Salim, "A New Tunable Dual-Mode Dual-Band Square Cavity SIW Bandpass Filter," *Progress In Electromagnetics Research C*, vol. 118, pp. 113-123, 2022, doi:10.2528/pierc21120306

[11] M. Abdelfattah, R. Zhang and D. Peroulis, "High-Selectivity Tunable Filters With Dual-Mode SIW Resonators in an L-Shaped Coupling Scheme," *IEEE Transactions on Microwave Theory and Techniques*, vol. 67, no. 12, pp. 5016-5028, 2019, doi: 10.1109/TMTT.2019.2944365.

[12] C. X. Zhou, C. M. Zhu and W. Wu, "Tunable Dual-Band Filter Based on Stub-Capacitor-Loaded Half-Mode Substrate Integrated Waveguide," *IEEE Transactions on Microwave Theory and Techniques*, vol. 65, no. 1, pp. 147-155, 2017, doi: 10.1109/TMTT.2016.2613053.

[13] 5G NR specifications, document TS 38.101-1 V15.4.0 3GPP Release15, Dec. 2018.

[14] J. S. G. Hong, and M. J. Lancaster, "*Microstrip filters for RF/microwave applications*,"John Wiley & Sons, 2004.



**Md. Atiqur Rahman** received his B.Tech degree in Electronics and Communication Engineering from North Eastern Hill University-Shillong in 2015 and M.Tech degree in Electronics and Communication Engineering from North Eastern Hill University-Shillong in 2017. Presently he is pursuing his Ph.D. from North Eastern Hill University- Shillong. His research interest lies in the area of microwave passive circuit design, antenna. Several of his conference papers received the best paper award.

**Pankaj Sarkar** received his M.Tech degree from Burdwan University and Ph.D. from Jadavpur University in the year of 2009 and 2016, respectively. He worked one year in Space Applications Center-Ahmedabad as a trainee for M. Tech project entitled as "Design of MMIC Mixer at 50-60 GHz". He initiated his teaching carrier from ITER (Siksha "O" Anusandhan University-Bhubaneswar), after that he served Sikkim Manipal Institute of Technology and National Institute of Technology-Sikkim. Presently he is an Assistant Professor in Electronics and Communication Engineering Department of North-Eastern Hill University (A Central University)-Shillong.

He has more than 50 publications in various National/International journals and conferences. He is the reviewer of various journals such as IEEE Transactions on Microwave Theory and Techniques, IEEE Transactions on Industrial Electronics, IEEE Microwave and Wireless Components Letters, Electronics Letters, IET Microwaves, Antennas and Propagation, Progress in Electromagnetics Research (PIER), Microwave and Optical Technology letters and so forth. His research interest lies in the area of microwave passive circuit design, metamaterials, MMIC, antenna. He has been a member of various program committee for several international conferences. He chaired various technical session for the international conferences.

Received: 30 December, 2022, Revised: 06 February 2023, Accepted: 07 February, 2023, Online: 22 February, 2023

DOI: https://doi.org/10.55708/js0202002

# Applied Salt Technique to Secure Steganographic Algorithm

**Bo Bo Oo***

Edinburgh Napier University, School of Computing, Edinburgh, EH10 5DT, UK

*Corresponding author: Bo Bo Oo, +44 77 7863 0269, bobooo.1249@gmail.com

**ABSTRACT:** Digital multimedia assets, including photographs, movies, and audio files, have become a staple of contemporary life. Steganography is a method for undetectable information concealment in these files. One can communicate messages to another by modifying multimedia signals so that a human would be unable to tell the difference between the original signal and the altered one. The widespread use of digital data in practical applications has prompted the development of new and efficient methods for ensuring its security. Steganographic techniques can be used to, at least in part, achieve efficient secrecy. There have been suggested new and adaptable audio steganographic techniques. By using cryptography, readable language is converted to unintelligible data. In order to send and receive text, multimedia, or other important digital files safely, this paper discusses secure communication media. To have secure communication tools, the tools must lessen potential risks and weaknesses. Therefore, the primary factor to take into account for creating a solid communication system is transferred media. The objective of steganographic systems is to find a secure and reliable method to hide a significant amount of secret data. This research focuses on digital image audio steganography, which has become a popular method for data concealment.

**KEYWORDS:** Steganography & Cryptography, Secure communication media, Salt Encryption, AES, Steganography with SHA-256

## 1. Introduction

In order to share information across many geographies through digital communication, a number of new technologies are constantly developing. Information can sometimes include user privacy, confidential data, and other sensitive material that needs to be segregated. Secure communication media should be used to communicate this information. Even if a crucial piece of information is given to a person who is acting strangely, unforeseen events that could result in dangerous situations could still happen. Therefore, this information is shielded from corruption or breach by a malevolent hacker using the data concealing approach. The majority of data concealment techniques use steganography, cryptography, and digital watermarking.

The message should first be encrypted using a secure cryptographic procedure before being encoded using the steganography algorithm. In that case, not even steganographic algorithms can simply decode the message. The message will be converted into ciphertext, rendering it unintelligible to attackers. The algorithms used in cryptography methods are numerous. In essence, key management infrastructure is used. To improve the encryption algorithm, symmetric and asymmetric cryptographic key management approaches are used. To confirm that the sender and receiver are the authorised users, the symmetric key is originally provided with both parties. Steganography doesn't really make message authentication better. To protect messages for visual detection from sender and receiver, numerous encryption techniques are used.

The mechanism through which steganography and cryptography will interact to create secure media is being developed in this secure communication medium. Additionally, steganalysis will be used to find stego-objects in developed material using a variety of analysis tools and evaluation results from various hashing techniques. Python programming will be used to carry out the implementation. This study will outline an improvement strategy for using secure media to transmit private information.

## 2. Related work

### 2.1. Steganography

Frequency domain and spatial domain are the two main domains that can be utilised to identify data embedding in image processing that uses pixels, according to an analysis of steganography techniques. The measurement of image quality and quantity distinguishes the two domains most proposed in [1]. Quantity is determined by using image sensitivity. Based on the results of the peak signal to noise ratio (PSNR) or the structural similarity index metric, the quality measure is examined (SSIM). Based on the results of bits per pixel, the quantity measurement is examined. In addition to these two, imperceptibility and robustness are important considerations. Robustness is the ability to clearly degraded modified image from partial attacks to lose data integrity. The human eye can detect significant changes that point to the existence of embedded data. The study of this perceptible is referred to as imperceptibility. Using bit numbers, the spatial domain integrated the simple text into the cover image.

In LSB methods, bit numbers of the message are substituted for the image's least significant bits. There will be 3 bytes for red, green, blue, and alpha when decomposing the pixel (RGBA). There are 8 bits in each byte, and one byte is used to represent each colour. The least significant bit (LSB) for each byte is the one on the right, while the most significant bit (MSB) is the one on the left (MSB). An image with an RGB value of 800x600 pixels can hold up to 180,000 bytes for embedding explained in [1].

#### 2.1.1. Image Steganography

The use of a picture as a cover to conceal a message is known as image steganography. The image can be used with a variety of image formats, including Portable Network Graphics (PNG), Bitmap (BMP), and Joint Photographic Experts Group (JPEG) (PNG). The JPEG image format compression is a popular format for lowering the size of the image described in [2]. Using an image as compression enables you to maintain aesthetic characteristics that are still evident. Since the human naked eye cannot breakdown the veiled information contained within the cover image, this information is difficult for humans to see.

#### 2.1.2. Audio Steganography

A steganographic method called Audio Steganography involves encoding data using an audio-based file structure. Waveform Audio (WAV), Audio (AU), and MPEG Audio Layer III are all acceptable audio file formats (MP3). It is extremely difficult to embed the message in audio, however many different methods have been tried. An enhanced least significant bit modification technique for audio steganography shows large amounts of data can be compressed using audio, and it is difficult to hack in [3]. However, maintaining an audio signal becomes more challenging as more data are encoded. It primarily serves to safeguard digital copyright.

### 2.2. Cryptography

Encryption and decryption are the two main operations involved in cryptography. private information is transformed into bizarre, cryptic text with a variety of odd marks in order to prevent unauthorised access. It's called encryption. The output of encryption is referred to as ciphertext, which is difficult to decipher visually. Decryption is the process of converting this ciphertext back to plaintext (the original text). It is not possible to restore the ciphertext to plaintext using some cryptographic methods. The cryptography technique is carried out in these two operations using the key exchange infrastructure. The plaintext is converted to a cypher using a pseudorandom key or user-defined key, which is then utilised again during the decryption process. These three techniques are hash functions, symmetric cryptography (public-key cryptography), and asymmetric cryptography (secret-key cryptography). These three techniques are frequently used to send messages more securely in [4].

#### 2.2.1. Asymmetric cryptography

Asymmetric cryptography, also known as public-key cryptography, uses two different kinds of keys: public and private. Public key infrastructure, digital signature, channel security, and tamper detection are the main applications for public key. A digital signature is used to confirm the message's validity and provide proof that it originated with the sender. Additionally, it has the capacity to confirm the non-repudiation and data integrity. The signature enables the sender to notify the recipient if the encrypted communication is changed or expanded upon described in [5]. Plaintext, ciphertext, an encryption method, a decryption algorithm, a private key, and a public key are the different parts of a public key infrastructure.

#### 2.2.2. Symmetric cryptography

Symmetric cryptography, also referred to as secret-key cryptography, encrypts and decrypts data transformations using a single common key that is passed into a mathematical formula. Secret-key cryptography is used specifically to improve the privacy and confidentiality of data.

AES is a symmetric encryption method since it employs the same key for both both encryption and decryption. Additionally, it employs numerous rounds of the SPN (substitution permutation network) method to encrypt data. The impenetrability of AES is a result of

these encryption rounds, which are impossible to break through due to their sheer number in [6]. The United States National Institute of Standards and Technology (NIST) developed the Advanced Encryption Standard (AES) as a specification for the encryption of electronic data in 2001. Despite being more difficult to build, AES is still commonly used because it is substantially stronger than DES and triple DES. Three key lengths—128 bits, 192 bits, and 256 bits—are used in the AES encryption and decryption process. For, a fixed block length of 128 bits is used. For 128-bits, 192-bits, and 256-bits, AES uses 10, 12, and 14 rounds, respectively.

#### 2.2.3. *Hash Function*

One of the cryptographic methods that enables the complete transformation of the plaintext to the given varied fixed number is the hash functions. Digesting is the term for this transformation process. The hash functions do not need keys. Fundamentally, hash functions are used in digital signatures, password security enhancement, random number creation, and message authentication. The one way is another name for it explained in [4]. For instance, the message "Hello" is encrypted using the MD5 cryptographic hash function technique. "Hello" will result in a digest message of 128 bits rather than 16 bytes. The result will be 128 bits when another plaintext "World" message is similarly encrypted in that manner (16bytes).

Table 1: MD5 Hash Table

| Plaintext | Hash value (MD5) | Output size |
|---|---|---|
| Hello | 8b1a9953c4611296a827abf8c47804d7 | 128 bits (16bytes) |
| World | f5a7924e621e84c9280a9a27e1bcb7f6 | 128 bits (16bytes) |
| Hello World | b10a8db164e0754105b7a99be72e3fe5 | 128 bits (16bytes) |

There are hundreds of different hashing algorithms available, and each one is tailored for a certain sort of data, speed, security, etc. Secure Hashing Algorithm, or SHA. There are two variants of the algorithm: SHA-1 and SHA-2. They differ in the bit-length of the signature as well as in creation (how the resultant hash is made from the original data). The National Institute of Standard of Technology released SHA (NIST). The hash value produced by FIPS 180-4 SHA can be MD. It generates a higher hash value than MD, is faster, and is more secure than MD. The output of SHA is a hash value of 160 bits (20 bytes) with 20 rounds.

As a hashing algorithm response to developing BCrypt assaults, SCrypt was developed. SCrypt is used in many software programmes to implement the protection against password cracking. For the purpose of generating the peak time for password processing, SCrypt uses a specific amount of their hardware resources in their farm. However, employing a specific amount of memory allows you to restrict an attacker's capacity to find passwords using high-tech gear. SCrypt is used to strengthen the encryption algorithm based on the findings.

### 2.3. *StegAnalysis*

The method known as steganalysis aims to counter steganography by locating the concealed data and extracting or erasing it. For law enforcement organisations, it becomes essential to decipher the communication or at the very least render it useless to the recipient, as is the case with nearly all such approaches. Through steganalysis, the primary attribute of a stego-object is analysed based on its robustness, capability, and imperceptibility. The steganalysis is carried out in the steganography studio to look at the detection of images that show the presence or absence of steganographic information using various algorithms and various image format types in [7]. In order to identify the cover image, steganalysis is performed using server tools like Openpuff and Steganography Studio. Visual analysis (examining with human visual abilities to perceive the existence of information) and statistical analysis (examining of modification in statistical properties to the images). To improve security assessments, steganalysis can be researched on cutting-edge technologies like artificial intelligence, neural networks, fuzzy logic, and genetic logic by extracting data more thoroughly through statistical qualities as a progressive digital forensic.

## 3. Proposed System

In steganography, there are three main cover file formats that are utilised. They are steganography for audio, steganography for video, and steganography for images. Data steganography in audio and video is a very dedicated approach because even little changes can cause significant noise affects. This had a negative impact on the original quality and greatly affected the capacity of the human visual system (HAS) and human auditory systems (HVS). HAS is more sensitive than HVS when compared to each other. In order to see the variations in noise in an image file, you must look at it in great detail for a few seconds. The development of communication medium is more adaptable and trustworthy when using image and audio steganography. The effectiveness of audio steganographic techniques is influenced by a number of factors. Each feature's significance and effect vary depending on the application and the transmission environment. The durability to noise, compression, and signal manipulation, as well as security and the ability to hide concealed data, are among the most crucial characteristics shown in [8]. The robustness criteria is the

most difficult to meet in a steganographic system when paired with data hiding-capacity because it is closely related to the application.

The most practical approach based on the spatial domain is called least significant bit (LSB). The image is broken up into a large number of pixels as part of the spatial domain process. A pixel has 24 bits in total. Red, blue, and green are represented by each 8-bit colour. The least significant bit of these three values is used in the LSB algorithm's processing. The first step of the method is to read the image and transform it into image pixels. The message is then transformed into a bit as well. The LSB of the picture is used to replace the message bits to create the stego-image. The image is not lost when the LSB is changed, and great perceptual transparency is supported. As a result, these changes are not easily visible to humans. In order to hide data, several image steganography programs alter bits using the least significant bit (LSB) technique. In low resolution pictures with 8-bit colour, changing the LSB could cause a noticeable shift in the colour palette, making it simple to spot hidden material. Another sign that there is hidden information present in an image is padding or cropping. The Hide-and-Seek tool can only be used to create fixed-size graphics.

## 4. Methodology

By using data hiding techniques on the communication carrier, the process can be divided into two primary parts: encryption and decryption. There will be two actors while employing a communication carrier: a sender and a receiver. Before sending the carrier, the sender must complete the encryption process. The system needs three user inputs for the encryption method: a cover image, a message, and a secret key. Stego-object as well as a shared secret key are needed for decryption. the symmetric communication mechanism that uses encryption. The sender must enter the secret and message into the system in order for symmetric communication to flow.

Utilizing the LSB approach, steganography and cryptography are combined in this system. The entered file is chosen as an audio file in this system. After that, the communication is encrypted using just one secret key. The Image Steganography and cryptography are also combined as different mechanism for encryption and decryption. Both systems are suggested and employ the LSB algorithm to conceal the message in communication media. Utilizing various essential communication networks has its benefits. Depending on the user's decision during encryption, the stego-object can be either an image or an audio file.

The AES algorithm first converts the secret key into a hash digest value. The salt will be generated prior to hashing the AES in order to combine the secret key. This procedure is only used in one-way operation. The hash value cannot be converted back to its original form and cannot be used to determine the secret key's value.

The hash value and encrypted message are base64

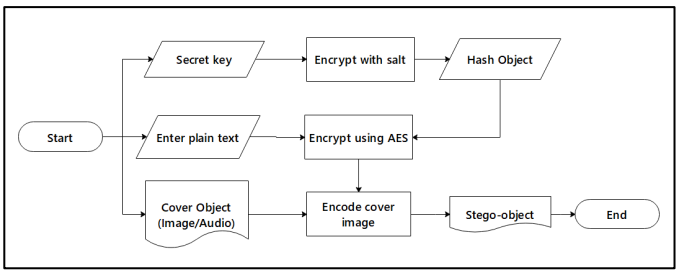


Figure 1: Encryption Algorithm

encoded into unintelligible ciphertext. The cover object is additionally mixed with the ciphertext using the LSB steganography algorithm. The ciphertext of the encrypted communication is converted to binary format. First, an RGBA format conversion is performed on the cover image. These binary-formatted data are also converted to hexadecimal form. By using a delimiter, the modified binary value of the message is inserted into the hexadecimal format value of the cover image. The system will return the cover image as the stego-image to deliver the message over communication media to the recipient once all of the transform values have been fully included into the cover image.

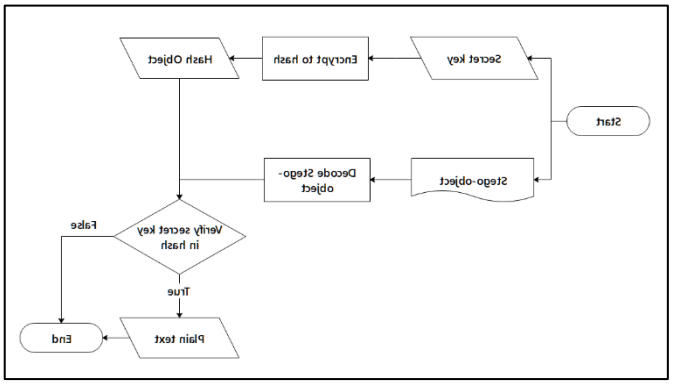

Figure 2: Decryption Algorithm

On the other side, High data embedding capacities are possible with the LSB method, which is also reasonably simple to use alone or in combination with other hiding methods. This method's limited resistance to noise addition, which makes it susceptible to even straightforward attacks, lowers its security performance. The data will probably be lost if the stego-audio is filtered, amplified, has noise added to it, or is compressed using lossy techniques. Without impacting the perceived transparency of the stego audio signal, it has extended the depth of the embedding layer from the fourth to the sixth and eighth LSB layers to improve the robustness of the LSB approach against distortion and noise addition. The other bits can be switched to create a new sample that is more similar to the original in order to reduce embedding error.

The communication carrier (stego-object) is extracted on the recipient side using a shared key. The stego-object is initially broken down into an acceptable format by identifying a delimiter to recreate the binary data. By converting to binary, these hexadecimal values are retrieved back into plaintext. The system begins ciphertext decryption once the ciphertext has been successfully obtained. There is a password verification function that must be passed through in order to acquire the original message prior to the decryption of the ciphertext. The system extracts the salt from the ciphertext before encrypting the newly entered password from the receiver and converting it to a hash value. The system then compares the newly created hash value to the other hash value that was derived from the stego-object. The generated hash must be verified in order to ensure that the password is valid. The system unpads the result and sends the message to the recipient after the ciphertext has been decrypted.

The suggested steganography system's encryption and decryption procedures are shown in the diagram below. The encryption procedure for both audio and image steganography requires the cover file, password, and secret message in order to produce a new stego-image. The application simply needs a password and stego-object to decrypt data.

```
(app) G:\My Drive\Master course\Napier MSc Computing\Advanced Software Development\Final\app\App>py stego.py

Select the type of steganography:
1)Audio Steganography
2)Image Steganography
3)exit

Your Choice:2

1)Encyption
2)Decryption
Your Choice:1
Enter a new password:
Enter a message to hide: This is a secrect message.

Starts Image Encyption..
Enter name of the image file (with extension): test_image.jpg
 >>>>> Succesfully encoded inside stego_test_image.jpg
```

Figure 3: Encryption Process

```
(app) G:\My Drive\Master course\Napier MSc Computing\Advanced Software Development\Final\app\App>py stego.py

Select the type of steganography:
1)Audio Steganography
2)Image Steganography
3)exit

Your Choice:2

1)Encyption
2)Decryption
Your Choice:2
Enter password:

Starts Image Decryption..
Enter name of the image file (with extension): stego_test_image.jpg
This is a secrect message.
```

Figure 4: Decryption Process

## 5. Experimental Results

The two techniques from the data hiding techniques will be used to produce the secure stego-object. The evaluation of each method will be done separately from this implementation of data concealing strategies. For the steganography, the evaluation will be performed on the changes of stego-object and original cover object.

The system's performance is controlled by the local host machine: Storage: 1TB HDD with read/write speeds of 100 MB/s, CPU Processor: Intel(R) Core (TM) i7-7500U CPU @ 2.70GHz, 2901 Mhz, 2 Core(s), and Operating System: Windows 10 Pro 64 bit As a result, utilising this local machine, the results of both encryption and detection with cryptography are acquired.

As a result of the changes in their pixel construction and attributes, the difference between the original cover image and stego-object is compared. These outcomes were acquired using the output characteristics of https://www.textcompare.org/image/. Size in bytes, dimension, bit depth, horizontal resolution, and vertical resolution are all aspects of an image's attributes. Bit depth is the term used to describe the colour information stored in an image. The image can store more colour values due to the huge number of bit depth values. The measurement of pixel density, known as horizontal and vertical resolution, is typically expressed in dots per inch (dpi). A 1-inch square has a grid of pixels that is 72 pixels wide by 72 pixels high when a picture has a resolution of 72 dpi. Changes in size, bit depth, and horizontal and vertical resolution can be seen in these findings. Comparing the stego-picture to the cover image, the size has risen. Then the bit depth increased by roughly 8 and both stego-object resolutions were displayed at 96 dpi.

The bytes that will be embedded in the cover picture will be located initially from the above and stored until the final hiding with the pink areas, based on the results of the difference in images. The only way to see these allocations is by employing a tool for comparing and contrasting.

The steganalysis is performed to investigate the presence of the encrypted message. In this steganalysis, the stego-object are used to detect with several steganography. The detection process is performed with decoding the stego-image into text information.

Table 2: Steg-analysis Tools Table

| No. | Steg-analysis Tools | Detection Results |
|---|---|---|
| 1. | Stegdetect | Failed |
| 2. | Mcafee Steganography Defense Initiative | Failed |
| 3. | Steghide | Failed |
| 4. | Steganography Online | Failed |
| 5. | VSL | Failed |

The difference between the cover image and the stego image is being compared in this experiment's results. The test is carried out using Guiffy Image Diff (11.11). The highlighted portion of the stego-object showed a small discrepancy between the stego-image and the original image. The secret data is totally encrypted after starting at the beginning of the image and being put in that highlighted bit.

Figure 5: Original Image

Figure 6: Stego-Image

Figure 7: Image Difference between Original Image and Stego-image

Audio steganography is used on fixed LSBs to determine the point at which the difference between the host message and stego message may be heard. Every sample of the host message's fixed bits is replaced with bits from the secret message without employing the randomness suggested in Bit Selection and Sample Selection. In this following, it is simpler to conceal the existence of noise or secret data. A frequency study of the same data, however, makes it clear that there is foreign data in the media. The main goal of the suggested approach was to keep noise levels low by minimising the disparity between original audio and stego audio. There is no discernible difference between the stego signal and the original signal, even after stegano-manipulation.

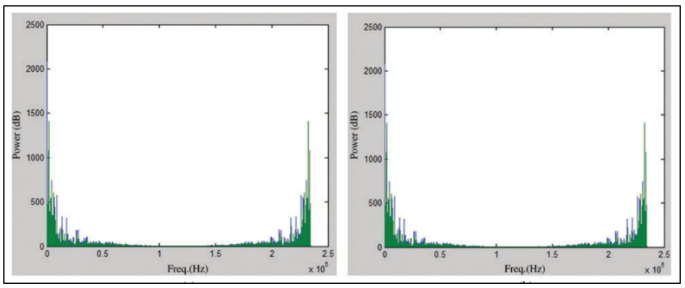


Figure 8: Comparison between Original Audio and Stego-audio

## 6. Conclusion

The system that was put into place had benefits for protecting communication medium thanks to data-hiding algorithms. With base 64 encoding and the SHA-256 hashing technique, the message and secret key can be compressed thanks to the robust security of AES encryption. Utilizing the most recent hashing algorithm development raises the security level of password authentication. Controlling the resilience and lowering the level of suspicion in a visual attack on a carrier using LSB. The techniques based on audio steganography primarily work with audio and spoken signals for a protective communication. While evaluating these techniques, the key steganographic characteristics of capacity, security, and resilience are taken into account. The difference image in the performance section shows the modifications and differences between the original and the stego-image. Because of the LSB approach and base64 encoding, the final output size does not vary even when a significant quantity of data is inserted into the cover image.

## Acknowledgment

I would like to thank my Supervisors at Edinburgh Napier University, for her kind support throughout this research process.

## Conflict of Interest

The authors declare no conflict of interest.

## References

[1] P. Rajkumar, R. Kar, A. K. Bhattacharjee, H. Dharmasa, "*A Comparative Analysis of Steganographic Data Hiding within Digital Images*," International Journal of Computer Applications, vol. 53, no. 1, pp. 1–6, 2012, doi:10.5120/8382-1981.

[2] V. Lokeswara Reddy, Dr.A. Subramanyam, Dr.P. Chenna Reddy, "*Stegnography Rajarao Kaviliga Related papers Implementation of LSB Steganography and its Evaluation for Various File Formats*," J. Advanced Networking and Applications, vol. 868, , pp. 868–872, 2011.

[3] M. Asad, J. Gilani, A. Khalid, "*An enhanced least significant bit modification technique for audio steganography*," Proceedings - International Conference on Computer Networks and Information Technology, pp. 143–147, 2011, doi:10.1109/ICCNIT.2011.6020921.

[4] G. Kessler, "*An Overview of Cryptography (Updated Version 24 January 2019)*," Publications, 2019.

[5] D.S.Abdul. Elminaam, H.M.A. Kader, M.M. Hadhoud, "*Performance Evaluation of Symmetric Encryption Algorithms on Power Consumption for Wireless Devices*," Undefined, pp. 343–351, 2009, doi:10.7763/IJCTE.2009.V1.54.

[6] Rūta Rimkienė, *What is AES Encryption and How Does It Work? | Cybernews*, https://cybernews.com/resources/what-is-aes-encryption/, 2022.

[7] Y. JinaChanu, Kh. Manglem Singh, T. Tuithung, "*Image Steganography and Steganalysis: A Survey*," International Journal of Computer Applications, vol. 52, no. 2, pp. 1–11, 2012, doi:10.5120/8171-1484.

[8] F. Djebbar, B. Ayad, K.A. Meraim, H. Hamam, "*Comparative study of digital audio steganography techniques*," Eurasip Journal on Audio, Speech, and Music Processing, vol. 2012, no. 1, pp. 1–16, 2012, doi:10.1186/1687-4722-2012-25/FIGURES/12.



**Bo** received his BSc in Hons Computing from Edinburgh Napier University and is currently pursuing his MSc in Computing from the same university. Additionally, he is attending Contemporary Technology University for an MSc in Computer Science (Data Science and Applied Artificial Intelligence). His research interests include Data Analytics and Wrangling, Scripting for Cybersecurity and Networks, Software Security and cryptography.

Received: 01 December 2022, Revised: 01 February 2023, Accepted: 07 February 2023, Online: 22 February 2023
DOI: https://dx.doi.org/10.55708/js0202003

# Blockchain Tokens for Agri-Food Supply Chain

**Ricardo Borges Dos Santos**[*,1], **Rodrigo Palucci Pantoni** [2], **Nunzio Marco Torrisi**[1]

[1]UFABC, Center of Mathematics, Computing and Cognition, Federal University of ABC, Campus São Bernardo do Campo, São Paulo 09606-070, Brazil
[2] Department of Eletrical Engineering and Computer Science, Federal Institute of São Paulo, Campus Sertãozinho, São Paulo 14169-263, Brazil
[*]Corresponding author: Nunzio Torrisi, nunzio.torrisi@ufabc.edu.br

**ABSTRACT:** The aim of this research is to suggest and analyze a framework to give universal publicity to food properties certificates from any certification authorities. The focus is the certification of agro product instances, i.e. unique for every single harvest, using smart contracts and blockchain non fungible tokens minted by third-party authorities. The development and testing of a set of smart contracts used the newly established ERC-1155 Ethereum token standard to implement Non-Fungible Tokens (NFT)s. The ERC-1155 tokens allow for representing both the uniqueness, thus non-fungibility, between different harvests as well as the quantitative elements within a specific harvest, e.g. mass fractions of product from the same harvest, which can be interchanged, thus fungible. The framework was developed, deployed, and tested on the Ethereum test net blockchain and submitted to extensive testing. The blockchain data is accessible through general-purpose block scanners and can be read through an Android App used by regular consumers during a supermarket visit. The goal is to give consumers easy access to the Third-party Certificates (TPC) URLs available at the public Ethereum blockchain. The benefit for food safety of widespread TPC visibility through web applications can not be underestimated, since the use of blockchain tokens controlled by smart contracts injects trust in the traceability of the merchandise, reducing counterfeiting and green-washing. The broadcasting of the TPCs with the corresponding discipline of tokens transfer and smart contact restriction to possible abuses increases agro-food supply chain transparency. Trust and transparency foster sustainable buying habits by many consumers and transparency in the complete production and distribution links.

**KEYWORDS** Third Party Certification, Smart Contracts, Non-Fungible Tokens, Food Certification, Blockchain

## 1. Introduction

In 1990, the Organic Foods Production Act (OFPA) established standards for agricultural producers of commodities that claimed to use organic methods. The methods, practices and substances used in agricultural practice, including sowing; growing; and harvesting; as well as handling crops and processed agricultural products, restrict the wording on the product labels and marketing. Since OFPA, the US consumer has been continuously increasing demand for certified organic foods brands that claim to use organic production processes. Nevertheless, these organic farm certification methodologies have shown limitations and criticism: the authors of [1] conclude that the "current regulatory framework is not only inadequate to the task of regulating domestic organics, but also incapable of ensuring the integrity of imported organics. Thus, the USDA Organic seal misleads consumers.".

### 1.1. Justification

Several studies have recently claimed that the certification of products holds great beneficial potential, such that [2]: "Product certification is one of the most promising and developed instruments to reward the socially and environmentally friendly practices of market producers".

Third-party certification (TPC) differs from first and second-party certification mainly because the third-party authority that issues the certificate has no interest in the transaction. A TPC involves an "independent Organisation with expertise to provide an assessment and verification of the company's compliance with standards or legal requirements" [3].

TPC can be very useful to ascertain product physical, chemical, or organoleptic properties and is allowing bolder certification of social, environmental, and sustainability properties. According to the work in [4]: "TPC also offers opportunities to create alternative practices that are more socially and environmentally sustainable".

Although the farming procedures may be certified according to criteria such as quality, sustainability, or social fairness, there is no form of ensuring that certification of the typical farming methods, such as USDA Organic certification methodology, avoids specific harvests being stained by malpractices such as agrochemical exposure or used hidden child labor.

Each harvest of a specific crop is unique. The difference may lie in the seeds used for that particular season or in the total hours of sunshine in that specific location during the crop's growth.

One good example is the wine industry, where consumers know that the time and the different weather conditions between harvests of different years even from the same farm will influence the wine quality. Organoleptic tests of wine produced from grapes of different years and locations evidence these differences. The wine counterfeit problem can be summarized as avoiding that larger quantities of more valuable wine from grapes harvested on better years or regions reach retail than the volume actually produced. This fraud is academically known as the mass balance [5] or the double spending problem [6] and has a negative impact on the luxury goods business as it can hurt the reputation of premium brands. This fraud also hurts products that are geographically traceable to a specific region, i.e., reserved by local laws under the protected designation of origin (PDO) concept.

### *1.2. Related Work*

The work in [7] provides a comprehensive overview on the application of blockchain technology to agri-food value chains. These are in line with the work in [8] which concludes that the use of blockchain technology can improve sustainability from social, environmental, and market perspectives. Recent literature [9] presents a blockchain-enabled supply chain architecture to ensure the availability of a tamper-proof audit trail for foods free of COVID-19 contamination Further [10] conducts an extensive literature review on the integration of blockchain into traceability systems. Discussion on a blockchain strategy to trace organic food products is presented in [11]–[12] . Attempts to use less costly distributed data structures such as the interplanetary File System (IPFS) for food traceability are discussed in [13]. These and other articles are convergent in stating that blockchain tools are possibly the most appropriate technologies to meet the various requirements the rapidly expanding food value chains such as traceability, auditability, fault tolerance, and flexibility [14]–[15]. Research on certification using blockchain [16]–citecreydt2019blockchain has also evolved with many interesting sustainability findings and efforts.

Nevertheless, no research has been found where harvests are recognized as being unique, thus their yield not interchangeable between different harvests. This approach, where the produce or yield of the different harvests are not interchangeable except within the same harvest, leads this research to use Non-Fungible Tokens (NFT) of the type ERC-1155.

### *1.3. Proposed Solution*

It is proposed to use Ethereum-based tokens and smart contracts pointing to TPC certificates for keeping track of certificates for individual harvests of each farm. In this manner, we show that it is possible to track the exact origin and quantity of each harvest from farm to consumer, offering the benefits of TPC available to the last links of the chain. Practical economic incentives to the chain participants are described allowing for effective productive usage. The focus is on information availability, reliability, synchronization to the physical flow of goods, and, above all, ensuring good publicity of the certificate at the consumer level.

This research paper is structured as follows. Section 2 presents relevant concepts and literature of traceability, blockchain, smart contracts, and distributed ledger technology (DLT) and the Ethereum-based non-fungible token (NFT). Section 3 discusses the requirements and implementation of a token passing TPC framework using the ERC-1155 token smart contracts and analyses the results obtained. Section 5 presents the conclusions pinpointing the research's main contributions and limitations.

## 2. Blockchain Key concepts applied to Certification

A chain of transactions, organized into cryptographically linked blocks, could, for the first time, reach a consensus, even within a (limited) number of unreliable (traitor) nodes. For a more detailed description of the data structures involved see in [17, 18]. Albeit the eventually synchronized nature of the protocol and possible temporary partitions in the network, the linear block of data is re-established after a partition and regains consistency and availability.

Consistency of distributed data within a predetermined time frame is achieved, avoiding the double spending [6] of the digital asset.

The technology behind blockchain successfully implements consistency and access discipline for collaborative data in a diffuse globally distributed accessible trustless environment. The consistency achieved by the underlying data structures and control mechanisms with validation through the consensus of third party validators or miners shows that this technology is an important step towards supply chain transparency and traceability data [19]–[20].

A blockchain is a cryptographically auditable, append-only, tamper-resistant, distributed and replicated data structure, accessible to anyone employing a web browser.

Blockchain can store proof of structured data as well as methods or programs to process this data according to deterministic program steps known as smart contracts. Blockchains require no central trust mechanism, thus there exists no central point of failure. The main strengths of Blockchain Technology (BCT) are listed below.

- Tamper resistance, i.e., cryptographic hashes to previous block, in practice, make it impossible to change data that has been recorded;
- Pseudo-anonymity, i.e., data are available publicly but encoded through hashed keys that allow for trust on the existence and on the authorship;
- Distributed presence, i.e., the data structures are replicated maintaining several copies with no single point of failure and keeping integrity between data sets;
- Software-driven, i.e., the Blockchain mechanism does not require human privileged operators to maintain the transactions, thus the system is not prone to bribery;

- Allows for certification of the tamper-proof storage of off-chain data by means of side blockchain. These are hierarchically hash-certified sub-database that can store larger volumes of data, including multimedia, and provide evidence and tools for more detailed analysis.

Ethereum [21] expanded the concept of the blockchain to distributed ledger technology by including tokens and programs called smart contracts that are executed independently of human intervention. These are open-source, human-readable high-level programs that are stored on the blockchain and run inevitably, without any human intervention, strictly as implemented thus avoiding any risk of downtime, censorship, or fraud [22]. The Ethereum Virtual Machine implements "unstoppable" and "unavoidable" Turing-complete computer processes. Smart contracts use open-source code and are developed to establish standard behavior between blockchain stakeholders and other contracts. They allow for extensive development and precise control, ensuring transparency of each data manipulation and thus trust. Digital blockchain tokens are capable of representing object properties, assets, or rights that have strict transactional behavior and ownership. The execution of smart contracts is immune to any human interference and therefore allows for transparent systematic transactions. Tokens can be used to represent supply chains, intellectual properties, voting, or identity management systems, among other objects. The associated smart contracts assure discipline to the corresponding state transitions of token balances and thus generate trust to the parties without a trusted third party thus no single point of failure. This assures transparency and prevents possible "double-spending" frauds in the certification system.

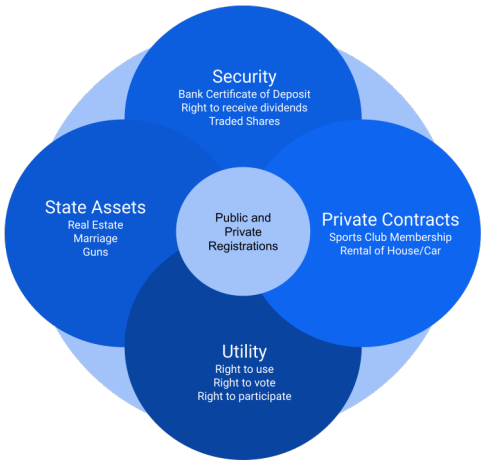


Figure 1: Families of assets and rights according to registration requirements.

### 2.1. *Digital Tokens*

Tokens are digital objects that represent specific rights or assets. They should be understood as assets that can be negotiated or used as guarantees. Note that the necessary and sufficient condition for full ownership of the balance of the token on a public address is the knowledge of its private key. Figure 1 shows a diagram for most common assets and rights, grouped into families along with their corresponding registration requirements.

The registration of the rights and property of assets, if required by law or regulation, will usually be centralized at a government-trusted centralized database. Because these data are maintained in centralized databases they are prone to corruption, fraud, censorship, downtime, or misuse. On the other hand, distributed registration schemes based on replicated databases, such as distributed ledgers, provide very high availability, are fraud-resistant, are fault-tolerant, and typically cannot be censored. Security and utility assets can reliably be represented, registered, and easily traded as cryptographic tokens. Automated processes through smart contracts allow high availability, low costs of the transaction, full traceability, non-repudiation, and pseudo-anonymity.

In order to be useful, tokens should not be copyable (i.e., should not be prone to double spending attacks) or suffer arbitrary changes. Thus, they need to follow strict discipline at each change of state to usefully represent real-world objects.

The development of digital objects to simulate real-world objects requires that the object's properties and behaviour are modeled through common data structures and coded procedures. Smart contracts manipulating tokens must respect some standard to allow for multiple users and contracts to share functionalities among different applications. Application independence and fungibility of digital objects could be achieved with a minimum set of functionalities. The ERC-20 token fungible objects standards are key to the success of many cryptocurrencies and many Ethereum decentralized applications. Because the ERC-20 token metadata structure holds all relevant property data within the blockchain, they can be freely transferred from one blockchain to another, allowing these to be exchanged for other ERC-20 assets.

It is important to note that like a real estate property record, which entitles the bearer to have full use and ownership of a real estate asset, the possession of a private key of a token on one blockchain entitles that person or smart contract to unrestricted use of that token for payment, exchange, deposit as warrant or collateral, lending or selling this assets at his discretion.

Further, it is important to recognize that objects can be categorized in fungible objects and non-fungible objects. Fungible objects are those that need not be distinguished from one another. The important question here is "How many of these objects?". Non-fungible objects, on the other hand, are those that are distinguishable from similar objects. The decisive question here is "Which of these similar, although unique, objects?"

The distinctive property between fungible and non-fungible tokens is that the former are fully exchangeable and thus can be added, e.g., coins of the same face type and value can be added or subtracted at will. The latter, not being exchangeable, can only be transacted as unique identifiable objects.

A non-fungible token (NFT) is a unique blockchain-based digital entity which can represent a non-fungible object. If this token follows a protocol such as the ERC-1155 or ERC-721, it can be traded as an asset between various stakeholders in possibly multiple applications.

The methods defined in the ERC-1155 standard assure consistent behavior, transparency, no double spending, and a verifiable auditable trail to families of similar, yet unique, objects. An ERC-1155 compliant NFT has one identifier that points to a specific URL, in which typically all properties and details are described. Additionally, an overview of these main differences is outlined in Table 1 and a numerical characteristic of the ERC-1155 object is also available (https://github.com/ethereum/EIPs/blob/master/EIPS/eip-1155.md accessed on 26 November 2022).

Table 1: Comparison between ERC-721 and ERC-1155 tokens

| | ERC-721 | ERC-1155 |
|---|---|---|
| **Fungible** | N | Y( within same family) |
| **Non Fungible** | Y | Y |
| **Smart Contract** | One instance | Multiple instances |

### 2.2. Harvest TPC Algorithm

For decades, important crops have been traded as commodities. Commodities are intrinsically fungible. Once the product is classified in a certain grade, according to purity, size, or maximum cross-contamination levels, then, the lot is handled as a commodity. Global trading standards and procedures require that a certain measure of a commodity, say, a bushel of a certain grade of wheat, is fully fungible with the same measure of this same commodity, i.e. another bushel of the same wheat grade. However, a specific harvest should be regarded as a unique object. No other harvest possesses the exact same physical, chemical or organoleptic properties, therefore harvests should be handled as non-fungible physical objects. To track this object appropriately, it is necessary to record all relevant data which will individualize and keep the history of that specific harvest product.

Each harvest of a specific crop is unique. The difference may lie in the seeds used during that particular season or in the total number of hours of sunshine in that specific location during the crop's growth.

In several agricultural sectors, especially in the wine trade, expert consumers recognize the crop timing and the different characteristics between harvests of different years even from the same farm. The analysis of the organoleptic properties of the wine produced recognizes differences in the year and location of the harvest of grapes. In the wine sector, the wine counterfeit problem can be summarized as avoiding that larger quantities of more valuable wine from grapes harvested on better years or regions reach retail than the volume actually produced. This fraud is also known as the mass balance problem [5] or double spending [6] and is very deleterious to the business as it can stain the reputation of premium producers. Products that are geographically traceable to a specific region, i.e., reserved by local laws under the protected designation of origin (PDO) concept are also frequently affected by this type of fraud. A harvest TPC mechanism with tamper-resistant certificates which are easily available to any stakeholder via internet devices is very helpful to avoid double spending and can significantly boost trust along the supply chain stakeholders.

Thus, we researched the following main research questions (MQ1) and subsidiary research questions (SQ2, SQ3):

**MQ1:** "Is it possible to establish a harvest TPC mechanism with tamper resistant certificates easily available to anyone, even previously unknown food supply chain stakeholder via public blockchain access?"

**SQ2:** "If a TPC mechanism is possible, who will carry the data input and maintenance costs? In other words, how will each stakeholder be incentivized to use this mechanism?"

**SQ3:** "If a TPC mechanism is possible, what will a typical time of response for a certification query be, in other words what quality of service can be expected by the end consumer?"

To answer the Research Questions MQ1 and the subsequent research questions SQ2 and SQ3 a systematic method was used which involves designing all smart contracts needed, deploying and subjecting them to testing. The test evaluated compliance to functional and non functional design requirements. The procedure is depicted in the Algorithm 1 which shows a step-by-step description of the methodology for harvest TPC validation using a set of 7 smart contracts as a Proof-Of-Concept (PoC).

**Algorithm 1:** Methodology Systematic

```
Result: Write here the result
User Requirements;
while Register Request do
    SmartContract(ProofOfConcept);
    if TPC Authority exist then
        Token Transfer;
        Consumer Tracking Access;
    else
        Evaluate(ProofOfConcept);
    end
end
```

In summary, the algorithm develops a systematic methodology by means of the following steps:

- 1—Elicit and define user requirements (both Functional and Non-Functional).
- 2—Harvest Traceability - Define and Identify Traceable Units - Discipline data collection, i.e., when and what needs to be collected.
- 3—Design and implement proof-of-concept (PoC)—Deploy smart contracts.
- 4a—Analyze if third-party certification authority is capable of issuing tokens easily and transferring them along the Supply Chain Participants.
- 4b—Analyze if a token transfer allows the URL information to be made accessible to the token buyer along the Supply Chain Participants.
- 5—Analyze if consumers can access URL for TPC with internet applications easily, reliably, and fast (MQ1).

- 6—Evaluate PROOF OF CONCEPT and respective results and improve implementation.

Besides the blockchain immutability permit to trace of all the test runs and deployments of the smart contracts. This allows the research methodology and procedures to be easily reproducible and traceable (Examples of blockchain scanners are https://www.etherchain.org/, https: //www.EthPlorer.io or https://www.Etherscan.io accessed on 29 August 2022 ). In other words, both the smart contract source code as well as all the test runs of all tests performed to the PoC can be followed in detail on any browser.

### 2.3. Requirement Analysis

The desired functionalities of the system, i.e., the functional requirements are listed below.

- to allow for farmers to request any third person authority to inspect and certify properties that a specific harvest may have;
- to allow the inspection authority to issue a certificate on any website including quantitative data about the desired property of the yield;
- to allow the authority to create ("mint") tokens, i.e., digital objects representing the harvest and carrying the URL linked to the certificate, representing information about the mass of product inspected (yield);
- to allow these tokens to be "passed on" along the chain of buyers of the product ( yield);
- to allow the buyer that applies the package, wrapper, or label to the food product to write the URL to an easily and freely accessible reliable database and
- to destroy ("burn") , after a predetermined time, these tokens once the food product is consumed, to avoid garbage accumulation or misuse.

As for the nonfunctional requirements, it is important to ascertain that the system satisfies the following:

(a) Universal access: allowing any supply chain participant, even previously unknown, to use the tool without previous registration;

(b) Tamper free auditabilty: enforcing tamper-free, auditable transactions between any parties;

(c) Robustness to faults: allowing the writing to a common persistent information layer in a robust manner;

(d) No double spending fraud: avoiding that token balances are used more than once;

(e) Universal read access: allowing any potential consumer to freely read the certificate by means of an internet device

(f) Interoperability: allowing usage with different systems and devices and

(g) Cost effectiveness: allowing information to be recorded in an inexpensive manner;

(h) Usability: allowing for comfortable user experience.

(i) Quality of Service: guaranteeing that response to a consumer query returns to the requesting device within a short time period;

(j) Scalability: allowing for a much larger number of transactions running within the acceptable quality of service i.e performance.

### 2.4. Persistence Layer Design: Do we need a Blockchain?

If harvests are to be certified for the benefit of the entire chain of potential stakeholders in the food industry, which type of data structure would be required to keep this information useful and trustworthy? Is it necessary to use a blockchain to record and make all relevant information consistently available to all stakeholders?

Figure 2, derived from [23] summarizes a structured approach to optimize the data structure architecture to be used for a specific application. In this case, the particular requirements for the TPC of Harvest in the Food Supply Chain recommend the use of a public permissionless blockchain as the best architecture. The sequence of questions we would ask is:

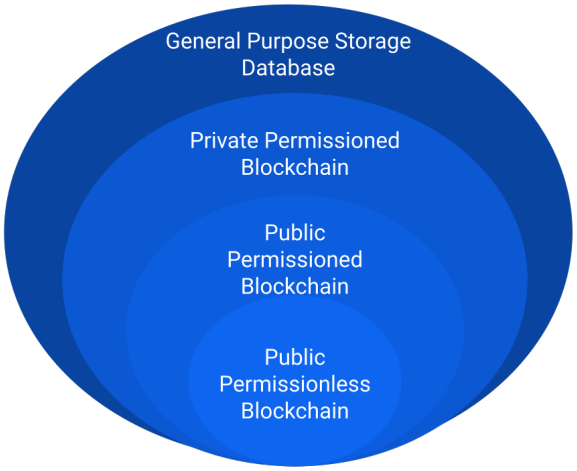


Figure 2: Scale of Requirements to define the type of data persistence layer (database or blockchain)

- Is it necessary to store current State (Current Custodian on Supply Chain)? YES;
- Is a Trusted Third Party available online? NO;
- Is WRITE access needed outside your organization? YES; (because of the possibly many unknown chain participants).
- Are all Writers known? NO.

Thus, the recommended architecture is Public Permissionless Blockchain. Because it is desired that the system maintains allows for new participants to join the supply chain such as new farmers, known farmers with new crops, new mills, new re-sellers, new comminglers or new retailers,

the choice of a permissioned blockchain such as Corda or Hyperledger was discarded[24, 23].

Because Ethereum tokens meet the non-functional requirements (a–i) listed above, the public Ethereum environment with the non-fungible token ERC-1155 standard protocol was chosen. Ethereum also meets all of the non-functional requirements today including (j): scalability.

## 3. Smart Contract Implementation

The smart contract code used for ingredient certification in [25] was modified to implement the non-fungible token (NFT) discipline that better represents each instance of a crop with the use of the ERC-1155 ( https://github.com/enjin/erc-1155 accessed on 29 August 2022 ) objects and methods.

The fully documented source code for all the smart contracts in the Solidity programming language was published in the Ethereum main net where all variables and algorithms are fully commented on and documented. The code was developed, tested, deployed, and made available at https://rinkeby.etherscan.io/address/0x841c5c79d9ae35db8fb4f216a478cd184fdae634#code ( accessed on 4 august 2021). The source code shown in the link is the full smart contract code and is divided as follows: The ERC-1155 standard code and the standard libraries used are shown up to line 772. The specific smart contract code responsible for the application is shown as of line 772 and comprises the following methods:

- *farmerRequestCertificate*- This routine allows for the sale of ingredients along with the respective IGR token transfer
- *certAuthIssuesCerticate*- This routine is used to allow for certification authorities to confirm that ingredients are trustworthy as well as quantity, URL where published, product, details of IGR value property, location, date of harvest).
- *sellsIngrWithoutDepletion* - This routine allows for the simple sale of ingredients along with the respective IGR token transfer ( with URL).
- *sellsIntermediateGoodWithDepletion* - This routine allows for the sale of intermediate products made from certified ingredients along with the respective IGR token transfer ( with URL) i.e.: allows only the pro-rata quantity of semi-processed InGRedient tokens to be transferred.
- *genAddressFromGTIN13date* - This is an auxiliary function to generate an ethereum address for the specific food item visible numbers GTIN-13 + date of validity in format YYMMDD. This is used by the method comminglerSellsProductSKUWithProRataIngred to allow anyone such as e.g. by a consumer with an App or block-scanner to query the exact blockchain address where the certificate URL is stored(Figure 4).
- *transferAndWriteUrl* - This is also an auxiliary routine to transfer the balance from the token owner's account to the 'to' account. Note that the owner's account must have sufficient balance to transfer, that zero value transfers are allowed.
- *comminglerSellsProductSKUWithProRataIngred* - This code allows for the sale of the final-consumer product with resp SKU and Lot identification with corresponding IGR transfer with URL. In other words, it warrants that only the pro-rata quantity of semi-processed InGRedient tokens be transferred to the consumer-level package(SKU)

The smart contract code described can be viewed also as a class UML diagram. Generation of UML class diagrams from published Solidity programming language source code on the Ethereum blockchain can be obtained by an automated functionality of the Etherscan blockchain scanner, as shown in ( https://rinkeby.etherscan.io/viewsvg?t=1&a=0x841c5c79d9ae35db8fb4f216a478cd184fdae634.

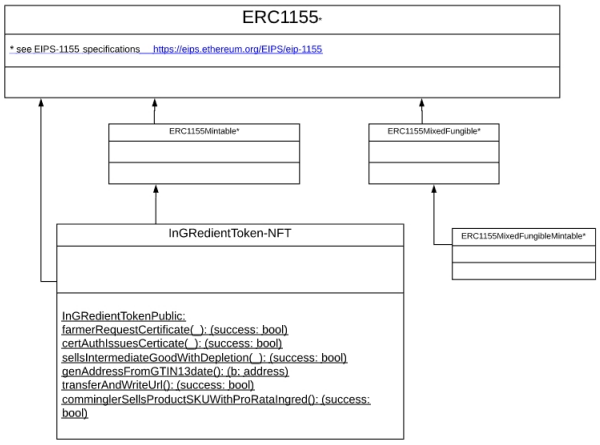


Figure 3: IGR Token class as a dependent class of the ERC 1155 class. ( simplified by author from auto-generated UML class diagram from Etherscan).

## 4. Results and Discussion

A set of public blockchain smart contracts govern the token synchronization framework to positively identify each harvest along the food supply chain to the end consumer.

At each transactional change to the product such as change of custody, mixing, usage, or depletion of the product, tokens are exchanged.

Using a modification of the IGR token set of smart contracts rewritten for ERC1155, in Figure 3, the farmer responsible for the harvest can freely choose the properties to be certified between:

- functional - e.g. minimum size of fruit or grade.
- organoleptic - e.g. color or aroma.
- social - e.g. free of child labor cultures.
- environmental - e.g. "grown in certified no forest devastation areas"or "organic—no xyz herbicide", or non Genetic Modified seeds only.

as well as the appropriate authority that will audit and issue the corresponding certificate for each harvest.

The authority is then invited to audit the farm at harvest time. After the appropriate auditing procedures, including inspection of the farm and qualitative and quantitative evaluation of crop yield, the authority formalizes the audit results by publishing the certificate as a web page at the authority's domain web server.

The link to this certificate, in the form of the URL is part of the minting process. Further, this smart contract will issue the exact number of tokens to match the numerical mass yield of that specific harvest in grams.

Thus the ERC-1155 unified resource identifiers (URL) descriptor will point to the web page containing the full technical details of the certified "consumer-valued properties", including the original mass of goods in grams. The number of IGR tokens issued will represent this specific mass of ingredients.

By using the delegated transfer "setApprovalForAll()" and "safeBatchTransferFrom()" primitive in the smart contracts, it is not possible for the farmer to issue or make first-person claims on the certificate. Only the Authority has this capability, thus enforcing strict true third-person certification (TPC).

Comparing the current approach to the previously published certification using the ERC-20 IGR Ethereum token, the main improvement was to avoid tokens obtained from different harvests, thus with different characteristics, being mixed. The ERC-1155 discipline allows for the farmer to sell part of the harvested product whilst avoiding possible attempts to mix tokens from distinct harvests.

Further, as in blockchain distributed ledgers, "double spending" frauds are not possible.

The necessary information in order to evidence to a final consumer that a specific harvest or food ingredient raw material was effectively inspected and certified by a third party to hold some "consumer value property" is handed over from one chain participant to the next, all the way to the recipe final processor.

The farmer, can freely define any property that may be useful or cherished by his consumers and the certifying authority by using the smart contract *farmerRequestCertificate()*. After an inspection of the farm, the certification authority will confirm the quality, quantity, and date of the lot harvested. He will then include all relevant information in the certificate web page at the authorityś web domain. *certAuthIssuesCert()* The smart contract mints for this specific lot of crop an equivalent quantity of IGR tokens such that one IGR token corresponds to one gram of that certified ingredient. The authority issues IGR tokens through the smart contract including nature, quantity, location, and time of the harvest. The token will hold the URL to the web page of the full TPC. Note that only the certification authority has permission to mint or not mint the tokens or determine the correct quantities. This assures a truly independent third-party certification and avoids potential conflicts of interest.

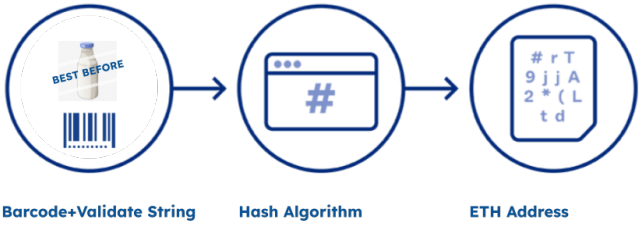


Figure 4: ETH Address generation from *genAddressFromGTIN13date*

The final processor, sometimes also known as commingler or packer, uses information printed on the product retail label to generate a public key which is linked to the certificate URL. The barcode (GTIN-13 SKU identifier) appended to the validity "best before" date on the wrapper are hashed to provide a unique public key in the Ethereum blockchain. Thus, the hash of the "GTIN-13 + Date" string is the public key on the Ethereum blockchain. Querying the blockchain at this address returns the URL link to the certificate.

This new ERC-1155 smart contract code retains the original functionalities while extending the framework to allow for non-fungible objects such as harvests of food products to be certified as unique objects. It has a major new focus on the conception, validation, and usability of smart contracts for TPC of non-fungible objects.

### 4.1. *Answers to Research Questions*

The research questions **MQ1** and subsidiary research question **SQ2** and **MQ3** can be answered as follows:

**MQ1:** Yes, the IGR token smart contracts after being modified to ERC-1155 are capable of truly evidencing harvest TPC with tamper-free certificates and are available to anyone, including new entrants to the food supply chain through simple internet devices, as shown by the PoC running on a test net as described.

**SQ2:** Yes, price incentive mechanisms are established for each stakeholder. The premium to the price that the final consumer is willing to pay for access to the TPC certification of products will be shared with the supply chain participants. The sum of the incentives along the links of the supply chain is approximately as large as the premium the consumer actually pays.

**SQ3:** The typical time for the response for an end consumer to a certificate query using the HTTP protocol is linear because it uses only one direct hashed access to the blockchain (linear data structure) plus one direct URL web access to the certificate, both of which are accessible in linear time. This is due to the fact that, at each change of custody, the URL to the certificate is "handed over" to the next in the chain all the way to the commingler or packer. The public key information (GTIN-13 + lot date) to the certificate URL saved on the blockchain can be scanned directly from the product label. This can be achieved conveniently using an Android App https://play.google.com/store/apps/details?id=com.igrtoken&hl=en&gl=US&pli=1

In summary, the modified IGR-token smart contracts suite using the ERC-1155 tokens allows for the synchronization of the transfer of custody of the crop with the corresponding IGR token representing each gram of the yield instantiated for each different harvest. The modifications to the IGR-token code to use the ERC-1155 have kept all original functionalities adding the necessary non-fungible discipline. The main enforcement is that yields from different harvests now may not be added.

The framework can not detect if a physical counterfeit of packaging, within a short period, i.e., re-utilization of original packaging material with counterfeit content, whilst the spent tokens are still "live".

## 5. Conclusions and Future Work

Farmers are systematically urged towards more sustainable farming methodologies whilst becoming more competitive. Some producers use the information on labels to induce customers to believe that their ingredients are harvested in environmentally and socially friendly manners without proper evidence. Third-party certification along with better availability of this information to the general public and supply chain actors can help fight this green-washing and promote consumer trust. Reliable publicity of the certificates with fast and easy access is paramount. A possible practical solution is the use of distributed ledger technology using tokens carrying the URL pointing to the certificate at the authority's website. This information is transferred at each change of custody from harvest along the chain.

This research shows that a TPC, via the certificate URL at the authority's website, can easily and publicly be made available through internet Apps. To allow for credibility among the target consumers, the certification authority can be freely chosen by the farmer. The authority is free to decide and has full control on whether or not to certify or deny certification. The architecture has a practical appeal because it allows economic incentives to be shared by stakeholders along the agro-supply chain links.

The major contribution of this research is to show a method for public access to URLs with TPC of harvests as unique objects, as opposed to a more generic certification of a farm.

**Conflict of Interest** The authors declare no conflict of interest.

## References

[1] C. Liu, "Is usda organic a seal of deceit: The pitfalls of usda certified organics produced in the united states, china and beyond", *Stan. J. Int'l L.*, vol. 47, p. 333, 2011.

[2] F. DeClerk, J. F. Le Coq, B. Rapidel, J. Beer, *Ecosystem services from agriculture and agroforestry: measurement and payment*, Routledge, 2012.

[3] B. Tanner, "Independent assessment by third-party certification bodies", *Food control*, vol. 11, no. 5, pp. 415–417, 2000.

[4] M. Hatanaka, L. Busch, "Third-party certification in the global agrifood system: an objective or socially mediated governance mechanism?", *Sociologia ruralis*, vol. 48, no. 1, pp. 73–91, 2008.

[5] T. Hirbli, "Palm oil traceability: Blockchain meets supply chain", Ph.D. thesis, Massachusetts Institute of Technology, 2018.

[6] U. W. Chohan, "The double spending problem and cryptocurrencies", *Available at SSRN 3090174*, 2021.

[7] G. Zhao, S. Liu, C. Lopez, H. Lu, S. Elgueta, H. Chen, B. M. Boshkoska, "Blockchain technology in agri-food value chain management: A synthesis of applications, challenges and future research directions", *Computers in industry*, vol. 109, pp. 83–99, 2019.

[8] J. Kasten, "Blockchain on the farm: A systematic literature review", *Journal of Strategic Innovation and Sustainability*, vol. 15, no. 2, pp. 129–153, 2020.

[9] A. Iftekhar, X. Cui, "Blockchain-based traceability system that ensures food safety measures to protect consumer safety and covid-19 free supply chains", *Foods*, vol. 10, no. 6, p. 1289, 2021.

[10] K. Demestichas, N. Peppes, T. Alexakis, E. Adamopoulou, "Blockchain in agriculture traceability systems: A review", *Applied Sciences*, vol. 10, no. 12, p. 4113, 2020.

[11] X. Lin, S.-C. Chang, T.-H. Chou, S.-C. Chen, A. Ruangkanjanases, "Consumers' intention to adopt blockchain food traceability technology towards organic food products", *International Journal of Environmental Research and Public Health*, vol. 18, no. 3, p. 912, 2021.

[12] G. d. S. R. Rocha, L. de Oliveira, E. Talamini, "Blockchain applications in agribusiness: a systematic review", *Future Internet*, vol. 13, no. 4, p. 95, 2021.

[13] D. Prashar, N. Jha, S. Jha, Y. Lee, G. P. Joshi, "Blockchain-based traceability and visibility for agricultural products: A decentralized way of ensuring food safety in india", *Sustainability*, vol. 12, no. 8, p. 3497, 2020.

[14] A. Upadhyay, S. Mukhuty, V. Kumar, Y. Kazancoglu, "Blockchain technology and the circular economy: Implications for sustainability and social responsibility", *Journal of Cleaner Production*, vol. 293, p. 126130, 2021.

[15] J. F. Galvez, J. C. Mejuto, J. Simal-Gandara, "Future challenges on the use of blockchain for food traceability analysis", *TrAC Trends in Analytical Chemistry*, vol. 107, pp. 222–232, 2018.

[16] F. Zhao, X. Guo, W. K. Chan, "Individual green certificates on blockchain: A simulation approach", *Sustainability*, vol. 12, no. 9, p. 3942, 2020.

[17] J. Zhang, S. Zhong, T. Wang, H.-C. Chao, J. Wang, "Blockchain-based systems and applications: a survey", *Journal of Internet Technology*, vol. 21, no. 1, pp. 1–14, 2020.

[18] M. Choi, S. R. Kiran, S.-C. Oh, O.-Y. Kwon, "Blockchain-based badge award with existence proof", *Applied Sciences*, vol. 9, no. 12, p. 2473, 2019.

[19] A. Rejeb, J. G. Keogh, S. Zailani, H. Treiblmaier, K. Rejeb, "Blockchain technology in the food industry: A review of potentials, challenges and future research directions", *Logistics*, vol. 4, no. 4, p. 27, 2020.

[20] R. Cole, M. Stevenson, J. Aitken, "Blockchain technology: implications for operations and supply chain management", *Supply Chain Management: An International Journal*, 2019.

[21] E. Wood, "A secure decentralised generalised transaction ledger, ethereum proj", *Yellow Pap*, , no. 151, p. 1.

[22] W. Ethereum, "Ethereum whitepaper", *Ethereum. URL: https://ethereum. org [accessed 2023-01-01]*, 2014.

[23] L. Wu, "Blockchain smart contracts in megacity logistics", 2018.

[24] K. Wüst, A. Gervais, "Do you need a blockchain?", "2018 Crypto Valley Conference on Blockchain Technology (CVCBT)", pp. 45–54, IEEE, 2018.

[25] R. B. dos Santos, N. M. Torrisi, E. R. K. Yamada, R. P. Pantoni, "Igr token-raw material and ingredient certification of recipe based foods using smart contracts", "Informatics", vol. 6, p. 11, MDPI, 2019.

**Ricardo Borges dos Santos** has completed his Bachelor in Mechanical Engineering degree from PUC-RJ University in 1984 with honors. He has obtained a Computer Engineer Degree from UNIVESP, Sao Paulo in 2020 as well as a MS degree in Mechanical Engineering at Penn State University in 1989. He has earned his PhD degree in Computer Science from the Center of Mathematics, Computation e Cognition of the Universidade Federal do ABC in 2019.

His research activities are mainly related to Distributed Systems, Cryptography, Blockchain and Energy. He has over 20 articles on Food Traceability, Distributed Systems, Energy Efficiency and Supply Chain Management.

**Rodrigo Palucci Pantoni** He received the Computer Science degree in 2000 and subsequently received the M.S. in 2006 and PhD in 2012 at the University of São Paulo (USP).

He now teaches "Industrial Informatics" at the Department of Electrical Engineering and Computer Science of Federal Institute of São Paulo. His research activities are mainly in the area of Industrial Informatics with focus on development activities including Internet of Things and Industry 4.0.

**Nunzio Marco Torrisi** He received the Master degree and the PhD in Computer Engineering from the University of Catania, Italy, in 2002 and 2006, respectively.

He registered a Brazilian patent, published his work in international journals and magazine and since 2009, he has been an associate professor at the Federal University of ABC in São Paulo (UFABC).

Received: 22 November, 2022, Revised: 10 February 2023, Accepted: 24 February, 2023, Online: 23 March, 2023

DOI: https://doi.org/10.55708/js0203001

# Designing Critical and Secondary Information in Augmented Reality Headsets for Situational Awareness

**Julia Woodward[1*], Jesse Smith[2], Isaac Wang[3], Sofia Cuenca[4], Jaime Ruiz[2]**

[1]Department of Computer Science and Engineering, University of South Florida, Tampa, Florida, 33620, USA
[2]Department of Computer and Information Science and Engineering, University of Florida, Gainesville, Florida, 32611, USA
[3]Department of Computer Science, James Madison University, Harrisonburg, Virginia, 22807, USA
[4]Department of Computer Systems, Farmingdale State College, Farmingdale, New York, 11735, USA
*Corresponding author: Julia Woodward, 4202 E. Fowler Ave ENG030, Tampa, FL, 33620, USA, juliaevewoodward@usf.edu

**ABSTRACT:** Augmented Reality (AR) headsets are being used in different contexts (e.g., the oil industry, healthcare, military); however, there is a lack of research and design recommendations on how information should be presented in the AR headset displays, especially for aiding users' situational awareness. We present two studies: one examining if existing findings on the perceptibility of three types of visual stimulus (color, text, shapes) can be applied to AR headsets for *critical information*, and one analyzing three different presentation styles (Display, Environment, Mixed Environment) for textual *secondary information* in AR headsets. Our study on secondary information is an extension of prior work. For critical information, we found that existing visual perception findings can be applied to AR headsets; there is a hierarchy of salient visual features. Understanding that we can utilize prior work on visual features helps in designing salient critical information for AR headset displays. For secondary information, we found that having the text in the Display and Environment presentation styles assisted in participants' perception and comprehension when compared to the Mixed Environment presentation style. Based on our results, we provide design recommendations on how to present critical and secondary information in AR headset displays to aid in users' situational awareness, which is essential in safety crucial domains such as the military.

**KEYWORDS:** Augmented Reality, Situational Awareness, Design

## 1. Introduction

Augmented reality (AR) systems combine virtual elements with the real-world environment [1]. Compared to more traditional AR platforms (e.g., tablets, smartphones, computers), AR headsets are becoming more popular due to providing more mobility, hands-free capabilities, and user immersion [2,3]. AR headsets are entering the consumer market [4], and are also being employed in industrial settings [5]. However, prior research studies have focused on examining the applicability of using AR headsets in various environments and not on investigating how to design the information in the display, especially for aiding users' situational awareness. Situational awareness consists of three levels: perception and detection of elements in the environment (level 1), comprehension and interpretation (level 2), and prediction of the future status of the environment (level 3) [6,7]. Situational awareness is separate from users' decision making [7] and is essential in safety crucial domains [8]. A lack of situational awareness has been attributed to tragedies, such as aircraft crashes [8], oil spills [9], and errors in anesthesia [10].

Since AR keeps users aware of their surroundings while providing additional virtual information in real-time, AR has the capability to increase users' situational awareness. Prior work has examined applying AR headsets for users' situational awareness in a wide range of contexts, such as the military [11], maintenance [12], construction [13], and healthcare [14]. However, prior work has mainly studied the applicability of AR instead of investigating how to design the visual information for aiding users' situational awareness (e.g., [14–17]). In addition, there has been conflicting results with using AR, such as both higher and lower situational awareness [15,16,18] and cognitive workload [19,20]. Therefore, it is important to study how the design of information affects users' situational awareness, since not considering the design and simply applying AR to situations may not be beneficial (e.g., lower situational awareness).

In this paper, we examine how the presentation of visual information in AR headsets can affect users' situational awareness (i.e., level 1 perception and level 2 comprehension). In terms of information necessity, visual information can be separated into two categories: central or critical information (e.g., hazard warnings, essential information) and peripheral or secondary information (e.g., current time, nonessential information) [21]. Critical information is essential to comprehend when completing a task, while secondary information may be beneficial but not necessary. Therefore, we conducted two separate studies focusing on critical and secondary visual information. In our critical information study, we focused on *perception* through examining if existing findings on the perceptibility of three types of visual stimulus (color, text, shapes) can be applied to AR headsets. Previous work in visual perception has found a hierarchy of salient features. For instance, people can more easily detect color than shapes and text [22,23]. However, it is unclear if these findings translate to AR headsets due to these headsets possessing technological and perceptual challenges. The low resolution and loss of visual acuity in AR headsets can negatively affect legibility, object recognition, and depth perception [24,25]. Also, the environment and transparency of virtual elements can impact users' color perception in AR headsets [24,26]. Understanding if we can apply existing perception findings to AR headsets will aid in the design of salient critical information. In our experiment, participants had to monitor visual stimulus in an AR headset while completing math problems on a tablet, and press a physical button when they noticed a specific visual condition in the headset (Figure 1). The math problems were used as a cognitively demanding task for the participants to focus on. The visual stimulus was locked to the AR headset display view. We designed the stimulus to always be present because critical information should be prominent and immediately perceptible [27,28].

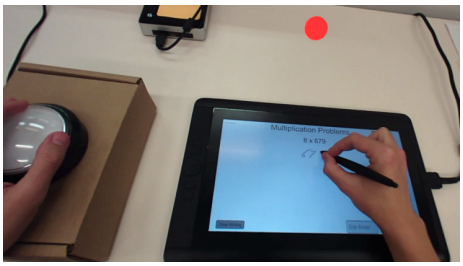

Figure 1: Study setup for critical information study: view from right-handed participant during color visual condition (color red is in AR headset display).

While visual saliency is essential for critical information, secondary information does not have this restriction, and therefore can display larger quantities of detailed information as text (date, time, descriptions, etc.). Since secondary information does not need to be as visually salient, there are more opportunities to integrate it with the environment. Therefore, for our second study, we investigated three different presentation styles for textual secondary information in the context of aiding both *perception* and *comprehension*: locked to the display view (Display), located in the environment (Environment), and a mix of both (Mixed Environment). As in the critical information study, participants had to monitor the textual information in an AR headset while solving math problems. Our study on secondary information is an extension of prior work [29]. This paper updates and expands upon the original work by adding additional literature, an exploratory study on the location of elements, the experiment on critical information, and more results from the study on secondary information.

In our critical information study, we found similar results to prior work with participants having a faster response time for color, and a slower response time and higher cognitive workload for text. In our secondary information study, we found that the Display and Environment presentation styles improved perception and comprehension of textual secondary information; participants had a higher recall of information. Our results provide a new understanding of how different types of visual stimulus for critical information and different presentation styles for textual secondary information in AR headsets can aid users' situational awareness. We contribute design recommendations on how to present visual information in AR headsets for users' situational awareness. Recognizing how to design visual information in AR headsets to improve situational awareness has a wide range of implications in safety crucial environments, such as surgery.

## 2. Related Work

We focus our review of prior work on two categories: (1) using AR for situational awareness and (2) examining the presentation of information in AR headsets.

### *2.1. AR for Situational Awareness*

Prior work has started studying using AR for users' situational awareness in safety domains, such as the military [14,16,17,30,31]. The authors in [31] created an AR system (FlyAR) to support Unmanned Aerial Vehicle (UAV) flight navigation. FlyAR supports live flight supervision by overlaying the flight path onto a live video stream on a tablet PC, as well as using graphical elements to show height and distance between points. The authors in [16] also developed an AR system for UAV operators, in which flight data was overlaid onto a video stream of the flight on a computer screen. Before the AR system, operators would have to look at two separate screens. The authors found that the AR system improved the operators' situational awareness. In the security domain, [32] proposed a conceptual AR computer-based design for combining social media data (e.g., twitter posts) with

contextual information (e.g., Google Maps) to increase emergency operators' situational awareness. The authors iterated on the design based on a workshop with AR and situational awareness experts but did not implement and evaluate the designs in a real-world context.

AR has also been analyzed in the context of driving [17,33,34]. In [17], the authors proposed an AR car windshield system to increase drivers' situational awareness by providing warning information to the driver. For example, it would detect another vehicle and add color depending on how close the vehicle was. The authors in [33] designed an AR driving system that provides warnings on the car windshield for pedestrian collision (e.g., a yellow outline). The authors conducted a driving simulator study and found that the AR visual cues enhanced drivers' awareness of pedestrians. In [34], the authors examined object segmentation visualizations for automated vehicles. They found that including the segmentation visualizations over the car windshield, instead of a tablet on the console, resulted in participants having lower cognitive workload and higher situational awareness, especially for color segmentations over both dynamic and static objects.

While the studies listed above investigated using AR for situational awareness, they only analyzed traditional displays (e.g., car windshields, computer screens), not AR headsets. AR headsets provide more user immersion and freedom, as well as contextual integration with the environment. Previous studies have started to examine using AR headsets for aiding users' situational awareness, such as to monitor patient information [14,15]. In [14], the authors investigated if AR headsets can aid anesthesiologists in monitoring patient information during surgery. They conducted a simulated operating environment study and found that the anesthesiologists that used the AR headset spent less time looking at the anesthesia machine and detected patient events faster. The authors in [15] analyzed if AR headsets could help nurses' patient alarm management decisions and situational awareness by showing patient vital signs. The authors found that using the AR headsets resulted in nurses having higher situational awareness, less errors in recognizing alarms, and faster alarm reaction times.

Prior work has also examined employing AR headsets in the military and security domains [11,30,35,36]. In [11], the authors developed an AR headset system that displays tactical information (e.g., navigation waypoints) for soldiers on foot. The authors in [35] analyzed using an AR headset to show real-time navigational information for the US Coast Guard. They ran a training simulation and found that the AR headset increased operator track keeping and situational awareness; however, it lowered operator responsiveness. For remote pilots of UAVs, [36] investigated using AR headsets to show telemetry details. The authors found that the AR headsets allowed the pilots to focus more on keeping the aircrafts in their field of view, instead of looking at the ground control station. In [30], the authors examined using AR headsets to provide distributed team awareness, specifically in the security domain (e.g., collecting evidence). One team member would be physically present in the environment with an AR headset while a remote team member would be watching a video stream from the headset camera on a computer screen. The remote member could add and edit virtual content displayed in the collaborator's headset (e.g., arrow pointing to specific evidence). They found that the team member wearing the AR headset had higher cognitive workload and lower alertness, while the remote team member had a higher understanding of the situation.

AR headsets are also being utilized in other domains to aid in users' situational awareness, such as firefighting [37,38] and agriculture [39]. The authors in [37] analyzed a proof-of-concept design for using an AR headset in a simulated fire scenario. In the design, the optimal path to the fire would be displayed, as well as fire extinguisher locations. They found that the proof-of-concept reduced travel distance and improved firefighting efficiency. In [38], the authors designed and built an AR headset prototype, which displayed thermal imaging and object segmentation visualizations to help firefighters see their environment during situations with limited sight (e.g., heavy smoke). For agriculture, [39] created an AR system to help farmers monitor their agricultural machines. The locations and status of the machines would be shown in the AR headset display.

These studies highlight the applicability of using AR headsets in domains that require situational awareness; however, they did not analyze *how* to present the visual information in the headsets. None of the studies compared different designs of information, which can impact users. Prior work has shown that AR headsets can result in slower completion times [40,41], higher discomfort [42], and higher cognitive workload [43] when compared to traditional methods (e.g., paper instructions). Therefore, not considering the design of information and simply applying AR headsets to different contexts may not be beneficial. We go beyond prior work by examining different types of visual stimulus for critical information and different presentation styles for secondary textual information in the context of situational awareness.

### *2.2. Presentation of Information in AR Headsets*

Prior work has started to examine the presentation of information in AR headsets [23,44–49]. During a maintenance assembly task, [48] compared using an AR headset (3D animations vs. video instructions) to traditional paper-based instructions. The authors found an improvement in participants' task performance (e.g.,

faster completion time, fewer errors) when using the AR headsets compared to paper instructions. For the AR headset, while it varied between 3D animations and video instructions, the participants could always see textual instructions and an image of the current tool they needed; the text design remained the same. The authors found that 3D animations, when compared to videos, in an AR headset lowered task completion times. In [47], the authors investigated different AR headset interface designs during a warehouse job simulation (i.e., finding order parts). The designs included text-based versus graphic-based designs, as well as always-on versus on-demand information. They found that graphic-based and always-on information helped users' task performance by reducing completion times and errors. The authors in [49] examined user preferences on how to convey information in industrial AR interfaces. The study consisted of a questionnaire with mockup images of an AR interface. The 3D CAD models were the most preferred, with text being the least preferred. However, the study only focused on assembly, did not use an actual AR device, and did not examine different designs and presentations of text. In addition, prior work recommends that text should not be completely removed for task instructions [50].

In [51], the authors developed an AR headset prototype to help users understand conversations in a noisy echoic environment. The prototype distinguishes between speakers by putting a symbol above their head (i.e., a blue triangle with a white flag and number). When a speaker talks, the audio is transcribed and displayed in the AR headset. The text is shown in black on a static off-white panel at the bottom of the display along with the number associated with the current speaker. The authors did not look at different text designs, only feasibility of the prototype. In [44], the authors analyzed different text positions in an AR headset for reading. When the text was in the top-right, users had higher cognitive workload and lower comprehension when compared to the center and bottom-center locations. The center and bottom-center locations resulted in users having lower cognitive workload and higher comprehension. They also examined two presentation styles: line-by-line scrolling and word-by-word. The word-by-word style resulted in higher user comprehension when users were sitting and reading, while the line-by-line scrolling style had higher comprehension when users were walking and reading.

Previous studies have investigated text and background panel colors in AR systems. The authors in [52] found that using white text with a blue panel background was the best for user readability in AR headsets. In [53], the authors conducted a crowd-sourcing study on user preferences for colors for text and background panels in AR smartphone applications. Most of the participants preferred red or blue background panels with white text. However, prior work has also recommended transparent backgrounds [45], which was not an option for participants in [53]. The authors in [45] conducted a user study, in which participants organized items in a grocery store while viewing product information in an AR headset in two modes: see through mode (i.e., transparent) or panel overlay (i.e., opaque background). The participants preferred the product text to be displayed in the center of the headset in see through mode (i.e., no background) for readability, as well as being able to easily switch between the information and environment. In [54], the authors tested different AR headset text magnification designs for low-vision users. The authors found that the participants liked the transparent background panels and that anchoring content in 3D space can support a more natural and flexible reading experience.

These prior studies examined the presentation of information in AR headsets, but mainly focused on readability and user preferences instead of situational awareness. It is important to examine how information should be presented in AR headsets to aid in users' awareness since these devices are being used in a wide range of contexts that require situational awareness (e.g., healthcare). For our studies, we focused on analyzing how different presentation styles for textual secondary information and different types of visual stimulus for critical information in AR headsets can aid in users' perception and comprehension (i.e., the first two levels of situational awareness).

## 3. Exploratory Study: Location

We first conducted an exploratory study to determine the best location to place the visual stimulus in our experiments. We wanted to choose the location, in which the participants would have the fastest reaction time possible. For this study, participants had to press a physical button when they noticed a dot appear in a Meta 2 AR headset [55]. The study was conducted in a windowless room with consistent lighting and took 5 to 10 minutes. In the application, a white 3D cube (25.4 millimeter (mm) edge length) remained in the middle of the field-of-view, while white dots (6.35 mm diameter) would appear in different locations along the periphery. Even though prior work has shown that reaction time increases for stimulus in the periphery [56,57], we focused on peripheral locations because we wanted to examine the perception of information that would not block the users' view or distract them from their main task. The participants were instructed to focus on the 3D cube and to hit the button when they noticed a white dot appear. The dot would appear in one of sixteen locations along the periphery; there was 75 mm between each dot to create all sixteen locations. When the participant pressed the button or if the participant did not notice the dot after 2 seconds,

the dot disappeared. The next dot would then appear in a different location after a random time interval (1-4 seconds). Each participant viewed 80 dots total (5 dots per location). The location order was originally randomized, and then the same order was used for every participant. Participants volunteered without compensation.

### *3.1. Equipment*

The AR application was created using Unity [58], and was run on a Meta 2 AR headset [55]. The headset features a 90-degree field-of-view with a 2560 x 1440 resolution. The physical button had a 76.2 mm diameter. We used a rectangular cardboard box (228.6 mm x 152.4 mm x 76.2 mm) as a base for the button.

### *3.2. Participants*

We had a total of 12 adult participants (M = 23.42 years, SD = 3.55); however, we excluded one female participant for not wearing their corrective lenses. Therefore, we had a total of 11 participants for analysis (M = 23.09, SD = 3.53). Out of the 11 participants, six participants were female, one participant was left-handed, and five participants had used an AR headset at least one time before. All of the 11 participants had normal or corrected-to-normal vision (e.g., eyeglasses).

### *3.3. Data Analysis and Results*

For analysis, we examined the participants' response time by location. Response time was calculated as the time it took a participant to press the button after a dot appeared in the headset. We excluded the times in which the participant did not notice the dot and it disappeared. We grouped the 16 individual locations into three categories: left, center, and right. The center included the six dot locations at the top and the bottom not located on the left and right edges. A Shapiro-Wilks test found that the data was normal; however, a Mauchly Test for Sphericity showed that the data did not have equal variances ($p < 0.01$). A one-way repeated measures ANOVA (RM-ANOVA) with a Greenhouse-Geisser correction found a significant main effect of location on response time ($F_{1.17,10.54} = 9.48$, $p < 0.01$). A Bonferroni post-hoc comparison showed that the participants had a significantly faster response time for the center locations (M = 0.399s, SD = 0.086) compared to the right-side locations (M = 0.444s, SD = 0.172); this is similar to prior work, which has found lower detection accuracy for the right-side of the visual field [59]. There was no significant difference in response time between the center and left-side locations (M = 0.418s, SD = 0.138).

To further analyze the locations, we examined: (1) the corner locations compared to the remaining locations, and (2) the top locations versus the bottom locations. For both the corner locations and the top versus bottom locations, a Shapiro-Wilks test found that the data was normal, and a Levene's test showed that the data met the assumption of equal variances. A paired-sample t-test found a significant main effect of corner locations on response time ($t(9) = 2.92$, $p < 0.05$). The participants had a significantly slower response time (M = 0.452s, SD = 0.202) for the corner locations compared to the remaining locations (M = 0.408s, SD = 0.102). A paired-sample t-test found no significant difference between the top and bottom locations ($t(9) = 1.27$, n.s.).

Based on our results, we decided to place the different types of visual stimulus in the top-center of the field-of-view for our first study on critical information, to increase perceptibility. For our second experiment on presentation styles for secondary information, we placed the textual information on the left-side of the field-of-view (avoiding the corner locations). We decided to place the secondary information on the left-side because we did not want the quantity of the information to block the participant's view, and there was no significant difference in response time between the center and left-side locations. Also, people exhibit a leftward visual bias, known as *pseudoneglect* [60,61], which results in higher detection accuracy and faster motion processing for elements on the left when compared to the right [59,61,62]; even for computer screens [59]. Although pseudoneglect occurs in both right-handed and left-handed people, it is not evident in cultures that read right-to-left [63]. Therefore, it is important to keep in mind users' cultural groups and differences when placing elements in headset displays.

## 4. Experiment 1: Critical Information

In our critical information study, we focused on examining three different types of visual stimulus in an AR headset: color, text, and shapes. These types of visual stimulus are commonly utilized to denote information, such as in warning signs [64]. The goal was to analyze if prior results on the perceptibility of types of visual stimulus could be applied to AR headsets. Previous work in visual perception has found a hierarchy of salient features. For instance, people more easily detect color than shapes and text [22,23]. However, it was unclear if these findings translate to AR headsets due to these headsets possessing technological and perceptual challenges. The low resolution and loss of visual acuity in AR headsets can negatively affect legibility, object recognition, and depth perception [24,25]. Also, the environment and transparency of virtual elements affects users' color perception in AR headsets [24,26]. Determining if we could apply existing findings to AR headsets allows us to further understand how to design critical information.

### *4.1. Participants*

We had a total of 37 adults participate (M = 22.19 years, SD = 5.59); however, we excluded one female participant due to equipment failure, resulting in a total of 36

participants for analysis (M = 22.22 years, SD = 5.67). Twelve participants were female, two participants were left-handed, and ten participants had used an AR headset before. We did not recruit participants who were color-blind or dyslexic, and all of our participants had normal or corrected-to-normal vision.

*4.2. Method and Design*

While wearing an AR headset, participants completed multiplication problems on a touchscreen tablet and different types of visual stimulus appeared in the headset: color, text, or shapes (Figure 2). The participants would only see one type of visual stimulus at a time, not a mix of all three. We placed the stimulus in the top-center of the headset field-of-view based on our results from our exploratory study.

For each visual stimulus type (e.g., color), the visual condition displayed would constantly change (e.g., switching between different colors). Participants were instructed to hit a physical button with their non-dominant hand when they saw a specific visual condition (e.g., color red). The participants took part in the study for approximately 60 minutes in a windowless room, and either volunteered without compensation or received extra credit in a course they were taking.

After consenting to participate, participants completed a demographic questionnaire. The participants then completed a 4-minute practice round of multiplication problems on the tablet without wearing the AR headset to get comfortable with the math application; which was not used in analysis. After the math practice, participants put on the AR headset and began the main study. In the main study, there were six study blocks (approximately 4-minutes each), two blocks per visual stimulus type (color, text, shapes). After completing two blocks for a visual stimulus type, the participants would take the NASA Task Load Index (TLX) [65] for that visual type, which is used to determine participants' perceived cognitive workload. The participants would then complete the next two blocks for a different visual type, the NASA TLX, and then move on to the last visual type blocks. The order of the visual types was counterbalanced across participants. After the participants completed the six study blocks, they were also asked questions about their subjective preference.

*4.2.1. AR Application Design*

Each visual stimulus type had a total of four different options that would constantly change in the headset in a randomized order and for a randomized duration. The four options for each type of visual stimulus included: (a) color: red, green, yellow, and blue; (b) text: "red", "green", "yellow", and "blue"; and (c) shapes: circle, triangle, star, and square. All types of visual stimulus had the same color saturation and brightness and had the same width (12.7 mm). For color, only the color of the circle changed (Figure 2a). Both the text and shapes (Figures 2b and 2c) were white, since black is transparent in AR headsets. The text height was 5 mm, which is consistent with Meta AR design recommendations [66], and in Liberation Sans font since prior work recommends using sans-serif fonts for text readability [67].

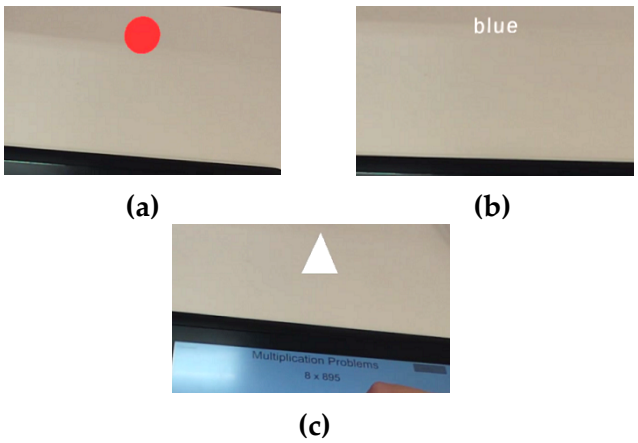


Figure 2: Types of visual stimulus from participant view from AR headset: (a) color, (b) text, and (c) shapes.

During each study block, the participant would view a total of 32 visual conditions (4 options x 8 occurrences). For example, if it was a color block it would constantly change between the four colors, and each specific visual condition (e.g., color blue) would appear eight times. The current visual condition (e.g., color red in Figure 2a) would remain in the headset display for a random time interval (6 to 9 seconds) before switching to the next visual condition. If the participant pressed the button it would automatically switch to the next visual condition, regardless of the amount of time left for the current visual condition. The last visual condition in that block would remain visible in the headset until the participant finished the current math problem and then both applications would end. Each study block was approximately 4 minutes. The blocks were not exactly 4 minutes because each visual condition would change after a random time interval, and the study block would not end until the participant finished the last math problem.

Since there were only two blocks for each type of visual stimulus, we had to determine the two visual conditions for when the participant would hit the button. For color, the participants hit the button when they saw the color red for one block and the color green for the other block because adults have faster reaction times for red and green colors, compared to yellow and blue [68]. For text, the participants hit the button when they saw the word "red" for one block and the word "blue" for the other block. Prior work has shown that word processing time increases as the number of letters increase [69], therefore we chose the two shortest words (out of the four options) to have

the fastest reaction time possible. For shapes, the participants hit the button when they saw a circle for one block and a triangle for the other block. We chose a circle and triangle because they are used by the International Organization for Standardization (ISO) to represent mandatory actions and warnings [64].

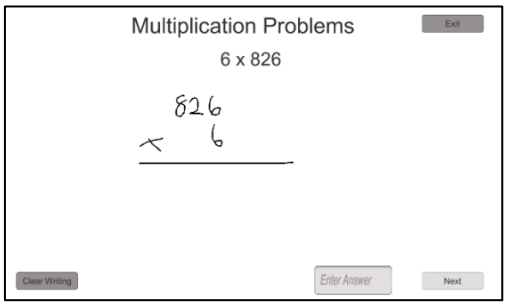


Figure 3: Screenshot from our math application.

#### 4.2.2. *Math Application Design*

We decided for the participants to focus on math problems while monitoring the visual stimulus in the AR headset because mental math calculation uses people's working memory [70]. Working memory falls under short-term memory and is necessary for sudden perceptual cognitive tasks, such as language comprehension and reasoning [71]. By having participants focus on a task that uses their working memory, we can examine the salient properties of the different types of visual stimulus in the AR headset. We purposefully designed our math application to be more cognitively taxing (i.e., utilize more working memory) in order to keep the participants' attention on the math application, instead of the visual stimulus in the AR headset; not primarily focusing on the information in the headset is consistent with demanding real-world settings (e.g., surgery).

Our math application consisted of single-digit x three-digit multiplication problems (Figure 3). We chose multiplication problems because they have a slower solve time compared to addition problems [72]; therefore, requiring more of the participants' attention. We also implemented other design decisions to make the application more cognitively taxing, such as presenting the single-digit first because prior work has shown that adults are slower when the smaller number is first [73]. The single-digit ranged from 2 to 9 because multiplication with 0 or 1 utilizes retrieving a rule (e.g., everything multiplied by 0 equals 0) instead of a solution [74]. The three-digit also did not end in 0 or 1, and did not include three of the same digit (e.g., 444) due to the tie-effect [75]. The tie-effect states that response time for an operand pair with identical digits is faster. None of the multiplication problems repeated in the math application.

Figure 3 shows a screenshot from our math application. The current math problem would appear at the top of the screen (e.g., 6 x 826). The participants had an area to work out the problem using a stylus pen, before inputting their answer and hitting a button to go onto the next problem. The participants had to input an answer to move on, but the answer did not have to be correct. Each participant finished the number of problems they could do in the set block time. We instructed the participants to take their time and focus on getting correct answers.

### 4.3. *Equipment*

Both the AR application and multiplication application were created using Unity [58]. The AR application was run on the same Meta 2 headset as the exploratory location study, and the math application was run on a Wacom Cintiq Companion Hybrid tablet [76]. The tablet has a 1080 x 1920 resolution, and the screen is 13.3 inches, measured diagonally. The physical button was the same button that was used in the location study.

### 4.4. *Data Analysis and Results*

We analyzed the types of visual stimulus (color, text, shapes) by examining the response time and error rate for the visual stimulus, the math solve time, and the participants' cognitive workload and preference.

#### 4.4.1. *Response Time*

We determined response time by calculating the time it took a participant to press the button after the correct visual condition appeared in the AR headset. When calculating response time, we did not include any incorrect button hits; for example, if the participant hit the button when the square shape appeared when the correct condition was a triangle. A Shapiro-Wilks test on response time per visual stimulus showed that the data was non-normal ($W = 0.97$, $p < 0.01$). We applied a log-transform [77] to the distributions and used the transformed data for analysis, but the mean response times we report are the actual measured values. A Mauchly Test for Sphericity showed that the data had equal variances. A one-way repeated measures ANOVA (RM-ANOVA) found a significant main effect of type of visual stimulus (color, text, shapes) on response time ($F_{2,70} = 34.84$, $p < 0.0001$). A Bonferroni post-hoc comparison showed that the participants had a significantly faster response time for color ($M = 1.33s$, $SD = 0.37$), than shapes ($M = 1.67s$, $SD = 0.4$) or text ($M = 1.92s$, $SD = 0.54$).

We further analyzed response time by examining all separate visual conditions (color red, color green, circle shape, triangle shape, "red" text, and "blue" text) (Figure 4). A Shapiro-Wilks test on response time per visual condition showed that the data was skewed ($W = 0.95$, $p < 0.0001$). We applied a log-transform [77] to the distributions and used the transformed data for analysis, but the mean response times reported in the paper are the actual measured values. A Mauchly Test for Sphericity showed that the data did not have equal variances ($p <$

0.05); therefore, we applied a Greenhouse-Geisser correction. A one-way RM-ANOVA found a significant main effect of type of visual condition (color red, color green, circle shape, triangle shape, "red" text, and "blue" text) on response time ($F_{3.99,139.41} = 23.03$, $p < 0.0001$). A Bonferroni post-hoc comparison showed that the participants had a significantly faster response time for color red (M = 1.17s, SD = 0.4) and a significantly slower response time for "blue" (M = 2.14s, SD = 0.68) when compared to all other visual conditions. There was no significant difference between the circle shape (M = 1.62s, SD = 0.59) and triangle shape (M = 1.69s, SD = 0.48). Altogether, participants had the fastest response time for color, more specifically for the color red, and had the slowest response time for text.

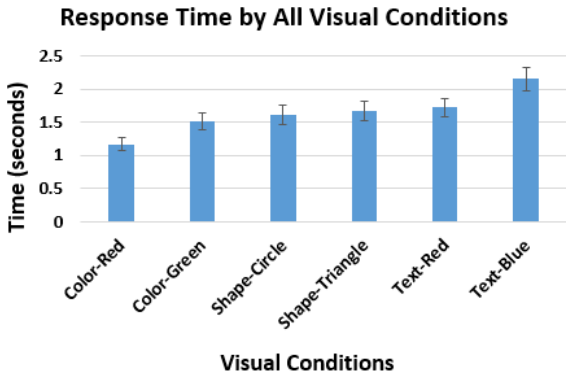


Figure 4: Average response time for all visual conditions. Error bars indicate 95% confidence interval.

### 4.4.2. *Error Rate*

In our study, we examined three possible types of errors: not hitting the button when the correct visual condition appeared (*missing the correct visual condition*), hitting the button for the wrong visual condition (*wrong button hit*), and overall error rate (i.e., combining the two types). A Shapiro-Wilks test on error rate per visual stimulus found that the data was severely skewed for all three types: missing the correct visual condition ($W = 0.68$, $p < 0.0001$), wrong button hit ($W = 0.56$, $p < 0.0001$), and overall error rate ($W = 0.77$, $p < 0.0001$). For overall error rate, a Mauchly Test for Sphericity found that the data met the assumption of equal variances; therefore, we applied the Aligned Rank Transform [78]. A one-way RM-ANOVA found no significant effect of visual stimulus type on overall error rate ($F_{2,70} = 2.89$, *n.s.*). All types of visual stimulus had a low error rate: color (1.65%), text (1.3%), and shapes (1.04%).

Next, we analyzed when the participants missed the correct visual condition. A Mauchly Test for Sphericity found that the data met the assumption of equal variances; therefore, we applied the Aligned Rank Transform [78]. A one-way RM-ANOVA found no significant effect of visual stimulus type on missing the correct visual condition ($F_{2,70} = 0.54$, *n.s.*). We analyzed the wrong hit errors (e.g., hitting the button for the text "green", when the condition was "blue"). A Mauchly Test for Sphericity showed that the data did not have equal variances ($p < 0.0001$). Since the data was not normal and did not meet the assumption of equal variances we conducted a Friedman test, which found a significant main effect of visual stimulus on hitting the button for the wrong condition ($\chi^2$ (2) = 9, $p < 0.05$). A Bonferroni post-hoc comparison showed that color had significantly more wrong hit errors than shapes and text; there was no difference between text and shapes.

To examine the wrong hit errors further, we analyzed all separate visual conditions (color red, color green, circle shape, triangle shape, "red" text, and "blue" text). A Mauchly Test for Sphericity showed that the data did not have equal variances ($p < 0.0001$). Since the data was not normal and did not meet the assumption of equal variances we conducted a Friedman test, which found a significant main effect of type of visual conditions on wrong hit errors ($\chi^2$ (5) = 34.8, $p < 0.0001$). A Bonferroni post-hoc comparison found that only color green had significantly more wrong hit errors than all other visual conditions. There was a total of 39 wrong hit errors, and 66.7% (26/39) of them were during the color green condition. During the color conditions, the colors red, green, blue, and yellow would cycle in the headset. We found that 96.15% (25/26) of the wrong hits during the color green condition were hit when the color was yellow. Participants frequently commented on having a hard time differentiating yellow and green. For instance, P6 stated "*Color required the least mental thought with the exception that the yellow and green are similar, and when I saw yellow I had to make sure it wasn't green.*" This is most likely due to the AR headset display quality, as it can affect users' color perception [24,26]. Generally, the three types of visual stimulus did not have a significant difference in error rate and participants discerned the correct visual condition, resulting in low error rates.

### 4.4.3. *Math Solve Time*

We examined the participants' math solve time to investigate if participants were focusing on the math application for each visual stimulus type. We were not interested in how fast the participants completed the math problems since we told the participants to take their time, but rather analyzed the math solve time to make sure they were consistently focusing on the math application between the different study blocks. A Shapiro-Wilks test on response time per visual stimulus showed that the data was non-normal ($W = 0.85$, $p < 0.0001$). We applied a log-transform [77] to the distributions and used the transformed data for analysis. A Mauchly Test for Sphericity showed that the data had equal variances. A one-way RM-ANOVA found no significant effect of visual stimulus type on math solve time ($F_{2,70} = 0.56$, *n.s.*). The consistency in solve time between the different types of

visual stimulus corroborates that participants considered the multiplication problems their main task.

#### 4.4.4. *Perceived Cognitive Workload*

The participants completed the weighted NASA TLX [65] for each type of visual stimulus (color, text, shapes). A Shapiro-Wilks test found that the data was normal, and a Mauchly Test for Sphericity showed that the data met the assumption of equal variances. A one-way RM-ANOVA found a significant main effect of type of visual stimulus on perceived cognitive workload ($F_{2,70} = 8.97$, $p < 0.001$). A Bonferroni post-hoc comparison found that text (M = 45.08, SD = 17.33) had a significantly higher perceived cognitive workload compared to color (M = 36.46, SD = 18.35) and shapes (M = 38.43, SD = 17.04); there was no significant difference between color and shapes. The participants found text to be more cognitively demanding.

### 4.5. *Subjective Preference*

At the end of the study, we asked the participants to rank the three types of visual stimulus in their order of preference: from most preferred to least preferred (1 to 3). A Friedman test found a significant relationship between preference rank and type of visual stimulus ($\chi^2$ (2) = 47.2, p <0.0001). A Bonferroni post-hoc comparison found that color (M = 1.31, SD = 0.52) and shapes (M = 1.81, SD = 0.52) were ranked significantly higher than text (M = 2.89, SD = 0.40). Color was highly preferred, with 72% (26/36) of the participants ranking it as their first choice. Text was overwhelmingly the least preferred, with 92% (33/36) of the participants ranking it last. The participants preferred color and shapes over text for critical information.

### 4.6. *Discussion*

For our experiment on critical information, we found that existing perception findings can be applied to AR headsets. Our results are consistent with literature on visual perception [23,79], which shows a hierarchy of salient visual features. People can more easily detect color, followed by shapes, and then text. Participants in our study frequently remarked about not having to divert their focus away from the math problems to discern the different colors. AR headsets can lead to difficulties in object recognition and legibility, as well as impact users' color perception [24]. Having an inaccurate perception of color comprises the users' interpretation of display elements which is necessary in contexts that rely on color-coding (e.g., military). Therefore, understanding that we can utilize prior work on visual features helps in designing salient critical information for AR headsets. Also, understanding how to design salient information in AR headsets is important because visual salience can help working memory [80], which is crucial during complex tasks. The AR headset system for helping farmers operate and monitor agricultural machines in [39] provided warnings in the display if something was wrong with the machines. The warning consisted of the word "ALERT" in black text on a red background in the periphery of the display. While the authors use color, it might be more beneficial to utilize a distinct shape instead of text. Also, the authors should place the warning in the center location instead of the periphery to increase saliency.

In addition, examining differences between specific conditions led to further insight into how to design critical information for AR headsets. When we analyzed the two separate visual conditions for color (red and green), we found a significant difference in response time. The participants had a faster response time for color red when compared to all other visual conditions, including color green, which is consistent with prior work [81]. Color also had significantly more wrong hit errors than shapes and text, which we found was due to the color green condition. The participants frequently confused yellow and green, which strengthens the argument for utilizing high contrast elements in AR [28], especially for critical information. Yellow and green are analogous colors, as they are grouped next to each other on the color wheel. Designers should consider color choice for critical information in AR headsets and avoid using analogous colors to denote separate information.

Shapes were the second most effective in aiding awareness for critical information. The majority of the participants (25/36) ranked shapes as their second choice, and shapes had the second fastest participant response time. One interesting factor that the participants mentioned was looking for specific aspects of the shapes to determine if it was the correct visual condition, such as corners. For example, P16 stated "*Shapes were a mix, since looking for points like a triangle could cause you to mix up shapes like stars as well*." In addition to designers avoiding analogous colors, designers should also avoid using shapes that have similar characteristics (e.g., points).

Text was the least effective in helping awareness for critical information; the participants had the slowest response time, highest cognitive workload, and lowest preference for text. The majority of the participants (33/36) ranked text as their least preferred, due to having to pay more attention and actually read the text. We did find a significant difference in response time between the two visual conditions in which the participant had to press the button ("red" and "blue"), which aligns with prior work on processing times based on word length [69]. Our study confirms that designers should consider word length when designing for critical information in AR headsets. Depending on the context, including text in an AR headset may be necessary to effectively communicate the desired information. For instance, prior work recommends that text should not be completely removed for instructions, as it can lead to fewer errors and faster learning times [50].

We recommend that there needs to be a balance between providing the information and not cognitively overloading the user. Based on our findings, designers should incorporate more visually salient information (e.g., color, shapes) when possible, for critical information in AR headsets to aid in situational awareness.

## 5. Experiment 2: Secondary Information

While visual saliency is essential for critical information, secondary information does not have this restriction, and therefore can display larger quantities of detailed information. Since secondary information does not need to be as visually salient, there are more opportunities to integrate it with the environment. Therefore, we examined three textual presentation styles for secondary information: locked to the display view (Display), located in the environment (Environment), and a mix of both (Mixed Environment). We chose to study text because it is commonly used to denote information in AR headset applications and may be necessary depending on the context [14,23,30,44,46]. This experiment is an extension of prior work [29].

### *5.1. Participants*

We had 33 adults participate in our study (M = 21.55 years, SD = 3.55); however, we excluded one male participant due to equipment failure and two participants (one female, one male) for self-reported peripheral vision loss. Therefore, we had 30 participants (M = 21.63 years, SD = 3.69) for analysis, which consisted of seventeen males, twelve females, and one non-binary participant. Two of the participants were left-handed, seventeen had prior experience with AR headsets, and all had normal or corrected-to-normal vision.

### *5.2. Method and Design*

During the study, participants completed multiplication problems on a touchscreen tablet (same as our first study) while viewing textual secondary information in an AR headset in three different presentation styles. The participants took part in the study for approximately 60 minutes in a windowless room, and either volunteered without compensation or received extra credit in a course they were taking.

The structure of the study was similar to our first experiment. After consenting to participate, participants completed a demographic questionnaire. The participants then completed a 5-minute practice round of multiplication problems on the tablet without wearing the AR headset to get comfortable with the math application; which was not used in analysis. After the math practice, participants put on the AR headset and completed three study blocks (5-minutes each), one per presentation style (Display, Environment, Mixed Environment). After completing a block, the participants would take the NASA TLX [65] for that presentation style, and then we would ask the participants to recall the last textual information displayed in the headset. We did not explain beforehand that we would ask them to recall the last presented information in the headset, which allowed us to examine if there was a difference in perception and comprehension. We counterbalanced the order of the presentation styles across participants.

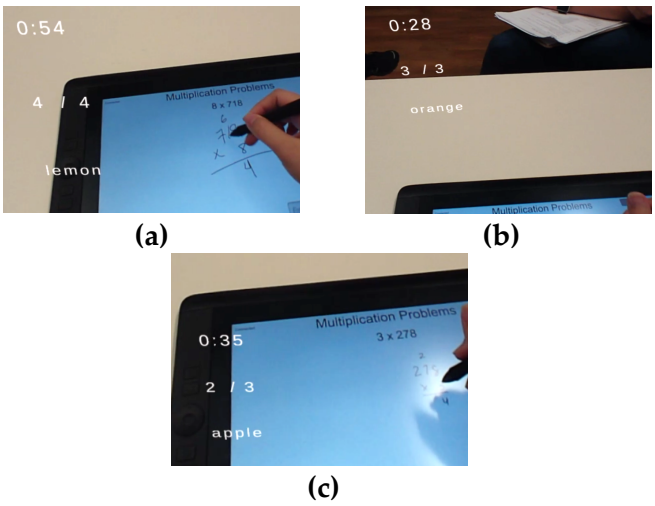


Figure 5: Presentation styles in AR headset: (a) Display, (b) Environment, and (c) Mixed Environment (Images from [29]).

#### *5.2.1. Secondary Textual Information*

The content of the secondary textual information included the participant's average math problem completion time, the participant's math accuracy, and a random word (Figure 5). Before the start of each study, we explained the content and how it would be presented in the headset to the participant; the information was always presented in the same order. Like in our first study, the text was in Liberation Sans font since prior work recommends using sans-serif fonts for readability [67]. Each textual element was placed 75 mm apart.

The participant's average math problem completion time was presented in minutes and seconds (e.g., "2:36"). The math accuracy was the number of correct problems over total completed (e.g., "2/3"). Both the average completion time and accuracy were updated in real-time after the participant completed a problem. For the random word, the text would randomly cycle between four words: "apple", "banana", "lemon", and "orange". Each word would remain in the headset for a random time interval (20 to 40 seconds) before switching. We used the random word as a substitute for information that may be necessary but not essential for situational awareness.

#### *5.2.2. AR Textual Presentation Styles*

The three different presentation styles included: Display, Environment, and Mixed Environment. For the *Display* presentation style, the textual information was

locked to the left-hand side of the AR headset field-of-view and superimposed over the users' environment (Figure 5a). As mentioned earlier, we decided to place the secondary information on the left-side because we did not want the quantity of the information to block the participant's view, there was no significant difference in response time between the center and left-side locations in our exploratory study, and people exhibit pseudoneglect (i.e., leftward visual bias) [60,61]. Same as our first experiment, text height was 5 mm and white, which is consistent with recommendations [66]. The information was always present in the AR headset field-of-view, which is different than the *Environment* presentation style. For the Environment style, the text was superimposed and fixed in the environment to the left of the participant; therefore, it was more conformal to the environment. Consistent with design recommendations, the text was 500 mm away from the participant with a height of 10 mm [66]. In Figure 5b of the Environment style, the participant is looking directly at the text in the headset. If the participant looked away from the text (e.g., down or to the right) they would not be able to see the information. The *Mixed Environment* presentation style was a mix of both of the previous styles. The text was superimposed and always present in the AR headset field-of-view (same as Display) but was 500 mm away from the participant with a height of 10 mm (same as Environment). Although the text was always present in the headset, having the text 500 mm away from the participant placed the textual information more into the participant's central view (Figure 5c).

### 5.3. Equipment

Both the AR application and multiplication application were created using Unity [58]. The AR application was run on the same Meta 2 AR headset [55] as the previous studies, and the math application was run on the same Wacom tablet [76] as the critical information study.

### 5.4. Data Analysis and Results

We analyzed the presentation styles by investigating participants' accuracy of recalled information, math solve time, cognitive workload, and subjective preference.

#### 5.4.1. Information Recall

After each study block, we asked the participants to recall the last textual information that was displayed in the AR headset (i.e., average math time, math accuracy, random word). The participants were unaware that we were going to ask this information; therefore, they were truly unsuspecting for the first study block but became aware for the remaining two study blocks. To capture this difference we split our analysis into two categories: *first response* recall (first presentation style) and *habituated response* recall (other styles). *First response* recall captures the natural perceptibility of the presentation styles, while *habituated response* recall is more aligned with real-life settings in which the users are conscious of what information they have to monitor. For both *first response* and *habituated response* recalls, we calculated the percentage of correct answers for each participant's presentation style. A participant's answer had to directly match the last information presented in the AR headset to be considered correct. A Shapiro-Wilks test showed that the data was non-normal for both *first response* recall ($W = 0.85$, $p < 0.001$) and *habituated response* recall $W = 0.87$, $p < 0.0001$). They both met the assumption of equal variances, so we applied the Aligned Rank Transform [78].

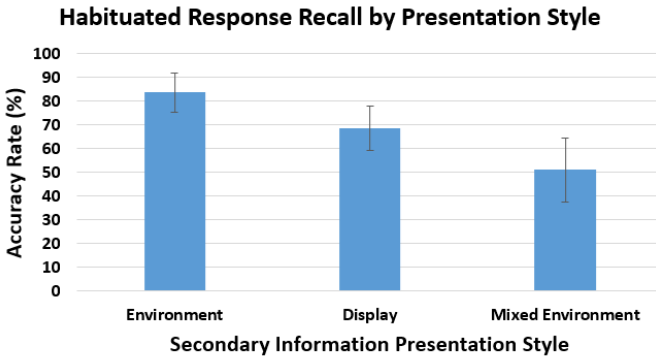


Figure 6: Habituated response recall accuracy by secondary information presentation style. Error bars represent 95% confidence interval.

For *first response* recall, a one-way ANOVA found no significant effect of type of presentation style on recall accuracy ($F_{2,27} = 1.64$, *n.s.*); there was no significant difference between the Display ($M = 60.0\%$, $SD = 21.1\%$), Environment ($M = 67.5\%$, $SD = 23.7\%$), and Mixed Environment ($M = 50.0\%$, $SD = 20.4\%$) styles. However, for *habituated response* recall, a one-way RM-ANOVA found a significant main effect of type of presentation type on recall accuracy ($F_{2,44.05} = 8.91$, $p < 0.0001$). A Bonferroni post-hoc test showed that participants had a significantly higher *habituated response* recall accuracy for the Environment style ($M = 83.8\%$, $SD = 18.6\%$) than the Mixed Environment style ($M = 51.2\%$, $SD = 30.9\%$) (Figure 6); there was no significant difference between the Environment and Display ($M = 68.8\%$, $SD = 21.3\%$) styles. We examined each secondary information separately, and only found a significant effect of presentation style on the random word accuracy ($p < 0.001$, Fisher's exact test [82]). A pairwise test of independence with a Bonferroni correction only found a significant difference between the Environment and Mixed Environment styles. The Environment style had a higher number of correct recall events for the random word than the Mixed Environment style (18 correct vs. 6 correct).

#### 5.4.2. Math Solve Time

As in the first study, we examined the participants' math solve time to investigate if participants were focusing on the math application for each presentation

style. A Shapiro-Wilks test found that the data was severely skewed ($W = 0.70$, $p < 0.0001$) and a Mauchly Test for Sphericity showed that the data did not have equal variances ($p < 0.0001$). Since the data was not normal and did not meet the assumption of equal variances we conducted a Friedman test, which did not find a significant effect of presentation style on math solve time ($\chi^2(2) = 3.27$, *n.s.*). The consistency in solve time between the different types of presentation styles corroborates that participants considered the math as their main task.

#### 5.4.3. *Perceived Cognitive Workload*

We analyzed the participants' perceived cognitive workload for each presentation style. A Shapiro-Wilks test on cognitive workload per presentation style showed that the data was non-normal ($W = 0.96$, $p < 0.05$), and the data met the assumption of equal variances using a Mauchly Test for Sphericity; therefore, we applied the Aligned Rank Transform [78]. A one-way RM-ANOVA found no significant effect of type of presentation style on perceived cognitive workload ($F_{2,58} = 0.12$, *n.s.*). There was no significant difference in participants' perceived cognitive workload between the three presentation styles: Display ($M = 31.5$, $SD = 17.5$), Environment ($M = 31.73$, $SD = 16.04$), and Mixed Environment ($M = 30.9$, $SD = 13.89$).

#### 5.4.4. *Subjective Preference*

After the participants completed the study blocks, we asked them to rank the three types of presentation styles in their order of preference: from most preferred to least preferred (1 to 3). A Friedman test found no significant relationship between preference rank and type of presentation style ($\chi^2(2) = 4.2$, *n.s.*). There was no significant difference in preference between the styles: Display ($M = 1.9$, $SD = 0.8$), Environment ($M = 1.8$, $SD = 0.85$), and Mixed Environment ($M = 2.3$, $SD = 0.75$).

### 5.5. *Discussion*

The only significant difference we found between the three presentation styles (Display, Environment, Mixed Environment) was for *habituated response* recall accuracy. The Environment presentation style had a higher *habituated response* recall accuracy than the Mixed Environment style. With further examination, we only found a significant effect of presentation style on the random word accuracy. During the study, participants frequently mentioned that they were more interested in the math completion time and accuracy, instead of the random word, since they were related to the main task and their performance. Therefore, the Environment presentation style resulted in higher user perceptibility, since it aided in the awareness of information that did not capture the participants' attention (i.e., random word).

For the Mixed Environment style, having the textual information further into the participants' central field of vision made it more distracting to the participants. For example, P13 stated *"The mixed environment was too distracting and put too much pressure on me to get more problems right"*, and P21 stated *"It [The Mixed Environment style] would block some of my work or the math problem."* With the Environment presentation style, the participants could look at the information when they wanted. One participant (P8) stated *"[The Environment style] didn't get in my way so I didn't have to block it out of my vision while completing the math problems. It was nice to look up at it when I felt the need to."* Although the Display style was always present in the headset field-of-view like the Mixed Environment style, participants remarked that it was easier to disregard since it was more in the periphery. Both the Display and Environment presentation styles allowed the participants to view, as well as tune out, the secondary information whenever they preferred. This resulted in a stronger focus when the participants did pay attention to the information, which led to higher recall accuracy.

Both the Display and Environment styles aided user perception and comprehension for secondary textual information. However, prior work has found that text notifications locked to the field-of-view in both virtual reality (VR) [83] and AR [84] headsets result in a higher sense of urgency. For instance, the authors in [83] found that text notifications locked to a VR headset display resulted in users viewing them as more imperative than text notifications in the environment. Also, the authors in [84] conducted a study examining different locations of notifications in an AR headset display during social conversations. The notifications placed in the direct center of the field-of-view were perceived as urgent and intrusive, when compared to notifications that were slightly offset. Secondary information should be subtle and in the background, while, as mentioned in our first experiment, critical information should be salient and require promptness [27]. Therefore, we recommend that AR headset application designers use the Environment style for supplementary secondary information and the Display style for information that requires urgency to increase users' perception and comprehension.

## 6. Limitations and Future Work

Our results provide insight into the design of critical and secondary information in AR headset displays for users' situational awareness (i.e., perception and comprehension); however, there are some limitations. First, we only examined three types of visual stimulus for critical information and three secondary information presentation styles. In addition, we mainly focused on perception (level 1). Future work can analyze different types of information, as well as comprehension (level 2) and prediction (level 3). Another limitation for the first study was that the visual stimulus constantly changed, which could have prompted the participants to be more

aware and closely monitor the stimulus. Prior work has found that *motion* has a high perception accuracy for peripheral visual notifications on computer screens (i.e., participants were able to quickly perceive the notifications), but it can also distract from the primary task [59,85]. Although the constant change may have prompted the participants, it does not detract from our main goal of comparing different types of stimuli.

## 7. Conclusion

We conducted two studies on how to present critical and secondary information in AR headsets to aid in users' situational awareness: one examining if existing findings on the perceptibility of three types of visual stimulus (color, text, shapes) can be applied to AR headsets for critical information, and one analyzing three presentation styles for textual secondary information (Display, Environment, Mixed Environment). Our results showed that the Display and Environment presentation styles improved the awareness of textual secondary information; participants had a higher recall of information when compared to the Mixed Environment presentation style. For critical information, we found similar results to prior work; the participants perceived color faster, and had a slower response time and higher cognitive workload for text. We contribute design recommendations on how to present critical and secondary information in AR headset displays to aid in users' situational awareness, which is essential to understand in safety crucial domains such as the military and healthcare.

## Institutional Review Board Statement

All participants consented before they participated in the studies. The studies were conducted in accordance with the Declaration of Helsinki, and the protocols were approved by the University of Florida Institutional Review Board.

## Conflict of Interest

The authors declare no conflict of interest.

## Acknowledgment

This work is partially supported by National Science Foundation Grant Award #IIS-1750840 and the National Science Foundation Graduate Research Fellowship under Grant No. DGE-1842473. Any opinions, findings, conclusions, and recommendations expressed in this paper are those of the authors and do not necessarily reflect these agencies' views.

## References

[1] D.W.F. van Krevelen, R. Poelman, "A Survey of Augmented Reality Technologies, Applications and Limitations," *The International Journal of Virtual Reality*, vol. 9, no. 2, pp. 1–20, 2010, doi:10.1155/2011/721827.

[2] S. Vardomatski, Augmented And Virtual Reality After Covid-19, https://www.forbes.com/sites/forbestechcouncil/2021/09/14/augmented-and-virtual-reality-after-covid-19/?sh=1b886d882d97, 2021.

[3] A. Olney, Augmented Reality | All About Holograms, American Library Association: 1–16, 2019.

[4] Meta, Meta Augmented Reality, https://www.metavision.com/, Apr. 2019.

[5] Augmented Reality Is A Game Changer For Oil & Gas, https://oilprice.com/Energy/Energy-General/Augmented-Reality-Is-A-Game-Changer-For-Oil-Gas.html, May 2022.

[6] M.R. Endsley, "Toward a Theory of Situation Awareness in Dynamic Systems," *Human Factors*, vol. 37, no. 1, pp. 32–64, 1995, doi:10.1518/001872095779049543.

[7] M.R. Endsley, "Design and Evaluation for Situation Awareness Enhancement," *Proceedings of the Human Factors Society Annual Meeting*, vol. 32, no. 2, pp. 97–101, 1988, doi:10.1177/154193128803200221.

[8] N.A. Stanton, P.R.G. Chambers, J. Piggott, "Situational Awareness and Safety," *Safety Science*, vol. 39, no. 3, pp. 189–204, 2001, doi:10.1016/S0925-7535(01)00010-8.

[9] T.W. Reader, P. O'Connor, "The Deepwater Horizon Explosion: Non-technical Skills, Safety Culture, and System Complexity," *Journal of Risk Research*, vol. 17, no. 3, pp. 405–424, 2014, doi:10.1080/13669877.2013.815652.

[10] C.M. Schulz, V. Krautheim, A. Hackemann, M. Kreuzer, E.F. Kochs, K.J. Wagner, "Situation Awareness Errors in Anesthesia and Critical Care in 200 Cases of a Critical Incident Reporting System," *BMC Anesthesiology*, vol. 16, no. 4, pp. 10pp, 2016, doi:10.1186/s12871-016-0172-7.

[11] E. Gans, D. Roberts, M. Bennett, H. Towles, A. Menozzi, J. Cook, T. Sherrill, "Augmented Reality Technology for Day/Night Situational Awareness for the Dismounted Soldier," in: Desjardins, D. D., Sarma, K. R., Marasco, P. L., and Havig, P. R., eds., in *Display Technologies and Applications for Defense, Security, and Avionics*, International Society for Optics and Photonics: Article 9470, 2015, doi:10.1117/12.2177086.

[12] Z. Zhu, V. Branzoi, M. Wolverton, G. Murray, N. Vitovitch, L. Yarnall, G. Acharya, S. Samarasekera, R. Kumar, "AR-Mentor: Augmented Reality Based Mentoring System," in *IEEE International Symposium on Mixed and Augmented Reality (ISMAR '14)*, IEEE: 17–22, 2014, doi:10.1109/ISMAR.2014.6948404.

[13] M. Wallmyr, T.A. Sitompul, T. Holstein, R. Lindell, "Evaluating Mixed Reality Notifications to Support Excavator Operator Awareness," in *IFIP Conference on Human-Computer Interaction (INTERACT ' 19)*, Springer, Cham: 743–762, 2019, doi:10.1007/978-3-030-29381-9_44.

[14] D. Liu, S.A. Jenkins, P.M. Sanderson, M.O. Watson, T. Leane, A. Kruys, W.J. Russell, "Monitoring with Head-Mounted Displays: Performance and Safety in a Full-Scale Simulator and Part-Task Trainer," *Anesthesia & Analgesia*, vol. 109, no. 4, pp. 1135–1146, 2009, doi:10.1213/ANE.0b013e3181b5a200.

[15] M.T. Pascale, P. Sanderson, D. Liu, I. Mohamed, B. Brecknell, R.G. Loeb, "The Impact of Head-Worn Displays on Strategic Alarm Management and Situation Awareness," *Human Factors*, vol. 61, no. 4, pp. 537–563, 2019, doi:10.1177/0018720818814969.

[16] S. Ruano, C. Cuevas, G. Gallego, N. García, "Augmented Reality Tool for the Situational Awareness Improvement of UAV Operators," *Sensors*, vol. 17, no. 2, pp. Article 297, 2017, doi:10.3390/s17020297.

[17] B.-J. Park, C. Yoon, J.-W. Lee, K.-H. Kim, "Augmented Reality Based on Driving Situation Awareness in Vehicle," in *International Conference on Advanced Communication Technology (ICACT'15)*, IEEE: 593–595, 2015, doi:10.1109/ICACT.2015.7224865.

[18] D. Aschenbrenner, N. Maltry, J. Kimmel, M. Albert, J. Scharnagl, K. Schilling, "ARTab - Using Virtual and Augmented Reality Methods for an Improved Situation Awareness for Telemaintenance," *IFAC-PapersOnLine*, vol. 49, no. 30, pp. 204–209, 2016, doi:10.1016/J.IFACOL.2016.11.168.

[19] K.-H. Kim, K.-Y. Wohn, "Effects on Productivity and Safety of Map and Augmented Reality Navigation Paradigms," *IEICE TRANSACTIONS on Information and Systems*, vol. E94-D, no. 5, pp. 1051–1061, 2011, doi:10.1587/transinf.E94.D.1051.

[20] L. Hou, X. Wang, "A Study on the Benefits of Augmented Reality in Retaining Working Memory in Assembly Tasks: A Focus on Differences in Gender," *Automation in Construction*, vol. 32, , pp. 38–45, 2013, doi:10.1016/J.AUTCON.2012.12.007.

[21] M.-C. Chen, R. Klatzky, "Displays Attentive to Unattended Regions: Presenting Information in a Peripheral-Vision-Friendly Way," *International Conference on Human-Computer Interaction (HCII'07)*, vol. 4551, , pp. 23–31, 2007.

[22] C.G. Healey, K.S. Booth, J.T. Enns, "High-Speed Visual Estimation Using Preattentive Processing," *ACM Transactions on Computer-Human Interaction*, vol. 3, no. 2, pp. 107–135, 1996, doi:10.1145/230562.230563.

[23] Y. Ishiguro, J. Rekimoto, "Peripheral Vision Annotation: Noninterference Information Presentation Method for Mobile Augmented Reality," in *Proceedings of the Augmented Human International Conference (AH'11)*, ACM Press, New York, New York, USA: 1–5, 2011, doi:10.1145/1959826.1959834.

[24] E. Kruijff, J.E. Swan, S. Feiner, "Perceptual Issues in Augmented Reality Revisited," in *IEEE International Symposium on Mixed and Augmented Reality (ISMAR '10)*, IEEE: 3–12, 2010, doi:10.1109/ISMAR.2010.5643530.

[25] M.A. Livingston, J.L. Gabbard, J.E. Swan, C.M. Sibley, J.H. Barrow, Basic Perception in Head-Worn Augmented Reality Displays, Springer New York, New York, NY: 35–65, 2013, doi:10.1007/978-1-4614-4205-9_3.

[26] J.L. Gabbard, J.E. Swan, J. Zedlitz, W.W. Winchester, "More Than Meets the Eye: An Engineering Study to Empirically Examine the Blending of Real and Virtual Color Spaces," in *IEEE Virtual Reality Conference (VR '10)*, IEEE: 79–86, 2010, doi:10.1109/VR.2010.5444808.

[27] M.R. Endsley, "Designing for Situation Awareness in Complex System," in *Proceedings of the Second International Workshop on Symbiosis of Humans, Artifacts and Environment*, 14pp, 2001.

[28] S. Ganapathy, Design Guidelines for Mobile Augmented Reality: User Experience, Springer New York, New York, NY: 165–180, 2013, doi:10.1007/978-1-4614-4205-9_7.

[29] J. Woodward, J. Smith, I. Wang, S. Cuenca, J. Ruiz, "Examining the Presentation of Information in Augmented Reality Headsets for Situational Awareness," in *ACM International Conference on Advanced Visual Interfaces (AVI '20)*, ACM Press: 1–5, 2020, doi:10.1145/3399715.3399846.

[30] S. Lukosch, H. Lukosch, D. Datcu, M. Cidota, "Providing Information on the Spot: Using Augmented Reality for Situational Awareness in the Security Domain," *Computer Supported Cooperative Work (CSCW '15)*, vol. 24, no. 6, pp. 613–664, 2015, doi:10.1007/s10606-015-9235-4.

[31] S. Zollmann, C. Hoppe, T. Langlotz, G. Reitmayr, "FlyAR: Augmented Reality Supported Micro Aerial Vehicle Navigation," *IEEE Transactions on Visualization and Computer Graphics*, vol. 20, no. 4, pp. 560–568, 2014, doi:10.1109/TVCG.2014.24.

[32] J. Fromm, K. Eyilmez, M. Baßfeld, T.A. Majchrzak, S. Stieglitz, "Social Media Data in an Augmented Reality System for Situation Awareness Support in Emergency Control Rooms," *Information Systems Frontiers*, vol. 25, no. 3, pp. 303–326, 2021, doi:10.1007/S10796-020-10101-9.

[33] Minh Tien Phan, I. Thouvenin, V. Fremont, "Enhancing the Driver Awareness of Pedestrian Using Augmented Reality Cues," in *IEEE International Conference on Intelligent Transportation Systems (ITSC '16)*, IEEE: 1298–1304, 2016, doi:10.1109/ITSC.2016.7795724.

[34] M. Colley, B. Eder, J.O. Rixen, E. Rukzio, "Efects of Semantic Segmentation Visualization on Trust, Situation Awareness, and Cognitive Load in Highly Automated Vehicles," in *Proceedings of the SIGCHI Conference on Human Factors in Computing Systems (CHI '21)*, Association for Computing Machinery: 11pp, 2021, doi:10.1145/3411764.3445351.

[35] A. Rowen, M. Grabowski, J.P. Rancy, A. Crane, "Impacts of Wearable Augmented Reality Displays on Operator Performance, Situation Awareness, and Communication in Safety-Critical Systems," *Applied Ergonomics*, vol. 80, , pp. 17–27, 2019, doi:10.1016/J.APERGO.2019.04.013.

[36] J. Coleman, D. Thirtyacre, "Remote Pilot Situational Awareness with Augmented Reality Glasses: An Observational Field Study," *International Journal of Aviation, Aeronautics, and Aerospace*, vol. 8, no. 1, pp. 10pp, 2021, doi:https://doi.org/10.15394/ijaaa.2021.1547.

[37] H. Chen, L. Hou, G. (Kevin) Zhang, S. Moon, "Development of BIM, IoT and AR/VR technologies for Fire Safety and Upskilling," *Automation in Construction*, vol. 125, no. 103631, 2021, doi:10.1016/J.AUTCON.2021.103631.

[38] M. Bhattarai, A.R. Jensen-Curtis, M. Martinez-Ramon, "An Embedded Deep Learning System for Augmented Reality in Firefighting Applications," in *IEEE International Conference on Machine Learning and Applications (ICMLA '20)*, IEEE: 1224–1230, 2020, doi:10.1109/ICMLA51294.2020.00193.

[39] J. Huuskonen, T. Oksanen, "Augmented Reality for Supervising Multirobot System in Agricultural Field Operation," *IFAC-PapersOnLine*, vol. 52, no. 30, pp. 367–372, 2019, doi:10.1016/J.IFACOL.2019.12.568.

[40] E.R. Velamkayala, M. V. Zambrano, H. Li, "Effects of HoloLens in Collaboration: A Case in Navigation Tasks," *Human Factors and Ergonomics Society Annual Meeting*, vol. 61, no. 1, pp. 2110–2114, 2017, doi:10.1177/1541931213602009.

[41] J. Blattgerste, B. Strenge, P. Renner, T. Pfeiffer, K. Essig, "Comparing Conventional and Augmented Reality Instructions for Manual Assembly Tasks," in *Proceedings of the International Conference on Pervasive Technologies Related to Assistive Environments (PETRA '17)*, ACM Press, New York, New York, USA: 75–82, 2017, doi:10.1145/3056540.3056547.

[42] S. Wang, M. Parsons, J. Stone-McLean, P. Rogers, S. Boyd, K. Hoover, O. Meruvia-Pastor, M. Gong, A. Smith, "Augmented Reality as a Telemedicine Platform for Remote Procedural Training," *Sensors*, vol. 17, no. 10, pp. Article 2294, 2017, doi:10.3390/s17102294.

[43] D. Datcu, S. Lukosch, H. Lukosch, "Comparing Presence, Workload and Situational Awareness in a Collaborative Real World and Augmented Reality Scenario," *IEEE ISMAR Workshop on Collaboration in Merging Realities (CiMeR '13)*, pp. 6pp, 2013, doi:https://research.tudelft.nl/.

[44] R. Rzayev, P.W. Wozniak, T. Dingler, N. Henze, "Reading on Smart Glasses: The Effect of Text Position, Presentation Type and Walking," in *Proceedings of the SIGCHI Conference on Human Factors in Computing Systems (CHI'18)*, ACM Press, New York, New York, USA: 9pp, 2018, doi:10.1145/3173574.3173619.

[45] A. Albarelli, A. Celentano, L. Cosmo, R. Marchi, "On the Interplay between Data Overlay and Real-World Context using See-through Displays," in *Proceedings of the Biannual Conference on Italian SIGCHI Chapter (CHItaly'15)*, ACM Press, New York, New York, USA: 58–65, 2015, doi:10.1145/2808435.2808455.

[46] J. Orlosky, K. Kiyokawa, H. Takemura, "Managing Mobile Text in Head Mounted Displays: Studies on Visual Preference and Text Placement," *ACM SIGMOBILE Mobile Computing and Communications Review*, vol. 18, no. 2, pp. 20–31, 2014, doi:10.1145/2636242.2636246.

[47] S. Kim, M.A. Nussbaum, J.L. Gabbard, "Influences of Augmented Reality Head-Worn Display Type and User Interface Design on Performance and Usability in Simulated Warehouse Order Picking," *Applied Ergonomics*, vol. 74, , pp. 186–193, 2019, doi:10.1016/J.APERGO.2018.08.026.

[48] D. Ariansyah, J.A. Erkoyuncu, I. Eimontaite, T. Johnson, A.M. Oostveen, S. Fletcher, S. Sharples, "A Head Mounted Augmented Reality Design Practice for Maintenance Assembly: Toward Meeting Perceptual and Cognitive Needs of AR Users," *Applied Ergonomics*, vol. 98, , pp. 103597, 2022, doi:10.1016/J.APERGO.2021.103597.

[49] M. Gattullo, L. Dammacco, F. Ruospo, A. Evangelista, M. Fiorentino, J. Schmitt, A.E. Uva, "Design Preferences on Industrial Augmented Reality: A Survey with Potential Technical Writers," in *IEEE International Symposium on Mixed and Augmented Reality (ISMAR '20)*, IEEE: 172–177, 2020, doi:10.1109/ISMAR-ADJUNCT51615.2020.00054.

[50] N. Irrazabal, G. Saux, D. Burin, "Procedural Multimedia Presentations: The Effects of Working Memory and Task Complexity on Instruction Time and Assembly Accuracy," *Applied Cognitive Psychology*, vol. 30, no. 6, pp. 1052–1060, 2016, doi:10.1002/ACP.3299.

[51] K. Sekiguchi, A.A. Nugraha, Y. Du, Y. Bando, M. Fontaine, K. Yoshii, "Direction-Aware Adaptive Online Neural Speech Enhancement with an Augmented Reality Headset in Real Noisy Conversational Environments," in *International Conference on Intelligent Robots and Systems (IROS '22)*, 9266–9273, 2022, doi:10.1109/IROS47612.2022.9981659.

[52] S. Debernardis, M. Fiorentino, M. Gattullo, G. Monno, A.E. Uva, "Text Readability in Head-Worn Displays: Color and Style Optimization in Video versus Optical See-Through Devices," *IEEE Transactions on Visualization and Computer Graphics*, vol. 20, no. 1, pp. 125–139, 2014, doi:10.1109/TVCG.2013.86.

[53] J.J. Dudley, J.T. Jacques, P.O. Kristensson, "Crowdsourcing Design Guidance for Contextual Adaptation of Text Content in Augmented Reality," in *SIGCHI Conference on Human Factors in Computing Systems - Proceedings*, Association for Computing Machinery: 14pp, 2021, doi:10.1145/3411764.3445493.

[54] L. Stearns, L. Findlater, J.E. Froehlich, "Design of an Augmented Reality Magnification Aid for Low Vision Users," in *International ACM SIGACCESS Conference on Computers and Accessibility (ASSETS' 18)*, ACM: 28–39, 2018, doi:10.1145/3234695.3236361.

[55] R. Brown, Meta 2: Full Specification, https://vr-compare.com/headset/meta2, May 2022.

[56] S. Ando, N. Kida, S. Oda, "Central and Peripheral Visual Reaction Time of Soccer Players and Nonathletes," *Perceptual and Motor Skills*, vol. 92, no. 3, pp. 786–794, 2001, doi:10.2466/pms.2001.92.3.786.

[57] G. Berlucchi, W. Heron, R. Hyman, G. Rizzolatti, C. Umiltà, "Simple Reaction Times of Ipsilateral and Contralateral Hand to Lateralized Visual Stimuli," *Brain*, vol. 94, no. 3, pp. 419–430, 1971, doi:10.1093/brain/94.3.419.

[58] Unity, https://unity3d.com/, 2022.

[59] A. Mairena, C. Gutwin, A. Cockburn, "Peripheral Notifications in Large Displays: Effects of Feature Combination and Task Interference," in *Proceedings of the SIGCHI Conference on Human Factors in Computing Systems (CHI'19)*, ACM Press, New York, New York, USA: 12pp, 2019, doi:10.1145/3290605.3300870.

[60] D. Bowers, K.M. Heilman, "Pseudoneglect: Effects of Hemispace on a Tactile Line Bisection Task," *Neuropsychologia*, vol. 18, no. 4–5, pp. 491–498, 1980, doi:10.1016/0028-3932(80)90151-7.

[61] N.A. Thomas, O. Schneider, C. Gutwin, L.J. Elias, "Dorsal Stream Contributions to Perceptual Asymmetries," *Journal of the International Neuropsychological Society : JINS*, vol. 18, no. 2, pp. 251–259, 2012, doi:10.1017/S1355617711001585.

[62] S.D. Christman, C.L. Niebauer, "The Relation Between Left-Right and Upper-Lower Visual Field Asymmetries: (Or: What Goes Up Goes Right While What's Left Lays Low)," *Advances in Psychology*, vol. 123, , pp. 263–296, 1997, doi:10.1016/S0166-4115(97)80076-3.

[63] A.K. Smith, I. Szelest, T.E. Friedrich, L.J. Elias, "Native Reading Direction Influences Lateral Biases in The Perception of Shape From Shading," *Laterality*, vol. 20, no. 4, pp. 418–433, 2014, doi:10.1080/1357650X.2014.990975.

[64] ISO 7010:2011 Graphical symbols, https://www.iso.org/standard/54432.html, 2011.

[65] S.G. Hart, "Nasa-Task Load Index (NASA-TLX); 20 Years Later," *Proceedings of the Human Factors and Ergonomics Society Annual Meeting*, vol. 50, no. 9, pp. 904–908, 2006, doi:10.1177/154193120605000909.

[66] P. Mealy, Planning Your Augmented Reality Project, John Wiley & Sons, Inc. : 159–161, 2018.

[67] L. Rello, R. Baeza-Yates, "How to Present More Readable Text for People with Dyslexia," *Universal Access in the Information Society*, vol. 16, no. 1, pp. 29–49, 2017, doi:10.1007/s10209-015-0438-8.

[68] D.J. McKeefry, N.R.A. Parry, I.J. Murray, "Simple Reaction Times in Color Space: The Influence of Chromaticity, Contrast, and Cone Opponency," *Investigative Opthalmology & Visual Science*, vol. 44, no. 5, pp. 2267–2276, 2003, doi:10.1167/iovs.02-0772.

[69] V. Kuperman, H. Stadthagen-Gonzalez, M. Brysbaert, "Age-Of-Acquisition Ratings for 30,000 English Words," *Behavior Research Methods*, vol. 44, no. 4, pp. 978–990, 2012, doi:10.3758/s13428-012-0210-4.

[70] R.H. Logie, K.J. Gilhooly, V. Wynn, "Counting on Working Memory in Arithmetic Problem Solving," *Memory & Cognition*, vol. 22, no. 4, pp. 395–410, 1994, doi:10.3758/BF03200866.

[71] A. Baddeley, "Working Memory," *Science*, vol. 255, no. 5044, pp. 556–559, 1992, doi:10.1126/SCIENCE.1736359.

[72] K. Miller, M. Perlmutter, D. Keating, "Cognitive Arithmetic: Comparison of Operations," *Journal of Experimental Psychology: Learning, Memory, and Cognition*, vol. 10, no. 1, pp. 46–60, 1984, doi:10.1037/0278-7393.10.1.46.

[73] J.I.D. Campbell, D.J. Graham, "Mental Multiplication Skill: Structure, Process, and Acquisition.," *Canadian Journal of Psychology*, vol. 39, no. 2, pp. 338–366, 1985, doi:10.1037/h0080065.

[74] P. Lemaire, M. Fayol, "The Role of Working Memory Resources in Simple Cognitive Arithmetic," *European Journal of Cognitive Psychology*, vol. 8, no. 1, pp. 73–103, 1996.

[75] G.J. Groen, J.M. Parkman, "A Chronometric Analysis of Simple Addition," *Psychological Review*, vol. 79, no. 4, pp. 329–343, 1972, doi:10.1037/h0032950.

[76] Wacom, Professional Hybrid Creative Tablet User's Manual About the Cintiq Companion Hybrid, 1–93, https://cdn.wacom.com/f/manual/0x0307/UM-EN.pdf, May 2022.

[77] O.N. Keene, "The Log Transformation is Special," *Statistics in Medicine*, vol. 14, no. 8, pp. 811–819, 1995, doi:10.1002/sim.4780140810.

[78] J.O. Wobbrock, L. Findlater, D. Gergle, J.J. Higgins, "The Aligned Rank Transform for Nonparametric Factorial Analyses Using Only Anova Procedures," in *Proceedings of the SIGCHI Conference on Human Factors in Computing Systems (CHI'11)*, ACM Press, New York, New York, USA: 143–146, 2011, doi:10.1145/1978942.1978963.

[79] C. Healey, J. Enns, "Attention and Visual Memory in Visualization and Computer Graphics," *IEEE Transactions on Visualization and Computer Graphics*, vol. 18, no. 7, pp. 1170–1188, 2012, doi:10.1109/TVCG.2011.127.

[80] M.S. Fine, B.S. Minnery, "Visual Salience Affects Performance in a Working Memory Task," *Journal of Neuroscience*, vol. 29, no. 25, pp. 8016–8021, 2009, doi:10.1523/JNEUROSCI.5503-08.2009.

[81] A. Batra, D. Jeph, S. Vyas, "Color Difference on Simple Visual Reaction Time in Young Volunteers," *International Journal of Clinical and Experimental Physiology*, vol. 1, no. 4, pp. 311–313, 2014, doi:10.4103/2348-8093.149771.

[82] H.-Y. Kim, "Statistical Notes for Clinical Researchers: Chi-squared Test and Fisher's Exact Test.," *Restorative Dentistry & Endodontics*, vol. 42, no. 2, pp. 152–155, 2017, doi:10.5395/rde.2017.42.2.152.

[83] R. Rzayev, S. Mayer, C. Krauter, N. Henze, "Notification in VR: The Effect of Notification Placement, Task, and Environment," in *Computer-Human Interaction in Play (CHIPlay'19)*, ACM Press: 199–211, 2019, doi:10.1145/3311350.3347190.

[84] R. Rzayev, S. Korbely, M. Maul, A. Schark, V. Schwind, N. Henze, "Effects of Position and Alignment of Notifications on AR Glasses during Social Interaction," in *Proceedings of the Nordic Conference on Human-Computer Interaction (NordiCHI '20)*, ACM Press, New York, NY, USA: 11pp, 2020, doi:10.1145/3419249.

[85] C. Gutwin, A. Cockburn, A. Coveney, "Peripheral Popout: The Influence of Visual Angle and Stimulus Intensity on Popout Effects," in *Proceedings of the SIGCHI Conference on Human Factors in Computing Systems (CHI '17)*, ACM Press, New York, New York, USA: 208–219, 2017, doi:10.1145/3025453.3025984.

Received: 21 December 2022, Revised: 09 February 2023, Accepted: 16 February 2023, Online: 27 March 2023
DOI: https://dx.doi.org/10.55708/js0203002

# Coding: First Steps from Kindergarten up to Primary School

**Elisa Benetti*** **, Gianluca Mazzini**
Lepida ScpA, Via della Liberazione 15, 40128, Bologna, Italy
*Corresponding author: Elisa Benetti & elisa.benetti@lepida.it

**ABSTRACT:** Computational thinking is now featured in many school curricula around the world. It is in fact defined as the "new English", emphasizing its universally recognized indispensability. Despite this, the subject is almost never addressed until primary school where, however, hours dedicated to it are often too limited. Our first training proposal, including basic coding concepts in kindergarten, led to better results than expected in terms of children's understanding and involvement. Our field training has led to a refinement and expansion of the program in these past three years. The primary objective is to begin the study of coding at the age of three, when the foundations of logical thinking are actually already present, due to get to the writing of the first programs in pseudocode and analysis of programming languages at the end of elementary school. All methodologies used are chosen on the basis of the possibility of following a single logical trend, which gradually increases the concepts to be learned and their difficulty, but always starting from already known bases, previously addressed. This allows to optimize learning times by minimizing the necessary hours and human resources and still obtaining the desired results. In addition to not burdening the number of hours available, a further firm point was not to burden schools economically either: costs were in fact always achievable without any problems. Having no impact either on the budget, or on the number of hours, or on the required staff makes this program easily feasible for any school.

**KEYWORDS:** Coding, Kidergarten, Primary School

## 1. Introduction

The concept of computational thinking was first introduced by Seymour Papert in the book Mindstorms [1], published in 1980, where in his theory of learning, known as Constructivism and based on the LOGO language he invented, he states how the computer is an important new medium for learning. Indeed, it is seen not only as a machine with which you can process information, but a tool for building, manipulating, learning, discovering and even making mistakes. A very important point of his theory for the purposes of the work presented in this article, in fact, is that error is not seen in a negative light, but as a constructive aspect of the learning process. To err is to explore in search of alternative solutions to the problem. More recently, in 2006, this concept has been taken up by computer scientist and MIT professor Jeanette Wing, who defines it as follows, "Computational thinking is a process of formulating problems and solutions in a form that is executable by an agent who processes information." [2] Indeed, we know that computers are used to solve problems, but even before solving a problem, it is important to understand by what means it can be solved, and it is computational thinking that enables us to do this.

The revolution of this concept is to note that it is not only important to solve problems, but more importantly to understand them, in order to formulate a process that leads to its resolution. This process can be performed by an agent or executor, figures that we will see in the exercises used, who implements instructions in a mechanical and unconscious manner, replicating human thinking. Computational thinking has been used in programming for the longest time, but recently also in coding, as well as in educational robotics. Tools used are not only technological and related to these disciplines, but also in normal life situations involving the decomposition of a problem, just to emphasize its importance in any aspect of life. Every day, without even realizing it, we find ourselves deciding on the expression of a solution by instructions and the execution of those instructions: finding the shortest route to a place, executing a recipe, assembling an object, assembling constructions. All of those listed are processes that involve computational thinking and presuppose a set of precise, orderly, clear, and repeatable instructions that will enable an effective solution to be reached by whoever is executing them. These instructions represent a de facto algorithm, that will certainly lead to the solution and can be applied to another identical problem with the same result, just as is the case with the algorithms behind any type of programming: from making decisions in a video game to performing an Internet search to managing interpersonal relationships on a smartphone.

Thus, computational thinking can be described by three main stages:

1. Abstraction: formulation of the problem;
2. Automation: expression of the solution;
3. Analysis: execution of the solution and evaluation.

All this is done by starting with the ability to break down a complex problem into several parts so that it can be tackled more easily. In this, coding is similar to mathematics: it is the logic of everything that works in a programmable way as mathematics is the logic of numbers and figures.

The International Society for Technology in Education [3], too, further highlights its importance in school education, pointing out that computational thinking allows people to:

1. Represent problem data through specific models;
2. Organize problem data in a logical manner;
3. Formulate and analyze problems so that they can be solved by a performer, computer or human;
4. Segment solutions into sequences of ordered, accurately described steps, or automate them through algorithms;
5. Identify possible solutions to implement the one that is the most effective and efficient in terms of effort and resources;
6. Abstract such processes for solving similar problems;

Computational thinking therefore is not only closely related to computer science and it is essential to develop it from an early age. One of the most effective ways to do this is to cultivate it through the use of coding tools, the process of writing languages and instructions intended for machines. Coding also constitutes a practical and immediate way to apply the theory of computational thinking and its previously illustrated steps and tools, while having fun, leaving room for creativity and imagination, while learning a new language and a new way of seeing problems and situations and expressing one's ideas and solutions clearly and effectively, thus also developing one's intelligence and critical thinking.

Coding, is not the only way to develop, or apply, computational thinking, but it has proven to be particularly effective because of the immediacy, interactivity, variety, availability and versatility of available tools. For this reason, its presence in school curricula is now worldwide recognized as indispensable as also explained in [4]. However, the training solutions and proposals available to date have been designed in limited areas. In fact, they are often focused only on the specific skills of an age: a lot of work has been done to exploit cognitive skills already in the pre-school context. For example, [5] shows how a coding course has led to an objective increase in problem solving skills and cognitive abilities in 4 and 5 year old children. On the other hand, children of various elementary schools in [6] used the Code.org site showing how, after following 8 coding activities, also in this case cognitive abilities increased, and not only that: children began to spend more time to planning, with increased ability to solve standardized planning tasks and in many cases even led to an inhibition of overbearing responses. In other researches, such as [7], the age analyzed is broader but the tool used is very specific, in this case apps. Both [8] and [9] searched in several elementary schools with a wider time range but in both cases using only the Scratch application. Therefore, in the existing literature, there are no proposals that lead to a general use for a long period. Our proposal therefore has the objective of choosing some of the tools available, designed for the different abilities relating to growing ages but sufficiently similar to allow the development of a fluid and continuous coding educational path. New complexities are, in fact, gradually added along the way, following this list of concepts gradually taught, starting from 3 years of age, reaching 11 years: instruction and sequence, coding through colors and symbols, algorithm, constraints, transcoding, programming a robot, programming on tablets or devices analogues, programming a hardware device using block programming, first approaches to a real programming language.

## 2. Dissemination of coding at school

The spread of coding in schools around the world has been gradual. Many countries have already implemented coding as a subject in primary education programs for years, recognizing its importance, and we can see the most striking examples, summarized in table 1.

Table 1: Summary of coding dissemination in the world

| | |
|---|---|
| Singapore | 2014 |
| France | 2014 |
| Denmark | 2014 |
| Spain | 2015 |
| UK | 2015 |
| Estonia | 2015 |
| Slovakia | 2015 |
| Philippines | 2015 |
| Australia | 2015 |
| Belgium | 2016 |
| Finland | 2016 |
| Poland | 2016 |
| Portugal | 2016 |
| United Arabian Emirates | 2017 |
| Qatar | 2020 |
| South Africa | 2020 |
| Italy | 2021 |
| Kenya | 2022 |

Australia as early as 2015 has noticed a growing need for technology talent recognizing that the future of work is toward technology, as seen in [10]. In order to properly train its younger generation by providing the technological knowledge necessary for their future, it started early to allocate significant economic sums. To reach kindergarten and basic education on programming, the Australian government spends 64 million dollars to fund school-based STEM (Science, Technology, Engineering, and Mathematics) and early learning initiatives under the Inspiring All Australians in Digital Literacy and STEM measure. As early as 2018, coding teaching from elementary school onward is mandatory in Australia.

In Asia, on the other hand, Singapore, which adopted computer science education in 2014 as shown in [11], quickly made it a compulsory subject, as early as 2020 and giving it

a lot of space in school curricula: coding, in fact, is usually done for 10 hours per week. The Singapore government, in 2017, released 3 million dollars allocated for the distribution of 100,000 coding pocket gadgets to school children before the start of compulsory coding and spent annual budget allocations for the program. Malaysia, Thailand, Vietnam, and Indonesia have already been investing economically for years in their turn for the dissemination of coding. In contrast, an Asian country that has more recently introduced programming as a subject in primary and secondary schools is the Philippines. Although the government, unlike those previously mentioned, spends much less on programming education, pupils show much interest in programming and are willing to learn programming in school. Interviews from 2015 already showed that about 97 percent of students in the Philippines were interested in learning about programming and 96 percent wanted programming to become a core subject in their schools.

South Africa was the first African country to adopt coding education at primary and secondary levels [12]. In 2020, it began by providing programs for teachers to learn how to teach programming as a first step in order to be able to pass the same knowledge on to students. On the other hand, Software Engineer turns out to be the most in-demand job in South Africa to date, and for this reason the government in South Africa is paying a lot of attention to technical education, understanding how necessary it is to equip the younger generation with relevant technical skills to adapt when it comes to future jobs. In the recent August 2022, the Kenyan government also announced the inclusion of programming as a subject in its educational curriculum for primary and secondary school pupils, becoming the second African country to adopt programming education at primary and secondary levels.

More than 90 percent of parents in the United Arabian Emirates wanted their children taught programming in schools as early as 2017, and in year 2020, about 35 percent of schools in the country have begun implementing programming courses for their students. The Arab country has immediately begun to transform the entire education system by adopting the use of e-books, robotics, and other emerging technologies in teaching and learning. Other countries have also more recently begun efforts to prepare new generations for the technological revolution that will shape future jobs, for example, Qatar since 2020 has been restructuring its education system to include programming.

In Europe, the first effort aimed at the importance of coding across a broad spectrum, is undoubtedly codeweek, [13], launched in 2013. The European Commission supports European Programming Week as part of its Digital Single Market strategy. In its Digital Education Action Plan, it especially encourages schools to join the initiative. European Programming Week is an event therefore aimed primarily at schools but not only, celebrating creativity, problem solving and collaboration through programming and other technology activities. The idea is to make programming more visible, show young people, adults and older people how to bring their ideas to life with programming, explain these skills and bring motivated people together to learn. The latest statistics regarding the event that took place in 2021 show that 4 million people from more than 80 countries around the world participated in European Programming Week. The average age of the participants was 11 years old, and 49 percent of them in 2021 were women or girls. Eighty-eight percent of European Programming Week events took place in schools, showing that efforts to strengthen teachers, during the 2021 campaign, were successful. Another experience is provided by the web site All you need is C<3DE , through which the European Coding Initiative has supported thousands of teachers across Europe in their efforts to integrate programming and coding teaching with a collection of open online courses, teaching materials, tools and lesson plans. To understand the uptake in compulsory schools it helps the JRC, which, in March 2022, published a new report [14] which examines the integration of computational thinking in compulsory schools in 29 countries, European and non-European: 18 european and 7 non-european countries have already made the teaching of coding compulsory, of the remaining 4 Denmark is carrying out a pilot initiative, while Italy, Slovenia and the Czech Republic have policies in this direction.

In fact, even Italian Parliament finally seems to have become convinced of the need and urgency, necessary requirements for law decrees, to also include coding as a basic learning skill The National Recovery and Resilience Plan(PNRR) is the plan approved in 2021 by Italy to revive its economy after the COVID-19 pandemic in order to enable the country's green and digital development. Among the measures foreseen with regard to schools can be found that, as of the school year 2025/2026, it will be mandatory in schools of all grades and levels to pursue the development of digital skills, including by fostering the learning of computer programming (coding), within the existing teachings. Albeit, quoting the text here, "with the human, instrumental and financial resources available under current legislation and in any case without or greater burdens on public finance". These resources, both human and financial, are far from substantial in Italy. In proposals regarding coding, therefore, it must also be taken into account that they should not be economically costly and should not weigh excessively on available school hours either. That is, programs must be proposed that optimize the number of hours needed with respect to the skills acquired by students, using material that is as low-cost as possible.

We have therefore seen how the importance of coding in the school curriculum is recognized worldwide and both strategic and economic plans are being implemented everywhere for its diffusion. Australia has been among the first to leave, as early as 2015. In Asia, Singapore in 2014, the Philippines in 2015 and the United Arab Emirates in 2017 started early, with a subsequent slowdown. However, since the Code for Asia project [15] was born in 2021, other countries are quickly aligning, such as Malaysia, Thailand, Vietnam and Indonesia. In Europe, the beginning was given by the codeweek in 2013, following which, between 2014 and 2017, most European countries began to promote initiatives for the diffusion of coding. Italy was among the last to join, in 2021. The continent that moved last was Africa, where South Africa was the first to introduce coding into primary and secondary schools in 2020, followed last year by

Kenya. In 2022, the AltSchool digital campus was born, with a purely technological curriculum, also attracting interest in Nigeria, Ghana, Uganda and Botswana. CodingAfrica [16] was also born in 2022, with the aim of promoting tech literacy in the rest of Africa. Our effort in trying to introduce coding already in preschool age started in 2019, with the first year of a pilot project in a kindergarten in the province of Bologna. These almost four years of proactive field experience have allowed us to already have a concrete and easily implementable solution in any school, even without any previous experience since teachers are provided with both the list of necessary materials and a series of lessons, ideas, exercises and software/hardware creations to copy or draw inspiration from. This opportunity is today very important in our territory, given the mandatory nature of coding in Italian school curricula by 2025/2026.

### *2.1. Gender Gap in STEM*

We devote a final space for reflection to how the introduction of coding in education can also help overcome existing gender gaps.

In Iraq, for example, coding has been, since 2020, a tool used for a dual purpose: to also help the gender gap present in education. Indeed, there are still to this day both strong regional differences within the country and more widespread structural, social and cultural barriers that prevent girls from fully and equally accessing and completing their education, thus making it more difficult for them to participate in the employment sector and also in society as a whole. To address this problem, Mercy Hands for Humanitarian Aid, in partnership with Mercy Hands Europe and with support from the Canadian Fund for Local Initiatives, has implemented an innovative project to strengthen girls' technology skills in Basra through computer and coding courses, benefiting both female students and teachers. The goal of the project is to improve girls' IT and programming skills by giving them more employability while training teachers on IT and coding in public schools in Shatt al-Arab.

In Europe there is a similar gender gap related to STEM (Science, Technology, Engineering and Mathematics) subjects. In fact, as explained in [17] and [18], there is a critical gender gap in STEM areas at all levels of education and the labor market. Various research and statisticsshow that globally, women obtain 53 percent of STEM university degrees, but in the EU only 34 percent of graduates in the field are women. Moreover, in 2018, only 41 percent of EU scientists and engineers were women, and only five EU member states had more women scientists than men: Lithuania, Bulgaria, Latvia, Portugal, and Denmark. Finally, note that there is also a "gender equality paradox," whereby women are less likely to obtain STEM degrees in wealthier societies with greater gender equality, such as Finland and Sweden.

Particularly in Italy we are at the bottom of the European rankings for female participation in the digital economy and society. To make up for this, fortunately already for a number of years there have been many organizations dedicated to promoting a better image of science and technology subjects and building a real sisterhood among girls who engage in these areas. Notable among them is definitely Girls who code [19], whose mission is to change the stereotypical image of the programmer. Girls who code, instead, offers several free courses and classes on programming and women working in the technology area. Another successful initiative is Coding Girls [20], born in 2014 and supported by the U.S. Diplomatic Mission in Italy, the Ministry of Education, University and Research, Roma Capitale and Microsoft. In subsequent editions, the project has grown to shape itself as an augmented educational program to train the next generation in STEAM, but more importantly, to help young female students gain confidence in science and navigate the careers of the future. There are also Girls Code it better project clubs, which organize workshops at various secondary schools in grades I and II. Girlstart, projectCSGIRLS and Technovation girls also carry out similar operations.

## 3. Coding in kindergarten and primary school

There are many reasons why primary school children should be taught programming, some of which have already been discussed in the preceding paragraphs. Among first reasons is the great ability of children in being able to learn new notions quickly, which is why from an early age they are induced to learn new foreign languages. If we consider the enormous influence that technological revolution is having in the world of work, learning coding and programming language allow children to have a greater understanding, from an early age, of how computers and technology work, skills that are indispensable today in the world of work as well as in everyday life. Benefits are not only technical: an additional one comes precisely from the possibility of developing, through educational coding programs, important general social and relational skills such as working in teams. Recognizing an error in a solution process helps to understand how making mistakes can be an opportunity for improvement and collaboration to reach the solution, also in an increasingly optimized way. Specifically, on the other hand, the final learning of programming languages is a great exercise for children in learning what can be called in effect a new language. Coding has proven in our experience to be an easily applicable tool as early as kindergarten because the basics of logical thinking, already broadly understood by age 3, can be taught very simply through fun games.

As we explained earlier, coding in schools started to spread as early as 8 years old, and in recent years many tools have been proposed that can be used in programs to be carried out in school and in specific events. Those chosen for this project were decided on the basis of two basic components, which are derived from the previously quoted sentence of the PNRR:

1. Possibly they must be no cost, where not possible they must be limited cost and allow with limited purchases ample opportunity for use.

2. They must fit the relative abilities of the age of the children to whom they are proposed while trying to create a uniform path with a smooth transition from one tool to the next more advanced one, all the way

from age 3 to 11, thus minimizing the hours needed to learn coding.

We then go on to illustrate first for kindergarten and then for primary school, all proposed exercises and tools chosen for this pathway.

### *3.1. Constraints and choices for preschool*

The most obvious constraint in preschool is that children are unable to read and write. Tools used must therefore rely on colors and symbols. The need to make lessons playful is high, especially in the early approach. Finally, although devices such as smartphones and tablets are now used from the earliest years of life, the concepts of programming and computer science as they are understood in the working world are far from the minds of children of this age. It therefore becomes essential to demonstrate how logical thinking is applicable, and often unconsciously already applied, in what they do every day. In addition, in order to minimize the hours needed for coding, the proposed exercises are integrated with other activities and topics covered in the school year.

### *3.2. Sequences and encodings*

The first approach with 3 and 4 year old children is done using two types of cards: codyfeet free and codycolor. As explained in [21] this decision was made in order to separate the concepts of sequencing and coding so that they can be learned gradually before combining them at a later stage. Interaction with children is crucial to maintain attention and the introduction is an example of this, starting by asking them if they want to guess what coding is, then suggesting that it is related to the word code. Already this first stimulus to reasoning has always brought out the link to passwords and secret codes. Asking what secret codes they know leads to the unlock code on their parents' tablet or smartphone. This already leads to the next level where teachers notice together with children that the codes are of several different types: some parents use numbers, some use signs, some use biometric data such as fingerprint or face recognition. Also when asked what they ask to unlock these devices for, the main reasons are: viewing videos on social channels or video games. This leads to the explanation that behind both there is a code that is called programming language, which programmers use. Programming is not only needed for games and applications but it can be found everywhere and the theacher can look with the children in what they do during the day or what they would like to do when they grow up, where the programming or coding is found. The amazement and interest in seeing that it exists in everything increases their interest: if they want to fly a plane they will use programmed controls, if they want to be police officers they will certainly know the coding of road signs, when they watch television it is a program that follow one cartoon to another at the same times but with different episodes, when they are in the car with mom and dad it is the programming of a "strange card called a control unit" that makes a sound to remind parents to add fuel or put on the seat belt. Once we get their attention, we return to coding related to computers and explain the first concept, that of sequence. Computer, in fact, executes a series of instructions that are given to it one after another. We must therefore as a first step decide on the right sequence of instructions to get to what we want.

To make children understand that instruction is nothing more than an action that you want them to perform, ask them to perform some elementary actions, e.g. 'Raise your hand' 'Clap your hands' ' Do no with your head'. Finally ask 'come to me jumping like a kangaroo' then having them analyze what movements they did: they stood up then performed N kangaroo jumps forward. This is a sequence. Often, without our realizing it, we are asked to do something that requires a sequence of instructions in order to do it, and we then illustrate the cody-feet free tiles that will be used to demonstrate this. The tiles are of 3 types, as shown in the Figure 1: beginning/instruction/end, and are recognizable by the way they can fit together like puzzle pieces, forming a long line of tiles, that is, a sequence. On top of the instruction tiles is a piece of velcro and it is explained that it is used to have fun playing different games depending on what you stick on it.

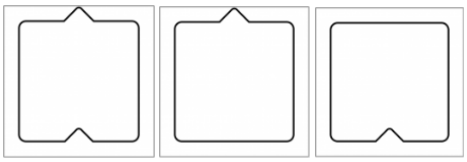

Figure 1: CodeFeetFree Cards

We can then play the first game with these tiles to explain the importance of putting the instructions in the right order in a sequence. We tell the children that their parents woke up particularly sleepy and have to get them dressed for school. As we tell in what order the clothes are put on, we create the sequence by sticking the clothes on the instruction velcro. The sequence will obviously be wrong, and we show at the end a drawing of how the parents would have sent them to school: with the underwear over the pants,the tank top over the vest, and the socks over the shoes! What should the correct sequence look like? By reasoning aloud with the group of children, they independently manage to dress correctly.

The second proposed game, on the other hand, combines coding and movement: each tile represents a movement to do, as shown in the Figure 2. Education tiles with the movements on them are made available to the children. They take turns choosing their favorite movement and, putting them in sequence, create a dance to try all together. This type of exercise can also be proposed during motor skills hours by changing the symbols as desired to create motor pathways for the children.

All the material used so far is paper-based and can safely be printed by the school at little cost. Not only that: exercises can also be suggested to be done at home with the relevant material. In fact, at the end of the illustrated lesson, suggestions of games to be played together at home were sent to parents, complete with cards, obviously of a small size, that can be printed, cut out and used. First suggested exercises were:

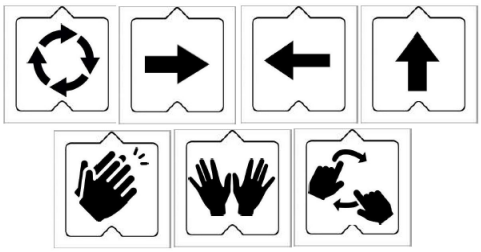

Figure 2: Dance with CodyFeetFree Cards Example

1. Practice discovering the sequences of instructions hidden in what we do: try to think together with the children about a job you do often and what is the right sequence of actions. For example to set the table, brush teeth, cook pasta. You can draw the actions together on instruction tiles and put them in sequence, then have fun shuffling them around to see how much the end result changes if you don't perform them in the correct sequence: if you drained the pasta before you turned on the stove, what would happen?

2. Dance battle: each family member proposes his or her own dance using the tiles already known from the lesson at school. The others will vote to see who is the best choreographer in the family.

3. Storytelling Inventory: tiles with good characters, bad characters, places and objects are also provided. The game is to create a sequence and invent a fairy tale by following it. A similar exercise can also be offered at school in storytelling hours, preparing tiles concerning the fairy tale that will be read and asking children to put them in the right sequence to recreate the story.

In a second lesson the term coding is introduced, starting with the explanation that it is nothing more than a simple way to explain an instruction to be executed. In the previous lesson, symbols were used, as they are also used for example on devices and remote controls: square for stop and trinagle for play are already known at age 3. It is not only symbols that are used for coding of course, and one of the most frequently used ways is certainly the use of colors, which can easily be explained to them by showing them a drawing of a traffic light. Color coding will also be used in later exercises, through the new codycolor tiles, explained in [22]: these have only one color but no interlocks. Tiles are large so they can walk on them. On gray they will step forward, on red they will turn to the right and step forward, and on yellow they will turn to the left and step forward. Since the concept of left and right is not yet clear to all children, 2 yellow and red bracelets are used to help them i understand which hand to turn toward. A first volunteer child is then sought to put the bracelets on and an object is placed on the floor: the other children in turn will have to choose the right tiles for the child to reach for the object. The teacher places the first one and the child stands on it, then it is decided where to spot in the room to go further, and which tile needs to be placed in front of the child's feet to reach the goal. The paths to take can be guided by imagination or by stories read at school, for example, one can imagine that the dragon is coming and a princess-doll needs to be collected and then placed safely in a container-castle. A variation may be, instead, to place an object in the center of the room, arrange some obstacles on the floor and form two teams that, starting from opposite corners of the room, will have to try to reach the object first.

The third and final lesson introduces the chessboard into the games. A large 5x5 chessboard is placed on the floor and they try to create a path together like the ones on the floor, but this time putting the tiles on the squares of the board. The first tile is placed by the teacher. When the path comes out of the chessboard then the teacher introduces the last two new tiles to the children, namely the start and end tiles of the path by putting the triangle before the first tile of the path and the circle at the end. Start and end now are put in retrospect, the following year they will instead become constraints to be respected: they will be set at the beginning and the children will have to make sure to create a path between the two. All the necessary information and tools for the next level have then been given.

The experience with 3 and 4-year-olds has been carried out with 3 different classes of children year after year. Every year it has been confirmed that through continuous interaction, playful exercises, and the presence of movement, the children's attention and interest always manages to remain high, often with requests from them to extend the lesson. After the first trial year, in which many parents asked for information following their children's enthusiastic stories, explanations and exercises that could be done at home were introduced. Obviously interest is subjective, but over the next two years 30 percent of parents shared with us fairy tales and dances invented together with their children or fun times when dad shaved his beard following the sequence specially scrambled by his own child. We initially expected this feedback to come from families in which at least one of both parents worked in the computer field or similar, and had clear concepts related to coding. Instead, we feel it is important to make explicit that the feedback was always related solely to the child's interest, and the parents who participated often asked for additional guidance because, completely distanced from the concept of coding and programming in their own work, they found themselves intrigued in turn.

### *3.3. Consolidation of acquired knowledge and introduction of Constraints and cycles*

This second part is offered to 5 and 6-year-olds. In the first lesson we start immediately with the chessboard but using tiles that combine the two concepts of sequence and coding, cody-feet cards. As explained in [21] and [23] these have both point and wedge shapes to fit together like a puzzle, and color, with the same coding as the codycolor tiles. The main change from the previous level of difficulty is that you do not create the path before, but during. The start and end tiles are placed a priori, then 3 children proceed at a time, each with a specific task: one of them will be the executor, that is, he will only follow the instructions given to him; one will be the analyst, who will decide on the sequence of instructions to achieve the goal; and one will be the programmer, who, starting from the solution identified by the

analyst, translates it into code to be executed. As much as this process has always been followed easily and naturally by children, we can see how complex it is: it involves doing teamwork while managing to keep each person in his or her specific role.

The first challenge to propose is to try to get the children to create an increasingly shorter path, until they achieve the shortest possible one. This explains the importance in achieving a goal with as few instructions as possible: it is achieved in less time and the performer gets less tired. The link to scheduling in the business world is becoming more and more evident, but there are still generalizable motivations: for example, planning better for a long journey allows one to arrive at the destination sooner, less tired and spending less money on fuel. Some planning concepts can then be explained through simple games, such as creating a tree of depth 5 by keeping the same starting point but, by choosing tiles from a predefined set, reaching different end points. By drawing each path on an A4 sheet of paper with the 5x5 checkerboard reproduced and going over it on tissue paper, the various paths found, when overlaid, will show just such a tree. Again, is sent a document to their parents, with an explanation of what was done, together with tiles and chessboards that they can print out to play with their children on A4 sheets. Some challenges proposed for home, and shown in Figure 3,are a first approach to the concept of constraint, which will later be explained at school. Using a 3x3 chessboard, how could it be filled using any tiles? How could it be filled if one had no yellow tiles? What if one had only two grays?

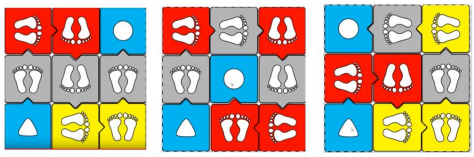

Figure 3: First Approach to Constraints Excercises

The concept of constraint in class is introduced with a google maps satellite map where they can see their school from above. Different groups of children are asked to draw the route they would take to reach a house nearby where they are having a big party. They may choose different routes, but instinctively they will follow the constraint of only being able to drive a car on one road: none of them go through a farmer's field or a park, even though doing so might take a shorter route! During exercises on the chessboard, constraints will be obstacles of various kinds to be avoided in order to reach the goal. Again, they develop concepts through themes they are dealing with in school or by linking them to a particular time of year. In this three-year project, for example, a game was proposed where the child had to program a robot to make it clean a room of garbage by managing a separate collection of items: paper, plastic and organic. As shown in the Figure 4 in order to clean up everything it will be necessary to start with one type of objects and then move on to the others.

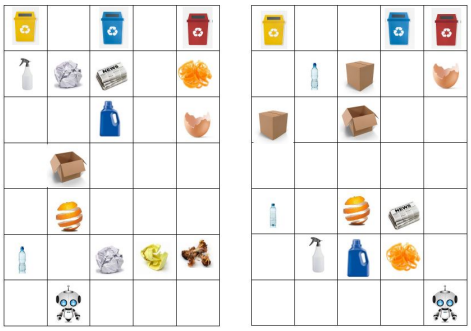

Figure 4: Garbage Collection Excercise

Both at school and at home, collection challenges have been proposed: the Easter Bunny's Easter egg collection, shown in Figure 5 where the child has to impersonate the rabbit and return to his burrow trying to put as many eggs in his basket as possible. Similarly, for the holiday season, a tale of a blizzard has been proposed at home, that dropped a lot of presents from Santa's sleigh, which he must now try to retrieve while being careful not to fly into high buildings.

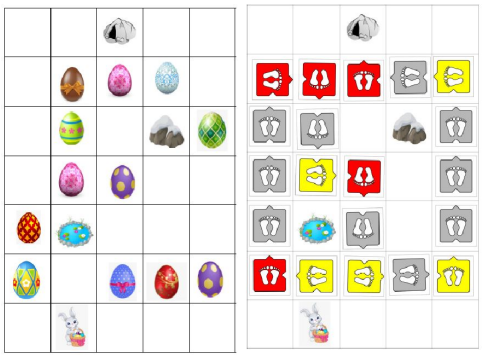

Figure 5: Easter Game Example with Solution

During the third year of the piloting of this program, the 2021/2022 school year, one section of the school was following a parallel experiment in which the section teacher, from the morning reception until the end of lunch, communicated with children only in english language. We then took advantage of this for a joint, more in-depth lesson on exercises related to one of the cycles of programming. The english teacher previously explained the key words IF THEN ELSE to the children. Next, taking a cue from the story of a bee that served as a thread for the various exercises on the board, children are divided into 3 groups. In the first group the bee, which cannot fly because it has injured a wing, will have to reach the hive while avoiding lakes and stones. In the second group the bee will be given a bulldozer and will be able to go over the boxes with stones. In the third group the bee with the boat will be able to cross the lakes. At the end of each of the three paths, the tiles used on the small checkerboards on the A4s are redrawn and overlaid on tissue paper. This time overlaying the 3 tissue papers will show the decision tree. The first real pseudocode is then made for the children to write. An A4 has already written IF <drawing bulldozer> then <free space> ELSE IF <drawing boat> THEN <free space> ELSE <free space>. In the three free spaces, the children will draw the sequence of colors they used in the three paths. This

simple pseudocode got them so excited thinking they were becoming real programmers that they wanted to do it again, with the results shown in the Figure 6.


Figure 6: If Then Else Pseudocoding Example

This second phase of teaching tended to have less feedback at home: 20 percent of parents reported examples of exercises done with the children. In contrast, there was a noticeable increase during lockdown periods when schools were not open: coding was gladly exploited at home to teach in a playful way. During these periods as many as 60 percent of parents shared paths, challenges, and even proposed new ideas followed by other parents in the school. The simplicity of these tools that can be used to stimulate computational thinking was certainly confirmed by showing how it is accessible to everyone and easily transformed into fun games that can be proposed even to very young children.

## 4. First approaches to technology

One of the main tools of coding is visual or block programming: this type of programming offers an intuitive approach, reducing syntactic rules to simple interlocking between blocks of complementary shape. In short: the program code does not have to be typed. Even for children as young as 5 or 6, who still need to learn to read and write, visual programming thus allows them to immediately experience the effect produced by the colored blocks on the characters, called sprites, that animate the story or game being created. As children play and invent stories, they have to work hard to figure out which colored blocks to choose and fit together to recreate what they have in mind. As they do this, they unknowingly write lines of computer code. Block programming is shown as a first approach to technology.

### 4.1. Block coding Example

Harking back to the previous lesson, we begin by showing, on old smartphones lent by parents and given to various groups of children, a game in which, using exactly the pseudocode written with them in lesson three, the bee makes the three different paths. The mblock platform was used for this purpose, as it easily allows one to create ad-hoc blocks and visually reproduce exactly the sequence that the children see on the sheets they filled in. In figure 7 we can see on the upper part the game and on the lower the code, with the color of the instructions that the children had chosen in the different paths.

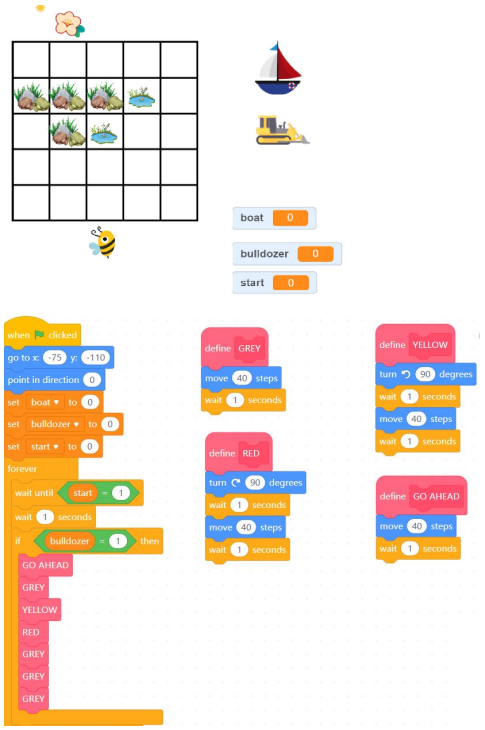


Figure 7: If Then Else Implementation with mBlock

### 4.2. Programming a robot

Certainly finishing kindergarten by programming a real robot was the winning choice. As explained extensively in [21], it is explained that depending on the object we want to program the coding to be used changes. In fact there are so many programming languages and often a programmer is faced with the need to transcode one of his sequences. Transcoding is necessary to transform the paths taken on the large chessboard into a sequence of keys to be pressed on a robot to make it take the same path on a chessboard of a suitable size for the length of the robot's step. The focal point of teaching at this last stage is actually the error. Easily children can make mistakes in the sequence on the robot, and at the first mistake you will cheer up the child by letting him know when the mistake is important to understand in order to correct and improve the path-it is nothing more than the debugging that every programmer does for a very high percentage of his working time! It is important to look very carefully at each step performed by the robot: when does it not do what we expect? That is exactly where there is the error that needs to be fixed!

It is also very interesting to introduce voluntary errors at 3 different points in the same sequence: at the beginning, towards the middle and almost at the end. The earlier we introduce an error the farther it will take us from the desired result.

Fortunately, also the robot was chosen not only for its easy transcoding but also for its decidedly low cost: this not only helped the school but also the parents. In fact, each year 25 to 30 percent of the seniors were so proud of the programming achievement that they asked their parents for the robot they used at school as an end-of-school gift.

## 5. Primary School

By primary school, manual dexterity has markedly improved, and all children are already familiar with smarthphones, tablets, and interactive whiteboards at school. Until they are yet able to read and write, a less paper-based and more technological approach to coding can still be given through online applications.

Despite this, a first approach that summarized the previously assimilated concepts proved to be effective. We had further confirmation of the easy adaptability of the tools chosen in this case as well: a specific school, for example, had chosen a ship of little pirates as the theme that would also act as a leitmotif in the textbooks. During the first year it was easy to organize courses related to this area, for example:

- drive the ship between rocks and sea monsters making it arrive at the treasure island
- follow a map and reach the treasure by passing through marked key points

Adding motor skills is still important especially in the first year, therefore both courses of this type and exercises via applications on tablets or interactive whiteboards have been proposed, in parallel.

Scratch is a programming language developed by MIT (Massachusetts Institute of Technology) and made freely available. It is a block programming environment used for coding that aids in logical reasoning. In this environment there is no need to type any lines of code, but simply drag and drop blocks. The block system allows the implementation of a series of commands by simply arranging the blocks in a particular order. Each block corresponds to a command and they are executed in the order in which they were placed, from top to bottom. These features make Scratch undoubtedly one of the most popular programming languages for children.

Scratchjr is a declination dedicated to younger children and can therefore be approached in first grade. In this case blocks do not have written description of the related instruction but explain it with an intuitive picture. Available blocks are divided into 6 groups according to their functions:

1. the yellow group contains all the possibilities for starting a sequence: when you press start, when you touch a character, when a message comes to the character, and so on;
2. the blue group contains all the movements the character can do;
3. the purple group allows you to perform certain actions such as making the character talk, making him zoom in or out, making him disappear or appear;
4. the orange group contains cycles and timings;
5. the red group only indicates whether the sequence at the end should be repeated in a loop or not.

During the first year ScratchJR is then used to learn how to use blocks in sequence.

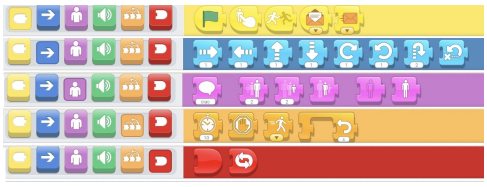

Figure 8: ScratchJR Blocks

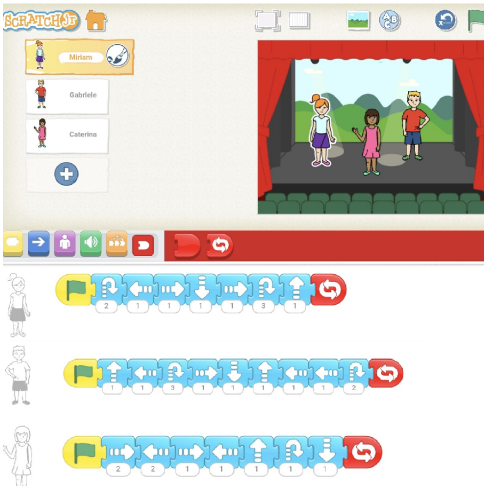

Figure 9: School Dance with ScratchJR

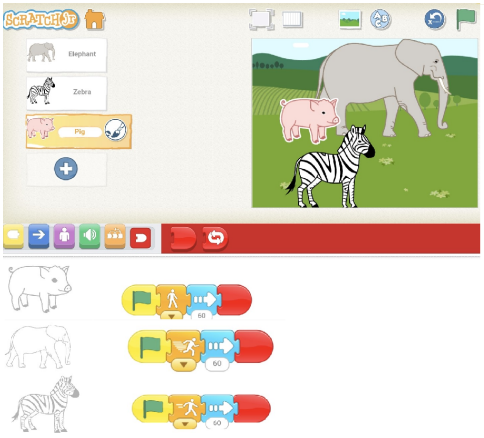

Figure 10: Race with ScratchJR

Exercises are aimed at recognizing the groups of blocks and using them creatively. The first one is, in fact, dedicated to the blue group that will lead the babies to organize the school dance. Each child chooses his character and his 10 moves. An example of an implementation performed by 3 children can be seen in Figure 9. Then, exploring the orange block, students can play a game of guessing who comes first among the chosen animals. One child in turn will choose 3 different animals, decide the speed of each one to the other children will decide which animal to bet on. In the example proposed in Figure 10 the child had the heavy elephant come first, the fast zebra second and the lazy piglet third. The level of difficulty is increased in subsequent lessons by proposing the creation of real stories. For example, this school year's class decided to fulfill the math and science teacher's dream by arranging for her to travel to the moon.

As can be seen from the Figure 11 sequence, movement, action and timing blocks were used.

As a last exercise they are stimulated in thinking of a more complex story with at least three characters interacting with each other. For example, one class proposed the following story: the child comes out of school and his mother takes him to his best friend's house to play together. Together with the teacher, the children first have to identify interactions, that is, when one character's action starts another character's sequence. In this case, the following interactions were identified:

Figure 11: Travel to the Moon with ScratchJR

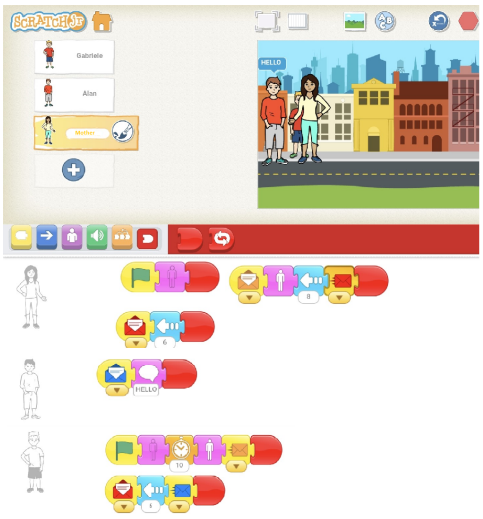

Figure 12: More Complex Interactions with ScratchJR

1. when the child appears outside school mom walks from home to school.

2. when mom comes to the child they go together to his friend's house, that is both child and mother start walking.

3. when they arrive the friend immediately says "hello".

In Figure 12 we see the implementation on scratchJR of the story. All interactions are expressed by sending colored letters, the receipt of which is the start of another sequence.

### 5.1. Deepening of block programming

With reading and writing skills established, the mBlock platform can be used in third and fourth grade. Makeblock, or mBlock [24], starts with scratch 3.0 and expands its opportunities by tying it to different types of hardware devices and the language C code hidden behind each block. Children can then approach this transitional version between the block world and real programming code. As on Scratch, blocks on mBlock also have the description of the corresponding instruction written in text. The first exercises proposed are similar to those done on scratch,for example implementing again the trip to the moon with mBlock. If the school where this program is being followed is in the same territory as the preschool and therefore there are many children who have followed the previous path, it is interesting to analyze with the newly acquired skills, the coding that the teacher had written for the exercise on the if,then,else cycle. The groups of available blocks, compared to scratchJR, obviously have many more instructions in them, and groups of operators and sound actions are added. The connection with programming languages is evident in the group of loops in which we find all the most frequently used ones.

### 5.2. Exercises with advanced circuits

Fourth grade concludes with an actual project, including hardware. The harware used can be an Arduino UNO or Elegoo UNO, there are kits for both including LEDs, sensors, displays and many other devices that can satisfy the children's creativity, at a very low cost, such that a school can buy enough of them for children to work on in small groups. The project involves developing a kit that lights up the Italian flag and plays the anthem at the push of a button and was explained specifically in [25].

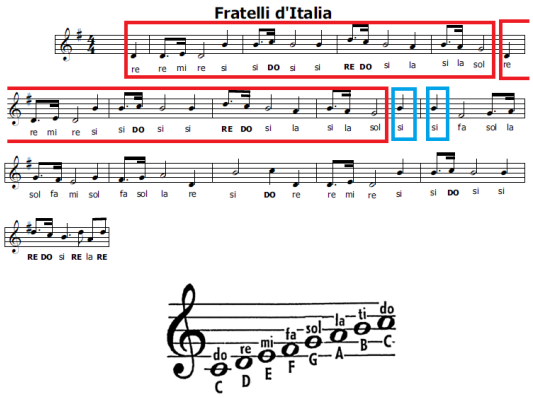


Figure 13: Looking for Repetitions and Notation Transformation

It first involves the music teacher, with whom the score of the anthem is analyzed looking for repetitions of groups of notes, as shown in Figure 13. Next comes a thorough understanding of the notes and their encoding in Anglo-Saxon notation, necessary for programming, through the transformation table in the same figure.

In Figure 14 we see the final real implementation of the project, thoroughly explained in [25]. Programming the hardware is done precisely through mBlock, already widely

used by children. The Arduino UNO device is simply added to the software, and by connecting the Arduino to the PC, the program written through the blocks is loaded to it.

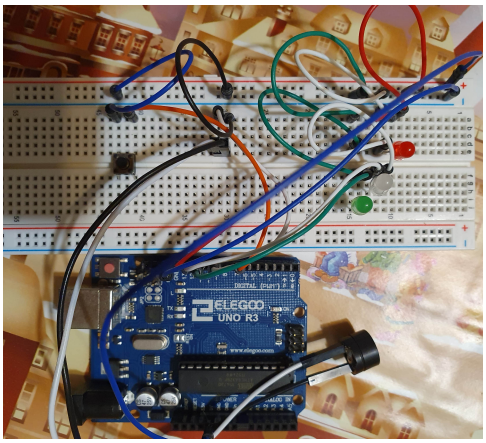

Figure 14: Real Implementation of the Anthem Project

Fifth grade is dedicated to creativity. The goal is to collaborate on the creation of an interactive landscape. The first part is devoted to analyzing what kits provided to the school include, getting inspired. The various proposals are then evaluated together, both from the point of view of feasibility and difficulty, deciding the number of people of each team that will develop the chosen ones. This project is still developing, enthusiasm is high, and many ideas have emerged, from which some choices have been made according to feasibility.

The simplest projects made by groups of two children will be as follows: The starry sky: several white and yellow LEDs with different on and off timings will be placed behind a blue veil, giving the idea of stars shining. A light sensor will be placed upstream so that the led circuit will be activated only if the sensor is in the dark or is dimmed. Design drawing and first draft of programming are respectively on the left and right side in Figure 15

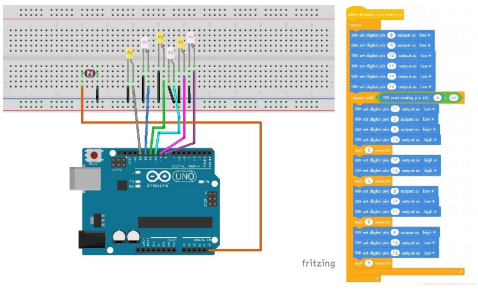

Figure 15: Starry Sky Project

Traffic management at an intersection: programming two traffic lights by reasoning about the timings needed to operate the 'intersection properly without causing accidents. The design drawing is in the left side of Figure 16, and, in the draft scheduling on the right part of the same figure, we see the timings of the two traffic lights studied through some simulations to see if they were suitable for cars to pass through without accidents.

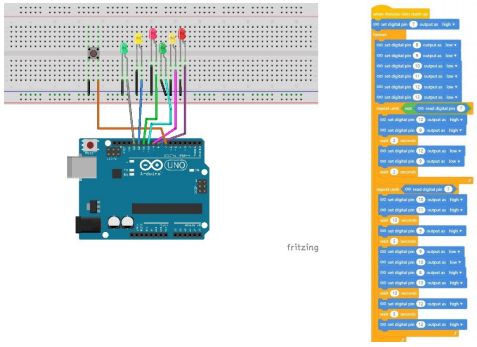

Figure 16: Traffic Lights Project

More complicated projects were then chosen to be carried out by larger groups. A group of three children will design an advertising panel in which LEDs are turned on in different ways to show different figures every minute. The main work was to understand the matrix of the LEDs and, by reproducing the designs by coloring squares on a checkerboard the size of the display used, translate them into block code.In addition, it is necessary to find the correct extension for managing the led matrix through blocks. On the left side of Figure 17 we see the design and, in Figure 18 on the right two examples of programming to make the image of a heart and an up arrow.

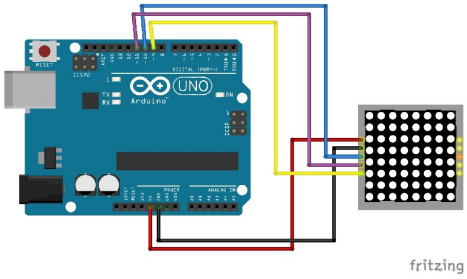

Figure 17: Advertising Panel Project

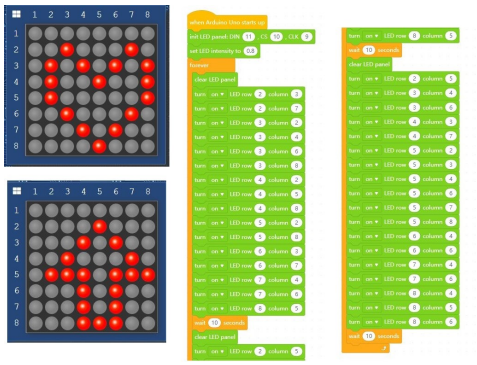

Figure 18: Matrix Programming Examples

Groups of four children will work on projects concerning the school that will be included in the landscape. The first is an automatic cooling system based on a temperature sensor that when a given threshold is exceeded activates a fan. In addition to finding the right extension to have suitable blocks to handle the sensor, this project was assigned to the children who had shown more interest in the electronic part.

In fact, of course with great help from the teacher, it was necessary to include other elements: a resistor, a diode and a transistor. In Figure 19 on the left we see the design and on the right the block programming. The second is a pad with security code for school entry. For ease of resolution, the code is a single digit. If the correct digit is pressed, the green LED lights up, otherwise the red one.

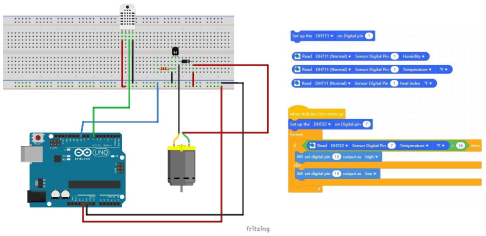

Figure 19: Cooling System Project

The main difficulty is connecting the pad and initializing it on mBlock, as well as having to find the correct extension to handle the pad here as well. Again we can see in Figure 20 on the left the design and on the right the programming.

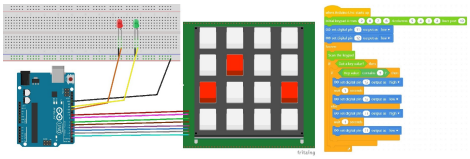

Figure 20: Security Code Pad Example

The low-cost kit proposed to the school contains many other devices not used here but which can lead to further projects that can be implemented in a primary school but with a great final functional impact. For example, it could be possible to automatically turn on the external lights of the school that is part of the project, using a proximity sensor. The cardboard model representing the school is equipped with some LEDs connected to a proximity sensor and an ultrasonic sensor is placed on the ground. When you place a hand at a predefined distance or less, all LEDs will light up for a certain number of seconds. The circuit diagram is shown in Figure 21. In Figure 22 we see a last example of a level crossing. In an infinite loop, for example every 5 minutes, the servomotor is activated so that the rod attached to it, colored to remember the level crossing, moves 90 degrees centigrade to close going into a horizontal position, lighting up the red LED parallel to the start of the movement. After 1 minute the servomotor will move 90 degrees in the opposite direction, so as to reopen returning to the vertical position, and finally the LED will turn off.

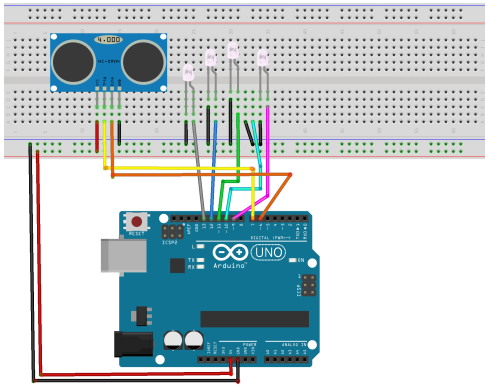

Figure 21: Switching on of Lights with Proximity Example

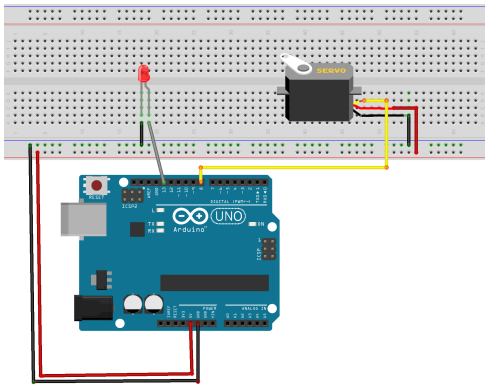

Figure 22: Level Crossing Example

The final step will be to show the programming code related to the blocks they used on mBlock and try to analyze it together, so as to have a first approach to the actual programming. The code in C language related to the hymn implementation blocks, being very simple and repetitive, lends itself well to being a first approach in which the structure of a program written in code is studied. As can be seen from the extract of Figure 23, the following can be highlighted: the inclusions of external libraries in the head of the file, the subdivision into functions, the initial setting of the variables, the main while and for loops,several calls to functions which will give an output relative to the variables that are passed as input. A more advanced analysis can instead be carried out thanks to the code relating to the exercise on the security access code. In Figure 24 students could, first of all, understand how the Pad matrix and its configuration on the hardware side are instantiated, so as to be able to uniquely encode each key pressed. The final challenge that can be proposed is to analyze the code to find the right point, shown in Figure 25, which must be changed to change the security code that should be pressed on the Pad.

Arduino C

```
#include <Arduino.h>
#include <Wire.h>
#include <SoftwareSerial.h>

float button = 0;

void _delay(float seconds) {
  long endTime = millis() + seconds * 1000;
  while(millis() < endTime) _loop();
}

void setup() {
  pinMode(7,OUTPUT);
  pinMode(7,INPUT);
  pinMode(11,OUTPUT);
  pinMode(12,OUTPUT);
  pinMode(13,OUTPUT);
  pinMode(9,OUTPUT);
  while(1) {
      digitalWrite(7,1);
      while(!(!(digitalRead(7))))
      {
        _loop();
      }
      digitalWrite(11,1);
      digitalWrite(12,1);
      digitalWrite(13,1);
      for(int count=0;count<1;count++){
          tone(9,294,0.5*1000);
          delay(0.5*1000);
```

Figure 23: Analysis of the C Language of the Hymn

```
const byte ROWS = 4; //four rows
const byte COLS = 4; //four columns
char keys[ROWS][COLS] = {
  {'1','2','3','A'},
  {'4','5','6','B'},
  {'7','8','9','C'},
  {'*','0','#','D'}
};
byte rowPins[ROWS] = { 9, 8, 7, 6}; //connect to the row pinouts of the keypad
byte colPins[COLS] = { 5, 4, 3, 2}; //connect to the column pinouts of the keypad

Keypad keypad = Keypad( makeKeymap(keys), rowPins, colPins, ROWS, COLS );
```

Figure 24: Analysis of the Pad implementation in C

```
while(1) {
    key_value = keypad.getKey();
    if(key_value != NO_KEY){
        if(String(key_value).indexOf(String("5")) > -1){
            digitalWrite(12,1);
            _delay(1);
            digitalWrite(12,0);

        }else{
            digitalWrite(11,1);
            _delay(1);
            digitalWrite(11,0);

        }
    }
```

Figure 25: Modification of the Security Code

Each group will have its own degree of interest and understanding of the programming code, so it will be decided from time to time what type of analysis to propose in terms of difficulty and depth.

## 6. Conclusion

Economic investments and initiatives aimed at introducing coding into schools are present, as we have seen, in all continents: the first started in 2014, the last in 2020 but the diffusion is now widespread and is slowly becoming even mandatory in most part of the countries. In Europe, Italy is one of the last to have confirmed its willingness to invest in this topic at a political level and our aim was to move proactively with the first pilot projects to arrive at a complete and structured proposal, easily applicable in every school, in the moment in which the obligation would also arrive in our country. To our great satisfaction we have reached our goal early: compulsory education in Italy will start from the 2025/2026 school year. This work, which continues to be ongoing and expanding to this day, has always aimed to define a project that can be used in schools to incorporate coding into the school curriculum. The proposed solution respects the need to have neither additional funding nor impacts on current hours and human resources, constraints imposed by the Italian government. The choices made, in fact, took into account many key aspects that we summarize here. First of all, continuity: the main idea is a program that starts in kindergarten with 3-year-old children and continues until the end of compulsory schooling. It can be seen that all tools chosen for teaching are: on the one hand optimized for the age-appropriate skills of the students, and on the other they have a common thread that leads naturally to the next level of learning, which always has points in common with what was used previously.

The concepts of instruction, its coding through colors or symbols, the algorithm seen as a sequence of instructions that allows to reach an objective are proposed first to 3 and 4 year olds. The computational complexity of proposed exercises already increases in children aged 5 and over by adding constraints, transcoding and using symbols for programming a robot. The change of school at the age of 6 starts with a recovery of the concepts seen, through exercises on the chessboard, however combining them with their implementation of increasing complexity, on applications for touch devices, thus introducing block programming. This same block programming is finally linked to the hardware, to give life to ever-changing projects, which start from the ideas of the children themselves, and lead to the creation of something functional and interactive. The discovery of the C language code hidden behind the blocks, its analysis and modification allows students to reach the end of primary school with a suitable preparation for learning real programming languages.

Although this work is focused on kindergarten and elementary school, the same tools can be used to continue teaching in the following years, moving to the actual programming language, analyzing it, testing it, fixing it and gradually abandoning the use of the block language.

These 3 years of experimentation have brought various results:

- student interest has always been high throughout the process;
- a minimization of hours needed has been obtained, since all the necessary basic skills are already present at each change in difficulty level and teaching is dedicated only to novelty in the strict sense;
- even in the primaries in which the project was not implemented, there was evidence of how the basic notions of coding already received in kindergarten had made it possible to immediately move on to more advanced coding;
- the appropriateness of the increasing difficulty pro-

posed in parallel with increasing age was confirmed by the students' understanding;

- paper instruments or electronic devices chosen, have always been tools with a negligible cost and easily accessible by public schools;
- it was possible to consolidate a list of already tested materials to offer to schools, accompanied by lessons, course examples, application exercises and examples of Arduino hardware that can be replicated or used only as a starting point.

LepidaScpA, among all its objectives for the citizens of the Emilia Romagna region, has always had computer literacy, aimed at schools but not only, and ensuring all schools broadband connectivity to better exploit the current media technologies. The channel of communication towards schools and citizens is therefore already open on these topics and this has led us to think, as a work for the near future, of providing a portal for the exchange of information on the topic of coding. Sharing is thought of at different levels:

- publicity of training and information events by the municipalities;
- sharing initiatives in schools;
- exchange of ideas, material and examples between the teachers of the schools themselves, making the material deriving from our training proposal available first;
- exchange of information and clarifications with the students' parents, trying to involve them in the process;
- exchange of ideas, projects and collaborations between students, both from the same school and from different schools.

The basic concept of the portal is that the exchange of opinions and ideas, in this first phase of the approach that Italy is having towards coding, leads to an increase in interest with a consequent natural generalized enrichment among participants, making it a facilitating tool in the diffusion of teaching coding in schools of Emilia Romagna Region. In the hope that it will be an inspiration for the whole national territory.

**Conflict of Interest** All authors declare that they have no conflicts of interest.

**Acknowledgment** Author Elisa Benetti thanks Lepida ScpA and Gianluca Mazzini, as general manager of the company, for giving her the opportunity to teach firsthand the coding program proposed here in a pilot school. The authors thank the Primi Giochi preschool in San Pietro Capofiume, Bologna, for their willingness during the first three years of testing the program.

## References

[1] S. Papert, *Children, Computers and Powerful Ideas*. New York: Basic Books, 1990. DOI: 10.1095592.

[2] J. M. Wing, "Computational Thinking," *Commun. ACM*, vol. 49, no. 3, pp. 33-35, Mar. 2006. DOI: 10.1145/1118178.1118215.

[3] S. Boss and J. Kraus, *Reinventing Project-Based Learning: Your Field Guide to Real-World Projects in the Digital Age*. International Society for Technology in Education, 2022.

[4] S. Bocconi et al., "Developing Computational Thinking in Compulsory Education," *European Commission, JRC Science for Policy Report*, 2016, p. 68. DOI: 10.2791/792158.

[5] C. S. Iftci and A. Bildiren, "The Effect of Coding Courses on the Cognitive Abilities and Problem-Solving Skills of Preschool Children," *Comput. Sci. Educ.*, vol. 30, no. 1, pp. 3-21, 2020. DOI: 10.1080/08993408.2020.1728600.

[6] B. Arfè, T. Vardanega, and L. Ronconi, "The Effects of Coding on Children's Planning and Inhibition Skills," *Comput. Educ.*, vol. 148, p. 103807, 2020. DOI: 10.1016/j.compedu.2020.103807.

[7] S. Papadakis, "Apps to Promote Computational Thinking Concepts and Coding Skills in Children of Preschool and Pre-Primary School Age," in *Mobile Learning Applications in Early Childhood Education*, IGI Global, 2020, pp. 101-121. DOI: 10.4018/978-1-7998-1486-3.ch006.

[8] J. M. Sáez-López, M. Román-González, and E. Vázquez-Cano, "Visual Programming Languages Integrated Across the Curriculum in Elementary School: A Two-Year Case Study Using Scratch in Five Schools," *Comput. Educ.*, vol. 97, pp. 129-141, 2016. DOI: 10.1016/j.compedu.2016.03.003.

[9] A. Wilson, T. Hainey, and T. Connolly, "Evaluation of Computer Games Developed by Primary School Children to Gauge Understanding of Programming Concepts," in *Proc. Eur. Conf. Games-Based Learn.*, Academic Conferences International Limited, 2012, p. 549.

[10] F. Heintz, L. Mannila, and T. Farnqvist, "A Review of Models for Introducing Computational Thinking, Computer Science and Computing in K-12 Education," in *2016 IEEE Frontiers in Education Conf. (FIE)*, 2016, pp. 1-9. DOI: 10.1109/FIE.2016.7757411.

[11] P. Seow et al., "Educational Policy and Implementation of Computational Thinking and Programming: Case Study of Singapore," in *Computational Thinking Education*, Springer, Singapore, 2019, pp. 345-361. DOI: 10.1007/978-981-13-6528-7_18.

[12] V. Lin and O. Shaer, "Beyond the Lab: Using Technology Toys to Engage South African Youth in Computational Thinking," in *Proc. 2016 CHI Conf. Extended Abstracts Human Factors Comput. Syst.*, 2016, pp. 655-661. DOI: 10.1145/2851581.2851634.

[13] Codeweek site, https://codeweek.eu/ Accessed: 2022-12-21.

[14] S. Bocconi et al., *Reviewing Computational Thinking in Compulsory Education*. Joint Research Centre (Seville site), 2022.

[15] Code for Asia Site, https://www.codefor.asia/ Accessed: 2023-02-07.

[16] Coding Africa Site, https://www.codingafrica.org/ Accessed: 2023-02-07.

[17] A. Garcìa-Holgado et al., "Trends in Studies Developed in Europe Focused on the Gender Gap in STEM," in *Proc. XX Int. Conf. Human Comput. Interact.*, 2019, pp. 1-8. DOI: 10.1145/3335592.3335607.

[18] A. Garcìa-Holgado et al., "Gender Equality in STEM Programs: A Proposal to Analyse the Situation of a University About the Gender Gap," in *2020 IEEE Global Eng. Educ. Conf. (EDUCON)*, 2020, pp. 1824-1830. DOI: 10.1109/EDUCON45650.2020.9125334.

[19] Girls Who Code Site, https://girlswhocode.com/ Accessed: 2022-12-21.

[20] Coding Girls Site, https://www.coding-girls.com/ Accessed: 2022-12-21.

[21] E. Benetti and G. Mazzini, "Coding Training Proposal for Kindergarten," in *2020 Int. Conf. Softw., Telecommun. Comput. Netw. (SoftCOM)*, 2020, pp. 1-5. DOI: 10.23919/SOFTCOM50211.2020.9238265.

[22] L. C. Klopfestein et al., "CodyColor: Design of a Massively Multiplayer Online Game to Develop Computational Thinking Skills," in *Extended Abstracts Annu. Symp. Comput.-Human Interact. Play Companion Extended Abstracts*, 2019, pp. 453-458. DOI: 10.1145/3341215.3356303.

[23] A. Bogliolo, "Unplugged Language-Neutral Card Games as an Inclusive Instrument to Develop Computational Thinking Skills," in *Proc. 9th Int. Technol., Educ. Dev. Conf. (INTED)*, 2015, pp. 7609-7615.

[24] mBlock Site, https://mblock.makeblock.com/en-us/ Accessed: 2022-12-21.

[25] E. Benetti and G. Mazzini, "Coding Training Proposal from Kindergarten to High School," in *2021 Int. Conf. Softw., Telecommun. Comput. Netw. (SoftCOM)*, 2021, pp. 1-5. DOI: 10.23919/SOFTCOM52868.2021.9559112.



**ELISA BENETTI** was born in Portomaggiore (FE) in 1981. In October 2006 she obtained a bachelor's degree in Computer and Automation Engineering from the University of Ferrara. In October 2008 she obtains her bachelor's degree at the same university with a thesis entitled "Efficient Systems with Authentication for Digital TV." The study of MHP services led her, from November 2008, to a one-year collaboration contract at Lepida SpA, within the LepidaTV project where she deepened her studies in the field of Digital Terrestrial and Audio/Video. In January 2009, he began his PhD in Engineering Sciences at the University of Ferrara, receiving his degree in January 2012 with a thesis entitled "Architectures, Services and Multimedia in New Media." From 2009 to the present, she has authored and coauthored some 20 publications in the areas of telecommunications, DataCenter infrastructure and coding dissemination in public schools. In January 2010 she is hired in LepidaSpA in the Ideation and Prototypes Area. Since 2014 she also started working in the Design and Development - DataCenter and Cloud area where to date she works full-time as a systems engineer.

**GIANLUCA MAZZINI** was born in 1968. He received his Master Degree and PhD from the University of Bologna in 1992 and 1996, respectively. Since 1996 he had a permanent position at the University of Ferrara. Since 1995 he taught courses on Telecommunications. He served as a tutor for 150 theses and supervised 15 PhD students. He published more than 280 international and peer-reviewed papers. He served has IEEE Associate Editor for 9 years. He managed 40 research projects, with the role of coordinator for 20. He served in 60 Technical Program Committee. He is an IEEE Fellow. He was member in the Scientific Council of: CNIT, GARR, Cento Technopole, Telematic Strategy for the Emilia-Romagna Region, ASTER, Iperbole Wireless for the Municipality of Bologna, Guglielmo Marconi Foundation. He served as R&D Director in LepidaSpA, as CEO in Cup2000ScpA, as member of the Board of Directors in LepidaSpA and as member ofthe Board of Directors in CNIT. Since 2009 he is CEO of LepidaSpA, reformed as LepidaScpA in 2019. Since 2019 he is a member of the Board of Directors of the Guglielmo Marconi Foundation.

Received: 27 December 2022, Revised: 03 March 2023, Accepted: 23 March 2023, Online: 28 April 2023
DOI: https://dx.doi.org/10.55708/js0204001

# Graph-based Tool for Bandwidth Estimation, Health Monitoring and Update Planning in Broadband Networks

**Gian Paolo Jesi**[*,1], **Andrea Odorizzi**[1], **Gianluca Mazzini**[2]
[1]Network Department, Lepida ScpA, Bologna, 40128, Italy
[2]Engineering Department, University of Ferrara, Ferrara, 44121, Italy
[*]Corresponding author: Gian Paolo Jesi, Lepida ScpA, Via della Liberazione 15, 40128 Bologna, Italy, Email: gianpaolo.jesi@lepida.it

**ABSTRACT:**
This paper focuses on the genesis and evolution of our specific Company tool. It is aimed to tackle the problem of verifying the health status and availability of residual bandwidth between any node over the Lepida ScpA broadband network. In fact, there must be a correspondence between active contractual obligations signed by local network operators and the physical bandwidth which we allocate. This is the key factor that must be addressed in the early phases when processing any bandwidth requests from local customers. Before the introduction of our tool, this verification process has been carried out almost manually with a substantial cost in terms of time. The adoption of this in-house developed tool allowed us to substantially shrink of the verification time required and to provide an overview of the network status. Our tool is grounded on building a graph representation of the network and on well known graph algorithms.

**KEYWORDS** Graphs, Network bandwidth, Broadband

## 1. Introduction

The access to broadband Internet connection for citizens and companies is considered critical for the social and economical development of a modern Country. The geographical diversity of the territory of Italy created a situation in which a non negligible amount of areas suffer from poor connectivity. Unfortunately, there are cases in which these areas are not covered at all. These situations pave the road to what it is usually called as "digital divide".

Trying to limit and hopefully eliminate this problem is on top of the National and European Union (EU) agenda. At a Regional level, our company -Lepida ScpA[1]- is the main operational instrument regarding the Regional Information and Communication Technologies (ICT) Plan implementation. It has been created in 2007 by the Emilia-Romagna Regional Government (as unique shareholder and founder); currently, it has several hundreds Public Administrations (PAs) and Public Entities (PEs) as shareholders, and its activities are dedicated to them.

In order to accomplish the Plan, Lepida ScpA manages the strategies of broadband networks and several other activities such as: ensures and optimizes the delivery of ICT services and develops cloud infrastructures. In addition, it implements and manages innovative solutions for the modernization of healthcare paths in order to improve the relationship between citizens and the Regional Health Service in accordance with the provisions of EU, National and Regional Digital Agendas.

One of the core businesses of Lepida ScpA is selling its fiber optics network bandwidth at fair prices to local network operators. In turn, network operators sell an Internet connectivity service to their customers. Often, these operators *offer their service to the specific niche of customers which are located in poorly covered areas or not covered yet*.

Knowing how much bandwidth Lepida ScpA can provide from a particular network location, is just the first basic step to provide a quality service. When the customer request cannot be satisfied, it has to be aborted. In this case, it is required to plan an action in order to update the infrastructure and to satisfy similar requests in the same area ad soon as possible.

The band allocation is just one step in a wider and more sophisticated process that allows our Company to manage, update and expand the Regional broadband network.

It is important to note that bandwidth checking or monitoring here has nothing to deal with traditional real time bandwidth consumption monitoring. What really matters for us, is that when we sell some band to a customer (i.e., an operator), the sum of all bands sold must be compatible with the actual physical network capabilities of the area where the service is going to be provided.

In the last few years, the process of checking the band availability over the network had a significant evolution and lead to the creation of a specific tool having a set of continuously growing capabilities. This tool, Banda Calculus, is a building block that is going to integrate with several other tools that are on the way. In this work we are going to show the evolution of Banda Calculus and we provide the vision of our end goal in which Banda Calculus will inter operate with the other company tools which are part of the process.

Banda Calculus started as a data science notebook dealing

with just one network node at a time, but now it is a standalone web application. Over the years, it become an holistic instrument capable of providing the bandwidth status of the whole network and to highlight the less capable parts or the ones already in a suffering state. The network topology is another key aspect when dealing with the healthy of a network. Identifying specific patterns that potentially lead to issues became one of the available features of Banda Calculus.

The remainder of this paper is organized as follows. In Section 2, we briefly review the current state of the art, then we discuss the specific scenario we tackle in Section 3. After presenting our algorithms and their implementations in respectively Section 4 and 5, we finally draw our conclusions in Section 6.

## 2. State of the Art

Since the kind of monitoring or sanity checks to the network topology are very dependent to our Company' specific needs, it is quite hard to make any comparison with existing tools.

In fact, there are plenty of monitorin] tools [2, 3] and estimation mechanisms available [4]–[5] on the market and in the open-source community which are suitable for bandwidth monitoring for example. Essentially, the idea behind these kind of tools is collecting data from network devices (such as: server hosts, routers or switches), usually via Simple Network Management Protocol (SNMP). Alerts can be set when specific parameters go beyond a predefined range. In particular, more sophisticated tools are not just limited to present charts in a dashboards, but they can also react to undesirable events by exploiting collected data with machine learning algorithms [6], [7] and making predictions.

However, our aim is different. We already have these kind of tools for monitoring network resource consumption, such as bandwidth, detecting anomalous behaviors and/or listening for alarms. Here, as stated in Section 1, *we are not interested in real-time monitoring or consumption of the bandwidth*.

Graph databases, such as Neo4J [8], are an emerging breed of tools coming from data science aimed to organize and gather data on complex structures such as graphs.

Neo4j would be ideal to build our network graph and to check its structural topology. Unfortunately, when an algorithm has to modify or add new node attributes and eventually change the structure links, it becomes highly complicated. Essentially these tools are mostly designed and optimized for querying complex structures but not for making modifications on the fly.

Since our needs are very specific and our algorithms are not just graph queries but complex procedures that shapes the structure in a specific manner, we decided to build an in-house, custom solution and to ground it on more general graph computing libraries and other high-level abstraction frameworks.

## 3. The General Problem

Table 1: Types of node elements in Lepida ScpA network. Unfortunately, for non-Italian speakers, many of their acronym come from their Italian name.

| Acronym | Description |
|---|---|
| PAL | Lepida ScpA Access Point (Italian: "Punto di Accesso Lepida") |
| AG | Aggregator (Italian: "Aggregatore") |
| PR | Radio bridge (Italian: "Ponte Radio") |
| DC | Data center |
| MIP | Final endpoint to the core network |
| END POINT | Union between the DC and MIP node sets |

The broadband network is make of several types of nodes (e.g., PAL, AG, PR, DCand MIP), which are listed in Table 1. This list in not exhaustive, but just the nodes significant for this paper are present.

The set of ENDPoints represent our *core* network, while the rest is the *access* part providing end-users up-links. In the core network we can manage the bandwidth by choosing between (i) tuning specific Quality of Service (QoS) strategies or (ii) upgrading the backbones. In the access network instead, where Banda Calculus comes into play, our policy is to do *not allow* any overbooking.

When an operator makes a bandwidth request, the requested band has to be booked for a specific network node, which is usually a PAL or AG node type. *The fundamental role of Banda Calculus is ensuring that the operator band requests are compatible with the current state of network bandwidth capabilities*.

The information that is adopted to build the network representation as a graph structure is mainly taken from our Network Management System (NMS). This is where the information about the whole broadband network infrastructure is stored. This knowledge is essentially maintained by human intervention through our NMS web interface. Since several people are involved in these maintenance activities, which are mostly manual, this process tends to be error prone. In this vein, our goal is to exploit Banda Calculus in order to perform sanity checks and to iron out the majority of mistakes. In fact, this focus on sanity checks is one of the latest updates we performed on our tool and we are going to address this topic in the next chapters. We exploited two (REST) APIs to ingest network data:

1. *single node oriented*: data from a single node can be queried by name[1]; it returns who are the node's immediate neighbor, details of each interface and the (total) *current bandwidth* reserved by operators. The former item is a key factor for bandwidth calculation. Unfortunately, this API has several limitations, such as: it has no access to PR nodes and it is slow.

2. *graph oriented*: it is the newest API and it has been built for the purpose of our tool. This service provides a representation of the whole network in a JSON format structure that is in turn converted into a directed graph object. Essentially, it has the same features of

[1]This is not a fully qualified DNS name, but follows an ad-hoc, internal naming scheme.

the previous API but non of its limitations. In fact, it has access to PR nodes and it is much faster, since it collects all data with a single call.

The fact of only considering a subset of network entities (see Table 1) leads to the chance of having a disconnected graph. In practice, this possibility becomes a certainty and our graph is actually disconnected and scattered in about 30 components. However, the not considered entities are not very relevant in topological terms. This allows us to have 98% of nodes inside the graph largest component, where the bandwidth algorithms are run.

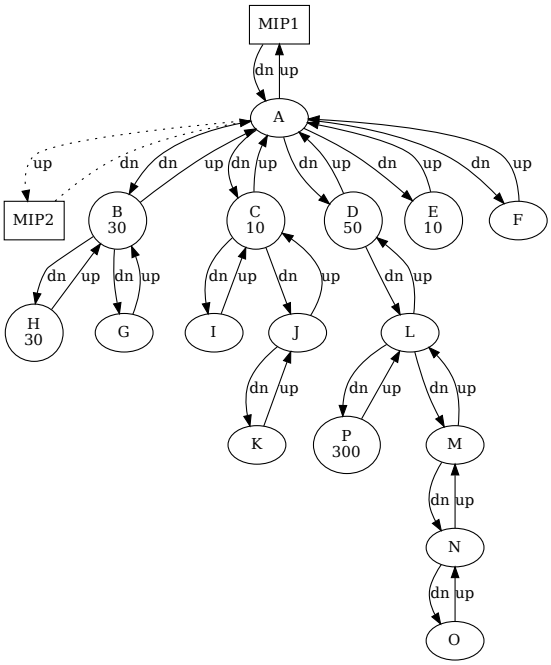


Figure 1: Network graph from which has been extracted the node *L* sub-graph. END POINTs are depicted as a rectangular box, while other nodes are elliptic boxes. When present, the number inside a node box represents the allocated, total operator bandwidth.

An simplified example of the particular structures (graphs) we have to deal with is provided in Figure 1, where a sub-graph for a *target node L* is shown. Suppose that an operator requests to allocate a band amount $x$ over node *L*. From the whole graph, we have to extract or isolate the sub-graph in which node *L* is located including its neighbors and their (eventual) sub-trees in a recursive fashion. More precisely, staring from node *L*, we add nodes until: (a) a leaf node is found or (b) an END POINT node is found. We remind the reader that the ENDPoints set is given by the union of MIP and DC node sets (see Table 1). In order to simplify the plot even further, all links speed is set 1 Gbit/s and it is not shown explicitly.

Since we have a directed graph, each node can have inbound and outbound edges which are respectively marked as *down-link* or *up-link*. Each connection between a pair of nodes it is actually implemented by a pair of edges: an up-link and a down-link edge. The route direction of up-link edges is towards an END POINT, while the route direction of down-links is towards leaf nodes.

Every node is enriched with its current reserved operator bandwidth (op_band) if it is $\neq 0$. Note that current reserved operator band parameter represents the *cumulative amount of band reserved by any operator on that node*. Dotted edges represents *inactive* links. This kind of edges usually connects a node *A* to one of the MIP nodes available. As depicted in Figure 1) node *A* is configured using an *active-standby* pattern, where the connection to MIP2 is the standby or back-up part which is exploited if and only if MIP1 link fails.

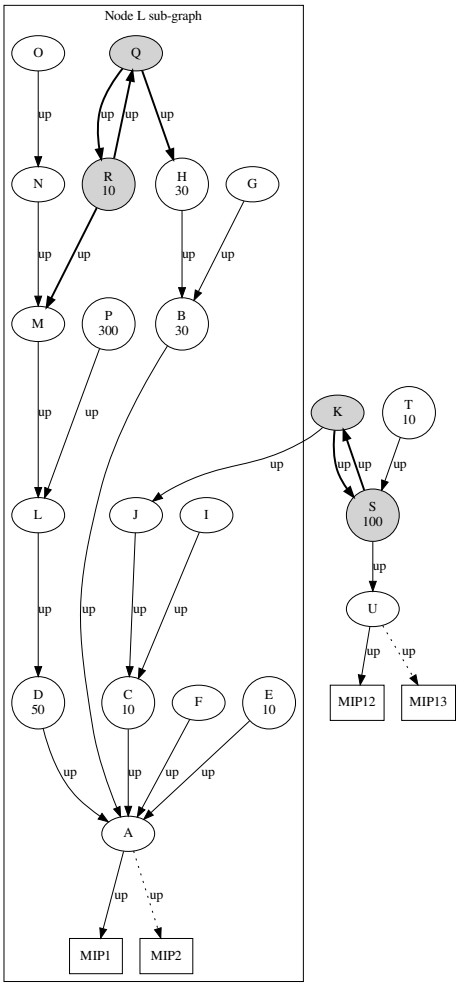


Figure 2: Prototypical, but more realistic representation of node *L* sub-graph. The gray filled shapes of nodes *Q*, *R*, *K* and *S* represent a *chain* structure where all edges are tagged as *up-links*. Two distinct pairs of MIP nodes are shown and are linked to distinct (PAL) nodes (i.e., *A* and *U*). The box on the left encloses node *L* sub-graph (*LG*) after the final filtering. Due to consecutive filtering processes, only up-links are left as they are exploited by the calculation algorithms.

From Figure 1 it is intuitive to understand that the available bandwidth from node *L* have to take into account any consumption at any node in the sub-graph; in other words, each node that stem from any down-link sub-tree might contribute to bandwidth consumption and it must be taken into account.

The general idea is to manipulate the graph structure by enriching edges with a parameter (i.e., AvailBand) which keeps track of the current band availability measured in Mbit/s.

This annotated graph is suitable to calculate the residual band between any node ad its END POINT by running any well known algorithm [9, 10]. The algorithm is going to

calculate the residual band on every edge in the sub-graph (by definition) and not just over the path between a target node and its END POINT.

Unfortunately, real world conditions often present more complex scenarios. Figure 2 shows a prototypical, but realistic representation of a target node ($L$) sub-graph in our broadband network.

This sub-graph exhibits two main peculiarities: (i) it has two *chain structures* and (ii) two pairs of END POINT nodes. The former peculiar structure represents an exception to previous schema in which for any node pair $(X, Y)$ we could only have one up-link and one down-link edge. Here, both edges are marked as up-links. This exception often allows the target node to reach multiple pairs of ENDPoints and this can complicate the band calculation as several (shortest) paths per END POINT becomes available. In addition, the larger the graph, the more challenging becomes its visualization and understanding.

In order to overcome these issues, we first need to clarify and impose that data traffic must follow the shortest path available to the *closest* END POINT and following the fastest links when possible. The closest MIP pair for a target node $L$ is identified by the first steps of the algorithm. In the sub-graph, the set of nodes ($LG$) sharing the same closest MIP with target node $L$ are the ones over which the actual band calculation is performed. In Figure 2, graph $LG$ is the portion enclosed in the box.

More formally, we can express the available or residual band ($RB$) of node $L$ in its sub-graph (i.e., see the box enclosed sub-graph shown in Figure 2) as:

$$RB\,(L) = \min\left(band\left(path_{L,ENDPOINT}\right)\right) \tag{1}$$

where the shortest path ($path_{(L,ENDPOINT)}$) is the smallest set of edges $\{e_{i,i+1}, e_{i+1,i+2}, \ldots, e_{i+(n-1),i+n}\}$ connecting $L$ to its END POINT. The band value for each $e_{i,j}$ is the difference between the edge link physical bandwidth and the (total) operator band associated with the $X_i$-th node of the edge:

$$band\left(e_{i,j}\right) = phyband\left(e_{i,j}\right) - op\_band\left(X_i\right) \tag{2}$$

However, in order to address any operator band contribution from any node in the sub graph that may affect the edges over $path_{(L,ENDPOINT)}$, we must consider all shortest paths starting from any node in the sub-graph having OP_BAND $\neq 0$. Essentially, in the case depicted by Figure 2, we have to consider the following set of paths and their corresponding band contribution over each edge:

$$\begin{cases} D \xrightarrow{50} A \xrightarrow{50} MIP_1 \\ P \xrightarrow{300} L \xrightarrow{300} D \xrightarrow{300} A \xrightarrow{300} MIP_1 \\ R \xrightarrow{10} M \xrightarrow{10} L \xrightarrow{10} D \xrightarrow{10} A \xrightarrow{10} MIP_1 \\ H \xrightarrow{30} B \xrightarrow{30} A \xrightarrow{30} MIP_1 \\ C \xrightarrow{10} A \xrightarrow{10} MIP_1 \\ E \xrightarrow{10} A \xrightarrow{10} MIP_1 \end{cases}$$

By summing all instances of the same edge $e_{i,j}$ in the above schema (e.g., $D \xrightarrow{300} A + D \xrightarrow{10} A = 310$ Mbit) we obtain the total amount of band consumption over each edge. Essentially, we can rewrite (2) as:

$$band\left(e_{i,j}\right) = phyband\left(e_{i,j}\right) - \sum_{k \in I} \left(e_{i,j}\right)_k \tag{3}$$

where $I$ represents the set of instances, as visible in the previous schema, for each individual edge $e_{i,j}$. In (3), for any edge $e_{i,j}$ we can actually calculate the (residual) band over an edge $e_{i,j}$ by subtracting all OP_BAND contributions from the physical bandwidth available on the edge link.

This approach [11, 12] allows us to calculate the available band for any target node in our broadband network no matter the complexity of the corresponding sub-graph.

### 3.1. Towards an 'holistic' approach

After being able to estimate the residual operator bandwidth for a single node in the network, we started to focus our efforts in extending the calculation to the entire broadband network. In fact, in order to monitor our network health from a topological point of view, the fact of being able to check one node at a time quickly became too limiting.

Since our basic mechanism is capable of calculation the residual band for (any) node $L$ and since each all sub-graphs adopted for the computation are not overlapping, extending the calculus over the whole graph[2] sounds straightforward at least on paper. By adopting this approach, we can provide a global view of the bandwidth status of the broadband network and, by knowing which are the zones where band availability is *suffering* or barely sufficient, we can plan for an infrastructure upgrade.

Actually, we can move even forward.

Our tool, while searching paths over the graph structure can collect many interesting information. In particular, checking any topological issue is a natural consequence of visiting/searching over the graph. For example, we realized that the two following main issues are more common: (i) a path between two nodes is absent or (ii) a node from the sub-graph is absent. Especially the latter issue might stem from a mis-configured link property lying on the NMS which triggered a node removal from the sub-graph in one of the filtering phases.

In addition, we can build a timeline or history of the band allocation for any node and showing its evolution over time in terms of band allocation and infrastructure upgrades.

Finally, our goal is to enable the following three new features or *sanity checks* into Banda Calculus:

1. extract all *critical path*. A critical path is a path between any two nodes $A$ and $B$ where the available band is lower than a threshold BAND_TSD. We are interested in all critical paths according to the currently selected band threshold (BAND_TSD).

2. provide human readable information about any topological issue eventually spotted by the algorithm while visiting the graph. The fact of having *readable* information is particularly important in order to simplify the

[2]Here, we consider the largest component of the original network graph.

task of fixing the (NMS) database, since it is carried out by a group of people.

3. build a time history about operator band for each node in order to be able to keep track of any change.

## 4. Algorithms

Our algorithm discussion is split into three distinct parts: the first one (a) is dedicated to the residual band calculation, the second one (b) is dedicated to the holistic sanity check features, while the latter (c) is about the graph visualization algorithm.

### *4.1. Bandwidth Algorithm*

The basic idea underlying the algorithm in order to calculate the residual band for a single node is to first annotate the graph with an AvailBand parameter and calculating the bandwidth, as previously stated in Section 3. The annotation process requires several filtering steps over the graph which are aimed to ensure data consistency and normalization. These steps are summarized as follows:

- *consistency check*: it guarantees that each record in the JSON structure coming from the NMS API contains all parameters which are relevant for the band calculation. It ensures that their values are in their corresponding ranges and are not null or NaN. A graph object $G$ is generated at the end of this step.
- *first filtering*: from the previous polished graph $G$ it is extracted a sub-graph $SG$ according top a selected *target* node $L$. The graph $SG$ is identified through a Breadth-First Search (BFS) over $G$ starting from node $L$. The search stops when an END POINT or a leaf node is found.
- *second filtering*: $SG$ sub-graph is refined a second time in order to just select only the relevant edges. More precisely, only edges with the following characteristics are kept:
  - edge parameter is_active is **true**
  - edge parameter template is not "NA"
  - edge parameter dir is "uplink"

  During this step, each edge is annotated with an AvailBand which is initialized to the current edge speed parameter value.
- *third filtering*: finally, graph $SG$ is further reduced in case multiple ENDPoints are present. According to the chosen target node $L$, its closest MIP (or MIP pair) is selected (i.e., MIP_closest) and all nodes sharing MIP_closest as their closest END POINT are kept in $SG$.

  This third filtering is only applied when the actual band calculation is triggered.

The requirement to address each allocation contribution provided by nodes in any graph sub-tree as well as in chain structures, forces the algorithm to consider all shortest paths *from every node to the MIP* and not just from leaf nodes.

Figure 3 shows the calculation algorithm using a pseudo-code notation. The code does not take into account the consistency check filter. It is basically split into three parts. The first one is dedicated to the filtering processes (i.e., lines 1-9).

The second one (i.e., lines 10-14) computes all shortest paths between every node and the sub-graph ENDPoints. paths is a map or dictionary structure which collects the path set for each node. The latter part instead (i.e., lines 15-28) perform the actual graph visit and updates the AvailBand field over each visited edge. During the visit, any node having allocated bandwidth - op_band field > 0 - and being still unknown, becomes part of the already known nodes in order to guarantee an *exactly once* semantic of the algorithm.

### *4.2. Sanity check algorithm*

The sanity checks algorithm, expressed in a pseudo-code notation, is depicted in Figure 4. The idea is simple and its actuation is scheduled at regular intervals (i.e., $\Delta$=24 hours). For each node in the main graph (component) $G$ we call the main function (*get_banda*()) which is the one depicted in Figure 3) which provides specific data structures required for our application needs. More precisely, it works as follows. The initialization phase (e.g, lines 1-4) prepares several data object, such as a set for basic nodes (i.e, no ENDPoints), a set for collecting topological issues and a database handle where the band history is actually stored.

The procedure runs until the node set is not empty (e.g., line 5). Nodes are pulled from the set one at a time in a (uniformly) random order and the residual band is calculated on the selection (e.g., lines 6,7). The *get_banda*() function invocation generates two structures: (a) a *banda_path* object holding the path from a target node to its MIP and the corresponding residual band and (b) a *subG* object which represents the target node sub-graph with nodes and edges enriched. Nodes are annotated with their allocated operator band, while edges are annotated with their respective residual band values.

At line 8, nodes belonging to the current target node sub-graph are removed from the node set since the band is computed for all nodes in the sub-graph. Any eventual node band update is propagated on stable storage over the database (e.g., line 9).

Finally (e.g., lines 11, 12), in case of exception, a handler manages any arising error. Three kinds of exceptions are actually trapped, which are the following:

- *NoPathException*: no path is found between node $A$ and $B$, where $B$ is a MIP. This exception may arise when there is a missing up-link edge between the two nodes. Actually, it is likely due to a mis-configuration in the NMS: in fact the edge can be present but it might have a wrong label, such as configured as 'down-link' instead of 'up-link'.
- *NoNodeFoundException*: a target node A or the MIP $B$ is not found in the graph. The reason for this exception is likely due to the removal of this node during one

```
G ← 1st_filtering()
G ← 2nd_filtering()
nodes ← G.nodes() ⋂ ENDPOINTS
avail_mips ← G.sample()
known ← SET()
if avail_mips.length > 2 then
    G.filter_closest_mip(target_node)
    avail_mips ← G.sample()
end
foreach node ∈ nodes do
    foreach mip ∈ avail_mips do
        paths[node] ← G.dijkstra(node,mip,weight=SPEED)
    end
end
foreach node ∈ paths do
    used_band ← 0.0
    path ← paths[node]
    source ← node
    foreach item ∈ path do
        cur_band ← G[source][item][AVAIL_BAND]
        if G.nodes[source][OP_BAND] > 0.0 ∧ source ∉ known then
            used_band ← used_band + G.nodes[source][OP_BAND]
            known ← source
        end
        G[source][item][AVAIL_BAND] ← cur_band - used_band
        source ← item
    end
end
```

Figure 3: Residual band algorithm pseudo code.

of the filtering processes. Again it is likely due to a NMS bad configuration: in fact a node might has been removed from the graph if all its edges are marked as 'down-link'.

- *BadLinkException*: in this case the system cannot calculate any path since there are no ENDPOINTS available in the sub-graph. Here, it is very likely that the sub-graph MIPis connected through 'inactive' edges and this triggered its removal from the graph. Again, the underlying reason is a badly configured NMS.

### 4.3. Visualization Algorithm

It is important to note that this algorithm just focuses on graph visualization and it does not affect the band calculation in any manner. While the graph objects we manage are not huge, their size is in a range that poses a challenge when trying to display them into a graphic interface window. In fact, it is not unusual to deal with a node whose sub-graph is about 1000 nodes in size. This especially happens when radio bridge (i.e., PR) nodes are involved: since all their edges are marked as *uplink*, they are likely to join distinct parts (sub-graphs) of the broadband network by creating loops that are not filtered out by the standard processing that is performed.

Even a few hundreds nodes and their edges end up in chaotic plot when trying to display them. In addition, this plotting effort is quite useless because it is likely that the vast majority of the (sub) graph does not participate to the bandwidth consumption: only the set of nodes having the same closest MIP as the target node are actually involved. We remind the reader that the third filtering step is only applied when the actual band calculation takes place. Therefore, the sub-graph is not simplified yet. However, even if the sub-graph would have been simplified at this time, it might be too large as well to obtain a non chaotic plot.

In any case, when dealing with such oversize sub-graphs we need to make a decision and choosing what we are really interested to. It is not a matter to choose or design a new plotting layout. When a user have to check the residual band for a target, the goal is to see the situation over the path that links the target node to its ENDPOINTS. The more we move far from this path, the less is the interest and the value for the information.

The amount of available band along this path is of course dependent by the eventual contribution coming from any sub-branch at each path node, but these contributions are calculated by the previous algorithm (see: 4.1) and affect the band availability at each edge.

According to what we just stated, the basic idea underlying the visualization algorithm is to first focus on the shortest path connecting the target node to its closest MIP (i.e., or

```
1  repeat periodically every Δ time units                    % Code executed every Δ=24 hours
2      nodes ← G.nodes() ⋂ ENDPoints
3      G_errors ← ∅
4      history ← DB.instance()
5      while nodes ≠ ∅ do
6          node ← nodes.sample(1)
7          banda_path, subG ← get_banda(G, node)
8          nodes.pop(subG.nodes())
9          history.update(node, banda_path, subG)
10     end
11     on GraphException : ex do
12         G_errors ← ⟨ ex.node, ex.info ⟩
13     end
14 end
```

Figure 4: Algorithm pseudo code for sanity checks calculation.

```
1  K_MAX ← 50;                    % Constant: max number of nodes for visualization graph
2  avail_mips ← G.getMips()
3  mip ← avail_mips[0]
4  path ← G.dijkstra(target_node, mip, weight=SPEED)
5  simple_G ← G.subgraph(path).copy()
6  foreach item ∈ path and simple_G.size() ≤ K_MAX do
7      if not item.isMIP() then
8          extra_nodes ← G.subgraph([G.allNeighbors(item) + item]).copy()
9          simple_g ← compose(simple_g, extra_nodes, K_MAX)
10     end
11 end
```

Figure 5: Banda Calculus Algorithm pseudo code for generating the simplified graph suitable for visualization.

MIP pair), then to expand this "graph-path" by adding the neighbors of each node belonging to the shortest path. Any $i$+1 level of nodes can be added by iterating the last step over the previous level of added neighbors. As a general rule, this process can stop when the graph size reaches *K_MAX* (e.g., with *K_MAX*=50).

In such a manner, we can plot what it is really required.

The actual algorithm pseudo code is depicted in Figure 5. The first four lines are in charge to detect the MIP nodes in the target node sub-graph (e.g., which is *G* in the code). Shortest paths are calculated using Dijkstra algorithm and a *simple_G* graph object is generated. This graph just contains the path items, the original sub-graph MIPs and their arcs.

The *simple_G* object is enriched by adding all neighbors for each node member of the shortest path (i.e., see lines 5-10). Any member being a MIP is skipped. The graph size is limited by the constant *K_MAX* both in the loop statement and by the commodity function *compose*() which actually merges two graphs together. More precisely, these graphs are: (i) the *simple_G* object and (ii) the graph made by the current loop node (i.e. *item*) and its neighborhood (i.e., see line 8). Any node or arc is added just once.

## 5. Implementation

Banda Calculus is implemented in Python3 language and through the adoption of other several frameworks for specific tasks.

Actually, the evolution of Banda Calculus leaded to several implementation over time since 2019 [11]. At first, it was designed as a Jupyter [13] notebook. This choice is quite common in the data science area and it turned out to be rewarding for our goal as well.

When started, this work shared many similarities with data science projects, where data sets have to be understood, analyzed and verified. For this reason, Jupyter turned out to be a stand out candidate for prototyping our tool. Usually, the best practice working with Jupyter involves trying ideas and distilling a corpus of functions or classes and use them as basic building blocks, then this process is iterated until the problem is solved.

By following this practice, we first designed the Banda Calculus application as a Jupyter notebook by exploiting exploits the set of modules we distilled. By mixing code and code and formatted text elements, a notebook can simplify documentation management. The notebook implementation helps the user in how to install a Python virtual environment and the required project dependencies. In

addition, the built-in documentation provides a user with a step by step explanation of (i) what he is supposed to do in order to use the tool and (ii) how it works.

Among the several solutions to manage a graph structure in Python, we selected *NetworkX*[14] library. The main reasons is that it is strongly supported by the Open Source community, it has a wide collection of state-of-the-art grade graph algorithms, and it is *symbol oriented*; in other words, any element identifier of a graph can be a symbol (e.g., a string or any complex object instead of a numeric id) and this simplifies data management. Symbolic graph libraries are not as fast as lower level ones, but the graph we are working with are in a manageable range (e.g., ~3550 nodes and ~8100 edges).

For visualizing graphs inside a notebook we adopted frameworks (e.g., *Holoviews* and *Panel*) taken from the data science world. These are high level frameworks suited for large data-sets.

Figure 6 shows the output of BANDA CALCULUS notebook application. It performs the following logical activities:

- *Graph creation*: the application downloads a graph structure using the API and stores the corresponding graph object on stable storage labeling the file with the current date in *graphml* format. However, if the current date matches the one of any available graph file, then this file is loaded instead. When the API fails for any issue, the most recent available file is loaded.

- *Target node selection*: through a Graphic User Interface (GUI) widget the user can select the desired target node from a drop-down list containing all valid nodes found in the graph. This choice is recorded and remains set for the entire notebook.

- *Sub-graph initialization and visualization*: graph initialization and its visualization are split in two distinct notebook cells. The output of the latter is depicted in Figure 6. The first two plots (see Figure 6(a) and (b)) are respectively dedicated to the visualization of nodes and edges attributes.
  The item color code is the following: target node is yellow, ENDPOINTS are green and standard nodes are blue. The edge color scheme instead is given by a (linear) color gradient function based on the corresponding SPEED field: faster edges are towards green, while slower ones are towards red. Any part of the sub-graph can be inspected by dragging any element or zooming. Due to their average length, node names are only visualized when moving the cursor close to their shape. By exploiting this visualization the user can check the current OP_BAND allocation and the edges SPEED field.

- *Operator band calculation and visualization*: the sub-plot in Figure 6(c) shows the target node sub-graph after the residual band calculation. As sub-plot (b), this visualization is edge focused. By inspecting the edge (i.e.: linking: 'ngn-pa-modigliana-co' → 'mip-07') we can see the AVAILBAND field annotated with the actual residual bandwidth. From the GUI it is possible to follow any path and inspecting the bandwidth at each hop. In addition, the output cell of the notebook shows bandwidth information along the path between the target node and its END POINT:

```
ngn-pa-modigliana-ai-alpi --[a. band: 700.00 Mbit/s]->
ngn-pa-modigliana-co
ngn-pa-modigliana-co --[a. band: 460.00 Mbit/s]-> mip-07
```

One of the notebook features we believe is very beneficial for our goal is the possibility to *convert it into a standalone web application* in a straightforward manner.

For example, this would open the road to deploy our tool in a container and serving users on the one with a traditional server approach.

Unfortunately, while the notebook app is up to the task of calculating the residual band and by exploiting the adopted frameworks it is possible to obtain a working web application with zero effort, the GUI offered by the notebook is too limiting and the documentation provided by the notebook itself is still too technical for non-tech users. Expanding and adding more sophisticated features to the notebook app is likely to became quite challenging. For this reason, we

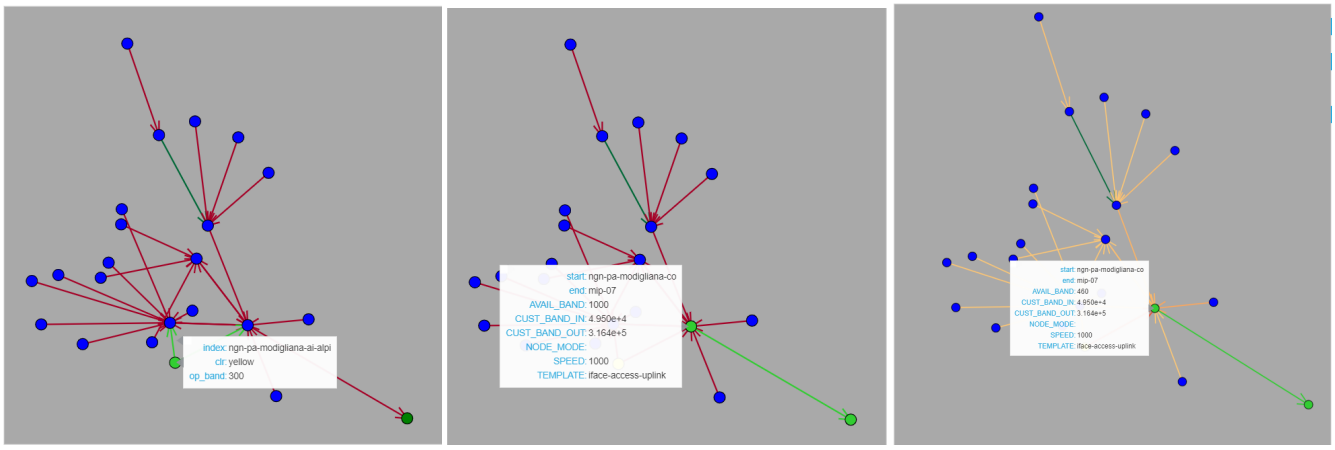


(a) (b) (c)

Figure 6: Notebook app (sub) graph visualizations. Plots (a) and (b) are respectively dedicated to node and edges. Plot (c) instead shows the graph residual band allocation after a run of the calculation algorithm. The node color schema is the following: target node is yellow, ENDPOINTS are green and standard nodes are blue.

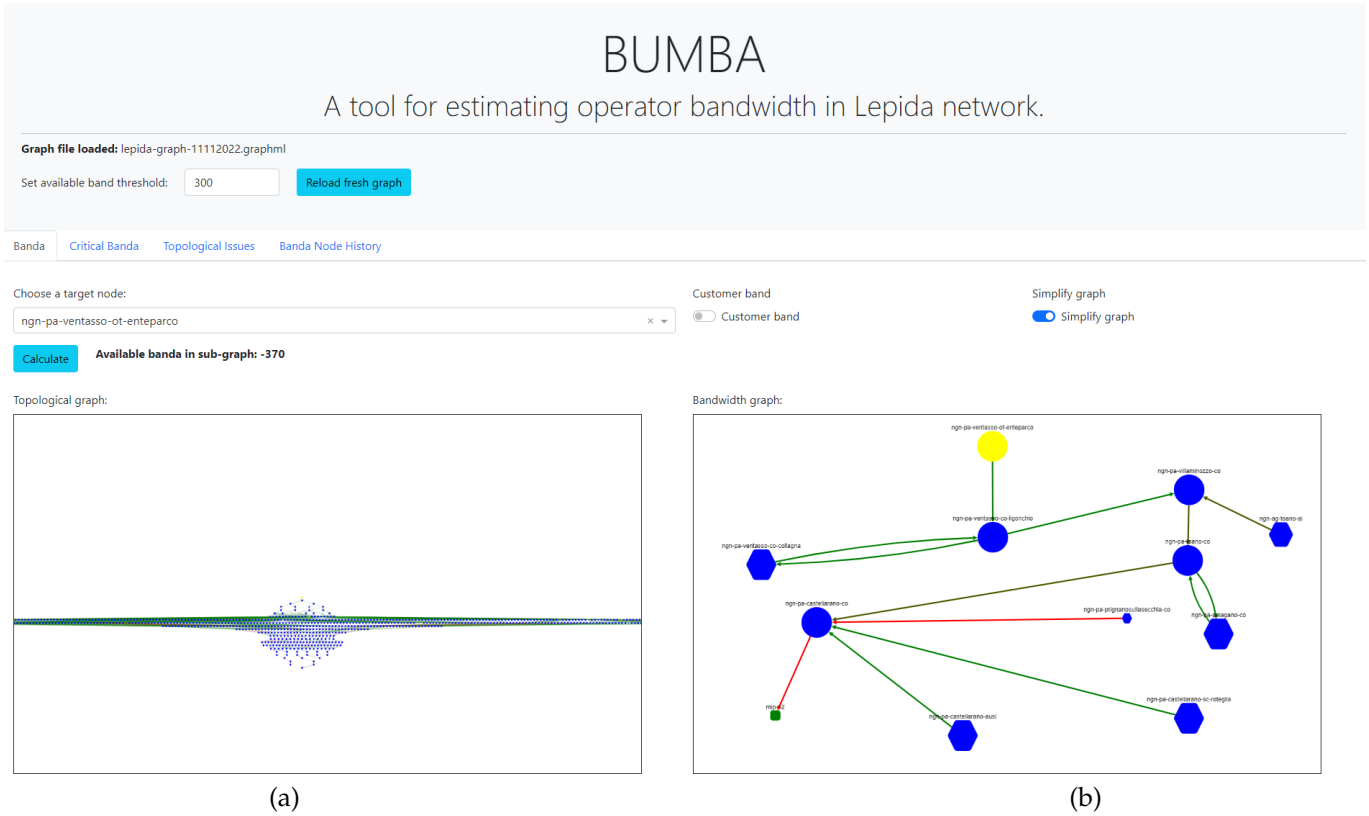


(a) (b)

Figure 7: The *Banda* tab is where the residual band is calculated for a single, selected target node. When the filtered graph is too large, as depicted in the left graph plot window (7a), by enabling the *Simplify graph* widget the graph is reduced and simplified while still retaining the information about the selected target residual band (7b).

decided to refactor our design and to switch to a different implementation capable of providing a full web application.

### 5.1. Web Implementation

Our implementation of the web version of the application and its 'holistic' features for network sanity checks is still grounded on Python3, but the adoption of another framework - Plotly-Dash [15] - is responsible of enabling the web interface without requiring any knowledge of standard web technologies (e.g., Javascript or CSS). Surprisingly, we managed to keep Jupyter in our design pipeline since Plotly-Dash is compatible with it and a single statement is just required to switch the application from running inside Jupyter to running standalone.

In other words, our approach of prototyping the basic functionalities into a Jupyter notebook [13] still holds.

Other frameworks has been adopted and are responsible for specific tasks such as Cytoscape [16] for rendering graphs on a web interface.

The new feature of keeping track of node band allocation over time requires some kind of database storage. Both a relational or NO-SQL approach are suitable and we decided to go for the traditional (relational) approach. In particular, we just adopted a SQL interface provided by the SQLite package and not a full database system. In fact, at the time of writing, the amount of stored data does not deserve a more sophisticated solution. However, this is likely going to change in the near future in order to improve the robustness and flexibility of the system. Since the application runs in a Docker container in our production environment, adding a database system is straightforward. Two persistent volumes has been added to the container to preserve data on stable storage which are respectively dedicated to: (a) database file and (b) daily graph files.

All sanity checks discussed in Section 3.1 are computed (once a day) when the application downloads the raw network data from the NMS API and builds an updated graph structure. Both sanity checks and the download procedure run inside a background service written in 100% Python as well. The web app exhibits the same behavior as in the previous implementation (see Section 5).

Figure 7 shows our tool GUI dedicated to the residual bandwidth calculation of a specific, single target node. In fact, note that the GUI has a first tab labeled as: "Banda" activated. The application GUI has been refreshed to better integrate the new features related to graph health.

The button labeled "Reload fresh graph" on the web Graphical User Interface (GUI) manually triggers the load of the freshest available graph from local storage. This tab performs the same task as the previous notebook application with some usability improvements.

After choosing a target node from the drop-down widget labeled "*Choose a target node*", the corresponding sub-graph is rendered in the "*Topological graph*" widget window. After applying the filtering process (until the second filter, see Section 4), the graph is still too large and its rendering provides little help to the user trying to visually verify the sub-graph topology. In these cases, enabling the switch labeled "*Simplify graph*" substantially simplifies the graph

rendering and allows users to concentrate over the interesting part of the sub-graph. After enabling the switch, by pressing the *Calculate* button the bandwidth calculation is performed and this triggers to effects: (i) the amount of available bandwidth appears close to the button and (ii) the simplified graph is rendered on the *Bandwidth graph* window. By enabling the simplified rendering before choosing the target node, it would have also simplified the rendering for the *Topological graph*. Here, only the graph on the right is simplified because the switch has been enabled after the target node selection.

In graph renderings, all nodes have a rounded shape except MIP nodes, which are squared and green. Target nodes instead are yellow and any other node is blue. When graph simplification is enabled (see 'Simplify graph' switch widget in Figure 7), *border nodes* are rendered in a hexagonal shape. Border nodes are neighbors of any node being part of the shortest path starting from the selected target node. Node size is dynamic and changes according to a linear function applied to its OP_BAND value.

The edge color meaning varies according to the particular graph window. In the topological graph widget (i.e. the left widget), the edge color represents the link speed: faster links are green, while slower links tends towards red. In the bandwidth graph widget instead (i.e., the right widget), the edge color shows the calculated residual band over that link. Its color scheme is the same as in the previous widget. Any edge connecting to a MIP node in standby mode is represented as a black dashed line and labeled by a red "standby" text on top.

Also in this application version, graph plots are dynamic and each element can be dragged and zoomed.

In addiiton to the "Banda" tab, this version has been enriched by three other tabs which respectively correspond to the graph *sanity check features*. The new tabs are named as follows: "Critical Banda", "Topological Issues" and "Banda Node History". In the following, we are going to focus on their respective interfaces.

The "Critical Banda" tab interface is shown in Figure 8. The graph plot shows the topology of a sub-graph which is the one in which lies the selected edge picked from the bottom table. The plot edges color shows their status. In fact, the selected edge is represented in red color as well as "ngn-pa-ozzano-ai-iaco" → "mip-13" edge.

The threshold that defines a critical link is towards the top of the GUI page and it stays visible no matter which tab is selected (see 7). The threshold (BAND_TSD) default is set to 300Mbit/s and can be overridden by editing its widget. Any edge whose residual band is less than the threshold is collected into the bottom table.

The table content can exported (in CSV format) through the "Export" button on the table top left corner.

The next tab is dedicated to topological issues and it is shown in Figure 9. Here, a table collects any exception error triggered by search algorithm over the graph (i.e., *G_errors* data structure). For each target node triggering an exception we have a table record with a corresponding "Node" column. The "Error" column contains all the required information (such as: node names, device interfaces, template description, ...) in a human readable form in order to fix the corresponding issue on the NMS. As in the previous tab, the table data can be downloaded for offline processing through the "Export" button.

Figure 10 shows the tab dedicated to node history. A user, by choosing a target node through the left drop-down widget, can query the underlying knowledge-base about any bandwidth allocation change over time. The node selection triggers the visualization of the corresponding information by populating the table on the right.

These new features allows to obtain an overview of the bandwidth status of the whole network graph and they focus on emphasizing those elements that are likely to deserve a special attention.

### 5.2. Banda Calculus API Integration

In order to support and integrate with other Company services, Banda Calculus implements a basic REST API in order to allow systems to interact together without human intervention. The API exposes a single resource via GET HTTP method. It is just sufficient to specify the target node symbol name as the only parameter. The back-end system reply is represented by a JSON structure as follows:

```
{
'target_node': <node_name>,
'avail_band': <band-int>,
'path_to_mip': [(<node-A>, <node-B>, <band-int>), ..., ()],
'from_graphfile': <graph_filename.graphml>,
'message': 'OK'
}
```

The object contains the target node symbol provided as parameter and the field `avail_band` shows the final result of the banda calculation process towards the closest MIP. In `path_to_MIP` field, a list of tuples depicts the exact path followed by the algorithm and specifies the residual band for each edge. Other information, such as the specific graphml file adopted as data source (i.e., `from_graphfile`) and a human readable outcome message (i.e., `message`). The former field contains the string `'OK'` or an error string in case of any issue.

## 6. Discussion and Conclusions

In this paper, we presented the problem we tackled when dealing with checking residual bandwidth availability in our Regional broadband network. Our ad-hoc and in house-developed solution, Banda Calculus, is coming from this particular need. Since the very beginning, the main benefit introduced by our tool is the substantial reduction (e.g., seconds versus hours) of the time required to calculate the residual available bandwidth over a specific node. Just this step turned out to be a game changer in order to provide our services to customers.

The benefits introduced by Banda Calculus are not limited to getting faster, streamlined business procedures. In fact, its evolution over time introduced several features addressing other needs. It first evolved in terms of (a) usability by becoming a web application deployed in our Intranet and in terms of (b) focusing on the whole network instead of a single node at a time. In particular, the latter avenue of evolution expanded the range of features at our disposal. These

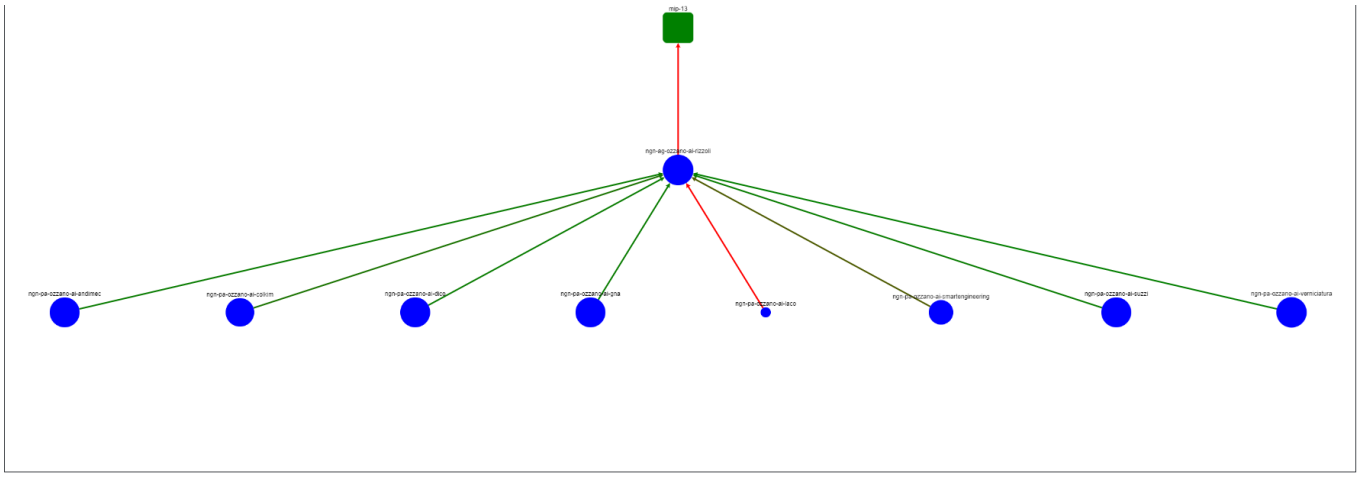

Critical paths:

Export

| | Source | Avail. Band | Destination |
|---|---|---|---|
| ○ | ngn-pa-cotignola-ai-vulcanflex | -1000 | ngn-ag-cotignola-ai |
| ○ | ngn-pa-langhirano-co | -1000 | dc-pr |
| ○ | ngn-ag-pc | -925 | mip-02 |
| ○ | ngn-ag-pc | -925 | mip-03 |
| ○ | ngn-ag-guastalla | -730 | mip-02 |
| ◉ | ngn-ag-ozzano-ai-rizzoli | -530 | mip-13 |
| ○ | ngn-pe-907 | -515 | mip-07 |

Figure 8: The *Critical Banda* tab is where paths considered *critical* from a residual band point of view are shown in a tabular format. By default, all links are ordered from most critical in a decreasing manner and the BAND_TSD is set to 300 Mbit/s as depicted in the text widget on top of the page. The selection of any table row shows triggers the sub-graph rendering in which the edge is located on the top windows for a visual examination. The table data set can also be exported in CSV format by the `Export` button.

Banda | Critical Banda | Topological Issues | Banda Node History

**Error Legenda:**

- **No path between X and Y** → missing uplink edge along the path between node X and MIP Y. The edge might be present, but marked as 'downlink' instead of 'uplink'.
- **Either source X or target Y is not in G** → means node not found. Bumba filtering removed node X or MIP Y from the graph. It is very likely that the filtering process has removed node X because all its in/out links are marked as 'downlink'. By removing any connection, node X is no longer part of the sub-graph.
- **A wrong INACTIVE link is likely present: no MIP DC for node: X** → the sub-graph generated by the filtering process has no ENDPOINT node (e.g., MIP). The edge with which the MIP node is connected to the rest of the sub-graph is marked as 'inactive'and this issue has removed the MIP node from the sub-graph.

Export

| Node | Error |
|---|---|
| ngn-pa-piandelvoglio-ot-piazza | Either source ngn-pa-piandelvoglio-ot-piazza or target mip-07 is not in G. Misconfigured link: 'ngn-pa-piandelvoglio-ot-piazza' --[IFACE: ge0-1-0, IS_ACTIVE: True, TEMPLATE: iface-access-downlink]--> 'ngn-pa-piandelvoglio-ot-118' Misconfigured link: 'ngn-pa-montearmato-trl' --[IFACE: ge0-0-0, IS_ACTIVE: True, TEMPLATE: iface-access-downlink]--> 'ngn-pr-montearmato-sanbenedettovaldisambro' |
| ngn-pa-rimini-sc-lettimi | Either source ngn-pa-rimini-sc-lettimi or target mip-07 is not in G. Misconfigured link: 'ngn-pa-rimini-sc-lettimi' --[IFACE: ge0-1-0, IS_ACTIVE: True, TEMPLATE: iface-cust]--> 'ngn-pa-rimini-co' Misconfigured link: 'ngn-pa-rimini-sc-lettimi' --[IFACE: ge0-1-0, IS_ACTIVE: True, TEMPLATE: iface-cust]--> 'ngn-pa-rimini-co' |
| ngn-pa-lizzanoinbelvedere-trl | A wrong INACTIVE link is likely present: no MIP or DC for node: 'ngn-pa-lizzanoinbelvedere-trl'. Misconfigured link: 'ngn-pa-lizzanoinbelvedere-trl' --[IFACE: ge0-0-10, IS_ACTIVE: True, TEMPLATE: iface-access-downlink]--> 'ngn-pr-lizzano-cellmon-querciola' Misconfigured link: 'ngn-pa-casteldicasio-trl' --[IFACE: ge0-0-1, IS_ACTIVE: True, TEMPLATE: iface-access-downlink]--> 'ngn-pr-casteldicasio-porrettatermeausl' Misconfigured link: 'ngn-pa-porrettaterme-ausl-3p' --[IFACE: ge0-1-0, IS_ACTIVE: True, TEMPLATE: iface-cust]--> 'ngn-pa-porrettaterme-ausl' Misconfigured link: 'ngn-pa-lizzanoinbelvedere-trl' --[IFACE: ge0-0-10, IS_ACTIVE: True, TEMPLATE: iface-access-downlink]--> 'ngn-pr-lizzano-cellmon-querciola' Misconfigured link: 'ngn-pa-casteldicasio-trl' -- |

Figure 9: The *Topological Issues* tab provides users a comprehensive view of any topological issue in the current graph. The view is implemented as a table where each row shows the node which triggered some kind of error and a verbose description of the error itself. The table data set can also be exported in CSV format by the `Export` button.

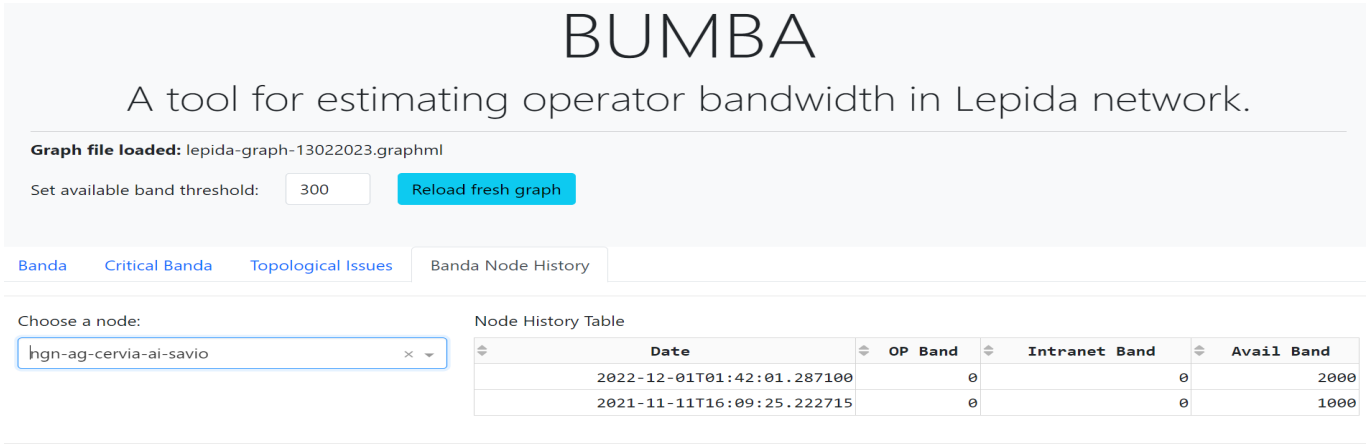


Figure 10: By first choosing a node using the combo-box widget on the left, the *Banda Node History* tab allows users to visualize the bandwidth availability for any node of the network over time.

features improve our monitoring and planning capabilities. We briefly summarize them in the following lines.

By exploiting the health monitoring features, operators can understand (c) in advance which parts of the (sub)graph might need un upgrade before it is too late (e.g., unable to provide any bandwidth). In addition, anything which is suspected of being a topological graph issue (d) is reported in a table and it is open to inspection. Also the graph visualization has been fine tuned and we adopted an in-house developed algorithm (e) that can be triggered when dealing with large graphs. Finally, in order to integrate Banda Calculus into our company processes and to allow automatic interactions between systems, we provided an API (f).

Our near future plans are actually focused on integration in order to automate and integrate as much as possible our business processes.

## References

[1] "LepidaScpA Home Page", 2022.

[2] "Nagios Monitoring Solutions", 2022.

[3] "Network monitoring with intuition", 2022.

[4] V. J. Ribeiro, J. Navrátil, R. H. Riedi, R. Baraniuk, L. Cottrell, "pathchirp: Efficient available bandwidth estimation for network paths", 2003.

[5] M. Allman, "Measuring end-to-end bulk transfer capacity", "Proceedings of the 1st ACM SIGCOMM Workshop on Internet Measurement", IMW '01, p. 139–143, Association for Computing Machinery, New York, NY, USA, 2001, doi:10.1145/505202.505220.

[6] "Elastic Stack", 2022.

[7] "Graphana Labs", 2022.

[8] "NEO4J Graph Data Platform", 2022.

[9] Y. Dinitz, *Dinitz' Algorithm: The Original Version and Even's Version*, pp. 218–240, Springer Berlin Heidelberg, Berlin, Heidelberg, 2006, doi:10.1007/11685654_10.

[10] Y. Boykov, V. Kolmogorov, "An experimental comparison of min-cut/max-flow algorithms for energy minimization in vision", "Third International Workshop on Energy Minimization Methods in Computer Vision and Pattern Recognition", vol. 23, pp. 1124–1137, 2004.

[11] G. P. Jesi, G. Mazzini, "Banda calculus: a tool for bandwidth estimation in broadband network infrastructures", "2020 International Conference on Software, Telecommunications and Computer Networks (SoftCOM)", pp. 1–5, 2020, doi:10.23919/SoftCOM50211.2020.9238312.

[12] G. P. Jesi, A. Odorizzi, G. Mazzini, "Exploit company knowledge from graphs with banda calculus", "2021 International Conference on Software, Telecommunications and Computer Networks (SoftCOM)", pp. 1–6, 2021, doi:10.23919/SoftCOM52868.2021.9559101.

[13] "Project Jupyter", 2022.

[14] "NetworkX - Network Analysis in Python", 2022.

[15] "Low-Code Data Apps", 2022.

[16] "Cytoscape - Network Data Integration, Analysis, and Visualization in a Box", 2022.



**Gian Paolo Jesi** graduated in Computer Science in 2002 at the University of Bologna. After a short experience in an ICT Company, he rejoined his Alma Mater in late 2003 and he received his Ph.D. degree in 2007 in the area of large distributed systems.

His research work focuses on distributed/complex systems, emergent behaviors and cognition. He served as a Research Associate in several universities in Italy and Europe until he had the opportunity to join Lepida ScpA in 2018. He is author of more than 25 papers in international conferences and journals.

**Andrea Odorizzi** received the B.S. and MSc. degrees in Electronic Engineering (summa cum laude) from the University of Ferrara respectively in 2003 and 2005. In 2009, he received his Ph.D. from the same Alma Mater.

His research work focuses on Cryptography, Peer-to-peer multimedia applications, sensor networks. He served as PhD fellow in University of Ferrara until he had the opportunity to join Lepida ScpA in 2008. He is

author of more than 20 papers in international conferences and journals.

**Gianluca Mazzini** graduated in Electronic Engineering (summa cum laude) and he received his Ph.D. degree in Electrical Engineering and Computer Science from the University of Bologna respectively in 1992 and 1996.

In 1996 he joined the University of Ferrara as an Assistant Professor and in 2002 he held the position of Associate Professor. His research work carried out since 1993 is related to: spread spectrum communications; applications of chaos to telecommunications; architectures for efficient radio local area networks, cellular and ambient; routing strategies in mobility sensor networks; capacity in telecommunications system; peer-to-peer networks; networks with multimedia traffic; information security. He is author or coauthor of more than 250 international publications in books, journals or conference proceedings. Google Scholar in November 2012 reports over 4700 citations with an h factor of 37 and an i10 factor of 58. His teaching shows more than 50 editions of university courses in 12 different categories. He has been the supervisor of over 140 theses and tutor for 14 Ph.D. students. He has been co-organizer of two international conferences, guest editor of the Proceedings of the IEEE, has served as Associate Editor for IEEE journals for nine years, and has served as TPC member for more than 40 international conferences. He has had roles in coordinating over a dozen projects at an international or national level, including four European projects. As first researcher in role for TLC in University of Ferrara, he founded the research group in TLC area and has established a structured series of collaborations with other organizations, including: ARCES at the University of Bologna, IEIIT at the CNR, CNIT. He has been a member of seven scientific committees and seven boards of directors or management. He was CEO of Lepida ScpA.

Received: 23 December 2022, Revised: 15 March 2023, Accepted: 24 April 2023, Online: 30 May 2023

DOI: https://doi.org/10.55708/js0205001

# Orthogonal Polynomials in the Problems of Digital Information Processing

**Yaroslav Pyanylo[1,*], Valentyna Sobko[1], Halyna Pyanylo[1], Oksana Pyanylo [2]**

[1] Pidstryhach Institute for Applied Problems of Mechanics and Mathematics, National Academy of Sciences of Ukraine Lviv, 79060, Ukraine
[2] CodeTiburon, Kharkiv, Ukraine
*Corresponding author: Yaroslav Pyanylo, Naukova str, 3/b, Lviv, 79060, Ukraine, danylo794@gmail.com

**ABSTRACT:** The paper examines spectral methods based on classical orthogonal polynomials for solving problems of digital information processing. Based on Jacobi polynomials, signal approximation methods are built to identify objects in the natural environment. Based on Chebyshev-Laguerre polynomials, methods of filtering multiplicative signal noises in linear filter models are proposed. Numerical experiments on model problems were conducted.

**KEYWORDS:** Spectral Methods, Digital Information Processing, Signal Approximation and Filtering, Object Identification

## 1. Introduction

To solve a broad spectrum of scientific and applied problems in many areas of natural science and technology, we use information that is stored in digital form. Input information is the value of measured parameters of the processes under investigation. The accuracy of the measured values depends on the measuring equipment and is not always high. Such problems as remote sensing data processing, electronic paramagnetic resonance (EPR), tomography, etc. [1] can be categorized as problems with unclear input information. Digital information is considered input for developing mathematical models of physical processes. Since the input information is specified with the inaccuracy of the measuring devices, their direct use in mathematical models can lead to significant differences in the desired results [2]. Consequently, preliminary processing of the input information is required [3, 4].

It becomes necessary to choose the processing method for cases when solutions to formulated applied problems that are based on digital input data should be obtained [3, 5, 6]. Considerable amount of software packages has been developed to process digital information. [7, 8]

The total amount of worldwide commercial software applications is measured by several dozen. However, the number of the most famous and widely used commercial software applications for geoinformation systems can be limited to ten to fifteen [7, 8]. The world leaders of the software are ESRI packages (ArcGIS Desktop products), the MapInfo Professional package, the Idrisi package (developed at Clark University, USA), AutoCAD, ERDAS IMAGINE, ENVI, and Digitals [4].

Every process in which digital information is used has its peculiarities. These peculiarities cannot always be factored into the existing application programs. As a rule, these software packages are protected and do not allow any modifications In this regard, it is necessary to develop methods of processing input data that should make it possible to consider the particularity that occurs when exploring numerous natural phenomena.

Signal approximation, information compression, and signal filtering are the main problems in information processing [1]. There are various methods to solve data processing problems. Not all of them meet the requirements associated with the tasks that must be resolved. Spectral methods in orthogonal bases with fast transformation algorithms are the most used. The analysis of the orthogonal bases presented in the literature shows that the classic orthogonal polynomials Jacobi and Chebyshev-Laguerre are highly effective for usage. [2, 3, 5, 6, 9 - 12].

The paper is aimed at research methods of classical orthogonal polynomials usage for solving applied problems, in particular, object identification based on the processing of discrete data of electronic paramagnetic resonance (EPR-dosimetry), remote sensing, and others. The identification of objects takes place based on the characteristic signs of the separation of the abnormal spectrum from the background spectrum. These signs may be extreme values of the digital spectrum. At the same time, not only the extreme values themselves are significant, but their coordinates as well.

It is worth noting, that digital information processing problems are also widely used in the mathematical modeling of natural and physical processes. In particular, for mass transfer modeling in complex pipeline systems and the filtration process in complex porous media. The peculiarity of such problems is that the input information is measured data. These data are obtained with low accuracy and at arbitrarily placed points. Direct implementation of such data in mathematical models can lead to unacceptable results in practice. Preliminary statistical and probabilistic data processing is necessary for effective input information implementation.

Adaptive algorithms based on classical orthogonal polynomials for solving many applied problems, such as approximation and filtering of signals, solving problems of mathematical physics, etc., are built in the current manuscript. The advantage of these algorithms over the existing ones is that these methods ensure the accuracy of the recovery of the problem solution based on the so-called constructive elements.

## 2. Definition of integral transformations where Jacobi and Chebyshev-Laguerre polynomials are cores.

A characteristic feature of the applied problems is that, in most cases, the data needed to set the initial and boundary conditions in an analytical form are unknown. This leads to the formulation of incorrect problems of mathematical physics under great uncertainty. To build a solution to problems of this type, it is necessary to use regularizing algorithms based on a priori information that is known in a non-formalized form.

One of the forward-looking approaches for resolving the formulated problems is operational and spectral methods usage. In computational experiments, these methods have several advantages related to the parametric (symbolic) problems solution at different stages. Such solutions allow us to study the influence of the parameters of the physical process on its progress and the stability of the solution regarding small perturbations of the input data. In those cases when the symbolic solution of the problem cannot be obtained, the value of these methods is partially retained, since it is possible to build a solution based on the images (in terms of the corresponding operators) based on the so-called constructive elements, for these cases the values of the images are then calculated with a predetermined accuracy.

Constructive elements are functions specified in some functional basis by a finite set of integers or rational numbers with accuracy up to the normalizing factor. This class of elements includes, for example, classical orthogonal polynomials; each such element has integer coefficients. Using the basis of structural elements allows you to organize the computational process of solving the problem with guaranteed accuracy. The calculation with guaranteed accuracy means the ability to build the calculation process in a way that arithmetic operations errors at each intermediate stage of the machine (hardware) implementation have such an order as to ensure the sufficient accuracy of the final result.

When numerically finding a solution to a problem with guaranteed accuracy, mainly method errors are left. If the numerical methods ensure sufficient accuracy of the problem solution recovery, then it can be assumed that the advantages of the symbolic solution in the computational experiment are maintained.

Let the function $\varphi(x)$ be defined on the interval of $[-1,1]$, and meet the conditions which allow it to be expanded into a series by Jacobi polynomials. [12, 13]. The Jacobian integral transformation $\varphi_n$ of $\varphi(x)$ function with the weighting function $\omega(x) = (1-x)^{\alpha}(1+x)^{\beta}$ $(\alpha > -1, \beta > -1)$ is defined as follows

$$\varphi_n = \int_{-1}^{1} \omega(x)\, P_n^{(\alpha,\beta)}(x)\, \varphi(x)\, dx\ . \qquad (1)$$

where $P_n^{(\alpha,\beta)}(x)$ – are Jacobi polynomials. If the images $\varphi_n$ for $n = 0,1,2\ldots$, are known, then the inverse of the integral transformation (1) is found by the formula

$$\varphi(x) = \sum_{n=0}^{\infty} \frac{\varphi_n}{r_n} P_n^{(\alpha,\beta)}(x)\ . \qquad (2)$$

For a function $f(t)$, $t \in [0,\infty)$, that expands in a series by $L_m^{\lambda}(t), \lambda > -1$ Chebyshev-Laguerre polynomials, we define the corresponding integral transformation as follows

$$f_m = \int_0^{\infty} t^{\lambda} e^{-t} L_m^{\lambda}(t) f(t) dt\ . \qquad (3)$$

In this case, $f_m$ is the Chebyshev-Laguerre image of the original function $f(t)$. The formula for the integral transformation inversion (3) has the form

$$f(t) = \sum_{m=o}^{\infty} \frac{m! f_m}{\Gamma(m+\lambda+1)} L_m^{\lambda}(t)\ . \qquad (4)$$

Analysis of the spectral methods implementation shows that the basis used to solve the problem must correlate with the domain of definition. That means that in

a case where the studied parameter changes over a finite interval, then Jacobi polynomials are advisable to use as this interval is reduced to an orthogonality interval by linear substitution. In the case of a semi-infinite interval, Chebyshev-Laguerre polynomials are recommended to be used. Chebyshev-Laguerre polynomials grow exponentially over increasing an argument. This property complicates the summation of the series (4). One of the methods to solve this problem is to use the modified Chebyshev-Laguerre integral transformation.

Let $\nu$ $(\nu < 0, \nu \neq 0)$ and $\mu(0 < \mu < \infty)$ are some constants. The modified integral Chebyshev-Laguerre transform is defined by the relation [5]

$$f_m(\nu,\mu) = \int_0^\infty t^{\nu\lambda+\nu-1} e^{-\mu t^\nu} L_m^\lambda(\mu t^\nu) f(t) dt \ . \quad (5)$$

For such an integral transformation, the original $f(t)$ is found by the formula

$$f(t) = \sum_{m=o}^{\infty} \frac{m! f_m(\nu,\mu)}{\Gamma(m+\lambda+1)} L_m^\lambda(\mu t^\nu) \ . \quad (6)$$

We note that the integral transformation (5) with the appropriate choice of parameters allows us to study rapidly oscillating functions effectively.

Spectral methods on a biorthogonal basis [11, 14], built based on classical orthogonal polynomials, have proved their worth. Their use makes it possible to apply the implicit regularization of the corresponding series to a greater extent.

Integral transformations (1) and (3) or similar ones are applied to solve many applied problems. They are the basis of spectral methods of digital information processing. The computation of the coefficients of the orthogonal series (integral transformations (1), (3), (6)) and finding the corresponding originals is the main essence of the spectral methods.

Quadrature formulas for calculating the integral transformations, the method of least squares, or other methods can be used to find generalized spectra when input values are given in the discrete form. [15, 16]. In some cases, depending on the method of specifying input information, it is possible to determine formulas that are optimal in the $L_2$ class for the calculation of the generalized spectra.

Let the polynomials $u_n(x)$ be orthogonal on the interval $[a, b]$ and the function $\varphi(x)$ is presented by an orthogonal series over the polynomials $u_n\ (x)$ [5], i.e

$$\varphi(x) \ = \sum_{n=0}^{\infty} \frac{\varphi_n}{r_n} \ u_n \ (x) \ . \quad (7)$$

It is known that the $N+1$-th orthogonal polynomial has $N+1$ a real root that belongs to the interval of orthogonality. Then an $L_2$ optimal quadrature formula is used to calculate the generalized spectra $\varphi_n$

$$\varphi_n \ \sim \sum_{j=0}^{N} \rho_j^2 \ u_n \ (x_j) \ \varphi(x_j) \ , \quad (8)$$

where $x_j$ - the roots of the equation $u_{N+1}(x_j) = 0$, a

$$\rho_j^{-2} \ = \ \sum_{i=0}^{N} u_i^2 \ (x_j).$$

## 3. Construction of biorthogonal systems of functions.

The advisability of constructing a biorthogonal basis may explain the following well-known fact: when a biorthogonal series converges slowly by one system of functions then it converges rapidly by another. Nowadays, there are not many works in literature that are devoted to the construction of biorthogonal systems of functions and the studying of their characteristics. The main ways of constructing an orthogonal basis are: using the Gram-Schmidt scheme, building eigenvalues and eigenfunctions, and building eigenvalues of integral operators. It must be taken into account that, in practice, the Gram-Schmidt scheme permits the construction of a small number of orthogonal functions as it comes down to solving a poorly conditioned system of algebraic equations.

The systems of the orthogonal polynomials $p_0, p_1, \cdots p_n$ , which are built based on tram-Schmidt's scheme, rely on the following algorithm. Let $g_n(x) = x^n$ be a polynomials system on the $x\epsilon[x_1, x_k]$ interval. Let's define a projector

$$proj_p(g) = \frac{\int_{x_1}^{x_2} f(x)g(x)W(x)dx}{\int_{x_1}^{x_2} (f(x))^2 W(x)dx}.$$

Then orthogonal polynomials are determined sequentially according to the scheme

$$p_0 = g_0,$$
$$p_1 = g_1 - proj_{p_0}(g_1),$$
$$p_k = g_k - \sum_{j=1}^{k-1} proj_{p_j}(g_k).$$

The given algorithm for constructing orthogonal polynomials belongs to the unstable class. The errors of decomposing rounding and numerical integration rapidly increase as the polynomial error increases during coefficient calculation.

Construction of quasi-spectral polynomials based on Chebyshev polynomials $T_n(x)$ . Consider an integral operator $L: L_{2,\rho}[-1,1] \to L_{2,\rho}[-1,1]$ with a weight function $\rho = 1/\sqrt{1-x^2}$, which matches the expression $f \in [-1,1]$ for the function

$$Lf(x) = \int_{-1}^{x} dx_1 \int_{-1}^{x_1} f(x_2)dx_2 = \int_{-1}^{x} (x - x_1) f(x_1)dx_1 \ (9)$$

It is known [12, 13, 17] that expression (9) has no non-zero eigenvalues. Therefore, we will consider the

corresponding quasi-spectral problem, based on the properties of the integral operator (9) in the Hilbert space $L_{2,\rho}[-1,1]$ instead of the spectral eigenvalue problem. Let's construct the operator

$$\pi_1^{\infty} L = \pi_1^{\infty} \int_{-1}^{x} \int_{-1}^{x_1} \quad : \pi_1^{\infty} \int_{-1}^{x} \int_{-1}^{x_1} \quad ,$$

which converts odd polynomials into even ones, and vice versa.

Definitions. Let $\tilde{L}_{2,1}[-1,1]$ is a complete subspace of Hilbert space $L_{2,\rho}[-1,1]$, all elements of which satisfy the $\int_{-1}^{1} u(x)dx = 0$ integral equation. The values of the $\pi_1^{\infty} \int_{-1}^{x} \int_{-1}^{x_1} \quad : \tilde{L}_{2,1}[-1,1] \to \tilde{L}_{2,1}[-1,1]$ operator, based on Chebyshev polynomials elements, differ from the values of the operator (1) by a zero summand of the Fourier-Chebyshev series. However, the spectral characteristics of these operators are radically different. The operator $\pi_1^{\infty} \int_{-1}^{x} \int_{-1}^{x_1}$ has characteristic values and eigenfunctions, but the spectral radius of a compact operator of the Volterra type has no eigenvalues that differ from zero [12, 13, 17].

Statement 1. If a polynomial

$$\bar{U}_{2i-1}^{2s-1}(x) = \sum_{j=1}^{s} \bar{c}_{2j-1}^{2i-1} T_{2j-1}(x),\ i = 1,\dots,s$$

meets the conditions

$$\int_{-1}^{1} \rho(x) U_{2i-1}^{2s-1}(x) \bar{U}_{2j-1}^{2s-1}(x) = \begin{cases} 0, i \neq j \\ \sigma_{2i-1}, i = j' \end{cases}$$

then the coefficients $c_{2j-1}^{2i-1}$ are computed according to the algorithm that is constructed in the works [4, 17].
Statement 2. If a polynomial

$$\bar{U}_{2i}^{2s}(x) = \sum_{j=1}^{s} \bar{c}_{2j}^{2i} T_{2j}(x),\ i = 1,\dots,s$$

meets the conditions

$$\int_{-1}^{1} \rho(x) U_{2i}^{2s}(x) \bar{U}_{2j}^{2s}(x) = \begin{cases} 0, i \neq j \\ \sigma_{2i}, i = j' \end{cases}$$

then its coefficients $c_{2j}^{2i}$ are computed by the algorithm presented in the works [4, 14].

Construction of quasi-spectral polynomials based on Lager polynomials. Consider an integration operator $L: L_{2,\varpi}[-1,1] \to L_{2,\varpi}[-1,1]$ with a weight function $\varpi(x) = \exp(-t)$, that $f(t) \in L_{2,\varpi}[0,\infty]$ matches the expression

$$Lf(t) = \int_{-1}^{t} dt_1 \int_{-1}^{t_1} f(t_2)dt_2 = \int_{-1}^{t} (t - t_1) f(t_1)dt_1 \quad (10)$$

Expression (10) does not have non-zero eigenvalues. Let's consider the corresponding quasi-spectral problem.

The quasi-spectral problem for an integral operator. For given $n = 1,2,\dots$ we should find the values of the parameter $\lambda$ at which the equation

$$\int_0^t dt_1 \int_0^{t_1} \varphi(t_2)\, dt_2 = -\lambda \left( \varphi(t) - \int_0^t \varphi(t_1) dt_1 \right) + \\ + \tau_1 L_{n+1}(t) + \tau_0 L_0(t)$$

has nonzero polynomial solutions $\varphi = \varphi(t) \in L_{2,\varpi}[0,\infty]$ of degree $\leq n$, where $\tau_1$, $\tau_0$ are some parameters, $L_{n+1} = L_{n+1}(t)$ and $L_0 = L_0(t)$ are given (and fixed) Lager's polynomials of power that equal to $n+1$ and zero, respectively.

The following equations are veritable

$$\int_0^{\infty} \exp(-t) \varphi_i^{n-1}(t) \varphi_j^{n-1}(t)\, dt = \begin{cases} 0, i \neq j \\ 1, i = j' \end{cases}$$

$$\int_0^{\infty} \exp(-t) \psi_i^{n}(t) \psi_j^{n}(t) dt = \begin{cases} 0, i \neq j \\ -\lambda_i, i = j \end{cases}.$$

Based on the constructed biorthogonal polynomials, adaptive algorithms for the computation of mode parameters of gas transport were built. These algorithms permit minimizing energy resources and optimizing the operation of the gas station according to various criteria. The fact that a significant number of parameters can be calculated with arbitrary precision and stored in computer memory is the advantage of using biorthogonal polynomials constructed to solve problems of mathematical physics. Their further usage for problem calculations reduces the accumulation of errors and saves time.

## 4. Moments in the processing of digital information and their relationship with spectral methods

Spectral moments in statistical and probabilistic methods of digital information processing should be used to reduce the error values that occur under the approach of the argument of the distribution function to the initial value. This error can occur by using distribution moments instead of the distribution function to simplify the analysis [1, 3, 4, 7, 11].

In contradistinction to the moments of the distribution, the spectral moments of the distribution do not depend on the shift of the distribution function along the axis of the argument. They can be initial and central, just as distribution moments. But in most cases, the spectral moments to the distribution functions are central [18].

The introduction of the concept of spectral distribution moments will simplify the computation of several errors summing up during their quantile evaluation [5, 8, 12-17, 19].

The initial moment of the k-th order of a random variable X is called the mathematical expectation of the k-th degree X, i.e.

$$M_k(X) = \int_a^b x^k f(x)\, dx = a_k,$$

The central point of the k-th order is called the mathematical expectation of the k-th degree of random variable deviation from its mathematical expectation, i.e.

$$\mu_k = \int_a^b (x - a_1)^k f(x)\, dx$$

The central moment of the first order is zero; the central moment of the second order is equal to the variance of the random variable: μ1 = 0; μ2 = D (X). The central moments are used to quantify the distribution of a random variable.

The asymmetry coefficient $C_s$ is the ratio of the central moment of the third order to the cube of the standard deviation

$$C_s = \frac{\mu_3}{\mu_2^{3/2}}.$$

The kurtosis coefficient of the random variables is calculated by the formula

$$E_s = \frac{\mu_4}{\mu_2^2} - 3.$$

Using orthogonal distributions permits solving some problems of digital information processing, for example, signal approximation and filtering from additive noise. At the same time, by the known coefficients, using the relationship between the coefficients of orthogonal distributions and statistical parameters, it is possible to estimate their probability and other probabilistic-statistical parameters.

Consider the relationship of moments with generalized spectral coefficients based on Jacobi polynomials.

If the function $\varphi(x)$ is decomposed into series

$$\varphi(x) = \omega(x) \sum_{n=0}^{\infty} \frac{\varphi_n}{r_n} P_n^{(\alpha,\beta)}(x),$$

then

$$\varphi_n = \int_{-1}^{1} \varphi(x)\, P_n^{(\alpha,\beta)}(x)\, dx .$$

The Jacobi polynomials $P_n^{(\alpha,\beta)}(x)$ are given in the form of

$$P_n^{(\alpha,\beta)}(x) = \sum_{j=0}^{n} \eta_{jn}(\alpha,\beta) x^j.$$

If through

$$\mu_j = \int_{-1}^{1} \varphi(x)\, x^j\, dx$$

denote the moments of the function $\varphi(x)$, then

$$\varphi_n = \sum_{j=0}^{n} \eta_{jn}(\alpha,\beta)\mu_j.$$

The last formula allows us to find the moments of the function for $n$ an arbitrary spectral coefficient $\varphi_n$

$$\mu_n = \frac{1}{\eta_{nn}(\alpha,\beta)}\left(\varphi_n - \sum_{j=0}^{n-1} \eta_{jn}(\alpha,\beta)\mu_j\right).$$

Below is an example of the implementation of statistical and probabilistic data processing. The works [2. 10, 11] are related to the mathematical model construction of the process of the Ukraine gas transportation system operation together with the underground gas storage operation. The input information is the measured pressure values and volumetric gas consumption at the measurement points. Based on this data, a range of practical problems are solved. In particular, the problem of determining gas reserves in pipelines can be solved. The GTS mostly operates in stationary mode. The calculation results of the gas reserve changes in the 122 km long and the 1,388 m diameter pipeline are presented in Figure 1. These results are calculated based on the measured data of the inlet and outlet pressures every two hours.

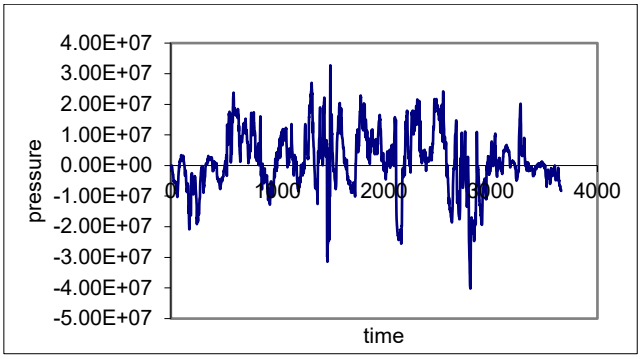


Figure 1: Dependency of gas reserves changes in the 122 km long and the 1,388 m diameter pipe, where calculations are based on measured data of inlet and outlet pressures every two hours.

The implementation of statistical and probabilistic input data processing allows stabilizing the process of the gas volume determination in the pipeline and determining the necessary processing parameters: the number of measurements, time interval, etc.

Identifying the nature of gas movement in the pipeline, stationary or non-stationary, is another objective, which is solved using the Fourier-Jacobi series. The zero Fourier-Legendre coefficient determines the arithmetic average of the measured value in the corresponding interval. The first coefficient expresses the mathematical expectation of a random value. Based on an analysis of the numerical results, we can follow up: if the first Fourier-Jacobi coefficient is smaller than one, then the gas movement process is stable; otherwise - it is non-stationary.

## 5. Inversion of one-dimensional Volterra convolution

Obtaining digital information about the explored objects is associated with various types of inaccuracies - additive or multiplicative. Additive inaccuracies are sufficiently well filtered by approximating the received signal. As a rule, filtering multiplicative noises is solved by integral equations, the cores of which are functions of the medium capacity. Quite often, integral equations may be approximated by convolutional integral equations

$$\alpha f(t) + \mu \int_0^t k'(t-\tau)\, f(\tau)\, d\tau = y(t), \qquad (11)$$

$$\mu \int_0^t k(t-\tau)\, f(\tau)\, d\tau = y(t). \qquad (12)$$

The problem of filtering multiplicative noises in linear filter models of signals, information processing, lidar equations, etc. may be solved by such equations [1, 5, 8, 20]. Here $\alpha$, $\mu$- some constants, $f(t)$- the desired function, $k(t)$- the equation core. Equations (11) and (12) can be easily solved by operational methods based on the integral Laplace transformation. When input information is presented as discrete data, then it is necessary to apply numerical methods. The main ways to solve integral equations of the 1st type convolution is the utilization of regularization algorithms of the Tikhonov type or the discretization of the direct origin equation. However, these methods have some disadvantages [2, 20].

The use of Tikhonov-type algorithms leads to a loss of Volterra stability, which significantly reduces the ability to restore the searched functions for the areas under consideration and demands the implementation of small grid steps.

The main disadvantage of the second method is the lack of accounting for the instability of the digital solution to inaccuracy in the input information. That leads to the case when the solution of the perturbed equation is beyond the set of correctness. Furthermore, not all quadrature formulas give rise to convergent methods.

Algorithm for solving integral equations (11) and (12) in the Chebyshev-Laguerre basis $L_n^{\lambda}(t)$, $\lambda > -1$. [5] It is assumed that the functions included in integral equations (11) and (12) satisfy the conditions that allow them to be represented by the Fourier-Laguerre series (4). Then, if $f(t)$ is the restoring signal, then the determination of the unknown coefficients $f_n$. will ensure the search solution.

Solution of equation (11). It is convenient to write equation (10) as follows

$$\big(\alpha - \mu\, k(0)\big)\, f(t) + \mu \frac{d}{dt} \int_0^t k(t-\tau)\, f(\tau)\, d\tau = y(t).$$

If $\lambda = 0$, then there is a formula for calculating the unknown coefficients

$$f_n = \frac{1}{\alpha + \mu(k_0 - k(0))} \left(y_n - \mu \sum_{m=1}^{n} k_m\, f_{n-m}\right). \qquad (13)$$

Here $k_m$ and $f_m$ are the Fourier-Laguerre coefficients of the functions $k(t)$ and $f(t)$, respectively. Since the coefficients $k_n$ and $y_n$ are known, the Lager spectrum of the unknown function $f(t)$.is determined by the formula (13). Thus, equation (11) can be considered resolved.

Similarly, the solution of equation (11) is obtained. Let the functions $k(t)$ and $f(t)$ be given in series by polynomials $L_n^{\lambda_k}(t), \lambda_k > -1$, and $L_n^{\lambda_f}(t), \lambda_f > -1$, respectively, then the Fourier-Laguerre coefficients for the desired solution are calculated by the formula

$$f_n = \frac{1}{k_0} \left(\frac{1}{\mu}\, y_n - \sum_{m=0}^{n-1} k_{n-m}\, f_m\right). \qquad (14)$$

Here $y_n$ are the Fourier-Laguerre coefficients of the function $y(t)$ at $\lambda = \lambda_k + \lambda_f + 1$.

One of the advantages of the considered method is that the discretization procedure is excluded since the integral convolution turns into a series convolution. Quadrature formulas and formulas (13) and (14) enable the computation of a limited number of coefficients. These are not always sufficient to restore the original with the required accuracy. For this disadvantage elimination, asymptotic formulas for large $n$ were derived in the research that applies a priori information. They allow building a regularizing algorithm for restoring the desired function $f(t)$ with an accuracy that is acceptable for practice.

Modification of the constructed scheme. It is advisable to modify the above spectral method of solving convolution-type integral equations in a way as to restore values $f(t)$ by values $y(t_i)$ at the given points. To do this, we write formula (14) in the form

$$y_n = \sum_{m=0}^{n} k_{n-m}\, f_m,$$

or in matrix form

$$K_N\, F_N = Y_N, \qquad (15),$$

where

$$K_N = \begin{pmatrix} k_0 & 0 & \dots & 0 \\ k_1 & k_0 & \dots & 0 \\ \vdots & \vdots & \ddots & \vdots \\ k_{N_1} & k_{N-2} & \dots & k_0 \end{pmatrix}, \quad F_N = \begin{pmatrix} f_0 \\ k_1 \\ \vdots \\ f_{N_1} \end{pmatrix}, \quad Y_N = \begin{pmatrix} y_0 \\ y_1 \\ \vdots \\ y_{N_1} \end{pmatrix}.$$

The unknown coefficients $f_n$ will be the solutions of the matrix equation (14)

$$F_N = K_N^{-1}\, Y_N.$$

Here $K_N^{-1}$ is the matrix inverted to $K_N$. In expanded form

$$f_n = \sum_{i=0}^{N-1} y_i\, z_{n,i}, \quad n = \overline{0, N-1}. \qquad (16)$$

The last formula $z_{n,i}$ contains the elements of the inverse matrix$K_N^{-1}$. Substitute formula (14) into the $N$-th partial sum of the Fourier-Laguerre series. As a result, we get approximate equality for recovery $f(t) \approx f_N(t)$

$$f_N(t) = \sum_{n=0}^{N-1} \eta_n^{\lambda}(t)\, y_n, \qquad (17)$$

where

$$\eta_n^{\lambda}(t) = t^{\lambda} \sum_{m=n}^{N-1} \frac{n!}{\Gamma(n+\lambda+1)}\, z_{n+1,m+1}\, L_m^{\lambda}(t).$$

The quadrature formula for calculating the expansion coefficients $y(t)$ in matrix form is written as follows

$$Y_N = W_{N,N}\, YT_N, \quad (18)$$

where $W_{N,N}$ is a square matrix $N * N$ with elements $\omega_{i,j}$, and $YT_N$ is a column matrix with elements $y(t_j)$, $j = \overline{0, N-1}$.

If the values of the function $f(t)$ are calculated in points$t_k, k = \overline{1,K}$, then equality (17) will be in the matrix representation

$$\begin{pmatrix} f(t_1) \\ f(t_2) \\ \vdots \\ f(t_K) \end{pmatrix} = \begin{pmatrix} \eta_0(t_1) & \eta_1(t_1) & \dots & \eta_{N-1}(t_1) \\ \eta_0(t_2) & \eta_1(t_2) & \dots & \eta_{N-1}(t_2) \\ \vdots & \vdots & \ddots & \vdots \\ \eta_0(t_K) & \eta_1(t_K) & \dots & \eta_{N-1}(t_K) \end{pmatrix} \begin{pmatrix} y_0 \\ y_1 \\ \vdots \\ y_K \end{pmatrix},$$

or

$$FT_K = \Theta_{K,N}\, Y_N. \quad (19)$$

Therefore, from formulas (17) and (18) we obtain the next formulas

$$FT_N = G_{K,N}\, YT_N, \qquad G_{K,N} = \Theta_{K,N}\, W_{N,N}. \quad (20)$$

Since the matrix $G_{K,N}$ is constructed, then equality (20) allows us to restore the values of the input signal based on the values of the output signal at the points $t_k$, $k = \overline{1,K}$.

The elements of the matrix do not depend on the values of the input and output signals. Therefore, it is possible to calculate their required number with specified accuracy by using specific software methods and storing them in the warehouse. This helps to save calculation time and reduce the accumulation of calculation errors.

## 6. Use of spectral methods in vegetation remote-sensing

The natural and physical phenomena investigation frequently is performed based on remote or spectroscopic data. This helps to obtain information on the studied objects without performing natural experiments, chemical or other analyses. The use of mathematical modeling allows us to save both financial and material costs, as well as research time.

Spectrometric surveys of objects using a remote method allow the detection of certain deviations in the spectra of the reflected signals from the background ones. Studying the difference between reflected and background signals makes it possible to identify these objects or detect the presence of impurities within them. Through remote spectrometric surveys, it is possible to detect certain deviations in the anomalous reflection spectra of plants from their background values [5, 6, 8, 18, 21]. Based on this, using the data of ground reconciliation and calibration works, the mapping of vegetation areas with anomalous spectral characteristics is easily performed. Effective methods for plant reflectance spectra processing, which must satisfy the given criteria, in particular, in terms of accuracy and extreme qualities should be developed to solve such type problems. The basis of Jacobi polynomials will be used to complete such problems. The input data for a specific interval of wavelengths is shown in Figure 2.

The reflected signal is approximated by the $N$ partial sum of the Fourier-Jacobi series

$$f(x) = \begin{Bmatrix} \omega(x) \\ 1 \end{Bmatrix} \sum_{n=0}^{\infty} \begin{Bmatrix} f_n \\ \hat{f}_n \end{Bmatrix} \frac{1}{r_n} P_n^{(\alpha,\beta)}(x), x \in [-1,1], \quad (21).$$

$$\begin{Bmatrix} f_n \\ \hat{f}_n \end{Bmatrix} = \int_{-1}^{1} \begin{Bmatrix} 1 \\ \omega(x) \end{Bmatrix} P_n^{(\alpha,\beta)}(x)\, f(x)\, dx.$$

It is advisable to use formula (8) to calculate the unknown coefficients $f_n$ as, during information processing, the values of the signals are known mainly at discrete points.

Contamination of plants by nitrates is known to cause disturbance of the reflected spectrum at wavelengths of 450 nm to 650 nm [5], and the number of nitrates may be determined after calibration by chemical samples for nitrate content by the deviation

$$\Delta f = f_{f\,max}(x_m) - f_{a\,max}(x_m)$$

at the maximum point $x = x_m$ (Fig. 1). Here, $f_f$ and $f_a$ are the value of the background and reflected spectra, respectively. Approximation of the reflected signal by various methods leads to the fact that the maximum point in the general case does not coincide with the background spectrum maximum point. This causes inaccuracy in the determination of the abnormal signal distribution $\Delta f$. Jacobi polynomials usage allows matching the coordinates of the background maximum and reflected spectra due to the presence of two free parameters $\alpha$ and $\beta$. Thus, the deviation of the reflected spectrum from the background spectrum is determined with specific accuracy.

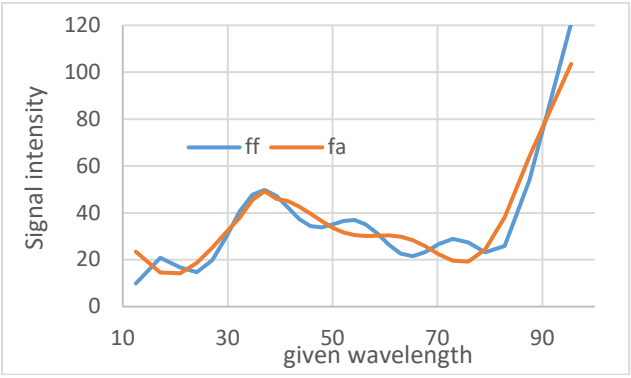


Figure 2: Dependence of background $f_f(\lambda_i)$ and reflected spectra on wavelength.

The identification algorithm is as follows.

a) The Fourier-Jacobi coefficients $f_{fn}$ and $f_{an}$ $(n = \overline{0, NV})$ are calculated based on the values of the $f_f(\lambda_i)$ background and $f_a(\lambda_i)$ reflected spectra.

b) The points of maximum $x_{fm}$ and $x_{am}$ for the background and reflected spectra at the given values $\alpha$ and $\beta$ in the interval 450-650 nm are obtained as solution of the below equations:

$$\sum_{n=0}^{NV} \frac{f_n}{r_n}\Big\{(\beta-\alpha-(\alpha+\beta)x)\,P_n^{(\alpha,\beta)}(x) + \frac{1}{2n+\alpha+\beta}\big((\alpha-\beta+(2n+\alpha+\beta)x)P_n^{(\alpha,\beta)}(x) - 2(n+\alpha)(n+\beta)P_{n-1}^{(\alpha,\beta)}(x)\big)\Big\} = 0$$

and

$$\sum_{n=0}^{NV} \frac{\hat{f}_n}{r_n(2n+\alpha+\beta)}\Big\{n(\alpha-\beta-(2n+\alpha+\beta)x)P_n^{(\alpha,\beta)}(x) + 2(n+\alpha)(n+\beta)P_{n-1}^{(\alpha,\beta)}(x)\Big\} = 0.$$

The values of $\alpha$ and $\beta$ are chosen in such a way that equality takes place $x_m = x_{fm} = x_{am}$.

c) The values of the background $f_f$ and $\Delta f$ anomalous $f_a$ reflected spectra and their difference $\Delta f = f_a(x_m) - f_f(x_m)$ are calculated at the found maximum point. The values of $x_m$ and $\Delta f$ at different values of $\alpha$ and $\beta$ are presented in Table 1. The row marked with I corresponds to the case when the multiplier before the sum in equation (21) is equal to one, while the row marked with II - $\omega(x)$. The analysis of the data presented in Table 1 illustrates that for each $\alpha$ there are such values $\beta$, at which $\Delta f$ is constant. Persistence of disturbance of the background spectrum $\Delta f$ serves as a criterion for the optimal choice of parameters $\alpha$ and $\beta$ for the remote data spectrometry of plants under processing.

Table 1: The value of disturbance of the background spectrum $\Delta f$ of plant reflection at the $x_m$ maximum point for different $\alpha$ and $\beta$ parameters.

| $\beta$ | | -0.6 | | -0.28 | | 0.04 | | 0.36 | | 0.68 | |
|---|---|---|---|---|---|---|---|---|---|---|---|
| $\alpha$ | | $x_m$ | $\Delta f$ | $x_m$ | $\Delta f$ | $x_m$ | $\Delta f$ | $x_m$ | $\Delta f$ | $x_m$ | $\Delta f$ |
| -0.5 | I | 577.6 | 3.84 | 578.1 | 3.89 | 578.5 | 3.70 | 578.9 | 3.54 | 579.3 | 3.43 |
| | II | 543.8 | 6.18 | 596.9 | 3.53 | 543.7 | 6.33 | 545.6 | 6.58 | 533.0 | 9.87 |
| 0.0 | I | 577.4 | 4.17 | 577.9 | 3.97 | 578.3 | 3.77 | 578.7 | 3.59 | 579.1 | 3.46 |
| | II | 544.4 | 6.47 | 597.4 | 0.43 | 544.2 | 6.42 | 545.3 | 6.58 | 548.8 | 6.85 |
| 1.0 | I | 577.0 | 4.32 | 577.5 | 4.16 | 577.9 | 3.98 | 578.3 | 3.80 | 578.7 | 3.64 |
| | II | 570.9 | 7.16 | 569.8 | 6.73 | 529.5 | 5.98 | 529.2 | 5.90 | 529.1 | 5.84 |

The deviations of the reflected spectrum from the background obtained during the computational experiment were compared with the corresponding results obtained based on chemical analysis during the natural experiment. The convergence of results was within 15%. Therefore, the presence of nitrates in plants and the estimation of their percentage rate can be detected by the processing of remote data of green areas. Similarly, it is possible to detect the presence of heavy metals in green vegetation. For this purpose, it is necessary to investigate the deviation of the reflected spectrum from the background in the so-called "blue shift" zone, that is, at wavelengths longer than 2000 nm. In particular, this will allow determining the area of radioactive contamination spreading by remote methods without the risk of exposure to specialists.

## 7. Conclusions and discussion.

An algorithm for remote and spectroscopic information processing using the spectral method based on orthogonal Jacobi and Chebyshev-Laguerre polynomials is presented in the current paper. This algorithm allows approximating signals by orthogonal series, calculating the derivatives of the specified series, and solving approximation and identification problems on this basis. The feasibility and effectiveness of orthogonal Jacobi and Chebyshev-Laguerre polynomials used to solve signal-processing problems have been confirmed based on real-life data. The problem of the summation of the orthogonal basis series is incorrect. The optimal choice of free parameters makes it possible to provide an "implicit regularisation" by applying the fast convergence series. Depending on the specifics of the problem, the procedures for speeding up the convergence of series or modifying the functions with orthogonal series may be utilized for this purpose.

Based on the input information, the Fourier-Jacobi series can be presented in the following form:

$$\varphi(x) = \omega(x)\sum_{n=0}^{\infty}\frac{\varphi_{\omega n}}{r_n}P_n^{(\alpha,\beta)}(x),$$

$$\varphi(x) = (1-x)^{\alpha}\sum_{n=0}^{\infty}\frac{\varphi_{\alpha n}}{r_n}P_n^{(\alpha,\beta)}(x),$$

$$\varphi(x) = (1+x)^{\beta}\sum_{n=0}^{\infty}\frac{\varphi_{\beta n}}{r_n}P_n^{(\alpha,\beta)}(x).$$

A similar procedure can be provided with the Fourier-Laguerre series.

One of the reasons for the usage of classical orthogonal polynomials widespread is that they are easy to use and theoretically justified. Recently, intensive research has been done regarding constructing and applying biorthogonal polynomials to solve applied problems.

Algorithms for filtering one-dimensional signals in linear filter models were built based on one-dimensional Laguerre polynomials. One of the advantages here is that the integral convolution moves directly to series convolution without using the discretization procedure. In practice, it is necessary to consider models of filtering

signals of higher dimensions, particularly two-dimensional ones. In such cases, it is advisable to use multidimensional orthogonal Laguerre polynomials. Studies of these polynomials types were conducted in works [15, 16, 19]. The results obtained in these works can be successfully used for filtering multidimensional signals. Note that in practice, as a rule, signal filtering models are non-linear. However, a considerable number of signal filtering problems in nonlinear models can be solved with sufficient accuracy for practice by approximating them with linear filter models.

## Conflict of Interest

The authors declare no conflict of interest.

## References

[1] B. Markus, *Spectral Analysis in Geophysics*. Moscow: Nedra, 1980, 535 p.
[2] Y. D. Pyanilo, *Projection-Iterative Methods for Solving Direct and Inverse Transfer Problems*. Lviv: Spline, 2011, 248 p.
[3] Y. Pjanylo and O. Hotra, "Methods of statistical processing of measurements data in the basis of jacobi polynomial for ecological monitoring," *Actual Problems of Economics*, no. 10, pp. 221–230, 2010.
[4] Y. Pyanylo, V. Sobko, H. Pyanylo, M. Petrus, and A. Demichkovsky, "Processing of digital information on the basis of orthogonal and biorthogonal polynomials," in *2020 IEEE 6th International Conference on Methods and Systems of Navigation and Motion Control, MSNMC 2020 - Proceedings*, 2020, pp. 114–117, doi: 10.1109/MSNMC.2020.9255422.
[5] V. I. Lyalko and Y. D. Pyanylo, "The use of classical orthogonal polynomials in remote sensing of vegetation," *Add. National Academy of Sciences*, no. 2, pp. 42-46, 1997.
[6] Z. M. Shportyuk, V. I. Lyalko, Y. D. Pyanilo, O. M. Sibirtseva, and H. M. Pyanilo, "Spectral methods of information processing and analysis in remote sensing of vegetation," *Preprint of NU TsMM IPPMM ANU*, no. 4-93, Lviv, 1993, 54 p.
[7] Global System of Observation of the Planet Earth [Online]. Available: https://goo.gl/uuhmCk.
[8] S. O. Dovgiy, V. I. Lyalko, S. M. Babiichuk, T. L. Kuchma, O. V. Tomchenko, and L. Ya. Yurkiv, *Basics of Remote Sensing of the Earth: History and Practical Application: Education Manual*. Kiev: Institute of the Gifted Child of the National Academy of Sciences of Ukraine, 2019, 316 p.
[9] J. Shen, "Efficient spectral-Galerkin method II. Direct solvers for second- and fourth-order equations by using Chebyshev polynomials," *SIAM J. Sci. Comput.*, vol. 16, pp. 74–87, 1995, doi: 10.1137/0916006.
[10] Y. D. P'yanylo, H. M. P'yanylo, and M. Y. Vasiunyk, "Application of orthogonal polynomials for analysis of input numerical data in the problems of mass transfer," *Mathematical Modeling and Computing*, vol. 2, no. 1, pp. 88–98, 2015, doi: 10.23939/mmc2015.01.088.
[11] Y. Pyanylo, V. Sobko, and O. Bratash, "The mass transfer research in complex porous media and pipelines by spectral methods," *Mathematical Modeling and Computing*, vol. 4, no. 2, pp. 187–196, 2017, doi: 10.23939/mmc2017.02.187.
[12] K. Lantsosh, *Practical Methods of Applied Analysis*. Moscow: Fizmatgiz, 1961, 524 p.
[13] S. Kachmazh and G. Shteinhaus, *Theory of Orthogonal Series*. Moscow: Fizmatgiz, 1958, 394 p.
[14] Y. D. P'yanylo and V. G. Sobko, "Construction and research of biorthogonal polynomials based on Chebyshev polynomials," *Applied Problems of Mechanics and Mathematics*, no. 11, pp. 135–141, 2013.
[15] N. U. Khan, T. Usman, and W. A. Khan, "A new class of laguerre-based generalized hermite-euler polynomials and its properties," *Kragujevac Journal of Mathematics*, vol. 44, no. 1, pp. 89–100, 2020, doi: 10.46793/KgJMat2001.089K.
[16] W. A. Khan and H. Haroon, "A new class of generalized Laguerre-based poly-Bernoulli polynomials," *Global Journal of Pure and Applied Mathematics*, vol. 13, no. 8, pp. 4175–4188, 2017 [Online]. Available: http://www.ripublication.com/gjpam.htm.
[17] Yu. Luk, *Special Mathematical Functions and Their Approximation*. Moscow: Mir, 1980, 608 p.
[18] Drones and satellites: monitoring the condition of crops during season [Online]. Available: https://smartfarming.ua/ua-blog/monitoring-sostoyaniya-posevov-vtechenie-sezona.
[19] W. A. Khan, S. Araci, M. Acikgoz, and A. Esi, "Laguerre-based Hermite-Bernoulli polynomials associated with bilateral series," *Tbilisi Mathematical Journal*, vol. 11, no. 2, pp. 111–121, 2018, doi: 10.32513/tbilisi/1529460026.
[20] A. N. Tikhonov and V. Ya. Arsenyn, *Methods of Solving Incorrect Problems*, 2nd ed. Moscow: Nauka: Main Edition of Physical and Mathematical Literature, 1979, 285 p.
[21] Heat balance of the Earth [Online]. Available: https://uk.wikipedia.org/Teplovy_balans_Zemli.